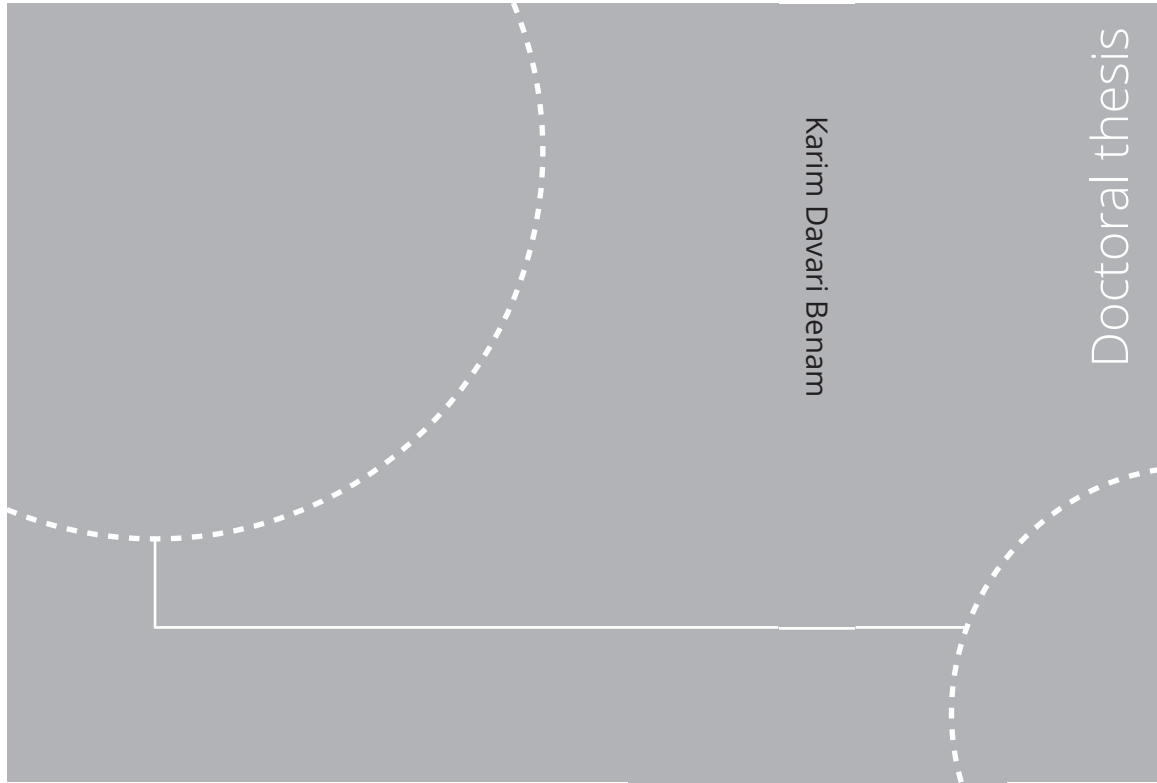


ISBN 978-82-326-7578-4 (printed ver.)  
ISBN 978-82-326-7577-7 (electronic ver.)  
ISSN 1503-8181 (printed ver.)  
ISSN 2703-8084 (electronic ver.)



Doctoral theses at NTNU, 2023:438

Karim Davari Benam

# Design and Implementation of the Dual-Hormone Artificial Pancreas in Animal Studies

A Model Predictive Control Approach with Intrapertoneal Hormone Injections

Doctoral theses at NTNU, 2023:438

**NTNU**  
Norwegian University of  
Science and Technology  
Thesis for the degree of  
Philosophiae Doctor  
Faculty of Information Technology  
and Electrical Engineering  
Department of Engineering Cybernetics

 **NTNU**  
Norwegian University of  
Science and Technology

 NTNU

 **NTNU**  
Norwegian University of  
Science and Technology

Karim Davari Benam

# Design and Implementation of the Dual-Hormone Artificial Pancreas in Animal Studies

A Model Predictive Control Approach with  
Intraperitoneal Hormone Injections

Thesis for the degree of Philosophiae Doctor

Trondheim, December, 2023

Norwegian University of Science and Technology  
Faculty of Information Technology  
and Electrical Engineering  
Department of Engineering Cybernetics



Norwegian University of  
Science and Technology

**NTNU**

Norwegian University of Science and Technology

Thesis for the degree of Philosophiae Doctor

Faculty of Information Technology  
and Electrical Engineering  
Department of Engineering Cybernetics

© Karim Davari Benam

ISBN 978-82-326-7578-4 (printed ver.)  
ISBN 978-82-326-7577-7 (electronic ver.)  
ISSN 1503-8181 (printed ver.)  
ISSN 2703-8084 (electronic ver.)

ITK-report: 2023-28 -W

Doctoral theses at NTNU, 2023:438



Printed by Skipnes Kommunikasjon AS

*Dedicated to the unwavering support of my  
Family, Professors, and Friends,  
who stood by me throughout this journey.*



## Abstract (English)

---

In this thesis, the exploration of new ways to help people with Type 1 Diabetes better control their condition is described. In this research, our primary focus was on the feasibility and benefits of utilizing the intraperitoneal (IP) route for insulin and glucagon injections in Type 1 Diabetes Mellitus (T1DM), chosen due to its significantly faster absorption and more rapid effects on glucose levels compared to the subcutaneous (SC) route. The core contribution of this research lies in the development of a fully automated dual hormone AP system and testing in various animal experiments.

In the first major part of this work, a new model is introduced, designed with a minimal number of parameters and states, exclusively intended for control applications within dual-hormone AP systems. Demonstrating remarkable prediction accuracy in over 30 animal experiments, this model represents a significant advancement that has the potential to facilitate future advancements in diabetes management.

Subsequently, an estimator based on the Moving Horizon Estimation (MHE) method is designed, incorporating embedded prior knowledge to effectively estimate non-measurable states of the model, as well as meals and exercises. The experimental evaluation showcases the high accuracy of the estimator, further validating its potential as a valuable tool in diabetes care future.

The work proceeds with the development of an MPC-based controller, adeptly incorporating practical considerations. Extensively tested in both *in vivo* and *in silico* experiments, the controller demonstrates high performance, surpassing existing Hybrid Closed-Loop AP systems in the market. Importantly, the proposed controller does not necessitate the meals and exercise announcements, enhancing its user-friendliness and autonomy compared to the commercial devices which all require meal announcements.

Beyond the primary research target, this study delves into various other areas within diabetes management. The investigation includes testing a two-layer PID controller scheme, developing a method to compensate for CGM sensor time lag, exploring sensor fusion techniques to enhance glucose measurements, and studying experimental design strategies to increase model parameter identification accuracy.

The findings of this research contribute to the advancement of diabetes

research, which in turn may result in advances in diabetes care. The proposed model, estimator, and controller collectively offer a comprehensive and efficient solution for achieving reliable glycemic control in T1DM patients with IP injections. Ultimately, this work represents a vital step forward in personalized care and opens new avenues for future research and technological innovations.

## Abstract (Norwegian)

---

I dette studiet har metoder for regulering av blodsukker i pasienter med diabetes type 1 blitt utforsket. Vårt primære fokus var å studere gjennomførbarheten og fordelene ved å bruke den intraperitoneale (IP) ruten for insulin- og glukagoninjeksjoner ved type 1 diabetes mellitus (T1DM). Hovedbidraget til dette forskningsfeltet var i utviklingen av et helautomatisert bihormonelt AP-system og testing i forskjellige dyreforsøk.

Den første delen av arbeidet bestod av å introdusere en ny modell, designet med et minimalt antall parametere og tilstander, samt eksklusivt beregnet for reguleringsanvendelser innen bihormonelle AP-systemer. Denne modellen viser en bemerkelsesverdig prediksjonsnøyaktighet i mer enn 30 dyreforsøk, og representerer et betydelig fremskritt innen diabetesbehandling.

Etterfulgt av dette ble en estimator designet basert på Moving Horizon Estimation (MHE)-metoden. Den inkluderer innebygd forkunnskap for effektivt å estimere ikke-målbare tilstander i modellen, samt måltider og trening/aktivitet. Eksperimentell evaluering viste at estimatoren har høy nøyaktighet, og validerte ytterligere dens potensiale som et verdifullt verktøy i diabetesbehandling.

Studiet fortsatte med utviklingen av en modellbasert regulering, inklusivt med innarbeiding av praktiske hensyn. Under omfattende testing, både i in vivo og in silico-eksperimenter, viser regulatoren høy ytelse, og overgår eksisterende Hybrid Closed-Loop AP-systemer på markedet. Regulatoren som presenteres her krever ikke kunngjøringer av måltider og trening, noe som øker brukervennligheten og autonomien.

Utover det primære forskningsmålet, gikk dette arbeidet også inn i andre elementer innen diabetesbehandling. Dette inkluderer testing av en tolags PID-regulator, utvikling av en metode for å kompensere for CGM-sensorens tidsforsinkelse, utforskning av sensorfusjonsteknikker for å forbedre målinger, og studier av eksperimentelle designstrategier for å øke nøyaktigheten av modellparameteridentifikasjon.

Resultatene fra dette studiet er et bidrag til diabetesforskning, som i fremtiden kan bli brukt til å forbedre diabetesbehandlingen. Den foreslåtte modellen, estimatoren og regulatoren tilbyr samlet en omfattende og effektiv løsning for å oppnå stabil glykemisk regulering hos T1DM-pasienter med IP-injeksjoner. Til syvende og sist representerer dette arbeidet et viktig skritt fremover innen personilpasset medisin og åpner nye veier for fremtidig forskning og teknologiske



innovasjoner.

## *Preface*

---

I have completed this thesis as a partial requirement for the degree of philosophiae doctor (PhD) at the Norwegian University of Science and Technology (NTNU). The research, conducted from January 2020 to October 2023, was primarily undertaken at the Department of Engineering Cybernetics and the Department of Clinical and Molecular Medicine at the Norwegian University of Science and Technology in Trondheim, Norway, within the research group of Artificial Pancreas Trondheim (APT).

The animal experiments for this study were conducted at the Comparative Medicine Core Facility (CoMed) at NTNU. The project received financial support from the Norwegian Research Council (project number 248872) and the Centre for Digital Life Norway.

Throughout this journey, I have had the pleasure of working with some of the most talented and inspiring individuals, including my supervisors, colleagues, and friends. I am deeply grateful for their support, encouragement, and guidance, without which this thesis would not have been possible.

In particular, I would like to express my gratitude to my supervisors, Anders Lyngvi Fougner and Sébastien Gros, for their unwavering support, invaluable insights, and patient guidance. Their expertise and encouragement have been instrumental in shaping my research and helping me navigate the challenges of the project.

I would also like to thank my colleagues and friends, who have been an endless source of inspiration, motivation, and laughter. Whether we were hiking, traveling, or working on long experiments, we always found a way to support each other, learn from each other, and have fun together. I am especially grateful for the unforgettable moments we shared during the COVID pandemic, which didn't stop us from progressing and having a bit of socially distanced fun along the way. Without their mentorship and encouragement, I may have never discovered my newfound addiction to coffee!

The experiments outlined in this thesis were conducted by Marte Kierulf Åm, Patrick Christian Bösch, Hasti Khoshamadi, Oddveig Lyng, and I. The authors would like to thank this team for their invaluable contribution to performing the experiments and collecting the data. We also like to thank Professor Sven Magnus Carlsen and Professor Øyvind Stavadahl for their help in designing the experiments and discussions.



**FIGURE 1.** On March 5th, 2021, we conducted our first 24-hour experiment on an anesthetized pig. In the upper left photo, you can see Patrick Christian Bösch uploading sensor data to the cloud every 5 minutes throughout the day to load it onto the controller. The upper right photo was taken on May 6th, 2021, during a hiking trip we took with Anders, Sébastien, Øyvind, and Hasti after the 24-hour animal trials. Anders and I were biking around Bymark on June 30th, 2021, when we took the lower right photo. Lastly, the lower left photo was taken on March 30th, 2023, at the University of Geneva when we were subject managers for an excursion trip for the NTNU students.

During certain stages of my PhD research, I collaborated closely with the students whom I co-supervised. Notably, Petter Skau-Nilsen, Martha Halvorsen, Eirik Jakobsen Daltveit, Christian Lillestrand, Mai Ve Bugge, and Jana Langholz played a significant role in the work closely related to the material presented in this thesis.

Furthermore, I would like to express my gratitude to Norway, where I had the privilege of studying and conducting research. Trondheim, in particular, stole my heart with its stunning nature, rich culture, and kind-hearted people.

Finally, I would like to dedicate this thesis to my family who have always been my biggest supporters, my source of love and strength, and my home away from home.

This journey wasn't without its challenges, especially during the COVID pandemic, but we adapted, persevered, and even managed to have some fun along the way. Attached to this preface, you'll find a picture of my professors and me hiking, biking, and a selfie with my colleagues during a long experiment that lasted for 24 hours. Yes, we were all sleep-deprived, but we were motivated and happy even in the middle of the night.

*Trondheim, April 2023,  
Karim Davari Benam*

## Contents

---

ABSTRACT	III	
ABSTRACT(NORWEGIAN)	V	
PREFACE	VII	
LIST OF FIGURES	XIII	
LIST OF TABLES	XV	
NOMENCLATURE	XVII	
CHAPTER 1	SCOPE AND CONTRIBUTIONS	1
1.1	Thesis Outline	1
1.2	Scope of the Thesis	2
1.3	List of Publications	3
1.4	List of Contributions	5
1.5	The Author's Individual Contributions in Co-authorships	10
1.6	Research Map	10
1.7	References	13
<hr/>		
<b>PART I</b>	<b>INTRODUCTION, BACKGROUND, AND DISCUSSIONS</b>	<b>15</b>
CHAPTER 2	INTRODUCTION	17
2.1	Background and Motivation	17
2.1.1	Diabetes Mellitus	17

2.1.2	Glucose Metabolism	19
2.1.3	Possible Treatments for Type 1 Diabetes	20
2.1.4	Artificial Pancreas	21
2.1.5	Insulin Injection Routes	21
2.2	Development of the Artificial Pancreas System	23
2.3	Research Groups and Their Designed Control Systems	27
2.3.1	Subcutaneous Artificial Pancreas systems	27
2.3.2	Interaperitoneal Artificial Pancreas systems	28
2.4	Story of the Presented Research	31
2.4.1	Step 1; Choosing the Control Strategy	31
2.4.2	Step 2; Streamlining MPC Implementation: Bridging Complexity for Developers, Delivering Simplicity for Clinicians and Patients	33
2.4.3	Step 3; Developing an Accurate Model with Simple or No Parameter Identification	34
2.4.4	Step 4; Designing an Estimator	35
2.4.5	Step 5; Design a Model Predictive Controller and Perform Experiments	35
2.5	References	36
<b>CHAPTER 3 DEVELOPMENT AND TESTING IN ANIMAL TRIALS</b>		<b>41</b>
3.1	Use of Animals in the Experiments	41
3.2	Hormone Injection and Glucose Measurement	42
3.3	Overview of the Designed Artificial Pancreas	43
3.3.1	Continuous Glucose Monitoring System	43
3.3.2	Sensor Fusion	44
3.3.3	Mathematical Model	45
3.3.4	Estimator	46
3.3.5	Control Design	47
3.3.6	Software Framework	50

3.4	References	51
<b>CHAPTER 4 DISCUSSION 53</b>		
4.1	Discussions on the Developed Dual-Hormone Intraperitoneal Model	53
4.2	Discussions on the Developed Dual-Hormone Intraperitoneal Moving Horizon Estimator	54
4.3	Discussions on the Developed Dual-Hormone Predictive Controller	55
4.4	Discussions on using Single Hormone or Dual Hormone Artificial Pancreas	57
4.5	Discussions on Using Intraperitoneal Route	58
4.6	References	60
<b>CHAPTER 5 CONCLUDING REMARKS 61</b>		
5.1	Conclusions	61
5.2	Future Work	62
5.2.1	From Research to Real-World Impact	64
5.2.2	Impact of This Research on Patients' Lives	64
5.2.3	Risk Assessment	65
5.3	References	65
<hr/>		
<b>PART II ORIGINAL PUBLICATIONS 67</b>		
<b>CHAPTER 6 ORIGINAL PUBLICATIONS 69</b>		
6.1	Paper 1	70
6.2	Paper 2	79
6.3	Paper 3	99
6.4	Paper 4	108
6.5	Paper 5	123
6.6	Paper 6	132

6.7	Paper 7	143
6.8	Paper 8	151
6.9	References	180

## List of Figures

---

1 Artificial Pancreas Trondheim (APT) viii

### CHAPTER 1

1.1 Research Map 11

1.2 Scope of the papers 12

### CHAPTER 2

2.1 Global incidence of type 1 diabetes 18

2.2 Glucose regulation system 19

2.3 Artificial pancreas 21

2.4 Insulin infusion routes 22

2.5 Peritoneal cavity 23

2.6 Advancements of artificial pancreas 25

2.7 Literature map 26

2.8 Categories of the artificial pancreas systems 27

2.9 Implantable pumps 29

2.10 Refilling of implantable pumps 30

### CHAPTER 3

3.1 Establishing of intraperitoneal route 43

3.2 Placement of sensor on pigs 44

3.3 Block diagram of the proposed artificial pancreas 45

3.4 Cost function of the designed controller 49

3.5 Designed Software and framework 50



CHAPTER 4

CHAPTER 5

5.1 Microglucagon mechanism 63

CHAPTER 6

## *List of Tables*

---

1.1	Contributions to Papers 1–8.	10
2.1	Important research groups and companies	28
2.2	MPC vs PID	33
CHAPTER 3		
CHAPTER 4		
CHAPTER 5		
CHAPTER 6		



## Nomenclature

---

### ACRONYMS

AP	Artificial Pancreas	MHE	Moving Horizon Estimation
BG	Blood Glucose		
BGL	Blood Glucose Level	MPC	Model Predictive Control
CF	Correction Factor		
CGM	Continuous Glucose Monitor	PI	Practical identifiability
CHO	Carbohydrate	PISA	Pressure Induced Sensor Attenuation
CSII	Continuous Subcutaneous Insulin Infusion	PK/PD	Pharmacokinetic/Pharmacodynamic
		SA	Sensitivity Analysis
DIP	Dual-hormone Intraperitoneal	SC	Subcutaneous
		SI	Structural identifiability
DM	Diabetes Mellitus	SMBG	Self Monitoring of Blood Glucose
EGP	Endogeneous Glucose Production		
		SVD	Singular Value Decomposition
EKF	Extended Kalman Filter		
HCL	Hybrid Closed Loop	T1DM	Type 1 Diabetes Mellitus
HOB	Glucagon on Board	T2DM	Type 2 Diabetes Mellitus
HWITL	Hardware in the Loop	UI	User interface
IG	Interstitial Glucose	UKF	Unscented Kalman Filter
IOB	Insulin on Board		
IP	Intraperitoneal	UVa-Padova	University of Virginia and Padova
KF	Kalman Filter		
MARD	Mean Absolute Relative Difference	VP	Virtual Patient



# CHAPTER 1

## *Scope and Contributions*

---

### 1.1 THESIS OUTLINE

The work is a paper collection-based thesis and is organized as follows:

- Chapter 1 (Scope and Contributions):** Outlines the extent of the thesis and explains the publications and contributions made in this current research endeavor.
- Chapter 2 (Introduction):** Introduces the reader to type 1 diabetes and the artificial pancreas. It describes the state of the art in control of blood glucose level and presents the challenges in the assessment and use of the currently available systems.
- Chapter 3 (Development and Testing in Animal Experiments):** In this chapter, we explore the concept of "Animal Experiments." Furthermore, we delve into the methods employed in the project, analyze the challenges faced, and highlight the strategies employed to overcome them.
- Chapter 4 (Discussion):** Puts the contributions and publications into context and discusses the strengths and weaknesses of the present work.
- Chapter 5 (Concluding Remarks):** Summarizes the work, defines relevant topics for future work, and concludes the thesis.
- Chapter 6 (Original Publications):** Contains seven published papers in facsimile, as well as one submitted journal paper manuscript.

## 1.2 SCOPE OF THE THESIS

This thesis aims to evaluate the feasibility and advantages of using the intraperitoneal (IP) route for insulin and glucagon injections in Type 1 Diabetes Mellitus (T1DM) patients. Additionally, it presents a fully automated dual-hormone artificial pancreas solution for T1DM patients, eliminating the need for meal or exercise announcements. In this thesis we:

- **Analyse:**

1. The **interactions** of Blood Glucose Level (**BGL**) with **intraperitoneal (IP) insulin and glucagon**,
2. The **feasibility** of having a fully closed-loop (**FCL**) artificial pancreas (**AP**) using the IP route,
3. The **pharmacokinetics (PK)** and **pharmacodynamics (PD)** of intraperitoneal (**IP**) insulin and glucagon **injections**.

- **Review:**

1. Existing **mathematical models** and **simulators** in the literature for IP AP systems,
2. Existing **estimation methods** for estimating the **non-measurable states** in the body,
3. Existing **control methods** for regulating the **BGL**.

- **Design:**

1. A **model** for **dual-hormone APs** for **control purposes**,
2. An **estimator** for consumed **meals** and the **non-measurable states**,
3. A dual-hormone **predictive controller** to regulate the **BGL**.
4. **Experiments** to evaluate the proposed methods.

- **Evaluate the proposed methods, through:**

1. **In silico** tests in 100 virtual subjects (simulated pigs),
2. **In vivo test** in six **anesthetized** pigs.
3. **In vivo test** in an **awake** pig.

### 1.3 LIST OF PUBLICATIONS

The research that forms the basis of this thesis has resulted in the following publications, listed and numbered in chronological order, and grouped by publication type:

#### Journal Papers:

---

**Paper 2** K. D. Benam, H. Khoshamadi, M. K. Åm, Ø. Stavdahl, S. Gros, and A. L. Fougner, "Identifiable prediction animal model for the bi-hormonal intraperitoneal artificial pancreas," *Journal of Process Control*, vol. 121, pp. 13–29, 2023.

DOI: 10.1016/j.jprocont.2022.11.008.

**Paper 4** K. D. Benam, S. Gros, and A. L. Fougner, "Estimation and prediction of glucose appearance rate for use in a fully closed-loop dual-hormone intraperitoneal artificial pancreas," *IEEE Transactions on Biomedical Engineering*, pp. 1–12, 2023, *in press*.

DOI: 10.1109/TBME.2023.3301730.

**Paper 8** K. D. Benam, M. K. Åm, P. C. Bösch, H. Khoshamadi, S. Chr. Christiansen, D. R. Hjelme, Ø. Stavdahl, S. M. Carlsen, S. Gros, and A. L. Fougner, "A Dual Hormone Predictive Controller for a Fully Automated Intraperitoneal Artificial Pancreas in Pigs", Submitted to *Automatica* on 15 Sep 2023.

#### Conference Papers:

---

**Paper 1** K. D. Benam, H. Khoshamadi, L. Lema-Pérez, S. Gros and A. L. Fougner, "A Nonlinear State Observer for the Bi-Hormonal Intraperitoneal Artificial Pancreas," 2022 44th Annual International Conference of the IEEE Engineering in Medicine & Biology Society (EMBC), Glasgow, Scotland, United Kingdom, 2022, pp. 171-176.

DOI: 10.1109/EMBC48229.2022.9871264.

**Paper 3** M. Halvorsen, K. D. Benam, H. Khoshamadi and A. L. Fougner, "Blood Glucose Level Prediction Using Subcutaneous Sensors for in Vivo Study: Compensation for Measurement Method Slow Dynamics Using Kalman Filter Approach," 2022 IEEE 61st Conference on Decision and Control (CDC), Cancun, Mexico, 2022, pp. 6034-6039.



DOI: 10.1109/CDC51059.2022.9992638.

**Paper 5** M. A. Ahdab, K. D. Benam, H. Khoshamadi, S. Gros, and A. L. Fougner, "Sensor Fusion for Glucose Monitoring Systems," IFAC World Congress, Yokohama, Japan, July 2023. *In press*.

**Paper 6** J. Langholz, K. D. Benam, B. Sharan, S. Gros, and A. L. Fougner, "Fully Automated Bi- hormonal Intraperitoneal Artificial Pancreas Using a Two-Layer PID Control Scheme," ECC, Bucharest, Romania, June 2023.

DOI: 10.23919/ECC57647.2023.10178295

**Paper 7** S. E. Engell, H. Bengtsson, K. D. Benam, A. L. Fougner, and J. B. Jørgensen, "Optimal Experimental Design to Estimate Insulin Response in Type 2 Diabetes," CCTA, Bridgetown, Barbados, August 2023. *In press*.

#### **Other Publications:**

-----  
**O.P 1** B. Aminian, K. D. Benam and D. Varagnolo, "ASAN: An Extendable Approach for Automatic Step-sizes Adjustment for Newton-Raphson Consensus Optimization Algorithms," 2022 IEEE International Conference on Systems, Man, and Cybernetics (SMC), Prague, Czech Republic, 2022, pp. 3026-3032,

DOI: 10.1109/SMC53654.2022.9945400.

**O.P 2** K. D. Benam, H. Khoshamadi, S. Gros, and A. L. Fougner, A. (2022, April) [Poster]. The bihormonal intraperitoneal artificial pancreas achieve fully closed loop control in anesthetized animals. In *Diabetes Technology & Therapeutics* (Vol. 24, pp. A97-A97). 140 Huguenot Street, 3rd Fl, New Rochelle, NY 10801 USA: Mary Ann Liebert, Inc.

## 1.4 LIST OF CONTRIBUTIONS

### **Paper 1** Title: *“A Nonlinear State Observer for the Bi-Hormonal Intraperitoneal Artificial Pancreas”*

This paper proposes a high-gain observer (HGO) for a modified model presented in [1] to estimate the amounts of insulin and glucagon in different compartments, as well as the glucagon sensitivity. In this paper, we assumed that the meals are announced, and the diffusion rates of insulin and glucagon from the peritoneal to the Portal Vein are high, with negligible absorption delay, similar to [2]. Hence, there is no need for estimating the amount of insulin and glucagon in the peritoneal cavity. Later in the research, we designed a different estimator (**Paper 4**) that does not require meal announcements and is based on a more accurate model (**Paper 2**). Consequently, the designed HGO was not utilized in the closed-loop experiments.

### **Paper 2** Title: *“Identifiable prediction animal model for the bi-hormonal intraperitoneal artificial pancreas”*

This paper is one of the main contributions of this thesis which explores the pharmacokinetics and pharmacodynamics of the intraperitoneal (IP) route for a dual-hormone Artificial Pancreas (AP) system. We presented a model for Model Predictive Control (MPC)-based dual-hormone IP APs and trained and tested it using data from 26 recorded experiments in anesthetized pigs.

We develop a technique that utilizes rich experimental data from prior experiments in other subjects to increase the identifiability of the model. Many parameters are modeled as functions of body weight or are common across animals, simplifying the identification process for each new subject while preserving essential details that enhance prediction capability.

The resulting model, named "meta-model," only requires the identification of five parameters for each new subject (pig). These parameters include the brain glucose consumption rate, the sensitivity of the liver and other organs to insulin, the sensitivity of the liver to glucagon, and the initial glycogen storage level. The meta-model is utilized in several subsequent papers (**Papers 4**, for developing a state estimator; **Paper 6**, develop a simulator to generate virtual subjects; and **Paper 8**, to develop a dual-hormone predictive controller).

### **Paper 3** Title: *Blood Glucose Level Prediction Using Subcutaneous Sensors for*

***in Vivo Study: Compensation for Measurement Method Slow Dynamics Using Kalman Filter Approach***

In our open-loop experiments, we were using a blood gas analyzer (BGA) to measure the BGL. In closed-loop experiments, we had to use a continuous glucose monitoring (CGM) system using the SC sensors since it was not feasible to take blood samples frequently. However, it measures glucose in interstitial fluid in subcutaneous tissue rather than directly in plasma. Measuring BGL in this method introduces a time lag in capturing the blood glucose level. This can reduce the quality of blood glucose regulation and result in hypo- or hyperglycemia.

The paper presents the development of a simple and practical linear Kalman filter to predict blood glucose concentration using CGM data and compensate for slow dynamics. A physiology-based, input-less model is used to describe glucose diffusion from plasma to interstitial fluid, with parameters obtained from the literature. The performance is evaluated using data from two animal experiments conducted on anesthetized pigs, which includes CGM measurements every 1.2 seconds and sporadic blood sample analysis during experiments. The results demonstrate that the proposed approach effectively compensates for the slow dynamics of CGM measurements when compared to blood glucose samples, as measured by statistical accuracy scores. This compensation can enhance the decision-making of control algorithms for glucose regulation during rapid changes in glucose concentration, such as during meals and exercise.

As a future practice, we will integrate this method with the method proposed in **Paper 5** to infuse the multiple sensor data and compensate for the time lag of the CGM systems from different brands.

**Paper 4 Title: “Estimation and Prediction of Glucose Appearance Rate for Use in a Fully Closed-Loop Dual-Hormone Intraperitoneal Artificial Pancreas”**

Another main contribution of this thesis is the proposed DIP-MHE. This study presents an estimator for glucose appearance rate (GAR) based on moving horizon estimation (MHE). The underlying cost function incorporates information about the lifestyle and diet of the subjects to improve estimation accuracy without the need for meal announcements.

The effectiveness and reliability of the estimations were tested by using data obtained from three 24-hour experiments on anesthetized animals. The estimator achieved an average 21.8% mean absolute percentage error (MAPE) in estimating GAR without meal announcements across six different scenarios. More importantly, it also achieved a promising

10.0% MAPE in four-hour blood glucose level (BGL) predictions when assuming future GAR was known. In addition, if future GAR is unknown, a predictor scheme is proposed to predict future GAR and BGL. For the predictions made over 120 minutes, the predictor achieved an average MAPE of 18.0% and 28.4% for GAR and BGL predictions, respectively.

As there is no comparable estimator available in the existing literature, the scores achieved cannot be directly compared with previous research. However, our findings demonstrate the effectiveness and reliability of the proposed estimator, especially in near-real-life scenarios. This estimator is well-suited for applications in closed-loop systems, particularly in the context of MPC methods.

**Paper 5 Title: “*Sensor Fusion for Glucose Monitoring Systems*”**

For a fully automated AP to function effectively, accurate BGL readings are crucial. However, the accuracy of commercially available sensors can be affected by various factors, such as sensor artifacts, connection loss, and poor calibration. Incorrect insulin/glucagon bolus administration may result from inaccurate sensor data when the patient is not supervising the system. In animal experiments, the situation may be further complicated as the pigs tend to play with the sensor and apply pressure.

To address this challenge, multiple sensors were mounted on the subjects (pigs) in the experiments to ensure correct measurements. A sensor fusion method then needed to be developed to automate the merging of data from multiple sensors and detect faults.

In this paper, we introduce and derive a Multi-Model Kalman Filter with Forgetting Factor (MMKFF) for fusing information from redundant subcutaneous glucose sensors. To evaluate its performance, we compared the MMKFF against other Kalman Filter (KF) strategies using experimental data from two different animals. The results demonstrate that the developed MMKFF provides a reliable fused glucose reading. Moreover, compared to the other KF approaches, the MMKFF exhibits superior adaptability to changes in the accuracy of the glucose sensors.

**Paper 6 Title: “*Fully Automated Bi-Hormonal Intra-peritoneal Artificial Pancreas Using a Two-Layer PID Control Scheme*”**

In the literature, MPC methods are widely utilized for AP systems, e.g., Control IQ. These methods are associated with computational challenges, the need for precise models, and estimators. As we are exploring the use of dual-hormone injections via the IP route, we tested the performance of PID controllers and assessed if they can deliver comparable results to the

MPC methods. For our study, we employed the meta-model presented in **Paper 2** as a simulator.

In this work, a bi-hormonal AP with IP infusions is designed to increase the time within the range of 3.9–10.0 mmol/l and alleviate the burden of meal announcements. A two-layer controller is designed to provide safe and effective insulin and glucagon delivery. The primary layer is based on classical PID controllers for insulin and glucagon, and the supervisory layer includes four parts: (A) Zone-based control settings, (B) Extrapolation of sensor data to compensate for sensor delay in SC tissue, (C) Auto-tuning of the PID parameters in the primary layer, and (D) Safety barriers. The controller is designed to prevent hypoglycemia after meals and during physical activity, as well as prevent postprandial hyperglycemia.

The results indicated that the designed PID controller effectively maintained the blood glucose levels within the acceptable range without the need for meal announcements. Moreover, the proposed method demonstrated significantly lower computational requirements compared to MPC methods.

**Paper 7** Title: *“Optimal Experimental Design to Estimate Insulin Response in Type 2 Diabetes”*

The quality of glycemic control is directly linked to the accuracy of the model and parameter identification. To ensure practical parameter identification, the collected data must be sufficiently rich and capable of exciting the necessary dynamics during the identification period. Moreover, the identification period should be carefully planned to maintain safe blood glucose levels for the patient.

This paper proposes an optimal experimental design for selecting the size of three meals and the hourly fast-acting insulin infusion rate over 24 hours. The designed experiment maximizes the sensitivity of blood glucose levels to the parameters of the Type 2 diabetes (T2D) model in [3], while also ensuring safety considerations. The results indicate that this optimal experimental design has the potential to enhance model-based algorithms and can serve as a qualitative tool when planning clinical experiments.

The collaboration between NTNU and the Technical University of Denmark (DTU) resulted in this paper. Sarah Ellinor Engell, who specializes in Type 2 diabetes (T2D) and optimal experimental design, visited us between January and March 2023. We are continuing our collaboration

with DTU to apply the same method to the meta-model presented in **Paper 2** and to patients with Type 1 diabetes.

**Paper 8** Title: “*A Dual-hormone Predictive Controller Framework for Fully Automated Intra-peritoneal Artificial Pancreas*”






The main contribution of this thesis is presented in this paper, where a dual-hormone predictive control (DHPC) framework is proposed for a fully automated artificial pancreas. The DHPC utilizes the proposed meta-model in **Paper2** and the DIP-MHE designed in **Paper4** to control the BGL without the need for meal announcements and with IP insulin and glucagon infusions.

A predictive control approach was designed and tested in animal experiments, involving six anesthetized pigs for 12-24 hours and an awake pig for five days. The proposed method achieved 73.1–94.2% time-in-range (TIR), surpassing the reported average TIR of commercially available SC hybrid closed-loop systems such as Medtronic MiniMed 670G (70%), Tandem t slim X2 with Control-IQ (72%), Omnipod 5 with Horizon (70%), and Diabeloop G7 (74% TIR).

























































The findings demonstrate the promise of the dual-hormone AP utilizing IP hormone delivery in terms of feasibility, safety, and superior fully automated BGL control. However, the paper also addresses the challenges and complexities associated with implementing the dual-hormone IP artificial pancreas system from the ground up. These challenges encompass BGL measurement, estimation, prediction, and surgical considerations in practical applications.

### 1.5 THE AUTHOR’S INDIVIDUAL CONTRIBUTIONS IN CO-AUTHORSHIPS

**TABLE 1.1.** Contributions to Papers 1–8.

Scale:	
	Has essentially done all the work independently (90–100%)
	Has done most of the work (70–90%)
	Has contributed considerably (40–60%)
	Has contributed to the collaboration (10–30%)
	No or little contribution (0–10%)

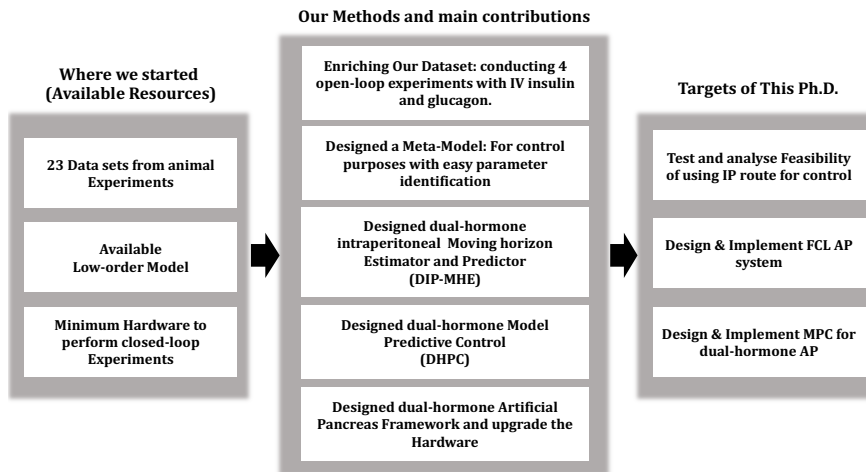
Contribution to Paper:	1	2	3	4	5	6	7	8
Identification of the scientific problem and Proposing the Topic								
Planning of experiments, data collection or literature review								
Design, development and implementation of methodology								
Preparation of the scenarios in the experiments/in the simulations								
Interpretation of results and preparation of the Figures								
preparation and writing of the first draft of the manuscript								
Finalization of the manuscript and submission								

### 1.6 RESEARCH MAP

In summary, the targets, approaches, and the initially available resources of this research are illustrated in [Figure 1.1](#). The main targets of the project were to analyze the feasibility of using the IP route to achieve a fully closed-loop artificial pancreas, design an AP, and test it in animal experiments. The available resources were rich data from the open-loop animal experiments, and the developed low-order model [1] in our research group.

To achieve the defined targets, we enriched our data set by conducting four

**FIGURE 1.1.** Summary and the Research Map of this work; AP, artificial pancreas; IP, intraperitoneal; IV, intravenous; FCL, fully closed loop; MPC, model predictive control.



new experiments involving intravenous insulin and glucagon infusions. These experiments were designed to study the pharmacokinetics of the hormones in pigs with different body weights, aiming to understand the effect of body weight on the parameters of the model. Moreover, a wide range of IP insulin and glucagon boluses were given to capture the impact of the hepatic first-pass effect.

Based on the findings from the new data set, we developed the model presented in **Paper2**, which facilitated easy parameter identification. Subsequently, in **Paper4**, an estimator was designed to estimate the glucose appearance rate in blood and the states of the proposed model. Utilizing the model and estimator, we then created a dual-hormone predictive controller (**Paper 8**) to regulate blood glucose levels in animal experiments.

Finally, we designed and implemented a dual-hormone artificial pancreas framework in Matlab to conduct the animal experiments. The block diagram of the implemented dual-hormone artificial pancreas, along with a summary of the scope of the papers, is illustrated in [Figure 1.2](#).



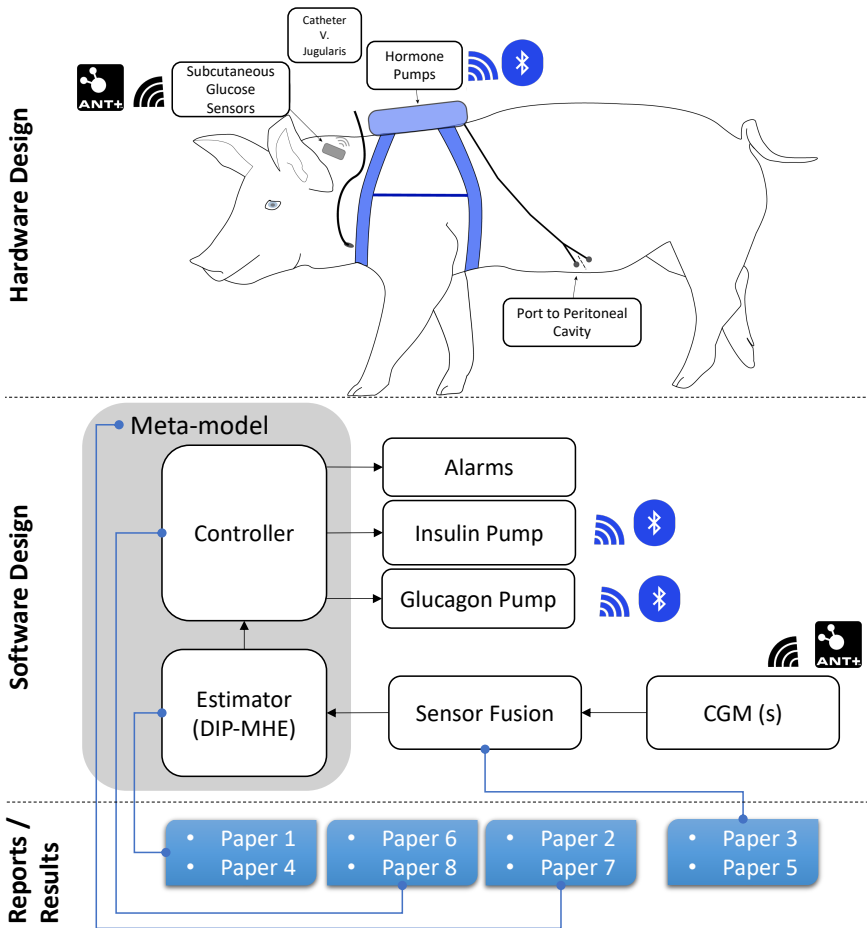


**FIGURE 1.2.** A schematic representation of the proposed scheme for the dual-hormone in-traperitoneal artificial pancreas, tested in animal experiments. The published papers and their respective scopes are visually depicted in blue boxes at the bottom.

## 1.7 REFERENCES

- [1] C. Lopez-Zazueta, Ø. Stavadahl, and A. L. Fougner, “Low-order nonlinear animal model of glucose dynamics for a bihormonal intraperitoneal artificial pancreas,” *IEEE Transactions on Biomedical Engineering*, vol. 69, no. 3, pp. 1273–1280, 2021. Cited on page/s 5, 10.
- [2] C. Toffanin, L. Magni, and C. Cobelli, “Artificial pancreas: in silico study shows no need of meal announcement and improved time in range of glucose with intraperitoneal vs. subcutaneous insulin delivery,” *IEEE Transactions on Medical Robotics and Bionics*, vol. 3, no. 2, pp. 306–314, 2021. Cited on page/s 5.
- [3] T. B. Aradóttir, D. Boiroux, H. Bengtsson, J. Kildegaard, B. V. Orden, and J. B. Jørgensen, “Model for simulating fasting glucose in type 2 diabetes and the effect of adherence to treatment,” *IFAC-PapersOnLine*, vol. 50, no. 1, pp. 15 086–15 091, 2017. Cited on page/s 8.



Part I

**INTRODUCTION,  
BACKGROUND, AND  
DISCUSSIONS**



## CHAPTER 2

### Introduction

---

*The aim of this chapter is to provide an introduction to T1DM and AP systems, as well as present the current state of knowledge regarding the control of BGL through exogenous insulin and glucagon. In addition, this chapter presents the "story" of the presented research in this thesis.*

#### 2.1 BACKGROUND AND MOTIVATION

##### 2.1.1 Diabetes Mellitus

The term "Diabetes Mellitus" has its origins in the Greek word *diabetes*, which translates to "siphon" or "to pass through," and the Latin word *mellitus*, which means "sweet." The civilizations of Ancient Greece, India, and Egypt recognized the sweetness of urine in individuals with similar symptoms, which led to the development of the term *diabetes mellitus* [1].

Diabetes mellitus is a type of disease that disrupts the metabolic balance controlled by insulin, leading to uncontrolled BGL. Type 1 diabetes mellitus (T1DM), also known as juvenile-onset diabetes mellitus or insulin-dependent diabetes mellitus, is caused by a complete lack of insulin due to the loss of insulin-producing beta cells in the pancreas [2]. The occurrence and frequency of type 1 diabetes vary considerably across the world (as shown in [Figure 2.1](#)). Finland has the highest incidence rates of type 1 diabetes, with over 60 cases per 100,000 people each year [3].

Type 1 diabetes has been on the rise worldwide for many decades, with reported annual increases in Finland, Germany, and Norway of 2.4%, 2.6%, and 3.3%, respectively. The incidence rates of type 1 diabetes have fluctuated in various countries, although Sweden has observed a plateau in recent years [3, 4]. The Nordic countries and North America exhibit a greater prevalence of T1DM cases, potentially attributed to the more advanced healthcare systems and enhanced accessibility to diagnoses in these regions.

Administering external insulin is the primary approach to control type 1 diabetes. The utilization of recombinant insulin analogs, insulin pumps, and

advanced monitoring devices has significantly enhanced glucose regulation in patients with this condition. Despite these advancements, existing therapies do not emulate the precise feedback control of insulin secretion observed in healthy individuals, which can result in sustained hyperglycemia in nearly all diabetes patients. Consequently, this can lead to severe long-term complications such as cardiovascular disease, neuropathy, retinopathy, and renal failure [2].

On the opposite end of the glucose spectrum, when BGL falls below 3.9 mmol/l, hypoglycemia may lead to convulsions, coma, or even death. Some patients are consistently anxious about hyperglycemia or the possibility of sudden hypoglycemia. These concerns, in addition to other disease-related burdens, result in three times the rate of depression among individuals with type 1 diabetes. In addition, T1DM issues can cause people to drop out of employment and thus also have an increased risk of financial and psychological problems.

The economic impact of diabetes in society is significant, with the cost of treating a diabetic individual being twice that of a non-diabetic individual. In Western countries, the cost is 560 billion euros per year or 2,600 € per patient annually [5, 6]. Hence, any automated system designed to manage BGL, thereby minimizing the need for patient intervention, is beneficial for both individuals and society.

The following section explores glucose metabolism and potential treatment options.

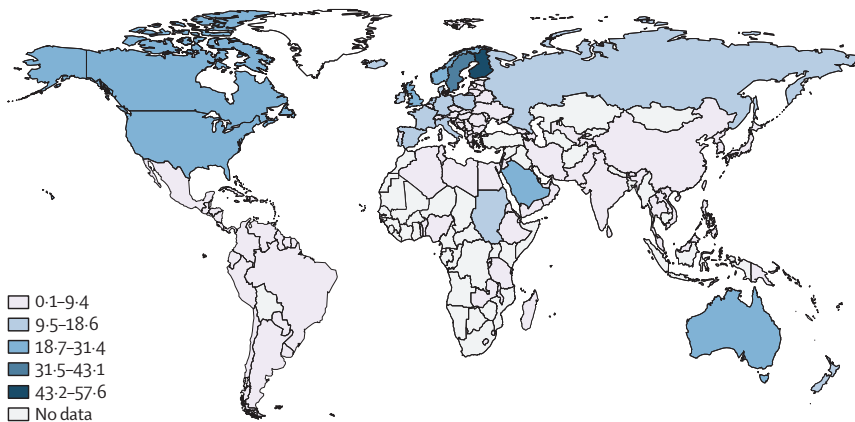


**FIGURE 2.1.** The estimated global incidence of type 1 diabetes, by region [3] (Copyright order number: 1357000 on [marketplace.copyright.com](http://marketplace.copyright.com)).

### 2.1.2 Glucose Metabolism

Glucose serves as a vital energy source for the body, particularly for certain cell types such as nervous tissue and red blood cells [7]. In healthy individuals who are fasting, BGL typically remains within the range of 3.5 to 5.5 mmol/L [8], while after a meal, it seldom increases beyond 7.8 mmol/L and returns to its pre-meal level within 2-3 hours [7]. The liver plays a significant role in glucose regulation, as it can switch between storing glucose and producing and releasing glucose depending on the glucose demands of the body [9].

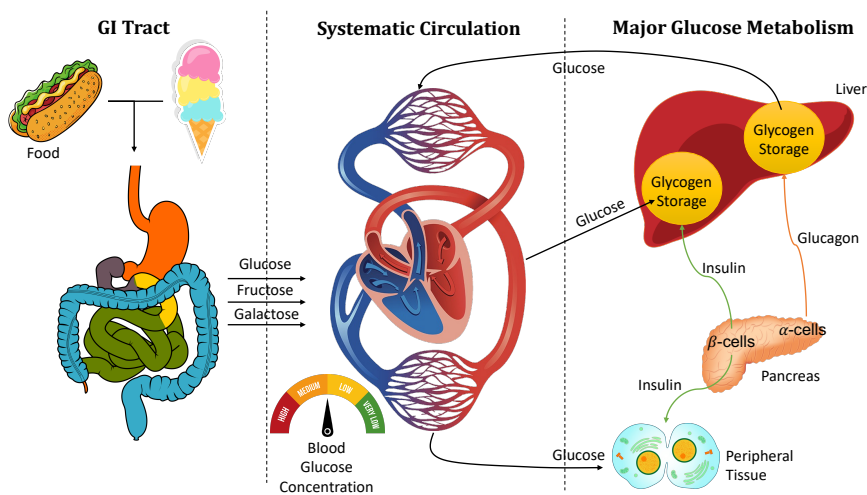


**FIGURE 2.2.** Simplified overview of glucose regulation system in healthy individuals; GI, gastrointestinal.

As shown in [Figure 2.2](#), eating carbohydrates causes an increase in BGL. Glucose can be detected by sensors in the taste buds on the tongue. Signals are sent to the central nervous system when glucose is absorbed from the intestines, and incretin hormones are released by enteroendocrine cells in response to glucose uptake [7]. Insulin is then released from the pancreatic  $\beta$ -cells due to direct stimulation by high BGL.

Postprandial insulin is secreted in a pulsive pattern, and insulin is transported into the hepatocytes to be converted into glycogen for storage. Insulin also activates the uptake of glucose by adipose tissue and muscle cells. In healthy individuals, both insulin and BGL return to their pre-meal level within 2-3 hours [7, 10, 11].

Insulin is the primary hormone that lowers BGL directly by allowing the organs to store or utilize the glucose. It also indirectly regulates BGL by inhibiting glucagon secretion, suppressing hepatic gluconeogenesis, and slowing the rate



of gastric emptying through the secretion of amylin in the  $\beta$ -cells [7, 12, 13].

Maintaining normal BGL is crucial for the proper function of many cells, particularly in the central nervous system (CNS). The CNS consumes a significant amount of glucose, and glucose uptake by CNS cells is primarily facilitated by insulin-independent glucose transporters [7]. When BGL drop, the brainstem and hypothalamus activate several physiological responses, including the sympathetic and parasympathetic nervous systems and the release of epinephrine from the adrenal glands. These pathways stimulate glucagon release by pancreatic  $\alpha$ -cells and glucose production by the liver to prevent hypoglycemia [14, 15].

Glucagon is a hormone that is released by the  $\alpha$ -cells into the pancreatic vein and transported directly to the liver, where glucagon receptors are primarily located. Glucagon triggers the production of glucose in the liver through the processes of glycogenolysis and gluconeogenesis. The liver produces the majority of the endogenous glucose in the fasting state by breaking down the stored glycogen, while the kidneys contribute a smaller amount [7]. Glucagon is primarily eliminated by the kidneys [16].

### 2.1.3 Possible Treatments for Type 1 Diabetes

As mentioned, the pancreas in T1DM patients produces no or little insulin. With the current progress in technology and science, two feasible treatments are pancreas transplant and external insulin therapy.

For certain patients, particularly those experiencing end-stage diabetic kidney disease, a pancreas transplant can be a viable treatment. The reason is that when they need a kidney transplant, a donor, and immunosuppressants, they can transplant the pancreas at the same time without much extra burden or risk.

This procedure can alleviate diabetic symptoms, however, the human pancreas is scarce, and immunosuppressive drugs can cause severe side effects. Norway has conducted around 25 pancreas transplants per year since 2011, with a total of 91 treated patients between 2001 and 2017. This treatment is still considered an experimental method in the United States [7].

In external insulin therapy, patients must administer insulin based on their needs. This involves measuring their BGL and infusing external insulin accordingly to regulate the BGL. With the currently developed technology, this procedure is relatively automated by using BGL sensors and insulin pumps. The automated system is called the artificial pancreas (AP).

### 2.1.4 Artificial Pancreas

As shown in Figure 2.3, the AP system utilizes a BGL sensor, an insulin pump, and a control algorithm to automatically regulate the BGL by injecting insulin. A dual-hormonal AP can deliver glucagon in addition to insulin to reduce the risk of hypoglycemia. At present, APs are developed to deliver insulin into subcutaneous (SC) tissues and use SC BGL sensors to measure BGL. The disadvantage of this method is the slow insulin absorption and its slow dynamics, which makes it challenging to achieve precise BGL control, particularly with unanticipated meals [17]. Therefore, in the commercially available single-hormone AP systems, the meals are announced to the controller before/during meal consumption.

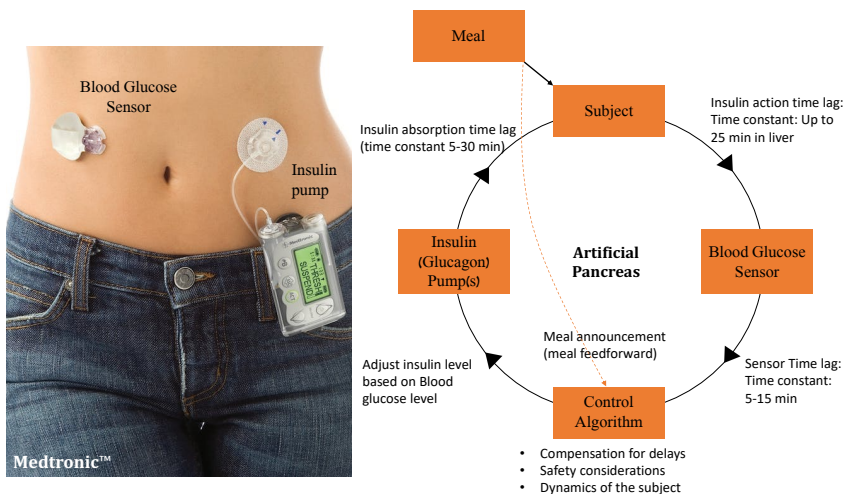


**FIGURE 2.3.** Basic concept of a hybrid closed-loop (HCL) system for type 1 diabetes therapy - artificial pancreas (AP). In HCL systems, an estimated size of the meals is announced to the controller before eating. The picture on the left is from [3] (Copyright order number: 1357000 on [marketplace.copyright.com](https://marketplace.copyright.com))

### 2.1.5 Insulin Injection Routes

Three main routes can be used to infuse insulin continuously into the body; The intravenous (IV) route, subcutaneous (SC) route, and intraperitoneal (IP) route.

When insulin is delivered via the IV route, as shown in Figure 2.4, it is distributed throughout the body by blood circulation. Despite the quickness and reliability of the IV route, blood clots and catheter-related problems make

it unsuitable for continuous insulin infusions. The SC route is safer and less invasive than the IV route [18]. Therefore, continuous subcutaneous insulin infusion (CSII) has become a widely used solution since the 1990s.

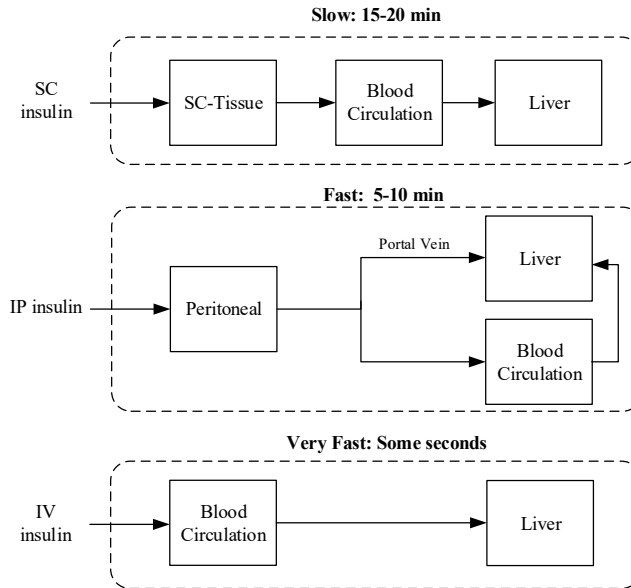


**FIGURE 2.4.** Comparison of the time delays and pharmacokinetics block diagram of the SC, IP, and IV insulin administration (the figure is from **Paper 2** - reuse of the figure is unrestricted).

Due to the intrinsic delay in the SC route and the slow dynamics of insulin absorption, no matter how advanced the control algorithms are, there is always a trade-off between the performance of the controllers and the risk of hypoglycemia episodes. The slow dynamics and delay can cause oscillations, especially if the control algorithm is aggressive (high gain). It requires precise control tuning to achieve a fully automated AP without meal announcements. Therefore, in commercially available single-hormonal APs, the carbohydrate content of each meal must be estimated and announced to the AP ahead of time [19]. However, it is challenging for some patients to remember meal announcements during the day or estimate the size of their meals.

In addition, a CSII delivers insulin to the entire body in equal concentrations, whereas the primary target organ of insulin is the liver. Under normal conditions, insulin is secreted from the pancreas and transported directly to the liver via the portal vein (PV). The insulin concentration is consequently much

higher in the liver than in the rest of the body. However, the non-physiological nature of CSII leads to a high concentration of insulin in peripheral tissues, which impacts the BGL control quality.

An alternative and feasible approach for delivering drugs to the liver is to deposit the drug into the peritoneal cavity [20–22]. As shown in Figure 2.5, the peritoneal cavity is a space within the abdomen enclosed by the peritoneal lining. It is lubricated by a small volume of peritoneal fluid that facilitates movements of the abdominal organs [23]. Although the peritoneal cavity is small in volume, it has a large surface area with many surrounding blood vessels within the lining. These vessels together with the blood vessels from the intestines, drain into the liver via the portal vein (PV). Therefore, the drugs in the peritoneal cavity will reach to the liver by diffusing into the PV. Drug injections via this route are called IP injections.

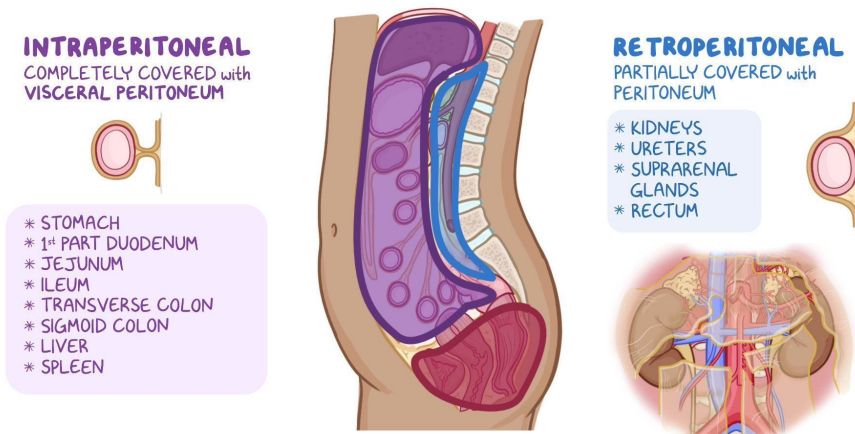


**FIGURE 2.5.** Human peritoneal cavity and the organs included in that area. The figure is taken directly from [24].

In addition to mimicking normal pancreatic function with IP injections, this route has significant control benefits, such as faster insulin appearance in the blood due to a higher absorption rate and also faster insulin disappearance rate due to the hepatic first-pass (HFP) effect [25]. The current challenges and solutions of using the IP route are discussed in [19].

## 2.2 DEVELOPMENT OF THE ARTIFICIAL PANCREAS SYSTEM

To design a practical AP system, it is necessary to have at least three components/modules:

- A real-time blood glucose monitoring (CGM) device,
- One insulin pump (two pumps for dual-hormone APs),
- A control algorithm to estimate the required amount of insulin (and glucagon for dual-hormone APs).

Although the idea of developing an AP system was conceived after the invention of insulin in the 1920s, it required significant advancements in CGM systems before it could be tested in real-life situations. The key inventions and events in the development of AP components are visually represented in [Figure 2.6](#) and the timeline of the important studies is presented in [Figure 2.7](#).

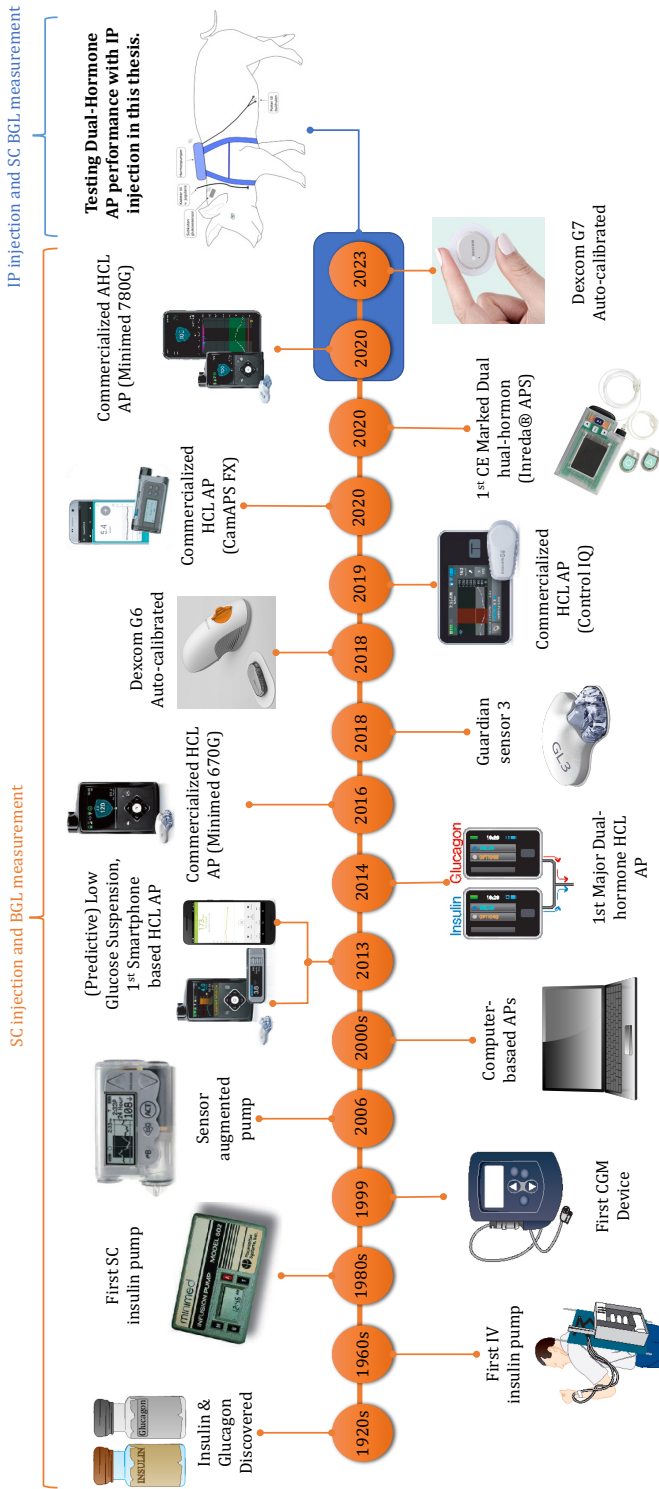
The first closed-loop system using the CGM devices was tested in the early 2000s [26], where the control algorithms were running on computers [27–29]. The next development was implementing the controllers in the pumps themselves or in the smartphones.

The development and improvement of various types of AP systems have been ongoing since the mid-2010s. [Figure 2.8](#) depicts the different categories of the AP systems. The initial step towards automating BGL control involved the use of sensor-augmented pumps (SAP), which were limited to providing only basal insulin with a binary on/off function. The SAP systems could halt insulin delivery when the BGL reached a low threshold. In subsequent developments, the SAP systems could anticipate hypoglycemia and suspend basal insulin administration in advance [30–32].

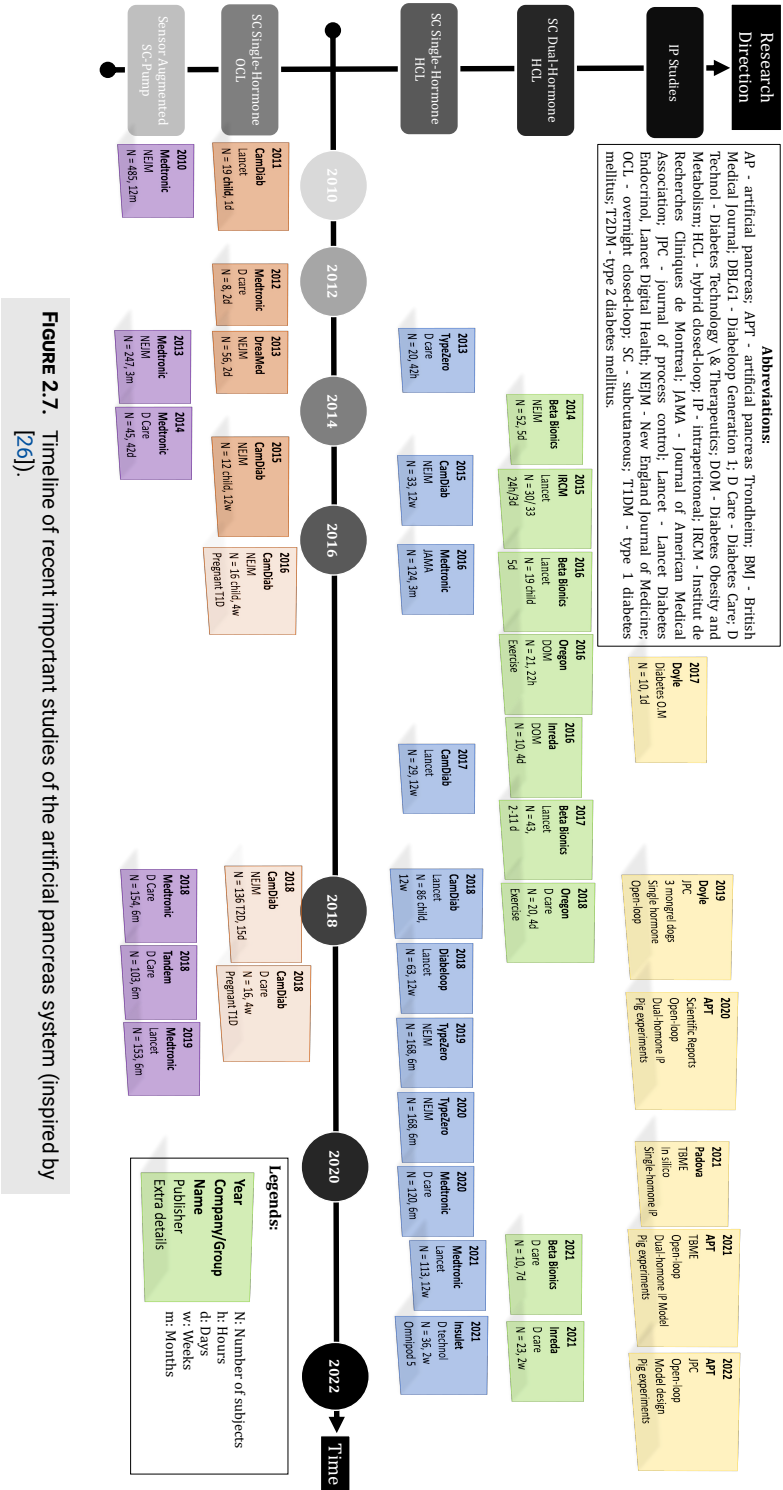
The initial automated closed-loop system was called the overnight closed-loop (OCL) system, as it regulated BGL during the fasting period while the user slept at night. The controller designed for OCL systems was relatively straightforward [26]. The subsequent generation of AP systems was the hybrid closed-loop (HCL) systems, in which the user would initiate the meal-insulin bolus before eating, and the controller would only regulate the basal insulin infusion. Subsequently, advanced hybrid closed-loop (AHCL) systems were developed that could automatically administer insulin correction boluses after the user initiated the insulin meal-boluses [29, 33–38].

Hybrid closed-loop (HCL) systems have been commercially available since the late 2010s. Meanwhile, dual-hormone closed-loop (DHCL) AP systems have also been tested in short-term studies since the mid-2010s [39–41].

Although the studies demonstrated the better safety margin of the DHCL over single-hormone APs, they have not been extensively investigated in practical settings due to the complexities of the DHCL controllers, technical limitations, and associated costs [18, 26]. In 2020, Inreda<sup>®</sup> Diabetic (Goor, the Netherlands) received the CE mark for their DHPC AP system which administers insulin and glucagon into SC tissue. Their AP system is claimed to



**FIGURE 2.6.** The progress and advancements of the components necessary for the artificial pancreas (inspired by [26]); SC, subcutaneous; IP, intraperitoneal; AP, artificial pancreas; APS, artificial pancreas system; BGL, BGL; HCL, hybrid closed-loop; FCL, fully closed-loop.



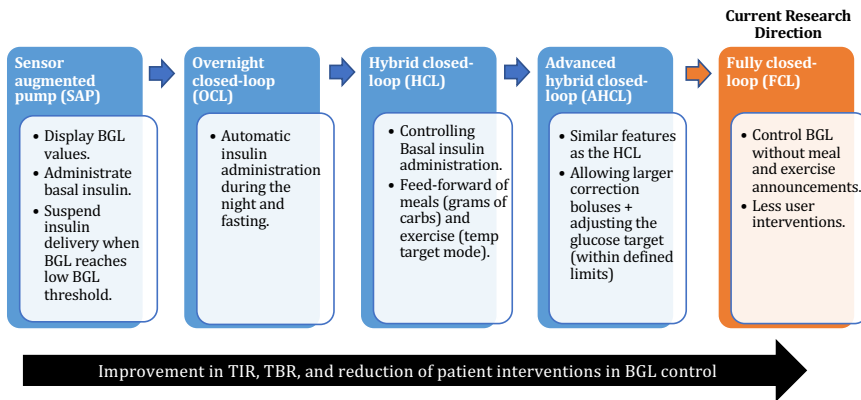


**FIGURE 2.8.** Different categories of the developed APs since today and their key features [26, 29, 33–38]; TIR, time in range; TBR, time below range.

achieve 86% time in range (TIR) of [3.9, 10] mmol/l with a fully closed-loop (FCL) controller.

The desired generation of APs under development is the FCL systems, which decrease user interventions and increase the time spent in auto-mode. To this end, new studies are being done to overcome the limitations of SC-insulin-based APs. For example, Peptide hormones, such as amylin analogs and agonists of the glucagon-like peptide 1 (GLP-1) receptor (GLP-1R), have been studied as well as the development of intraperitoneal (IP) insulin delivery systems [42–44].

## 2.3 RESEARCH GROUPS AND THEIR DESIGNED CONTROL SYSTEMS

### 2.3.1 Subcutaneous Artificial Pancreas systems

As previously stated, the current research direction is to create an FCL system, and multiple groups have devised different techniques to achieve this goal. The present advancements in this direction involve utilizing dual-hormone APs or employing more sophisticated control algorithms. Numerous groups are working on developing AP systems. However, a few of them develop successful products and test them in realistic situations. Table 2.1 categorizes the major companies in the field. Among them are companies such as CamDiab (Cambridge, UK), DreaMed (Petah Tikva, Israel), Medtronic (Minneapolis, MN, USA), TypeZero Technology (Charlottesville, VA, USA), Diabeloop in France, and the Insulet Group (USA), which are developing single hormonal APs/pumps with SC insulin injections [26, 33, 36, 45–49].



**TABLE 2.1.** Important research groups and companies developing artificial pancreas systems. MPC, model predictive control; PID, proportional integral derivative control; DBLHU, Diabeloop for highly unstable diabetes; IRCM, Institut de Recherches Cliniques de Montreal; PD, proportional derivative control; IRCM, Institut de Recherches Cliniques de Montreal; ALPHA, adaptive learning postprandial hypoglycemia prevention algorithm; AP, artificial pancreas; APT, artificial pancreas Trondheim; FMPD, fading memory proportional derivative control [26].

Subcutaneous Single Hormone Closed-Loop Systems		
Group/Company	Controller	Product name
CamDiab	MPC	CamAPS FX
DreamMed	MDlogic: PID with Fuzzy Logic	GlucoSetter, AdvisorPro
Medtronic	MDlogic with basal insulin, with correction boluses	Minimed 670G, and 780G
Dexcom/TypeZero	MPC (Contro IQ)	Dexcom, Tandem t:slim pump
Diabeloop	MPC	DBLHU
Insulet	MPC	Omnipod 5
Beta Bionics	PID	Single-hormonal iLet

Subcutaneous Dual-Hormone Closed-Loop Systems		
Group/Company	Controller (Insulin + Glucagon)	Product name
Beta Bionics	MPC + PD	Bihormonal iLet
Inreda®	PID-like controllers	Inreda® Diabetic AP
IRCM	MPC + Logic-based	None
Oregon	FMPD + ALPHA	None

Intraperitoneal Single Hormone Closed-Loop Systems		
Group	Controller	Detail
Montpellier (2009)	PID	8 Adults (Implantable Pump)
Doyle (2017)	MPC	10 Adults
Doyle (2019)	PID	3 Open-loop mongrel dogs
Padova (2021)	MPC	Simulator

Intraperitoneal Dual-Hormone Closed-Loop Systems		
Group	Controller (Insulin + Glucagon)	Detail
APT (This Study)	Dual-hormone MPC (DHPC)	Tested in Pigs

Some groups enabled their AP systems to administrate glucagon in addition to insulin to prevent hypoglycemia. The increased safety of dual-hormone AP systems compared to single-hormone APs allows for more aggressive control and an increase in TIR, even without meal announcements. Beta Bionics (Irvine, CA, USA), Inreda® Diabetic (Goor, the Netherlands), Institut de Recherches Cliniques de Montreal (Montreal, QC, Canada), and Oregon Health and Science University (Portland, OR, USA) are at the forefront of developing and testing dual-hormone APs [50–53].

### 2.3.2 Interperitoneal Artificial Pancreas systems

Several groups are trying to exploit the benefits of the IP pathway for AP systems. Two approaches are:

- Implantable Pumps.
- External pump with an established port to the peritoneal cavity.

The commercialized MiniMed implantable pump (MIP 2007D) from Medtronic (Northridge, USA) and the DiaPort system by Roche (Second Generation, Roche Diagnostics, Mannheim, Germany) are examples of the systems or equipment used in the intraperitoneal insulin infusions. The mechanism of the two approaches is illustrated in Figure 2.9.

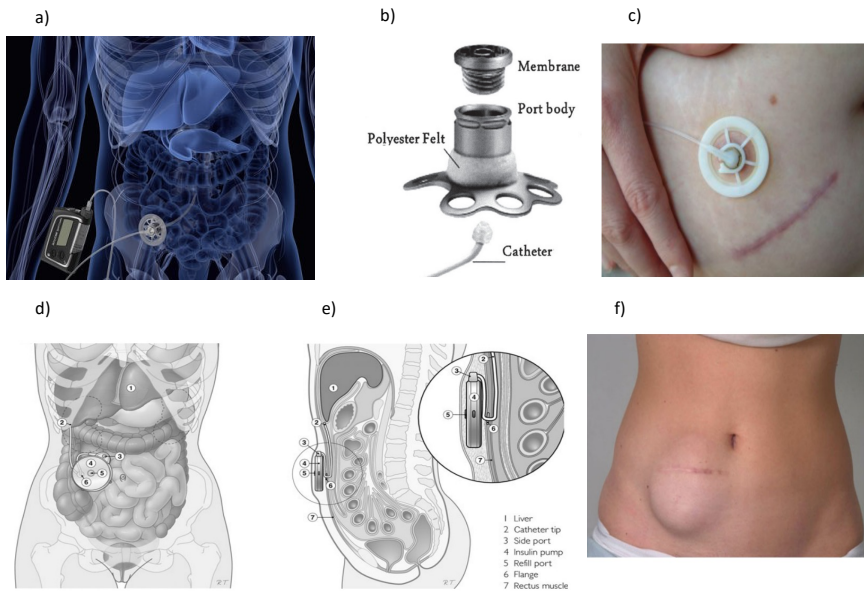


**FIGURE 2.9.** Panels a, b, and c illustrate the concept, mechanism, and implanted DiaPort system, respectively. In this mechanism, the insulin is administered via an external pump to the peritoneal cavity. The pictures are from [54, 55] (copyright IEEE © 2018). Panels d and e show where MMT2007D is located and implanted in the body. Panel f illustrates the implanted MMT2007D in patients. The panels d, e, and f are adapted from [56] (Copyright order number: 1357019 on marketplace.copyright.com).

Invasiveness, infections, occlusions, and the complexity of refilling the reservoir in implantable pumps have hindered their development and testing. As illustrated in Figure 2.10, Iacovacci *et al.* [57] have devised a mechanism for refilling the reservoirs in implantable APs. However, the product has not been launched yet. With the current technologies and developments and without having to implant a pump, more studies are being done using the DiaPort or other custom ports and catheters.

Dassau *et al.* [44] from Doyle group, used IP insulin administration to achieve FCL performance in 10 adults. The results suggested that with IP

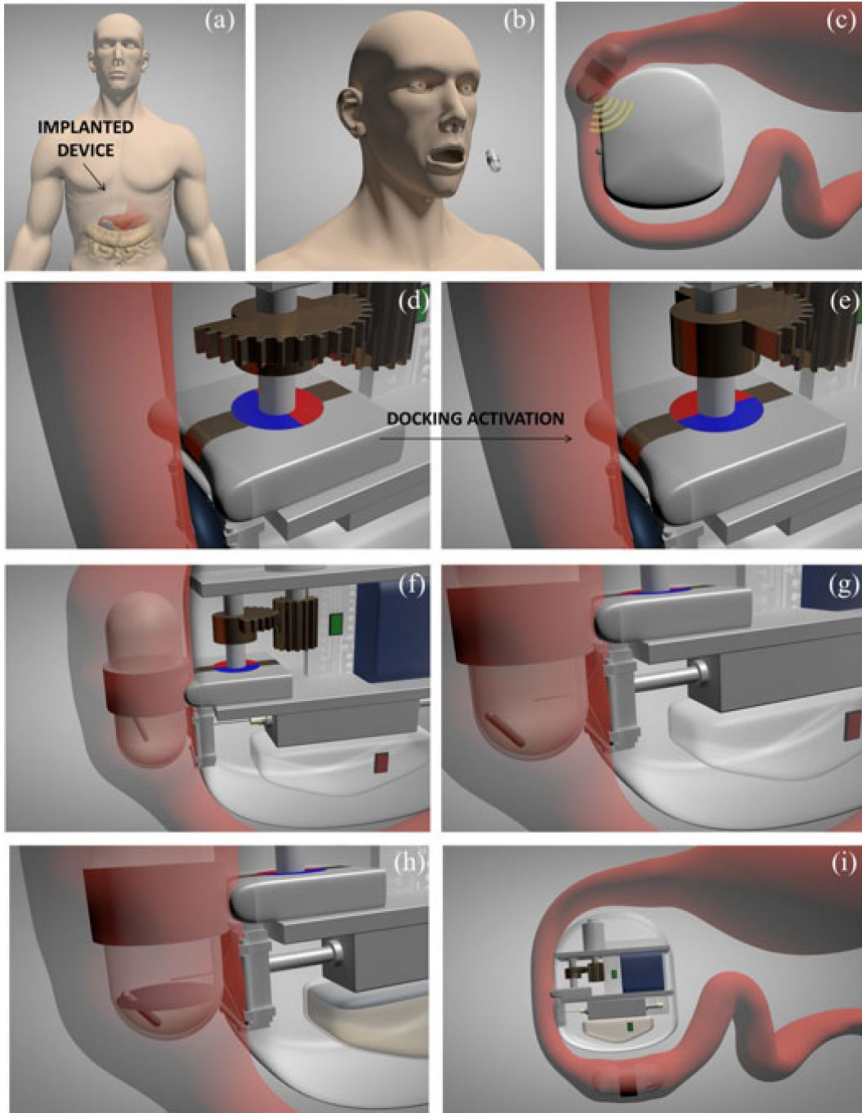


**FIGURE 2.10.** The sequence of the introduced mechanism to refill the insulin reservoir of the implantable artificial pancreas in [57]: (a) the device is implanted in a suitable location. (b) The patient ingests the insulin pill. (c) Once the capsule reaches a certain distance from the implant site, the device becomes detectable. The docking system transitions from its resting configuration (d) to its activated configuration (e) to enable capsule docking. (f) The capsule is attracted and securely docked. (g) A linearly actuated needle pierces the capsule. (h) The insulin inside the pill is extracted and transferred to a dedicated reservoir. (i) The capsule is undocked and naturally eliminated. The figures are reused from [57] copyright IEEE © 2015.

insulin there is no need for meal announcement compared to SC infusions. In addition, Chakrabarty *et al.* [17] performed open-loop IP insulin experiments on adult mongrel dogs to collect data and construct a model and controller for the IP insulin route. This model and controller were subsequently tested on a modified version of the UVA/Padova simulator [19].

## 2.4 STORY OF THE PRESENTED RESEARCH

The primary objective of the research team, known as Artificial Pancreas Trondheim (APT), revolves around reducing patient interventions required for controlling BGL while also eliminating the necessity of manually informing the AP systems about meal consumption. To achieve these goals, our approach commenced with the use of the IP route to enhance insulin absorption rates. Additionally, we included glucagon to increase safety margins and minimize the risk of hypoglycemia.

As depicted in [Figure 1.1](#), our work began in January 2020, and at that point, we possessed data from animal experiments. These experiments involved the administration of insulin and glucagon via the IP route, alongside the measurement of glucose, insulin, and glucagon levels in the bloodstream. Furthermore, a model had been previously developed by one of our former Postdoctoral researchers, as outlined in [58].

It's worth emphasizing that during this initial phase, our access to hardware was quite limited, and the available equipment had originally been designed for open-loop experiments. Moreover, the pumps in use were solely capable of manual operation. In order to integrate them into a closed-loop system, an equipment upgrade was imperative.

Our first step was to choose a control structure based on the available source.

### 2.4.1 Step1; Choosing the Control Strategy

When it comes to control systems, selecting the right controller is paramount to achieving desired performance, stability, and efficiency. While PID controllers have been the traditional go-to choice for many industrial applications, MPC has emerged as a powerful alternative in AP systems. For the following reasons we chose to use an MPC-based controller:

### **Predictive Capability**

As the name suggests, MPC is predictive in nature. It doesn't just react to current system conditions; it anticipates future states and optimizes control actions accordingly. This predictive capability allows MPC to better handle AP systems with significant delays, disturbances, or varying dynamics, where PID controllers may struggle to adapt quickly

### **Complexity of the AP Systems**

One of the most significant advantages of MPC is its ability to handle complex, nonlinear systems. MPC can work with intricate mathematical models of a system, making it suitable for our dual-hormone AP system.

### **Optimization is required**

MPC controllers solve an optimization problem at each control step. This means MPC can find the best control input while satisfying constraints and objectives, such as minimizing hormone consumption or maintaining the desired BGL range. In contrast, PID controllers rely on predefined parameters, making them less adaptable to changing conditions.

### **Multivariable System**

A dual-hormone AP is a multivariable system. MPC handles multivariable systems with ease, as it considers the interactions between variables, optimizing control actions across the entire system. PID controllers, when used in multivariable applications, can result in complex tuning.

### **Robustness**

The model-based controllers require an estimator to estimate the states and disturbances (e.g. glycogen storage level, meals, physical activities, insulin concentration of the blood, ...) that are not measurable. This extra information embeds more information to the controller than just feedback from BGL sensors. Therefore, an MPC with a reasonably tuned model is inherently robust to disturbances and uncertainties.

MPC continually recalculates control actions based on updated measurements, estimates, and predictions, ensuring the BGL stays on track even in challenging conditions. PID controllers may require additional tuning or the addition of advanced control strategies (such as complex feed-forward and structure design) to achieve similar robustness.

**TABLE 2.2.** Comparing features of advanced structures for PID with MPC methods in AP systems.

Feature	Advanced PID structures	MPC
Model-based	No	Yes
Predictive	No	Yes
Optimization	No	Yes
Handling constraints	Limited	Good
Adaptability to model changes	Limited	Good
Multivariable systems	Limited	Good
Robustness to disturbances	Limited	Good
Computational complexity	Low	High
<b>Complexity of Implementation</b>	<b>complex</b>	<b>Extremely Complex</b>
<b>Range of operation (due to nonlinearities)</b>	<b>Limited Range</b>	<b>Wide Range</b>
<b>Possibility of using clinicians' knowledge in tuning the controller</b>	<b>Low</b>	<b>High</b>
<b>Possibility of using the tuned controller in simulation in the real system</b>	<b>Low</b>	<b>High</b>
<b>Complexity of fine-tuning while in the experiments for the control designer</b>	<b>Very Complex</b>	<b>Complex</b>
<b>Complexity to understand and fine-tuning for non-technical people (e.g., patients and clinicians)</b>	<b>Extremely Complex</b>	<b>Complex</b>

#### 2.4.2 Step 2; Streamlining MPC Implementation: Bridging Complexity for Developers, Delivering Simplicity for Clinicians and Patients

In Table 2.2, a comprehensive feature comparison between PID and MPC structures is presented. When it comes to controller implementation, PID structures stand out as the preferred choice due to their simplicity in terms of model development and calculations. Nevertheless, it's crucial to emphasize that every controller requires tuning.

One noteworthy advantage of MPC methods lies in the meaningful nature of their tuning parameters, particularly the cost function. These parameters are designed to be intuitive and comprehensible, even for non-technical operators such as patients and clinicians. In stark contrast, the PID parameters can be considerably more challenging to grasp, lacking the straightforward interpretability found in MPC.

Patients and clinicians possess extensive experience in managing the BGL as an integral part of their daily routines. Conversely, many developers may not have the same level of firsthand insight. Therefore, MPC will unleash great potential for exploiting the clinicians' knowledge and:

- **Improve performance of the AP systems.**
- **Reduce the number of animal experiments.**
- **Maximize the duration of the closed-loop part of each animal experiment → Minimize the duration of the open-loop part.**
- **Pre-tune the controller on the simulator and then bring it to the real animal experiments.**
- **Fine-tune the controller “on the fly”**

The challenges associated with calculations and optimization become relatively manageable when we take into account the 5-minute sampling rate of the CGMs and the computing capabilities of the system we used in our animal experiments. When embedding this in an insulin pump, the computing capabilities and energy consumption will be a larger challenge, but we believe it will still be manageable. The primary hurdle in adopting MPC lies in designing a reliable model and addressing the complexities of parameter identification.

By addressing the complexity mentioned above and offering a reliable model that requires straightforward parameter identification, we can harness the advantages of MPC while ensuring ease of implementation.

### ***2.4.3 Step 3; Developing an Accurate Model with Simple or No Parameter Identification***

To expand the operating range of the low-order model [58], we integrate the observed effect of the hepatic first-pass effect into this model and improve some of the equations.

The availability of rich experimental data from 26 animal trials motivated the design of a technique (in **Paper 2**) to exploit this prior information to ensure the identifiability of our model. Through this technique, most parameters were either modeled as body weight functions or common among animals. The correlation between parameter values and body weight is discovered utilizing prior data from various animal experiments, such as blood glucose, plasma insulin, and glucagon levels, in which hormones were administered intraperitoneally or intravenously.

Through the application of this technique, the process of system identification is simplified for each new subject, all while retaining the crucial model intricacies that enhance predictive capabilities when compared to similar models.

#### 2.4.4 Step 4; Designing an Estimator

A fully automated artificial pancreas requires a meal estimator and predictions of blood glucose levels (BGL) to handle disturbances during meal times, all without relying on manual meal announcements and user interventions.

We designed a technique for estimating the glucose appearance rate (GAR) and predicting BGL using the developed model (in **Paper 4**). The estimator is designed based on the moving horizon estimation (MHE) approach, where the underlying cost function incorporates prior statistical information on the GAR in subjects over the course of a day. The animal experiments demonstrate the effectiveness and reliability of the proposed estimator and its potential for use in a fully automated artificial pancreas system.

#### 2.4.5 Step 5; Design a Model Predictive Controller and Perform Experiments

Once we completed the design of the model and estimator, the next step was to create a controller that could compute the necessary dosage of insulin or glucagon at each sampling interval. The formulation of the ultimate cost function for the dual-hormone predictive controller (DHPC) was achieved in **Paper 8**. This cost function was informed by practical insights gained from experiments and the collective experience of our team.

In our research group, we tested the performance of the designed AP using external pumps delivering insulin and glucagon to the peritoneal cavity through 2 Diaports (one for each hormone). The system performance was evaluated through a series of six experiments in anesthetized pigs and one experiment in an awake pig.



## 2.5 REFERENCES

- [1] A. Sapra and P. Bhandari, “Diabetes mellitus. 2021 sep 18,” *StatPearls [Internet]. Treasure Island (FL): StatPearls Publishing*, 2022. Cited on page/s 17.
- [2] D. W. Cooke and L. Plotnick, “Type 1 diabetes mellitus in pediatrics,” *pediatr Rev*, vol. 29, no. 11, pp. 374–84, 2008. Cited on page/s 17, 18.
- [3] M. A. Atkinson, G. S. Eisenbarth, and A. W. Michels, “Type 1 diabetes,” *The Lancet*, vol. 383, no. 9911, pp. 69–82, 2014. Cited on page/s 17, 18, 21.
- [4] M. Thunander, C. Petersson, K. Jonzon, J. Fornander, B. Ossiansson, C. Torn, S. Edvardsson, and M. Landin-Olsson, “Incidence of type 1 and type 2 diabetes in adults and children in kronoberg, sweden,” *Diabetes research and clinical practice*, vol. 82, no. 2, pp. 247–255, 2008. Cited on page/s 17.
- [5] T. Roy and C. E. Lloyd, “Epidemiology of depression and diabetes: a systematic review,” *Journal of affective disorders*, vol. 142, pp. S8–S21, 2012. Cited on page/s 18.
- [6] C. Toffanin, R. Visentin, M. Messori, F. Di Palma, L. Magni, and C. Cobelli, “Toward a run-to-run adaptive artificial pancreas: In silico results,” *IEEE Transactions on Biomedical Engineering*, vol. 65, no. 3, pp. 479–488, 2017. Cited on page/s 18.
- [7] M. Kierulf Åm, “The intraperitoneal artificial pancreas; glucose sensing and glucagon delivery.” Ph.D. dissertation, Norwegian University of Science and Technology, Trondheim, Norway, Faculty of Medicine and Health Sciences, Department of Clinical and Molecular Medicine, October 2020. Cited on page/s 19, 20.
- [8] M. Güemes, S. A. Rahman, and K. Hussain, “What is a normal blood glucose?” *Archives of disease in childhood*, vol. 101, no. 6, pp. 569–574, 2016. Cited on page/s 19.
- [9] K. D. Benam, H. Khoshamadi, M. K. Åm, Ø. Stavadahl, S. Gros, and A. L. Fougner, “Identifiable prediction animal model for the bi-hormonal intraperitoneal artificial pancreas,” *Journal of Process Control*, vol. 121, pp. 13–29, 2023. Cited on page/s 19.
- [10] R. Kahn, “Postprandial blood glucose,” *Diabetes Care*, vol. 24, no. 4, pp. 775–778, 2001. Cited on page/s 19.
- [11] N. Geidenstam, P. Spégel, H. Mulder, K. Filipsson, M. Ridderstråle, and A. P. Danielsson, “Metabolite profile deviations in an oral glucose tolerance test—a comparison between lean and obese individuals,” *Obesity*, vol. 22, no. 11, pp. 2388–2395, 2014. Cited on page/s 19.
- [12] E. G. Mietlicki-Baase, “Amylin-mediated control of glycemia, energy balance, and cognition,” *Physiology & behavior*, vol. 162, pp. 130–140, 2016. Cited on page/s 20.
- [13] D. L. Hay, S. Chen, T. A. Lutz, D. G. Parkes, and J. D. Roth, “Amylin: pharmacology, physiology, and clinical potential,” *Pharmacological reviews*, vol. 67, no. 3, pp. 564–600, 2015. Cited on page/s 20.
- [14] K. Guo, Q. Tian, L. Yang, and Z. Zhou, “The role of glucagon in glycemic variability in type 1 diabetes: a narrative review,” *Diabetes, Metabolic Syndrome and Obesity: Targets and Therapy*, pp. 4865–4873, 2021. Cited on page/s 20.
- [15] J. Walker, R. Ramracheya, Q. Zhang, P. Johnson, M. Braun, and P. Rorsman, “Regulation of glucagon secretion by glucose: paracrine, intrinsic or both?” *Diabetes, Obesity and Metabolism*, vol. 13, pp. 95–105, 2011. Cited on page/s 20.
- [16] C. F. Deacon, M. Kelstrup, R. Trebbien, L. Klarskov, M. Olesen, and J. J. Holst, “Differential regional metabolism of glucagon in anesthetized pigs,” *American Journal of Physiology-Endocrinology and Metabolism*, vol. 285, no. 3, pp. E552–E560, 2003. Cited on page/s 20.
- [17] A. Chakrabarty, J. M. Gregory, L. M. Moore, P. E. Williams, B. Farmer, A. D. Cherrington, P. Lord, B. Shelton, D. Cohen, H. C. Zisser *et al.*, “A new animal model of insulin-glucose dynamics in the intraperitoneal space enhances closed-loop control performance,” *Journal of process control*, vol. 76, pp. 62–73, 2019. Cited on page/s 21, 31.

- [18] C. Cobelli, E. Renard, and B. Kovatchev, “Artificial pancreas: past, present, future,” *Diabetes*, vol. 60, no. 11, pp. 2672–2682, 2011. Cited on page/s 22, 24.
- [19] C. Toffanin, L. Magni, and C. Cobelli, “Artificial pancreas: in silico study shows no need of meal announcement and improved time in range of glucose with intraperitoneal vs. subcutaneous insulin delivery,” *IEEE Transactions on Medical Robotics and Bionics*, vol. 3, no. 2, pp. 306–314, 2021. Cited on page/s 22, 23, 31.
- [20] J. A. Nelson, R. Stephen, S. T. Landau, D. E. Wilson, and F. H. Tyler, “Intraperitoneal insulin administration produces a positive portal-systemic blood insulin gradient in unanesthetized, unrestrained swine,” *Metabolism*, vol. 31, no. 10, pp. 969–972, 1982. Cited on page/s 23.
- [21] C. Botz, B. Leibel, W. Zingg, R. Gander, and A. Albisser, “Comparison of peripheral and portal routes of insulin infusion by a computer-controlled insulin infusion system (artificial endocrine pancreas),” *Diabetes*, vol. 25, no. 8, pp. 691–700, 1976. Cited on page/s 23.
- [22] A. Giacca, A. Caumo, G. Galimberti, G. Petrella, M. C. Librenti, M. Scavini, G. Pozza, and P. Micossi, “Peritoneal and subcutaneous absorption of insulin in type i diabetic subjects,” *The Journal of Clinical Endocrinology & Metabolism*, vol. 77, no. 3, pp. 738–742, 1993. Cited on page/s 23.
- [23] A. M. Albanese, E. F. Albanese, J. H. Miño, E. Gómez, M. Gómez, M. Zandomeni, and A. B. Merlo, “Peritoneal surface area: measurements of 40 structures covered by peritoneum: correlation between total peritoneal surface area and the surface calculated by formulas,” *Surgical and radiologic anatomy*, vol. 31, no. 5, pp. 369–377, 2009. Cited on page/s 23.
- [24] N. N. Armata, “Parietal peritoneum,” <https://www.osmosis.org/answers/parietal-peritoneum>, 2023, accessed on April 24, 2023. Cited on page/s 23.
- [25] M. Schiavon, C. Cobelli, and C. Dalla Man, “Modeling intraperitoneal insulin absorption in patients with type 1 diabetes,” *Metabolites*, vol. 11, no. 9, p. 600, 2021. Cited on page/s 23.
- [26] S. J. Moon, I. Jung, and C.-Y. Park, “Current advances of artificial pancreas systems: a comprehensive review of the clinical evidence,” *Diabetes & Metabolism Journal*, vol. 45, no. 6, pp. 813–839, 2021. Cited on page/s 24, 25, 26, 27, 28.
- [27] S. A. Weinzimer, G. M. Steil, K. L. Swan, J. Dziura, N. Kurtz, and W. V. Tamborlane, “Fully automated closed-loop insulin delivery versus semiautomated hybrid control in pediatric patients with type 1 diabetes using an artificial pancreas,” *Diabetes care*, vol. 31, no. 5, pp. 934–939, 2008. Cited on page/s 24.
- [28] E. Atlas, R. Nimri, S. Miller, E. A. Grunberg, and M. Phillip, “Md-logic artificial pancreas system: a pilot study in adults with type 1 diabetes,” *Diabetes care*, vol. 33, no. 5, pp. 1072–1076, 2010. Cited on page/s 24.
- [29] R. Hovorka, J. M. Allen, D. Eleri, L. J. Chassin, J. Harris, D. Xing, C. Kollman, T. Hovorka, A. M. F. Larsen, M. Nodale *et al.*, “Manual closed-loop insulin delivery in children and adolescents with type 1 diabetes: a phase 2 randomised crossover trial,” *The Lancet*, vol. 375, no. 9716, pp. 743–751, 2010. Cited on page/s 24, 27.
- [30] R. M. Bergenstal, D. C. Klonoff, S. K. Garg, B. W. Bode, M. Meredith, R. H. Slover, A. J. Ahmann, J. B. Welsh, S. W. Lee, and F. R. Kaufman, “Threshold-based insulin-pump interruption for reduction of hypoglycemia,” *New England Journal of Medicine*, vol. 369, no. 3, pp. 224–232, 2013. Cited on page/s 24.
- [31] D. M. Maahs, P. Calhoun, B. A. Buckingham, H. P. Chase, I. Hramiak, J. Lum, F. Cameron, B. W. Bequette, T. Aye, T. Paul *et al.*, “A randomized trial of a home system to reduce nocturnal hypoglycemia in type 1 diabetes,” *Diabetes care*, vol. 37, no. 7, pp. 1885–1891, 2014. Cited on page/s 24.
- [32] B. A. Buckingham, D. Raghinaru, F. Cameron, B. W. Bequette, H. P. Chase, D. M. Maahs, R. Slover, R. P. Wadwa, D. M. Wilson, T. Ly *et al.*, “Predictive low-glucose insulin suspension reduces duration of nocturnal hypoglycemia in children without increasing ketosis,”

- Diabetes Care*, vol. 38, no. 7, pp. 1197–1204, 2015. Cited on page/s 24.
- [33] M. Phillip, T. Battelino, E. Atlas, O. Kordonouri, N. Bratina, S. Miller, T. Biester, M. Avbelj Stefanija, I. Muller, R. Nimri *et al.*, “Nocturnal glucose control with an artificial pancreas at a diabetes camp,” *New England Journal of Medicine*, vol. 368, no. 9, pp. 824–833, 2013. Cited on page/s 24, 27.
- [34] H. Thabit, A. Lubina-Solomon, M. Stadler, L. Leelarathna, E. Walkinshaw, A. Pernet, J. M. Allen, A. Iqbal, P. Choudhary, K. Kumareswaran *et al.*, “Home use of closed-loop insulin delivery for overnight glucose control in adults with type 1 diabetes: a 4-week, multicentre, randomised crossover study,” *The lancet Diabetes & endocrinology*, vol. 2, no. 9, pp. 701–709, 2014. Cited on page/s 24, 27.
- [35] J. Kropff, S. Del Favero, J. Place, C. Toffanin, R. Visentin, M. Monaro, M. Messori, F. Di Palma, G. Lanzola, A. Farret *et al.*, “2 month evening and night closed-loop glucose control in patients with type 1 diabetes under free-living conditions: a randomised crossover trial,” *The lancet Diabetes & endocrinology*, vol. 3, no. 12, pp. 939–947, 2015. Cited on page/s 24, 27.
- [36] H. Thabit, M. Tauschmann, J. M. Allen, L. Leelarathna, S. Hartnell, M. E. Wilinska, C. L. Acerini, S. Dellweg, C. Benesch, L. Heinemann *et al.*, “Home use of an artificial beta cell in type 1 diabetes,” *New England Journal of Medicine*, vol. 373, no. 22, pp. 2129–2140, 2015. Cited on page/s 24, 27.
- [37] D. Eleri, J. M. Allen, K. Kumareswaran, L. Leelarathna, M. Nodale, K. Caldwell, P. Cheng, C. Kollman, A. Haidar, H. R. Murphy *et al.*, “Closed-loop basal insulin delivery over 36 hours in adolescents with type 1 diabetes: randomized clinical trial,” *Diabetes care*, vol. 36, no. 4, pp. 838–844, 2013. Cited on page/s 24, 27.
- [38] T. T. Ly, A. Roy, B. Grosman, J. Shin, A. Campbell, S. Monirabbasi, B. Liang, R. von Eyben, S. Shanmugham, P. Clinton *et al.*, “Day and night closed-loop control using the integrated medtronic hybrid closed-loop system in type 1 diabetes at diabetes camp,” *Diabetes Care*, vol. 38, no. 7, pp. 1205–1211, 2015. Cited on page/s 24, 27.
- [39] F. H. El-Khatib, J. Jiang, and E. R. Damiano, “A feasibility study of bihormonal closed-loop blood glucose control using dual subcutaneous infusion of insulin and glucagon in ambulatory diabetic swine,” *Journal of Diabetes Science and Technology*, vol. 3, no. 4, pp. 789–803, 2009. Cited on page/s 24.
- [40] F. H. El-Khatib, S. J. Russell, D. M. Nathan, R. G. Sutherlin, and E. R. Damiano, “A bihormonal closed-loop artificial pancreas for type 1 diabetes,” *Science translational medicine*, vol. 2, no. 27, pp. 27ra27–27ra27, 2010. Cited on page/s 24.
- [41] J. R. Castle, J. M. Engle, J. E. Youssef, R. G. Massoud, K. C. Yuen, R. Kagan, and W. K. Ward, “Novel use of glucagon in a closed-loop system for prevention of hypoglycemia in type 1 diabetes,” *Diabetes care*, vol. 33, no. 6, pp. 1282–1287, 2010. Cited on page/s 24.
- [42] A. Haidar, M. A. Tsoukas, S. Bernier-Twardy, J.-F. Yale, J. Rutkowski, A. Bossy, E. Pytka, A. El Fathi, N. Strauss, and L. Legault, “A novel dual-hormone insulin-and-pramlintide artificial pancreas for type 1 diabetes: a randomized controlled crossover trial,” *Diabetes care*, vol. 43, no. 3, pp. 597–606, 2020. Cited on page/s 27.
- [43] J. T. Ilkowitz, R. Katikaneni, M. Cantwell, N. Ramchandani, and R. A. Heptulla, “Adjuvant iraglutide and insulin versus insulin monotherapy in the closed-loop system in type 1 diabetes: a randomized open-labeled crossover design trial,” *Journal of diabetes science and technology*, vol. 10, no. 5, pp. 1108–1114, 2016. Cited on page/s 27.
- [44] E. Dassau, E. Renard, J. Place, A. Farret, M.-J. Pelletier, J. Lee, L. M. Huyett, A. Chakrabarty, F. J. Doyle III, and H. C. Zisser, “Intraperitoneal insulin delivery provides superior glycaemic regulation to subcutaneous insulin delivery in model predictive control-based fully-automated artificial pancreas in patients with type 1 diabetes: a pilot study,” *Diabetes, Obesity and Metabolism*, vol. 19, no. 12, pp. 1698–1705, 2017. Cited on page/s 27, 29.

- [45] R. M. Bergenstal, S. Garg, S. A. Weinzimer, B. A. Buckingham, B. W. Bode, W. V. Tamborlane, and F. R. Kaufman, "Safety of a hybrid closed-loop insulin delivery system in patients with type 1 diabetes," *Jama*, vol. 316, no. 13, pp. 1407–1408, 2016. Cited on page/s 27.
- [46] S. A. Brown, B. P. Kovatchev, D. Raghinaru, J. W. Lum, B. A. Buckingham, Y. C. Kudva, L. M. Laffel, C. J. Levy, J. E. Pinsker, R. P. Wadwa *et al.*, "Six-month randomized, multicenter trial of closed-loop control in type 1 diabetes," *New England Journal of Medicine*, vol. 381, no. 18, pp. 1707–1717, 2019. Cited on page/s 27.
- [47] P.-Y. Benhamou, S. Franc, Y. Reznik, C. Thivolet, P. Schaepeynck, E. Renard, B. Guerci, L. Chaillous, C. Lukas-Croisier, N. Jeandidier *et al.*, "Closed-loop insulin delivery in adults with type 1 diabetes in real-life conditions: a 12-week multicentre, open-label randomised controlled crossover trial," *The Lancet Digital Health*, vol. 1, no. 1, pp. e17–e25, 2019. Cited on page/s 27.
- [48] P.-Y. Benhamou, S. Lablanche, A. Vambergue, M. Doron, S. Franc, and G. Charpentier, "Patients with highly unstable type 1 diabetes eligible for islet transplantation can be managed with a closed-loop insulin delivery system: a series of n-of-1 randomized controlled trials," *Diabetes, Obesity and Metabolism*, vol. 23, no. 1, pp. 186–194, 2021. Cited on page/s 27.
- [49] G. P. Forlenza, B. A. Buckingham, S. A. Brown, B. W. Bode, C. J. Levy, A. B. Criego, R. P. Wadwa, E. C. Cobry, R. J. Slover, L. H. Messer *et al.*, "First outpatient evaluation of a tubeless automated insulin delivery system with customizable glucose targets in children and adults with type 1 diabetes," *Diabetes Technology & Therapeutics*, vol. 23, no. 6, pp. 410–424, 2021. Cited on page/s 27.
- [50] H. Blauw, A. J. Onvlee, M. Klaassen, A. C. van Bon, and J. H. DeVries, "Fully closed loop glucose control with a bihormonal artificial pancreas in adults with type 1 diabetes: an outpatient, randomized, crossover trial," *Diabetes Care*, vol. 44, no. 3, pp. 836–838, 2021. Cited on page/s 28.
- [51] S. J. Russell, F. H. El-Khatib, M. Sinha, K. L. Magyar, K. McKeon, L. G. Goergen, C. Balliro, M. A. Hillard, D. M. Nathan, and E. R. Damiano, "Outpatient glycemetic control with a bionic pancreas in type 1 diabetes," *New England Journal of Medicine*, vol. 371, no. 4, pp. 313–325, 2014. Cited on page/s 28.
- [52] A. Haidar, L. Legault, V. Messier, T. M. Mitre, C. Leroux, and R. Rabasa-Lhoret, "Comparison of dual-hormone artificial pancreas, single-hormone artificial pancreas, and conventional insulin pump therapy for glycaemic control in patients with type 1 diabetes: an open-label randomised controlled crossover trial," *The lancet Diabetes & endocrinology*, vol. 3, no. 1, pp. 17–26, 2015. Cited on page/s 28.
- [53] J. R. Castle, J. El Youssef, L. M. Wilson, R. Reddy, N. Resalat, D. Branigan, K. Ramsey, J. Leitschuh, U. Rajhbeharrysingh, B. Senf *et al.*, "Randomized outpatient trial of single- and dual-hormone closed-loop systems that adapt to exercise using wearable sensors," *Diabetes care*, vol. 41, no. 7, pp. 1471–1477, 2018. Cited on page/s 28.
- [54] "neuer weg bei der intraperitonealen insulingabe", howpublished = "https://www.diabetologie-online.de/a/neuer-weg-bei-der-intraperitonealen-insulingabe-1773515", "[Online; accessed 21-May-2023]". Cited on page/s 29.
- [55] R. W. Jones and F. Gianni, "Subcutaneous versus intra-peritoneal insulin delivery in the artificial pancreas," in *2018 13th IEEE Conference on Industrial Electronics and Applications (ICIEA)*. IEEE, 2018, pp. 508–513. Cited on page/s 29.
- [56] P. Van Dijk, S. Logtenberg, R. Gans, H. Bilo, and N. Kleefstra, "Intraperitoneal insulin infusion: treatment option for type 1 diabetes resulting in beneficial endocrine effects beyond glycaemia," *Clinical endocrinology*, vol. 81, no. 4, pp. 488–497, 2014. Cited on page/s 29.
- [57] V. Iacovacci, L. Ricotti, P. Dario, and A. Menciasci, "Design and development of a mechatronic system for noninvasive refilling of implantable artificial pancreas," *IEEE/ASME Transactions on Mechatronics*, vol. 20, no. 3, pp. 1160–1169, 2014. Cited on page/s 29, 30.

- [58] C. Lopez-Zazueta, Ø. Stavdahl, and A. L. Fougner, “Low-order nonlinear animal model of glucose dynamics for a bihormonal intraperitoneal artificial pancreas,” *IEEE Transactions on Biomedical Engineering*, vol. 69, no. 3, pp. 1273–1280, 2021. Cited on page/s 31, 34.

## CHAPTER 3

### *Development and Testing in Animal Trials*

---

*The title of the thesis is "Design and Implementation of the Dual-Hormone Artificial Pancreas in Animal Studies, A Model Predictive Control Approach with Intraperitoneal Injections." Chapter 2 provided an introduction to the concepts of dual-hormone artificial pancreas, equipment, and intraperitoneal injections. In this chapter, we discuss the term "Animal Experiments". In addition, it delves into the techniques employed in the project and examines the obstacles encountered, as well as the strategies used to overcome them.*

#### **3.1 USE OF ANIMALS IN THE EXPERIMENTS**

The utilization of animals for research is a topic that sparks controversy. According to a UK survey, the majority of the general public supports animal use under certain conditions where there are no alternatives available. However, 26% of the survey respondents advocate for a complete prohibition of animal use in research [1].

In Norway, the use of animals in research is regulated by national law, "Forskrift om bruk av dyr i forsøk," as well as the "Directive 2010/63/EU on the protection of animals used for scientific purposes." These legal regulations establish a baseline standard for animal use in research and stipulate that animals must be utilized in experiments aimed at addressing specific scientific questions while defining the treatments that the animals can receive. Any project involving animal use must seek and receive authorization from the appropriate authorities.

The guiding principle in animal research is "The three Rs," as stated in [1, 2], originally defined by Russel and Burch in 1959, which still stands as the core principle in animal experimentation. The three Rs represent Replacement, Reduction, and Refinement. Whenever possible, animal experimentation should be replaced, and data should be acquired through non-animal methods. If animal use is necessary, the number of animals utilized should be reduced to a minimum to obtain dependable and high-quality data. Refinement of animal experimentation is essential to achieve the best possible data while reducing

the burden on the animals involved.

The fundamental data of this thesis were obtained exclusively through animal experiments due to the scarcity of information and simulators available on BGL interactions with IP insulin and IP glucagon infusions. Investigating complex anatomical and physiological processes necessitated the use of animal experiments. All experiments were authorized by the Norwegian Food Safety Authority. We ensured that the number of animals used was kept to a minimum and that animals received appropriate treatments to minimize stress and pain. When possible, procedures were refined or animal experiments were replaced by the simulator.

We chose non-diabetic farm pigs (*Sus scrofa domesticus*) and suppressed their endogenous insulin and glucagon secretion using the methods presented in papers 2, 4, and 8. The reason for choosing the pig model was because of the physical, anatomical, and physiological similarities between humans and pigs [1, 3]. Although pigs and humans are similar in many ways, some differences might affect the results obtained in this study. For example, one obvious difference is that pigs lack the greater omentum in the peritoneal cavity [1].

### 3.2 HORMONE INJECTION AND GLUCOSE MEASUREMENT

Our research group, Artificial Pancreas Trondheim (APT), is focused on finding ways to expedite insulin absorption to achieve an FCL AP without user intervention. To accomplish this goal, we administered insulin and glucagon via the IP route, while using external pumps to infuse hormones into the peritoneal cavity. Before conducting human trials, we conducted tests on anesthetized pigs. During the initial phases, we made an incision in the abdominal region to insert both insulin and glucagon catheters, as illustrated in [Figure 3.1](#).

In the subsequent awake pig experiment, we placed two Diaports (Roche Medical) on the left side of the abdominal wall. Both ports were established on both sides of the incision, and the internal tubes from the ports were inserted into the abdominal cavity through the same intraperitoneal incision. We followed the guidelines of the manufacturer for the insertions, except for using two ports instead of one. The detailed procedures are described in **Paper 8**.

APT group has explored the use of IP fluid for measuring blood glucose levels as a way to overcome the time delay of current CGM devices [4]. Nonetheless, for closed-loop systems in this study, we opted for SC sensors due to their ease of use. [Figure 3.2](#) displays two examples of sensor placements on pigs. For the experiments in the anesthetized pigs, we attached the commercial sensors to the abdominal area to minimize the distance between the sensors and their

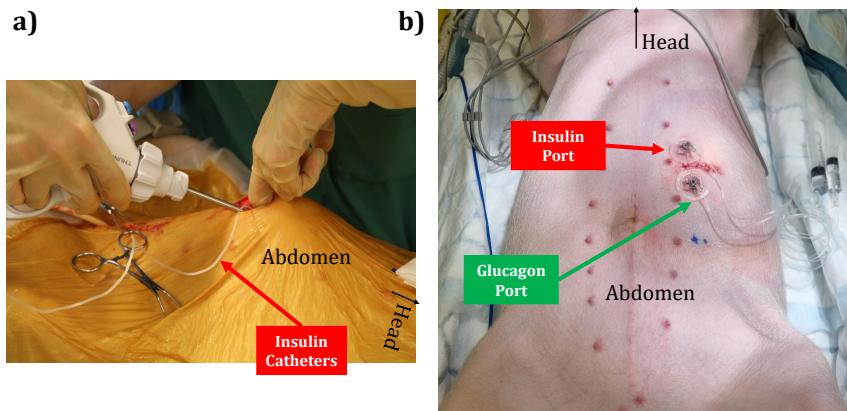


**FIGURE 3.1.** Picture (a) depicts the insertion of an insulin catheter into the peritoneal cavity through a 2–3 cm incision in the abdominal skin in an anesthetized pig experiment. A glucagon catheter was inserted through the same incision. Picture (b) demonstrates the placement of two Diaports in the abdominal region in the awake pig experiment.

receivers. However, in the awake animal experiment, the sensors were attached to the neck area as shown in the [Figure 3.2](#).

### 3.3 OVERVIEW OF THE DESIGNED ARTIFICIAL PANCREAS

In [Paper 8](#), we introduce a simplified block diagram that encapsulates the core functionalities of the DIP-AP. You can find this illustrative diagram in [Figure 3.3](#). This visual representation offers a concise overview of the fundamental components that constitute the DIP-AP system. Each part of the diagram is important for how the system works. To help you understand it better, we briefly explained the CGMs, Sensor Fusion, Estimator, and Controller blocks in the following sections. The rest of the blocks and hardware are explained in [Paper 8](#).

#### 3.3.1 Continuous Glucose Monitoring System

A fully automated AP relies heavily on precise BGL measurements. Nevertheless, the accuracy of commercially accessible sensors can be compromised by various factors. These factors encompass sensor distortions caused by pressure on adjacent tissues, connectivity issues, and inadequate calibrations. When patients are not actively monitoring the system, the AP might deliver an incorrect bolus based on faulty sensor data. This situation can be exacerbated in animal



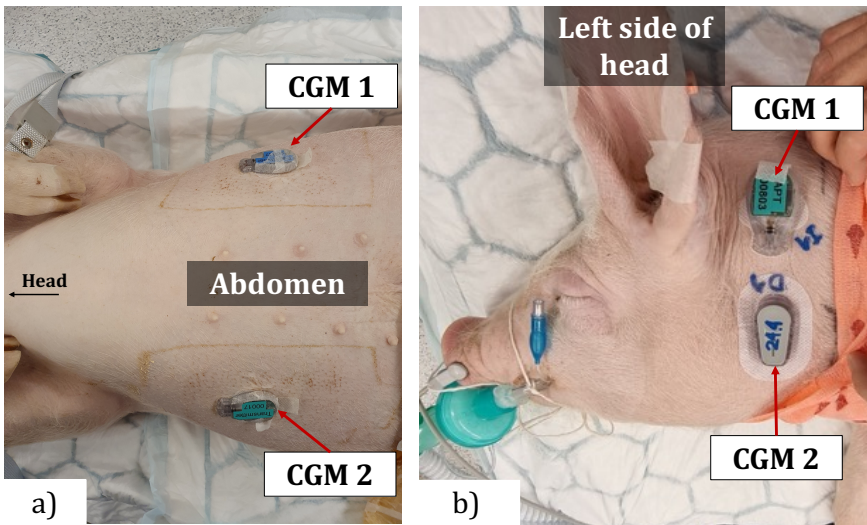


**FIGURE 3.2.** Pictures (a) and (b) show glucose monitoring sensors being attached to anesthetized pigs and awake pigs during experiments, respectively. To minimize sensor disconnections from the receivers during awake animal tests, the glucose monitoring sensors are attached to the neck, while the sensors are attached to the stomach area in the anesthetized pig experiments. This is because anesthetized pigs are kept sleeping on their backs, whereas awake pigs typically sleep on their stomachs.

experiments, where animals often exhibit curiosity and may tamper with the sensor or apply pressure to it.

As mentioned in Section 3.2, we used different sensors in the experiments to increase the reliability. For example in the awake animal experiment, due to the difficulty of obtaining frequent blood samples in awake animal experiments, we utilized two Dexcom G6 CGM systems (San Diego, CA) that are factory calibrated and two Medtronic Guardian sensors 3 (Northridge, Canada) with custom made transmitters provided by Inreda<sup>®</sup> Diabetic (Goor, the Netherlands).

These sensors are designed and made for humans. Therefore, some performance losses were expected. However, the sensors and the CGM devices were performed satisfactorily on the pigs. The performance of the sensors on pigs is compared with the blood gas analyzer in **Paper 3**.

### 3.3.2 Sensor Fusion

Since we used multiple sensors to measure the BGL, a sensor fusion unit was required in the control loop to merge sensor data from multiple CGMs and reduce noises and artifacts. In the experiments and to determine accurate read-

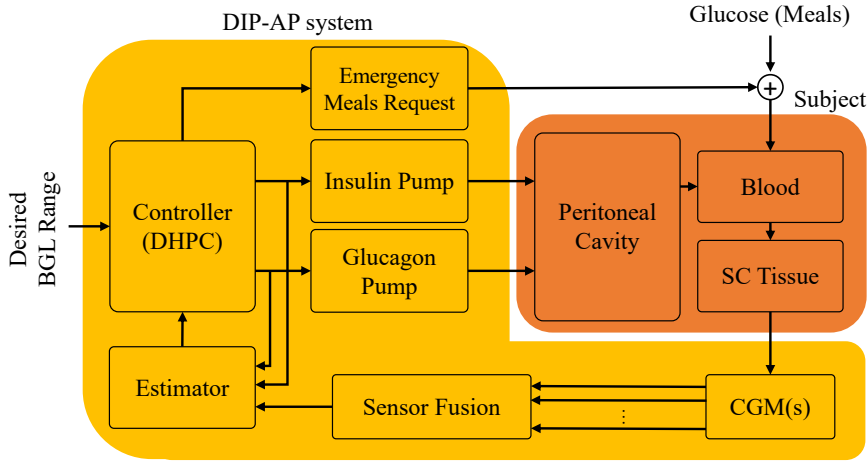


**FIGURE 3.3.** Schematic of the proposed dual-hormone intraperitoneal artificial pancreas; MPC, model predictive control; SC, subcutaneous; DIP AP, dual-hormone intraperitoneal artificial pancreas; CGM, continuous glucose monitoring; BGL, blood glucose level.

ings, we calculated the weighted average of the sensor data and assigned a trust value between 0 to 1 to each sensor based on its performance, as determined by an operator. Further work on sensor fusion and a proposed automated solution is proposed in **Paper 5** but was not used in the experiments.

### 3.3.3 Mathematical Model

Taking full advantage of the IP pathways in the AP systems necessitates having a mathematical model. The model used in this thesis is the meta-model presented in Paper 2. Meta model (3.1) describes the interactions of BGL with IP insulin, IP glucagon, and IV glucose infusions.

$$\frac{d}{dt} \begin{pmatrix} x_1 \\ x_2 \\ x_3 \\ x_4 \\ x_5 \\ x_6 \\ x_7 \end{pmatrix} = \begin{pmatrix} -(\beta_1 + \beta_2 \cdot x_2 + \beta_3 \cdot x_3) \cdot x_1 + HGP \\ \beta_5 (-x_2 + (\beta_7 \cdot \gamma_1 \cdot x_4 - F_{sat})) \\ \beta_8 (-x_3 + F_{sat}) \\ -\gamma_1 \cdot x_4 \\ \beta_9 (-x_5 + \beta_{10} x_6) \\ -\gamma_2 \cdot x_6 \\ \gamma_3 \cdot x_3 \cdot x_1 - \gamma_4 \cdot HGP \end{pmatrix} + \begin{pmatrix} \gamma_7 G(t) \\ 0 \\ 0 \\ \gamma_8 I(t) \\ 0 \\ \gamma_9 H(t) \\ 0 \end{pmatrix} \quad (3.1)$$

In this model,  $\{x_1, x_2, x_3, x_4\}$  are the states of the insulin sub-model including blood glucose level [mmol/l], effective insulin rate in the organs other than

the liver [U/min], effective insulin rate in the liver [U/min], and concentration of insulin in the IP fluid [U/ml], respectively. In this sub-model,  $I(t)$  is the IP insulin infusion rate [U/min], and  $G(t)$  is the IV glucose infusion rate [mmol/min]. In awake animals, we assume that  $G(t)$  is the GAR representing the meal digestion rate of the intestines.

The term  $F_{sat}$  is the saturation of the Hepatic first pass (HFP) effect, which is defined as follows:

$$F_{sat}(x_4) \triangleq \beta_6 \frac{\beta_{13} \gamma_5 x_4}{\beta_{12} + \beta_{13} \beta_7 \gamma_1 x_4} \quad (3.2)$$

The states  $\{x_5, x_6, x_7\}$  are the states of the glucagon sub-model that includes effective glucagon rate in the liver [mg/min], glucagon concentration in the IP fluid [mg/ml], and glycogen storage level [%].  $H(t)$  is the IP glucagon infusion rate [mg/min], and  $HGP$  is the hepatic glucose production rate modeled as follows.

$$HGP \triangleq \beta_4 x_5 \sqrt{x_7} \cdot \exp(-\beta_{11} \cdot x_3) \quad (3.3)$$

In (3.1), the parameter set  $\{\beta_1, \dots, \beta_4\}$  and the initial value of the glycogen storage level are needed to be identified individually. However, the parameters  $\beta_5, \dots, \beta_{13}$  are shown to be fixed among the different pigs, and they are identified using the prior information of the other subjects. The parameters  $\gamma_1, \dots, \gamma_9$  are body-weight dependant parameters that are known functions (See equations (16) and (17) in Paper 2).

### 3.3.4 Estimator

To develop a well-performing FCL artificial pancreas, independent of meal information, we must estimate the meal size to compensate them with the right insulin boluses. Furthermore, predicting BGL requires estimating non-measurable states of (3.1).

**Paper 4** presents an estimator for GAR based on the MHE method. The underlying cost function incorporates information about the lifestyle and diet of the subjects to improve estimation accuracy without the need for meal announcements. Besides estimating the GAR, the designed MHE estimates the non-measurable states of the meta-model which are essential for BGL predictions. Furthermore, it is shown that the proposed estimator is effective and reliable in near-real-life conditions and suitable for use in closed-loop systems.

### 3.3.5 Control Design

The control algorithm (often referred to as the *controller*) is a crucial component of the AP systems, responsible for determining the strategy to steer the BGL to a specific point or region. Typically, there are three strategies used in MPC methods: a) tracking a fixed point, b) tracking a trajectory, and c) reaching a desired zone. However, due to factors such as model mismatches, unannounced meals, and disturbances, trajectory-tracking approaches are not commonly used in AP systems. Within the context of AP systems, the strategy of tracking a fixed point is referred to as the "treat-to-target (T2T)" approach and the strategy of reaching a desired zone is called the "treat-to-range (T2R)" approach.

The T2T approach is designed to keep the BGL on a specific value. However, unforeseen meals, measurement errors, and discrepancies between the model and reality can result in BGL fluctuations and overuse of insulin and glucagon. The T2R approach, also known as "zone MPC" or "ZMPC" (as referenced in literature such as [5]), utilizes a set of set-point values (target range) that are considered equally acceptable by the objective function. T2R MPC methods are more conservative in sensor noise and disturbances compared to T2T methods. When the BGL (and predictions) fall within the target range, the ZMPC stops any control inputs, and only the basal insulin value is administered. The T2R method is more reliable and preferred in AP systems. For example, the T2R method explained in [6] is used in the commercial product Control IQ. The successful use of their algorithm in long-term real-world conditions is reported in [7].

The main idea behind the developed dual-hormone predictive control (DHPC) in this thesis is that the underlying penalty for BGL combines both the T2R and T2T methods to gain the advantages of both methods. To this end, we first defined the following zones:

- **Hypoglycemia:**  $BGL < 3.5$  mmol/l,
- **Severe Low:**  $BGL \in [3.5 \ 3.9)$  mmol/l,
- **Acceptable Low:**  $BGL \in [3.9 \ 4.5)$  mmol/l,
- **Desired point:**  $BGL = 4.5$  mmol/l,
- **Acceptable High:**  $BGL \in (4.5 \ 7]$  mmol/l,
- **Severe High:**  $BGL \in (7 \ 10]$  mmol/l,
- **Hyperglycemia zone:**  $BGL > 10$  mmol/l.

Then, we designed a zone-based penalty function as follows.

$$\Psi_g(g_k) := \begin{cases} (a_{ll} \cdot E)^2 + \beta_{ll} & g_k < 3.5 \\ (a_{sl} \cdot E)^2 + \beta_{sl} & 3.5 \leq g_k < 3.9 \\ (a_{al} \cdot E)^2 & 3.9 \leq g_k < 4.5 \\ 0 & g = 4.5 \\ (a_{ah} \cdot E)^2, & 4.5 < g_k \leq 7 \\ (a_{sh} \cdot E)^2 + \beta_{sh} & 7 < g_k \leq 10 \\ (a_{hh} \cdot E)^2 + \beta_{hh} & 10 < g_k, \end{cases} \quad (3.4)$$

Where  $g_k$  is the BGL at time  $k$ ,  $E := |g_k - 4.5|$  is the distance from the desired point,  $\{\beta_{ll}, \beta_{sl}, \beta_{sh}, \beta_{hh}\}$  are constant parameters that must be chosen to ensure the continuity of  $\Psi_g(g_k)$ , and  $\{a_{ll}, a_{sl}, a_{al}, a_{ah}, a_{sh}, a_{hh}\}$  are positive tuning parameters. An example of the BGL penalty for  $a_{ll} = 5$ ,  $a_{sl} = 4$ ,  $a_{al} = 3$ ,  $a_{ah} = 0.3$ ,  $a_{sh} = 0.4$ , and  $a_{hh} = 0.5$  is shown in [Figure 3.4](#).

Incorporating the BGL velocity into the BGL penalty function in MPC improves the performance of single-hormone AP systems and allows for better handling of moderate unannounced meals [5, 8]. To take this into account in the cost function, we defined “BGL velocity penalty” as follows

$$\Psi_{\delta g}(g_k, \delta g_k) = \begin{cases} \psi_1 \cdot g_k \cdot \delta g_k^2 & \delta g_k > 0 \\ \psi_2 \cdot (G_{\max} - g_k) \cdot \delta g_k^2 & \delta g_k \leq 0 \end{cases} \quad (3.5)$$

where

$$\delta g_k := g_k - g_{k-1} \quad (3.6)$$

is the rate of BGL change [mmol/5min],  $\{\psi_1, \psi_2\}$  are tune parameters, and  $G_{\max}$  is the highest acceptable BGL in the closed-loop system before an alarm is triggered for the patient. For negative slopes of BGL ( $\delta g_j \leq 0$ ), the penalty increases as BGL decreases, encouraging the controller to prevent hypoglycemia. Conversely, if  $\delta g_j > 0$  (positive slopes) and BGL is sufficiently high, the controller will be penalized to prevent a large hyperglycemia. An example of the velocity cost with  $\psi_1 = 1$ ,  $\psi_2 = 2$ , and  $G_{\max} = 15$  is shown in the lower-left panel of [Figure 3.4](#).

In summary, the BGL penalty function is defined as follows.

$$\Psi(g_k, \delta g_k) = \Psi_g(g_k) + \Psi_{\delta g}(g_k, \delta g_k) \quad (3.7)$$

An illustration of the BGL penalty function is shown in [Figure 3.4](#).

The suggested BGL penalty function provides enhanced user-friendliness for both patients and healthcare providers. This BGL penalty function can be readily comprehended and customized by modifying the zone ranges, target

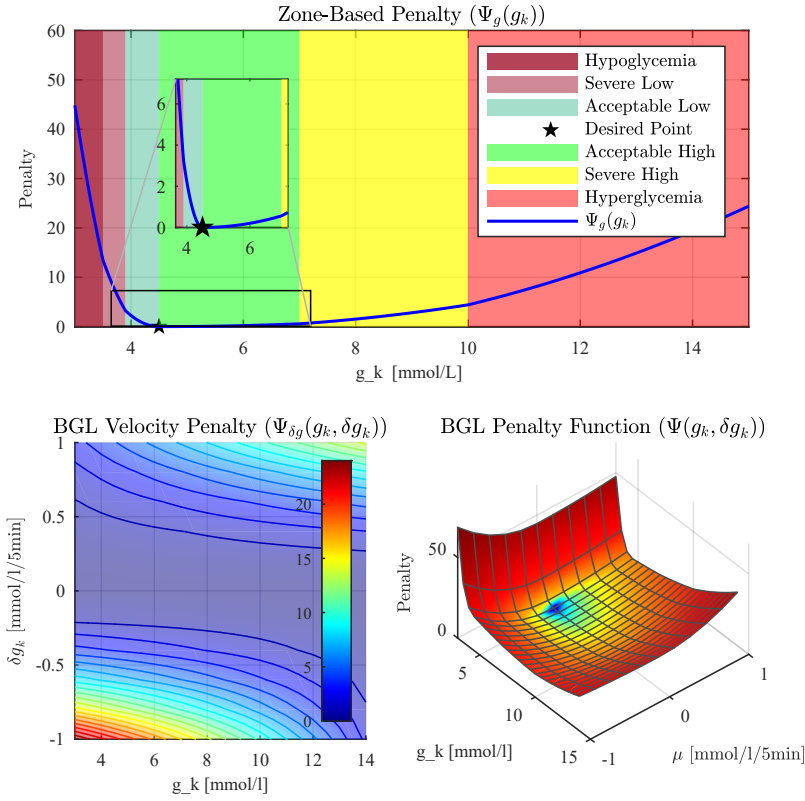


**FIGURE 3.4.** An example of the designed BGL penalty ( $\Psi_g(\cdot)$ ), BGL velocity penalty ( $\Psi_{\delta g}(\cdot)$ ), and the modified BGL penalty ( $\Psi(\cdot)$ ). The set point is at 4.5 [mmol/l] and  $\mu = 0$  [mmol/l/5min].

values, and the slope of the BGL penalty within each zone. This capability offers increased flexibility and adaptability to cater to the distinct requirements of individual patients, making it easy for patients or clinicians to fine-tune as needed.

**Paper 8** employed a model predictive control strategy with the designed cost function to determine the necessary insulin or glucagon. This cost function takes into consideration model mismatches, emergency scenarios, hardware malfunctions, sensor calibration points, and the avoidance of chattering caused by insulin and glucagon administration. Furthermore, the cost function addressed practical obstacles encountered during animal experiments.

### 3.3.6 Software Framework

The software framework developed for this thesis is a key component of the overall system. The framework was built on Matlab 2020 and later upgraded to Matlab 2022. As shown in Figure 3.5, the framework is responsible for fetching data from the sensors. The sensors have different sampling rates and start times, making it necessary to resample the data and synchronize the timing between the data streams. For example, the Dexcom G6 has a 5-minute sampling rate while the custom-made CGM from Inreda has a sampling rate of 1.2 seconds.

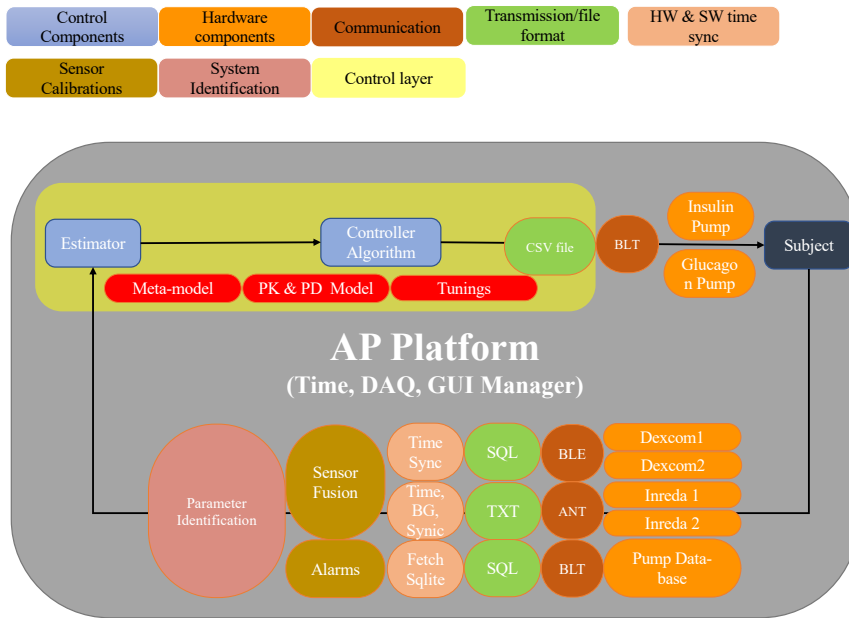


**FIGURE 3.5.** Different layers and components of the proposed artificial pancreas which is used in animal experiments; CSV, comma-separated values; BTL, Bluetooth; AP, Artificial Pancreas; DAQ, Data Acquisition; GUI, Graphic User Interface; BLE, Bluetooth Low Energy; ANT, Adaptive Network Topology. SQL, Structured Query Language; TXT, Text; BG, Blood Glucose; PK, Pharmacokinetics, PD, Pharmacodynamics.

After resampling and synchronization, the sensor fusion algorithm begins, where the data from different sensors are merged. In animal experiments, a simple sensor fusion algorithm was used, where the operator gave a trust value between 0 and 1 based on the performance, noise level, and calibration time of the sensors. The operator had access to a panel that allowed them to monitor the CGM measurements separately in the last 5 hours.

To inform the operator of critical situations, a flag, and sound alarm are implemented to alert them if the blood glucose level falls below 3.9 mmol/l or

rises above 15 mmol/l.

Once the sensor measurements have been merged, the framework initiates the estimator algorithm. After the estimations are completed, the framework begins the controller to estimate the required amount of insulin and glucagon. The framework then prepares the required file format and sends it via Bluetooth to the pumps for execution.

The explained procedure is repeated every 5 minutes. Overall, the software framework plays a crucial role in the successful operation of the system, ensuring that the sensor data are properly merged, the estimations are accurate, and the control loop responds effectively to maintain safe blood glucose levels.

### 3.4 REFERENCES

- [1] M. Kierulf Åm, "The intraperitoneal artificial pancreas; glucose sensing and glucagon delivery." Ph.D. dissertation, Norwegian University of Science and Technology, Trondheim, Norway, Faculty of Medicine and Health Sciences, Department of Clinical and Molecular Medicine, October 2020. Cited on page/s 41, 42.
- [2] S. J. Russell, F. H. El-Khatib, M. Sinha, K. L. Magyar, K. McKeon, L. G. Goergen, C. Balliro, M. A. Hillard, D. M. Nathan, and E. R. Damiano, "Outpatient glycemic control with a bionic pancreas in type 1 diabetes," *New England Journal of Medicine*, vol. 371, no. 4, pp. 313–325, 2014. Cited on page/s 41.
- [3] M. Swindle, A. Makin, A. Herron, F. Clubb, and K. Frazier, "Swine as models in biomedical research and toxicology testing (vol 49, pg 344, 2012)," *Veterinary Pathology*, vol. 49, no. 4, pp. 738–738, 2012. Cited on page/s 42.
- [4] A. L. Fougner, K. Kölle, N. K. Skjærvold, N.-A. L. Elvemo, D. R. Hjelme, R. Ellingsen, S. M. Carlsen, and Ø. Stavadahl, "Intraperitoneal glucose sensing is sometimes surprisingly rapid," 2016. Cited on page/s 42.
- [5] R. Gondhalekar, E. Dassau, and F. J. Doyle III, "Periodic zone-mpc with asymmetric costs for outpatient-ready safety of an artificial pancreas to treat type 1 diabetes," *Automatica*, vol. 71, pp. 237–246, 2016. Cited on page/s 47, 48.
- [6] S. D. Patek, L. Magni, E. Dassau, C. Karvetski, C. Toffanin, G. De Nicolao, S. Del Favero, M. Breton, C. Dalla Man, E. Renard *et al.*, "Modular closed-loop control of diabetes," *IEEE Transactions on Biomedical Engineering*, vol. 59, no. 11, pp. 2986–2999, 2012. Cited on page/s 47.
- [7] M. D. Breton and B. P. Kovatchev, "One year real-world use of the control-iq advanced hybrid closed-loop technology," *Diabetes technology & therapeutics*, vol. 23, no. 9, pp. 601–608, 2021. Cited on page/s 47.
- [8] D. Shi, E. Dassau, and F. J. Doyle, "Adaptive zone model predictive control of artificial pancreas based on glucose-and velocity-dependent control penalties," *IEEE Transactions on Biomedical Engineering*, vol. 66, no. 4, pp. 1045–1054, 2018. Cited on page/s 48.





## CHAPTER 4

### *Discussions*

---

*In the previous chapters, we have defined the problem and proposed solutions. This chapter summarizes the advantages and disadvantages of the proposed methods in this work. In addition, this chapter takes a broader perspective; Its main goal is to place our work in context and outline how our contributions can be applied in real-world scenarios to benefit patients, medical professionals, device manufacturers, and the broader research community within Artificial Pancreas.*

#### **4.1 DISCUSSIONS ON THE DEVELOPED DUAL-HORMONE INTRAPERITONEAL MODEL**

In **Paper 2**, a meta-model is presented that takes into account the physiology of the body. This model considers how insulin is transported directly to the liver through the portal vein. It is shown that the HFP effect has a significant impact on how the body responds to different insulin doses, leading to the development of a nonlinear model that incorporates this effect.

To identify the parameters of the proposed model, a significant number of experiments are required to stimulate all the system dynamics. However, invasive tests and measurements are not always applicable or safe for animals and humans or we cannot perform all the tests on each subject.

As an alternative, the meta-model concept is designed, which allows the tests to be distributed among different subjects. The results show that only five parameters need to be individually identified for each new subject to simulate blood glucose dynamics accurately. The remaining parameters are either constant across animals or can be calculated using body weight. The key advantages of the proposed meta-model are summarized as follows:

- **It is a dual-hormone model.**
- **Fewer individual parameters need to be identified compared to the existing models in the literature.**
- **Accurate predictions for a wide range of insulin and glucagon boluses.**

- **It is designed for control purposes which means it is fast and easy to identify its parameters.**
- **It is identified and tested with the data gathered from over 30 pigs in various scenarios including the anesthetized and awake experiments in pigs.**
- **Due to its accurate performance in fitting the data from animal experiments, it can be used as a simulator to reduce the number of animals used for future experiments.**

Due to limitations in anesthetized animals for open-loop experiments in **Paper 2**, the length of the experiments was shorter than 12 hours. Therefore, we assumed that the parameters remained constant throughout the experiments. One might need to consider intra-subject variation in extended experiments or human experiments. In addition, one may need more training data for longer experiments.

The ultimate goal of animal experiments is to develop the same methods for humans. We used IP and IV insulin and glucagon administrations with a wide range of bolus sizes in the anesthetized animal experiments. In addition, we took blood samples frequently to analyze. However, doing the same procedures might not be feasible in humans and the model might need to be simplified to reduce the complexity of the experiments.

During the experiments in anesthetized animals, IV glucose infusion was utilized instead of meals. However, when conducting experiments in awake animals and humans, meals will replace this input. Thus, future work may involve implementing an intestine model into the meta-model. Doing so will present additional challenges in identifying and ensuring the identifiability of the parameters.

## 4.2 DISCUSSIONS ON THE DEVELOPED DUAL-HORMONE INTRAPERITONEAL MOVING HORIZON ESTIMATOR

To achieve a fully automated artificial pancreas system, a meal estimator and BGL predictor are necessary to handle disturbances during meal times, all without requiring manual meal announcements or user interventions. The designed DIP-MHE in **Paper 4** estimates the states of the meta-model as well as the GAR.

We evaluated the performance of the proposed DIP-MHE in three 24-hour anesthetized animal experiments, under near-real-life conditions. Our results demonstrate that the DIP-MHE method is a reliable and efficient approach for estimating GAR and states of the meta-model. Moreover, the accuracy of the

estimator in estimating GAR from the intestines suggests that it can be used to develop and identify an accurate model for the digestive system. The successful implementation in animal trials indicates that it has the potential to be adapted for use in human trials. The key advantages of the proposed DIP-MHE are summarized as follows:

- **It provides accurate estimations in animal experiments.**
- **Due to embedded prior knowledge in the cost function, it provides reliable and stable performance in estimates.**
- **It does not need meal announcements.**

One drawback of MHE-based estimators lies in their computational demands, necessitating powerful computing units. Nevertheless, given the 5-minute sampling interval, the ongoing progress in embedded systems, and the battery capacities available, we can envision extending the application of our designed DIP-MHE to the existing single-hormone SC artificial pancreas systems. To achieve this, an equivalently accurate SC model is required to complement the IP meta-model.

During the experiments, CGM devices were utilized. It is important to note that these devices measure glucose concentration in interstitial fluid rather than blood. The diffusion of glucose from the blood to the interstitial tissue is a slow process which can result in a time lag and delay in the measurements. For the sake of simplicity, we have neglected measurement delays. However, a Kalman filter, as proposed in **Paper 3**, can be employed to compensate for the time lag in future studies.

The scenario in animal experiments is intended to last 24 hours due to the restrictions on the duration of the trials. One should create weekly or monthly routines to achieve more accurate probability distributions of the GAR and its derivative. Moreover, the exercise events must be studied more in detail in awake animal experiments or human studies. However, it was not feasible to perform the exercise in an anesthetized animal.

### 4.3 DISCUSSIONS ON THE DEVELOPED DUAL-HORMONE PREDICTIVE CONTROLLER

In the last two decades, numerous control algorithms have been developed for AP systems, clinically validated, commercialized, and used in actual practice for T1DM patients. A brief review of the AP systems is presented in **Paper 8** and [1].

In **Paper 8**, we developed an MPC method to control the BGL using IP insulin and glucagon administrations. This controller is called a Dual-hormone

predictive controller (DHPC). The meta-model (from **Paper 2**) and the DIP-MHE (from **Paper 4**) used in this work are developed specifically for control and predictions. Therefore, the controller offers several advantages, including a short identification time, precise predictions, and the ability to estimate meals or exercise. The designed control unit is a single-input and multi-output block specifically designed for dual-hormone artificial pancreas systems, incorporating safety considerations learned from practical experience. The key features of the DHPC can be summarized as follows:

- **It does not need meal or exercise announcements.**
- **It is designed based on the practical, physiological, and safety considerations of the system.**
- **It has optimal insulin and glucagon administration management to prevent overdosing and undesired oscillations.**
- **It is highly automated with embedded different emergency modes in the cost function. This minimizes the need for operator interventions.**
- **It achieved acceptable performance both *in vivo* and *in silico* experiments.**

Using glucagon as an active control input with insulin introduces certain complexities, such as the potential for oscillations. The cost function of the DHPC is designed to encompass safety considerations and emergency mode management. However, integrating all practical considerations into the cost function and control algorithm increases the number of parameters and computational challenges. The controller parameters are tuned using a trial-and-error approach on the simulator before being tested in animal experiments. However, we expect that employing an improved tuning method will yield enhanced performance and greater reliability from the DHPC.

The designed method is implemented in MATLAB and performed on a powerful experimental computer. The designed AP system is a prototype product and the ultimate goal is to implement this method in embedded systems with less computational capabilities. Therefore, the cost function and the controller must be optimized for use in embedded systems.

Simplifying the proposed DHPC can be achieved by implementing a logic-based emergency glucagon infusion rather than precisely calculating the required glucagon dosage. For instance, when the system detects a rapid drop in blood glucose levels and predicts an impending hypoglycemia event, the AP

system can administer a predetermined bolus of glucagon while suspending any insulin infusion until the hypoglycemia is resolved.

Implementing such methods and strategies can significantly alleviate the computational complexity associated with DHPC, DIP-MHE, and the parameter identification of the meta-model. By removing the glucagon sub-model and solely focusing on the insulin sub-model, we simplify process and enhance the computational difficulties.

#### 4.4 DISCUSSIONS ON USING SINGLE HORMONE OR DUAL HORMONE ARTIFICIAL PANCREAS

A single hormone artificial pancreas (SH-AP) has been shown to improve glucose control in people with type 1 diabetes. They can help to reduce the risk of both hypoglycemia and hyperglycemia and can improve quality of life. However, SH-APs do have some limitations. They can be less effective at controlling blood sugar levels during exercise or other times of high insulin demand. They also require the patient to be aware of their blood sugar levels and to be able to intervene if the SH-AP is not working properly.

Dual hormone artificial pancreas (DHAP) has the potential to provide even better glucose control than SH-APs and improve their safety margin. They can help to prevent hypoglycemia, which is a major risk for people with type 1 diabetes. However, DHAPs are still in development and are not yet widely available. They are also more expensive than SH-APs.

The decision of whether to use a single hormone or dual hormone artificial pancreas should be made between the patient and their healthcare provider. The best choice will depend on several factors, including individual needs and preferences, as well as the availability and cost of the different systems. Here are some of the factors to consider when making the decision:

- **Age and health status:** Younger patients and those with more severe diabetes may be more likely to benefit from a DHAP as they are more prone to hypoglycemia.
- **Activity level:** Patients who are active may be more likely to benefit from a DHAP, as they need more glucagon during the exercises.
- **Cost:** DHAPs are in the research phase and they will be more expensive than SH-APs.

The design of a single-hormone artificial pancreas is relatively straightforward. The system consists of a CGM, an insulin pump, and an algorithm that

automatically adjusts the insulin delivery. The algorithm is typically based on a mathematical model of glucose metabolism.

The design of a dual-hormone artificial pancreas is more complex than that of a single-hormone artificial pancreas. The system must not only monitor blood sugar levels and deliver insulin but also deliver glucagon. The glucagon pump is activated when blood sugar levels fall too low. The algorithm for a dual-hormone artificial pancreas is also more complex than the algorithm for a single-hormone artificial pancreas. It must take into account the effects of both insulin and glucagon on blood sugar levels.

In general, dual-hormone artificial pancreases are more complex to design and manufacture than single-hormone artificial pancreases. However, they provided better safety margins. Here are some of the disadvantages of DHAPs:

- **Complexity:** DHAPs are more complex to design, manufacture, and use than single hormone artificial pancreas. This can make them more difficult to troubleshoot and use.
- **Cost:** DHAPs are more expensive than single hormone artificial pancreas. This may make them out of reach for some people or their insurance companies.
- **Crystallization:** The infusion set for glucagon is more likely to get clogged since glucagon is an unstable solution. This necessitates changing the infusion set more often which is not desirable.
- **Infection risk:** More infusion sets installed in the body and changing them more often increase the risk of infection.
- **Acceptance:** Not all patients, companies, and stakeholders may readily embrace the concept of fully automated blood sugar control by machines. Many still prefer the familiarity and widespread use of traditional single-hormone artificial pancreas systems.

However, the dual-hormone artificial pancreas has many advantages and requires more research and experiments.

#### 4.5 DISCUSSIONS ON USING INTRAPERITONEAL ROUTE

This section will delve into the advantages and disadvantages of employing the IP route and compare it with the more traditional SC route. Advantages of the Intraperitoneal route [2]:

- **Rapid Absorption:** One of the most significant advantages of the IP route is the rapid absorption of substances into the bloodstream. Insulin and glucagon delivered via the IP route can act more swiftly, mimicking the physiological response of the pancreas more closely.
- **Reduced Delay:** Compared to SC injections, where there might be a delay in the onset of action, the IP route offers reduced delay, which is particularly advantageous when addressing fluctuations in blood glucose levels.
- **Consistency:** The IP route tends to provide more consistent absorption rates, reducing the variability in insulin and glucagon action commonly observed with SC injections. This can result in improved glycemic control.
- **Lower Insulin Doses:** Studies have suggested that lower doses of insulin are required when administered through the IP route, potentially minimizing the risk of hypoglycemia.

The IP route can be very suitable for those who have hypertrophy or other issues with SC delivery (such as antibodies that destroy the insulin before it arrives in the bloodstream). However, the use of IP route comes with the following list of disadvantages:

- **Invasive:** The IP route involves a surgical procedure to place a catheter into the peritoneal cavity. This invasiveness can deter some patients and may pose infection risks.
- **Technical Challenges:** Managing the IP route requires specialized equipment and expertise, which might not be readily available in all clinical settings.
- **Risk of Catheter Dislodgment:** There is a risk of catheter dislodgment, which can disrupt insulin and glucagon delivery and necessitate surgical repositioning.
- **Individual Variability:** While the IP route offers consistent absorption, individual patient responses may still vary, requiring careful monitoring and adjustment.

When it comes to choosing the insulin and glucagon infusion route, we should consider the following list as well as the advantages and disadvantages lists.



- **Patient Preference:** As mentioned, some patients may still prefer the SC route due to its non-invasive nature and familiarity.
- **Accessibility:** The SC route is more widely accessible and doesn't require specialized surgical procedures for catheter placement.
- **Versatility:** The SC route is well-established and versatile, accommodating various insulin and glucagon delivery pumps.

In conclusion, the use of the intraperitoneal route in AP systems offers advantages in terms of rapid and consistent absorption, potentially reducing insulin doses. However, it comes with the trade-off of invasiveness and technical challenges. The choice between IP and SC routes should be carefully considered, taking into account individual patient preferences, the clinical setting, and the desired glycemic control outcomes. Further research is warranted to explore the long-term efficacy and safety of the IP route in diverse patient populations.

## 4.6 REFERENCES

- [1] S. J. Moon, I. Jung, and C.-Y. Park, "Current advances of artificial pancreas systems: a comprehensive review of the clinical evidence," *Diabetes & Metabolism Journal*, vol. 45, no. 6, pp. 813–839, 2021. Cited on page/s 55.
- [2] I. Dirnena-Fusini, M. K. Åm, A. L. Fougner, S. M. Carlsen, and S. C. Christiansen, "Physiological effects of intraperitoneal versus subcutaneous insulin infusion in patients with diabetes mellitus type 1: A systematic review and meta-analysis," *Plos one*, vol. 16, no. 4, p. e0249611, 2021. Cited on page/s 58.

## CHAPTER 5

### *Concluding Remarks*

---

*This chapter summarizes the work, defines relevant topics for future work, and concludes the thesis.*

#### 5.1 CONCLUSIONS

This study aimed to evaluate the feasibility of utilizing the IP route in the AP system and achieving full automation without meal announcements. To achieve this objective, we designed a meta-model (in **Paper 2**), DIP-MHE (in **Paper 4**), and the DHPC approach (in **Paper 8**) for controlling BGL through IP insulin and glucagon administrations. We performed various experiments to evaluate the performance of the developed system in multiple scenarios, including:

- ***In Silico* 5-day tests in 100 virtual subjects.**
- ***In Vivo* tests in two anesthetized pigs for 12 hours.**
- ***In Vivo* tests in three anesthetized pigs for 24 hours.**
- ***In Vivo* tests in an awake pig for five days.**

The results and comparisons with the literature suggest that:

- IP Insulin and glucagon are absorbed fast enough to achieve FCL AP without meal announcements.
- Using glucagon in the AP system and with the proposed method provides reliable AP which can survive in unannounced challenges like exercise events.
- The controller must minimize dependency on glucagon usage due to the high probability of infusion set blockage.

The utilization of IP glucagon in practice was found to be challenging for long-term experiments, particularly in terms of replacing the glucagon infusion

set in the event of the infusion set blockage. However, it was observed that SC glucagon infusion proved to be equally effective in delivering glucagon while it has the advantage of easier infusion set replacement.

On the first day of the awake animal experiment, a single hormone IP AP system was implemented, which showed that the inclusion of glucagon as an input was not essential for achieving full automation. While the dual-hormone AP systems present several advantages, they also introduce the potential risk of glucagon infusion set blockage and place an increased burden on patients who need to change their infusion sets more frequently. In summary, we learned from the experiments that:

- The glucagon infusion set must be changed every 24 hours to prevent infusion set blockage, It is because the current formulation of glucagon is unstable and it is prone to cause such issues.
- With current developments, establishing and reestablishing the IP route is invasive and costly.
- Subcutaneously infused glucagon absorbed almost as fast as IP administrations in animal experiments.

In conclusion, the process of designing and implementing a fully closed-loop dual-hormone artificial pancreas system from the ground up is a complex and interdisciplinary target. It necessitates the integration of various fields and relies heavily on collaboration between engineering and medical disciplines. Despite facing technical and practical challenges during the awake animal experiment, the designed structure achieved significant results in the field. The simulations showed an average Time in Range (TIR) of 95.5% within the range of 3.5–10 mmol/l. In the anesthetized animal experiments, the average TIR was 94.0%. During the awake animal experiment on days 1, 4, and 5, with SC glucagon (no glucagon infusions on day 1), the TIR reached 77.3%. These findings indicate that the designed artificial pancreas system performs comparably in both simulation and real-world settings. This is achieved due to the high performance of the designed meta-model, DIP-MHE, and DHPC.

## 5.2 FUTURE WORK

In Papers 1–8 and Chapter 4, the future directions for enhancing each method and tool developed in this thesis are outlined individually. In this section, we will focus on discussing the potential future direction of the designed dual-hormone intraperitoneal artificial pancreas and explore potential strategies to overcome the limitations associated with the IP route.

The designed system is tested on a short-term and limited number of pigs. However, we believe more tests, especially on awake pigs, will reveal the important potentials and possible disadvantages of the method that are not found during the short-term experiments. Further studies must address safety issues such as infections in using IP insulin for long periods. In addition, a survey must be done to study how to implement the developed methods on humans with a minimum number of human trials.

Our future direction is replacing the IP insulin route with SC and accelerating insulin absorption by exploiting the vasodilative properties of glucagon. We found that SC micro-dose injections of glucagon can cause a significant increase in local blood flow in the surrounding tissue [1, 2]. In addition, the increased blood flow positively affected the absorption rate of insulin from the SC tissue of anesthetized pigs [3].

Therefore, in our future research, we will replace the IP infusion of insulin with the mechanisms illustrated in Figure 5.1. This mechanism is called "microglucagon" and injects a micro dosage of glucagon in the vicinity of the SC insulin infusion location (same «branch» of capillaries). This method is patented under International Application No. PCT/EP2022/067148 by our research group.

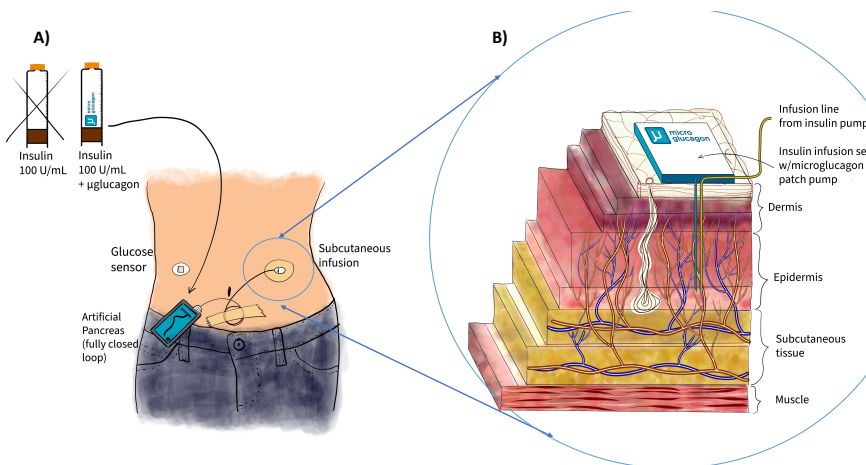


**FIGURE 5.1.** Infusion of mixed insulin and micro glucagon dose (A), and a mechanism to inject glucagon into the neighboring capillaries (B). The infusion of micro-doses of glucagon into the capillaries within subcutaneous tissue can induce vasodilation. This technique can be leveraged to enhance the absorption rate of subcutaneous (SC) insulin when glucagon is strategically injected into the same capillary branches through which SC insulin will diffuse. The invented method is called microglucagon and is patented under International Application No. PCT/EP2022/067148 by our research group.

### 5.2.1 *From Research to Real-World Impact*

While our research has primarily focused on the technical aspects, it's essential to consider how these advancements could translate into tangible benefits for diabetes patients and the broader healthcare landscape.

### 5.2.2 *Impact of This Research on Patients' Lives*

One of the core questions revolves around the potential impact of the methods developed in this research on patients.

The meta-model (discussed in **Paper2**), DIP-MHE (highlighted in **Paper4**), and the DHPC approach (covered in **Paper 8**) were designed using data from pig models. However, the adaptability of a similar approach for human subjects holds promise for the development of precise models and estimators.

This adaptability extends beyond intraperitoneal insulin and glucagon delivery. It can also be applied to subcutaneous insulin infusions, facilitating the creation of high-performance models and estimators. Implementing such models and estimators could significantly enhance the performance of Hybrid Closed-Loop AP systems. They could play a pivotal role in validating patient inputs and improving correction boluses by predicting glucose appearance rates accurately.

For this research to become a part of patients' lives, it would require collaboration with medical device manufacturers. Companies specializing in diabetes management systems, such as Inreda<sup>®</sup> Diabetic and Beta Bionics, could be potential partners. They would need to adapt and integrate our methodologies into their existing dual-hormone AP products or develop new ones to incorporate these innovations.

Companies and patients can benefit from using microglucagon strategy to accelerate insulin absorption rate. However, this also needs to be tested and explored in experiments.

### **Bringing it to Market**

Bringing our research to market involves several steps, including clinical trials, regulatory approvals, and product development. Companies interested in our work would need to invest in extensive testing to ensure the safety and efficacy of IP-based insulin and glucagon administration. They would also need to navigate the complex landscape of medical device regulations and work closely with healthcare professionals and regulatory bodies to obtain necessary approvals.

### 5.2.3 Risk Assessment

Like any transformative medical innovation, there are inherent risks and challenges. Our research paves the way, but there may be unforeseen obstacles in the path to commercialization, ranging from technical hurdles to market acceptance. Robust risk assessment and mitigation strategies are vital to address these challenges.

#### Beyond IP Delivery

Finally, while our research has a specific focus on intraperitoneal delivery, the methodologies developed, including the controller, estimator, and model, have broader applicability. These tools may find utility in other aspects of diabetes management, such as optimizing subcutaneous insulin delivery or aiding in the development of personalized treatment plans.

## 5.3 REFERENCES

- [1] M. K. Åm, E. Y. Munkerud, M. H. Berge, S. C. Christiansen, and S. M. Carlsen, "The effect of glucagon on local subcutaneous blood flow in non-diabetic volunteers; a proof-of-concept study," *European Journal of Pharmacology*, vol. 926, p. 175045, 2022. Cited on page/s 63.
- [2] I. A. Teigen, M. Riaz, M. K. Åm, S. C. Christiansen, and S. M. Carlsen, "Vasodilatory effects of glucagon: A possible new approach to enhanced subcutaneous insulin absorption in artificial pancreas devices," *Frontiers in Bioengineering and Biotechnology*, p. 1701, 2022. Cited on page/s 63.
- [3] S. M. Carlsen and S. C. Christiansen, "Effects of low-dose glucagon on subcutaneous insulin absorption in pigs." Cited on page/s 63.



Part II

# ORIGINAL PUBLICATIONS





## CHAPTER 6

### *Original Publications*

---

*This chapter contains seven published papers, as well as one submitted journal paper manuscript.*



► ORIGINAL PUBLICATIONS

**6.1 PAPER 1**

**Title: “A Nonlinear State Observer for the Bi-Hormonal Intraperitoneal Artificial Pancreas”**

Published in the Conference Proceedings of the IEEE Engineering in Medicine and Biology Society’s World Congress (EMBC 2021) in Glasgow, UK, July 2022 [1].



# A Nonlinear State Observer for the Bi-Hormonal Intraperitoneal Artificial Pancreas

Karim Davari Benam<sup>a,1</sup>, Hasti Khoshamadi<sup>a,2</sup>, Laura Lema-Pérez<sup>a,3</sup>,  
Sebastien Gros<sup>a,4</sup>, Anders Lyngvi Fougner<sup>a,5</sup>

**Abstract**—Currently, continuous glucose monitoring sensors are used in the artificial pancreas to monitor blood glucose levels. However, insulin and glucagon concentrations in different parts of the body cannot be measured in real-time, and determining body glucagon sensitivity is not feasible. Estimating these states provides more information about the current system status, facilitating improved decision-making by the model-based controller. In this regard, the aim of this paper is to design a nonlinear high-gain observer for a bi-hormonal artificial pancreas in the presence of measurement noises, model uncertainties, and disturbances. The model used in the observer is based on an existing intraperitoneal nonlinear animal model in the literature. This model is modified by assuming that insulin can directly transfer from the peritoneal cavity to the bloodstream. Based on a set of realistic assumptions, one model is considered after each hormone infusion, and two observers are separately designed. The model is divided into the insulin-phase and glucagon-phase models based on a set of realistic assumptions. Thereafter, two high-gain observers are designed separately for these phases contributing to estimating the non-measurable states. The observer error is proven to be locally uniformly ultimately bounded, and it is verified that any asymptotically stable control laws remain stable in the presence of the observer. The performance of the observers with different gains is evaluated for a scenario with multiple insulin and glucagon infusions. The proposed observer converges to a finite error, according to the results.

**Clinical relevance**— In Type 1 diabetic patients, the developed observer can be employed in a closed-loop artificial pancreas to improve the performance of model-based controllers. It estimates the key states, which are necessary for forecasting the body's response to insulin and glucagon boluses.

## I. INTRODUCTION

Glucose homeostasis is a mechanism of critical importance for sustaining life in humans through the use of glucose as a source of energy. One of the main organs involved in this mechanism is the pancreas. The pancreas regulates glucose in the body autonomously and continuously. The glycemic control is primarily achieved through the pancreas' endocrine hormones balanced through a negative feedback loop. Insulin and glucagon are the essential pancreatic hormones that affect the blood glucose level (BGL). Insulin (produced by beta cells in the pancreas) decreases BGL by either storing

excess glucose mainly in the liver and muscles or allowing body cells to utilize glucose as fuel. Glucagon (produced by pancreatic alpha cells) raises BGL by releasing glucose that has been stored as glycogen in the body.

Type 1 diabetes (T1D), or insulin-dependent diabetes, is a chronic disease where the pancreas produces no or little insulin. T1D has an unknown etiology. In most cases, T1D is caused by a reaction of the immune system destroying the beta cells of the pancreas. Other possible explanations include genetics, viral exposure, and other environmental variables. Impaired glucagon production and release are also common as a consequence of beta cells destruction. Therefore, the body becomes incapable of maintaining a normal BGL [1], [2].

An artificial pancreas (AP) that consists of subcutaneous BGL sensor(s), insulin/ and glucagon pump(s), and a control algorithm is the current treatment for T1D disease. It mimics the natural endocrine pancreas function by automatically delivering external insulin and glucagon in response to the changes in BGL. Different versions of single-hormone APs that infuse only insulin are currently available on the market [3]. However, since these systems lack glucagon, there is a substantial risk of low BGL if unannounced physical activities are performed. Dual-hormone APs are under development and the prior clinical trials show their advantages in reducing the number of hypoglycemia episodes [4].

It is possible to deliver hormones intravenously (IV), subcutaneously (SC), and intraperitoneally (IP). Although the IV route is fast, it is not a practical continuous solution due to the possible health complications. SC infusion is the most common approach in delivering insulin in current APs. However, due to the SC route's absorption delay, the existing APs, even with the most advanced control algorithms, are ineffective in dealing with unannounced meals [5].

The IP drug delivery pathway has been shown to have faster pharmacokinetics than the SC pathway [3]. Furthermore, in IP insulin infusion, the majority of the insulin absorbs into the portal vein (PV) and is then delivered to the liver. While in SC infusion, insulin first absorbs into the blood circulation system before reaching the liver. As a result, the IP insulin infusion seems to be physiologically more similar to pancreatic functionality. Moreover, Toffanin *et al.* tested their AP with IP infusion on the modified UVA/Padova simulator [6] and showed that the meal announcement is not needed [5].

Model-based controllers, such as model predictive control (MPC), are the most commonly used control approaches in

\*This research is funded by the Research Council of Norway (project no. 248872), and the Centre for Digital Life Norway.

<sup>a</sup> Department of Engineering Cybernetics, Faculty of Information Technology and Electrical Engineering, Norwegian University of Science and Technology (NTNU), O. S. Bragstads Plass 2D, 7034 Trondheim, Norway.

<sup>1</sup> karim.d.benam@ntnu.no

<sup>2</sup> hasti.khoshamadi@ntnu.no

<sup>3</sup> laura.l.perez@ntnu.no

<sup>4</sup> sebastien.gros@ntnu.no

<sup>5</sup> anders.fougner@ntnu.no

APs due to the constraints and the delays [7]. However, BGL is the only real-time measurable output of the system, while the other states essential for prediction must be estimated. In this paper, a high-gain observer is developed to estimate non-measurable states based on a modified version of the nonlinear bi-hormonal-glucose model proposed in [8]. High-gain observer is chosen due to its implementation simplicity and its robustness against large perturbations and model uncertainties. In spite of measurement noise, model mismatches, and disturbances, the proposed observer is proven to converge to a bounded error under some assumptions. Furthermore, the Lyapunov theorem is used to demonstrate that any asymptotically stable control approach will remain stable when the designed observer is used in the control loop.

The paper is organized as follows: In Section II, the modified version of the nonlinear bi-hormonal-glucose model is introduced and practical assumptions for designing the observer are made. Section III presents the high-gain observers designed for the insulin and glucagon phases and the convergence analysis. Results are discussed in Section IV. Finally, conclusions are exposed in Section VI.

## II. MATHEMATICAL MODEL AND ASSUMPTIONS

The nonlinear bi-hormonal-glucose model developed by Zazueta *et al.* [8] describes the interaction of BGL with IP insulin and glucagon, making it appropriate for bi-hormonal APs. In order to ensure structural identifiability, the effect of the insulin in the intermediate compartment is ignored and the order of the model is reduced in their final model.

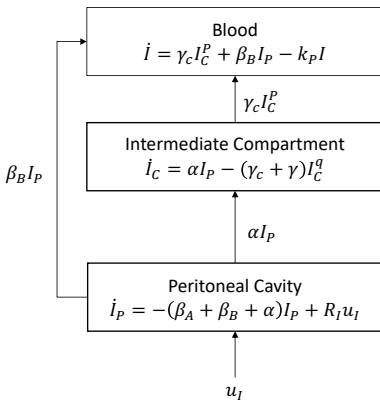


Fig. 1. Block diagram of the insulin compartment.

A modified version of this model is used to construct the observer in this paper. This modified version is as follows

$$\dot{G} = -[k_1 + k_I I + k_{I_c} I_c] G + k_H H f(\xi) + R \quad (1)$$

$$\dot{I} = \gamma_c I_c^p + \beta_B I_p - k_p I \quad (2)$$

$$\dot{I}_c = \alpha I_p - (\gamma_c + \gamma) I_c^q \quad (3)$$

$$\dot{I}_p = -(\beta_A + \beta_B + \alpha) I_p + R_I u_I(t) \quad (4)$$

$$\dot{H} = -nH + n_2 h_1 \quad (5)$$

$$\dot{h}_1 = -n_1 h_1 + R_H u_H(t) \quad (6)$$

$$\dot{\xi} = x_1 [(k_I I + k_{I_c} I_c) G] - x_2 [H f(\xi)] - x_3 \xi \quad (7)$$

where  $f(\xi) = \xi^a$  for  $0 < a \leq 1$  (where  $a = 1$  in the original model). As it is shown in Fig. 1, the pathway of direct insulin transportation from the peritoneal cavity to the blood is considered in this model as described in [9]. In addition,  $-x_3 \xi$  is added in (7) to model the glucagon sensitivity decrease due to the basal endogenous glucagon production. The states, inputs, and parameters of the model are described in Table I.

TABLE I  
STATES, PARAMETERS, AND INPUTS OF THE MODEL.

Symbol	Description	Unit
<b>States</b>		
$G$	Blood glucose concentration.	mmol/L
$I$	Blood insulin concentration.	mU/L
$I_c$	Insulin concentration in the intermediate compartment.	mU/L
$I_p$	Insulin concentration in peritoneal cavity.	mU/L
$H$	Blood glucagon concentration.	pmol/L
$h_1$	Glucagon concentration in peritoneal cavity.	pmol/L
$\xi$	Glucagon sensitivity.	dimensionless
<b>Inputs</b>		
$R$	IV exogenous glucose infusion.	mmol/L/h
$u_I$	IP insulin bolus.	U
$u_H$	IP glucagon bolus.	$\mu g$
<b>Parameters</b>		
$k_1$	Insulin-independent removal rate of glucose.	1/h
$k_I, k_{I_c}$	Insulin-dependent removal rates of glucose.	L/mU/h
$k_H$	Glucose response to glucagon rate.	1/h
$k_p, \gamma, \beta_A, n, \gamma_c, \alpha, \beta_B, n_1, n_2$	Consumption and degradation rates.	1/h
$a, p, q$	Transport rates.	1/h
$a, p, q$	Powers.	dimensionless
$R_I$	Conversion parameter.	1/L/h
$R_H$	Conversion parameter.	pmol/ $\mu g$ /L/h
$x_1$	Conversion parameter.	L/mmol
$x_2$	Conversion parameter.	L/pmol/h
$x_3$	Decrease rate of glucagon sensitivity due to endogenous glucagon production.	1/h

As mentioned in the introduction, a state observer is needed to estimate the non-measurable states for a model-based controller, such as an MPC, to make better control decisions. To design a high-gain observer, the following assumptions are considered:

- 1) The amounts of insulin and glucagon in the peritoneal cavity are represented by  $I_p$  and  $h_1$ . The inputs and parameters used in (4) and (6) are assumed to be known. Therefore these states can be calculated, and there is no need for the observer to estimate them.

2) Insulin and glucagon are hormones with reverse effects on BGL. It is not typical to design controllers in AP to use these hormones simultaneously or close to each other. Therefore, an observer during each of these hormone infusions can be designed separately.

3) For simplicity, it is assumed that  $p = 1$  and  $q = 1$ .

Two different models are considered, one during the insulin phase and the other during the glucagon phase, in order to design the observers:

• Insulin-phase Model

$$\dot{G}_I = -[k_1 + k_I I + k_c I_c] G_I + k_H \hat{H} f(\hat{\xi}) + R \quad (8)$$

$$\dot{I} = \gamma_c I_c + \beta_B I_p - k_p I \quad (9)$$

$$\dot{I}_c = \alpha I_p - \gamma_c I_c - \gamma I_c \quad (10)$$

$$y_m = G_I + v \quad (11)$$

where  $G_I$  is blood glucose concentration during the insulin phase,  $v$  is the measurement noise, and  $y_m$  is the measured BGL. Moreover,  $\hat{H}$  and  $\hat{\xi}$  are the estimated states from the glucagon phase.

• Glucagon-phase Model

$$\dot{G}_H = -[k_1 + k_I \hat{I} + k_{I_c} \hat{I}_c] G_H + k_H H f(\xi) + R \quad (12)$$

$$\dot{\xi} = x_1 \left[ (k_I \hat{I} + k_{I_c} \hat{I}_c) G \right] - x_2 [H f(\xi)] - x_3 f(\xi(t)) \quad (13)$$

$$\dot{H} = -nH + n_2 h_1 \quad (14)$$

$$y_m = G_H + v \quad (15)$$

where  $G_H$  is blood glucose concentration during the glucagon phase.  $\hat{I}$  and  $\hat{I}_c$  are estimations from the insulin phase.

It is worth mentioning that each of these models is observable. In the next section, a high-gain observer is designed, and its convergence and error bounds are analyzed.

### III. HIGH-GAIN OBSERVER AND CONVERGENCE ANALYSIS

The high-gain observer is one of the most commonly used nonlinear observers that considers both measurement noises and model uncertainties [10]. In this section, two high-gain observers are proposed for insulin phase and glucagon phase models.

#### A. Nominal Form of Models

To simplify the stability analysis and take advantage of the high-gain observer, each model must be transformed into a nominal form [11]. For this purpose, the new states for the insulin-phase and glucagon-phase models are defined as

$$S_1 \stackrel{\text{def}}{=} [p_1 \quad q_1 \quad r_1]^T \quad (16)$$

$$S_2 \stackrel{\text{def}}{=} [p_2 \quad q_2 \quad r_2]^T \quad (17)$$

where  $[p_1, q_1, r_1]^T$  and  $[p_2, q_2, r_2]^T$  are defined in (18) and (19), respectively. In these two equations,  $e_1 \triangleq k_I k_p$ ,  $e_2 \triangleq$

$-k_I \gamma_c - k_c (\gamma_c + \gamma)$ ,  $e_3 \triangleq k_c a + k_I \beta_B$ ,  $e_4 \triangleq (k_1 + k_I \hat{I} + k_{I_c} \hat{I}_c)$ , and  $e_5 = k_H f(\xi)$ .

The state-space models are transformed into the following equations for  $i=1,2$ :

$$\dot{S}_i = A S_i + B \varphi_i(S_i, u_i, R) \quad (20)$$

$$y_m = C S_i + v \quad (21)$$

where  $\varphi_i(S_i, u_i, R) \triangleq \hat{r}_i$ ,  $u_1 \triangleq I_p$ ,  $u_2 \triangleq h_1$ ,

$$A = \begin{bmatrix} 0 & 1 & 0 \\ 0 & 0 & 1 \\ 0 & 0 & 0 \end{bmatrix}, \quad B = \begin{bmatrix} 0 \\ 0 \\ 1 \end{bmatrix}$$

, and  $C = [1 \quad 0 \quad 0]$ . Furthermore,  $\|v\| < \mu$  for positive values of  $\mu$  as the maximum amplitude of measurement noise.

#### B. High-Gain Observer

A high-gain observer is designed based on the formulation proposed in [11], [12] as follows

$$\dot{\hat{S}}_i = A \hat{S}_i + B \varphi_{o_i}(\hat{S}_i, u_i, R) + \frac{1}{\varepsilon_i} H_i (y_m - C \hat{S}_i) \quad (22)$$

where  $\hat{S}_i$  for  $i = \{1, 2\}$  is the estimation of  $S_i$ ,  $\varepsilon_i$  is the inverse of observer gain, and  $\varphi_{o_i}$  is the nominal form of  $\varphi_i$ . It is notable that  $\varphi_i$  is locally Lipschitz function of  $S_i$  and  $u_i$ . In addition, for arbitrary positive values of  $\{a_{i1}, a_{i2}, a_{i3}\}$ ,  $H_i$  is defined as follows

$$H_i = \begin{bmatrix} \frac{a_{i1}}{\varepsilon_i} & \frac{a_{i2}}{\varepsilon_i^2} & \frac{a_{i3}}{\varepsilon_i^3} \end{bmatrix}^T \quad (23)$$

Moreover, the weighted observer error for  $\varepsilon_i \in (0, 1)$  is defined as

$$\eta_i = D(\varepsilon_i)_{3 \times 3} (S_i - \hat{S}_i) \quad (24)$$

with

$$D(\varepsilon_i) \triangleq \begin{bmatrix} 1 & 0 & 0 \\ 0 & \varepsilon_i & 0 \\ 0 & 0 & \varepsilon_i^2 \end{bmatrix} \quad (25)$$

In the rest of the paper, since both models are in the nominal form, the index  $i$  is removed to increase readability.

Using (20) and (24), the dynamics of the system and the weighted observer error can be augmented as below.

$$\dot{S} = f_s(S, S - D(\varepsilon)^{-1} \eta, R) \quad (26)$$

$$\varepsilon \dot{\eta} = A_0 \eta + \varepsilon^2 B g(S, S - D(\varepsilon)^{-1} \eta, R) + B_2 v \quad (27)$$

where  $f_s$  is the right-hand side of the (20) with assuming that  $u_i$  is function of observed states. Moreover,

$$A_0 = \begin{bmatrix} -a_{i1} & 1 & 0 \\ -a_{i2} & 0 & 1 \\ -a_{i3} & 0 & 0 \end{bmatrix}, \quad B_2 = \begin{bmatrix} -a_{i1} \\ -a_{i2} \\ -a_{i3} \end{bmatrix}$$

, and  $g(\dots) = \varphi(\dots) - \varphi_o(\dots)$ . In addition,  $\{a_{i1}, a_{i2}, a_{i3}\}$  should be selected in a way that eigenvalues of  $A_0$  lay at left-half plane.



$$\begin{bmatrix} p_1 \\ q_1 \\ r_1 \end{bmatrix} \stackrel{\text{def}}{=} \begin{bmatrix} G_I \\ -(k_1 + k_I I + k_c I_c) G_I \\ -(k_1 + k_I t I + k_c I_c)^2 G_I - (e_1 I + e_2 I_c + e_3 I_p) \end{bmatrix} \quad (18)$$

$$\begin{bmatrix} p_2 \\ q_2 \\ r_2 \end{bmatrix} \stackrel{\text{def}}{=} \begin{bmatrix} G_H \\ -(k_1 + k_I \hat{I} + k_{I_c} \hat{I}_c) G_H + k_H H f(\xi) \\ -e_4 \dot{G}_H + a e_5^{\frac{\alpha-1}{\alpha}} H (x_1 e_4 G_H - (x_2 H + x_2) e_5) + e_5 (nH - n_2 h_1) + e_4 G \end{bmatrix} \quad (19)$$

Based on the *Lemma 1* in [11], the observer error (27) converges to a bounded set for

$$\|g(S, D(\varepsilon)^{-1}\eta, R)\| < k_g. \quad (28)$$

*proof:* Since  $A_0$  is a Hurwitz matrix by design, a positive symmetric matrix  $E$  can be found such that  $EA_0 + A_0^T E = -I$ . Considering  $W(\eta) = \eta^T E \eta$  as a Lyapunov candidate function, its time derivation is

$$\dot{W} \leq -\frac{1}{\varepsilon} \|\eta\|^2 + 2\varepsilon \|\eta\| \|EB\| k_g + \frac{2}{\varepsilon} \|\eta\| \|EB_2\| \mu. \quad (29)$$

It can be shown that

$$\Sigma = \left\{ W(\eta(t)) \leq \|E\| \left( 4\|EB\| k_g \varepsilon^2 + 4\|EB_2\| \mu \right)^2 \right\} \quad (30)$$

is an invariant since  $\dot{W}(\eta(t)) < -2/\varepsilon \|E\|$  for  $W(\eta) \notin \Sigma$ .

While  $\|\eta\| \leq c_1 \varepsilon^2 + c_2 \mu$  for  $W(\eta) \in \Sigma$ , where  $c_1 \triangleq 4\|EB\| k_g \sqrt{\|E\|} / \sqrt{\lambda_{\min}(E)}$  and  $c_2 \triangleq 4\|EB_2\| \sqrt{\|E\|} / \sqrt{\lambda_{\min}(E)}$ . Therefore, the designed observer converges to a bounded error which can be found by

$$\|S(t) - \hat{S}(t)\| \leq c_1 \varepsilon + c_2 \frac{\mu}{\varepsilon} \triangleq F_r(\varepsilon, \mu) \quad (31)$$

### C. Stability of Closed-loop System in Presence of the Designed Observer

In this section, the stability of the closed-loop system in presence of the designed observer is analyzed as in [12].

We assumed that the closed-loop system is asymptotically stable for  $S \in \Omega$  when  $\eta = 0$ . Therefore, there is a Lyapunov function  $V(s) > 0$  (and  $V(S) = 0$  for  $S = 0$ ) in which  $\dot{V}(s) < -U(S)$ . Where  $U(S)$  is positive function for  $S \in \Omega$ . Since  $f(S, S - D(\varepsilon)^{-1}\eta)$  is bounded function and locally satisfies the Lipchitz conditions, one can write

$$\|f(S, D(\varepsilon)^{-1}\eta) - f(S, 0)\| \leq L_1 \|D(\varepsilon)^{-1}\eta\| \quad (32)$$

where  $L_1$  is positive constant. In addition, one can assume  $\|dV/dS\| \leq L_2$  for a positive value of  $L_2$ . Using this inequalities, for  $\eta \neq 0$ , one can write

$$\dot{V}(S) \leq -U(S) + L_1 L_2 F_r(\varepsilon, \mu) \quad (33)$$

As it proven in [12], for bounded values of  $\mu$  there is set of positive values for  $\varepsilon$  in which  $F_r(\varepsilon, \mu) < U(S)/L_1 L_2$ . That means the closed-loop system remains stable and  $(S(t), \eta(t))$  will remain in  $\{\Omega \times \Sigma\}$ .

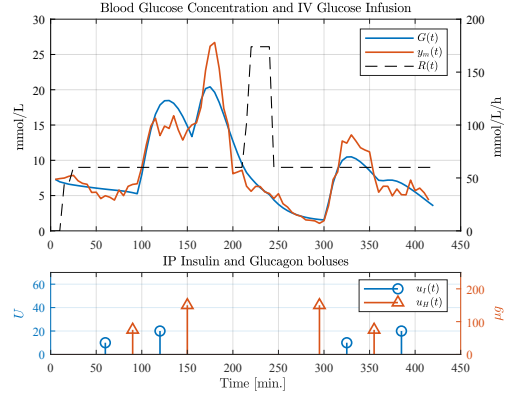


Fig. 2. The scenario used for evaluating the observer performance.

## IV. RESULTS

In the development of an AP, there are non-measurable states that must be estimated so that the controller can make better decisions in the control of BGL regarding the treatment of people with T1D. The high-gain observer was designed based on the modified nonlinear bi-hormonal-glucose model, and its convergence to a bounded error was evaluated.

To test the effectiveness of the observer, the scenario shown in Fig. 2 was considered where the sampling rate was set to 5 minutes, and four insulin boluses  $\{10, 20, 10, 20\}$ U, four glucagon boluses  $\{75, 150, 150, 75\}$ μg, and  $R(t)$  as IV glucose infusion were given. Furthermore, the measured BGL ( $y_m(t)$ ) was created by adding a measurement noise with the maximum amplitude of 2 mmol/L and a sinusoidal disturbance with amplitude 20% of the BGL and a frequency of 0.4 rad/h in order to evaluate the observer's robustness. Notably, 15% parameter identification error was considered to simulate the model uncertainties.

In order to analyze the error bound and time response of the observer, two cases are considered. In each case, there are two observers with the gain of  $\varepsilon_1$  and  $\varepsilon_2$ , respectively, for the insulin and glucagon phases. In the first case, relatively high values (near to one) were chosen both for  $\varepsilon_1$  and  $\varepsilon_2$  while these values were relatively low in the second case. The initial values were chosen randomly but the same for all observers in both cases.

In Fig. 3 and Fig. 4, the estimation results of the case 1 and

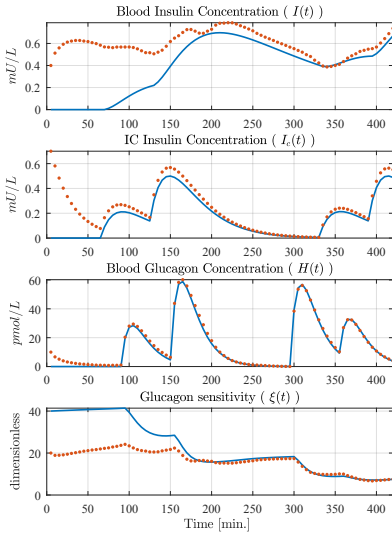


Fig. 3. Case 1: Performance of the designed observer with  $\varepsilon_1 = 0.9$  and  $\varepsilon_2 = 0.9$ . The constant blue lines in this figure show the values of the states derived from the model, while the red dots are the outputs of the observers.

2 are shown, respectively. As can be seen, the estimations of the states using the designed observers converged to actual values values with a bounded error. It can be noted that the performance of the designed observers with the lower gains (case 2) were faster while error boundaries increased.

As can be deduced from Fig. 3 and Fig. 4, there is a trade-off in selecting the observer gain,  $\varepsilon$ . The switching-gain observer concept described in [11] was used to address this issue. Based on this concept, it is better to initially have a small observer gain since it allows the observer to converge faster. Then, the observer gain can take a larger value  $T_s$  min after  $\|y_m - \hat{y}_m\|$  enters the switching zone to reduce the observer error. Notably,  $T_s$  should be selected in a way to prevent repetitive switching. The conditions for choosing the switching zone and the switching time are defined in [11].

The estimation results of the designed observers based on switching-gain concept is presented in Fig. 5. The initial gain set,  $\varepsilon_1 = 0.32$  and  $\varepsilon_2 = 0.45$ , was switched to  $\varepsilon_1 = 0.9$  and  $\varepsilon_2 = 0.9$ ,  $T_s = 45$  min after entering the switching zone. As expected, the observers convergence rates were shorter than Case 1 while their errors are less than Case 2. Therefore, in general, the performance of the observer was improved.

V. DISCUSSION

The model used in designing the observer is a modification of the animal model presented in [8] which, according to the best knowledge of the authors, is the only available bi-hormonal IP model for control purposes. The performance of

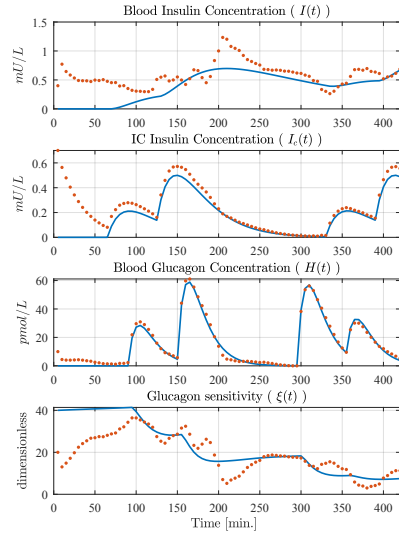


Fig. 4. Case 2: Performance of the designed observer with  $\varepsilon_1 = 0.32$  and  $\varepsilon_2 = 0.45$ . The constant blue lines in this figure show the values of the states derived from the model, while the red dots are the outputs of the observers.

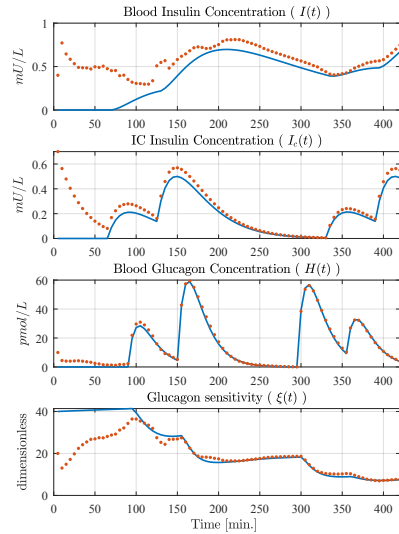


Fig. 5. Performance of the switching gain observer with  $\varepsilon_1 = 0.32$  and  $\varepsilon_2 = 0.45$  which switches to  $\varepsilon_1 = 0.90$  and  $\varepsilon_2 = 0.90$  at  $T_s = 140$  min. The constant blue lines in this figure show the values of the states derived from the model, while the red dots are the outputs of the observers.

the original model was tested on pigs. Due to the similarity between pigs and human physiology, the model can be used as an alternative for humans. However, the model's performance on T1D patients and consequently the performance of the designed observer can also be evaluated using human trials with realistic inputs.

In evaluating the performance of the observers, noise and the disturbances in measurements, as well as the 15% parameter identification error, were taken into account. The glucose appearance rate, on the other hand, was assumed to be known. However, as shown in (31) and (28), disturbance in  $R$  which can be due to an unannounced meal, is calculated in the observer error bound. Therefore, the observer will remain stable for adequately limited disturbances due to unannounced food intake.

## VI. CONCLUSIONS

Estimating non-measurable states in the bi-hormonal-glucose model provides a better understanding of the system status and improves the decision-making of a controller in AP. In this regard, two nonlinear high-gain observers were designed separately for the insulin and glucagon phases. It was mathematically shown that the observers are robust against measurement noises, model uncertainties, and disturbances and the closed-loop stability was proven for any asymptotically stable control approaches. Moreover, the simulation results, also confirmed the convergence of the observer to a bounded error. In addition, the performance of the observer was improved by utilizing the switching-gain approach. As a result, the intended observers can be employed in APs to help model-based controllers make better decisions. For example, whenever glucagon sensitivity is estimated to be low, the controller should be extra cautious about the dosage of insulin in order to prevent hypoglycemia.

## ACKNOWLEDGMENT

This research is funded by the Research Council of Norway (project no. 248872) and is part of the Centre for Digital Life Norway. We would like to thank Professor Jan Tommy Gravdahl for help in designing the observer and in the discussions.

## REFERENCES

- [1] A. Katsarou, S. Gudbjörnsdóttir, A. Rawshani, D. Dabelea, E. Bonifacio, B. J. Anderson, L. M. Jacobsen, D. A. Schatz, and Å. Lernmark, "Type 1 diabetes mellitus," *Nature reviews Disease primers*, vol. 3, no. 1, pp. 1–17, 2017.
- [2] P. Herrero, J. Bondia, N. Oliver, and P. Georgiou, "A coordinated control strategy for insulin and glucagon delivery in type 1 diabetes," *Computer methods in biomechanics and biomedical engineering*, vol. 20, no. 13, pp. 1474–1482, 2017.
- [3] C. Cobelli, E. Renard, and B. Kovatchev, "Artificial pancreas: past, present, future," *Diabetes*, vol. 60, no. 11, pp. 2672–2682, 2011.
- [4] S. J. Moon, I. Jung, and C.-Y. Park, "Current advances of artificial pancreas systems: A comprehensive review of the clinical evidence," *Diabetes & Metabolism Journal*, vol. 45, no. 6, pp. 813–839, 2021.
- [5] C. Toffanin, L. Magni, and C. Cobelli, "Artificial pancreas: In silico study shows no need of meal announcement and improved time in range of glucose with intraperitoneal vs. subcutaneous insulin delivery," *IEEE Transactions on Medical Robotics and Bionics*, vol. 3, no. 2, pp. 306–314, 2021.
- [6] C. D. Man, F. Micheletto, D. Lv, M. Breton, B. Kovatchev, and C. Cobelli, "The uva/padova type 1 diabetes simulator: new features," *Journal of diabetes science and technology*, vol. 8, no. 1, pp. 26–34, 2014.
- [7] B. W. Bequette, "Algorithms for a closed-loop artificial pancreas: the case for model predictive control," *Journal of diabetes science and technology*, vol. 7, no. 6, pp. 1632–1643, 2013.
- [8] C. Lopez-Zazueta, A. L. Fougner *et al.*, "Low-order nonlinear animal model of glucose dynamics for a bihormonal intraperitoneal artificial pancreas," *IEEE Transactions on Biomedical Engineering*, 2021.
- [9] V. Claassen, "Intraperitoneal drug administration," *Neglected factors in pharmacology and neuroscience research*, vol. 12, pp. 46–58, 1994.
- [10] H. K. Khalil and L. Praly, "High-gain observers in nonlinear feedback control," *International Journal of Robust and Nonlinear Control*, vol. 24, no. 6, pp. 993–1015, 2014.
- [11] J. H. Ahrens and H. K. Khalil, "High-gain observers in the presence of measurement noise: A switched-gain approach," *Automatica*, vol. 45, no. 4, pp. 936–943, 2009.
- [12] K. D. Benam, H. Talebi, and M. A. Khosravi, "Full order high gain observer design for image-guided robotic flexible needle steering," in *2019 27th Iranian Conference on Electrical Engineering (ICEE)*. IEEE, 2019, pp. 1151–1156.

## 6.2 PAPER 2

**Title: “Identifiable prediction animal model for the bi-hormonal intraperitoneal artificial pancreas”**

Published in Journal of Process Control, Volume 121, January 2023 [2].

**Errata:**

In equation (14b): the extra  $x_5$  in the 7th state must be removed since it is already included in  $HFP_{meta}$ . The equation must be as follows.

$$\frac{d}{dt} \begin{pmatrix} x_1 \\ x_2 \\ x_3 \\ x_4 \\ x_5 \\ x_6 \\ x_7 \end{pmatrix} = \begin{pmatrix} -(\beta_1 + \beta_2 \cdot x_2 + \beta_3 \cdot x_3) \cdot x_1 + HGP_{meta} \\ \beta_5 (-x_2 + (\beta_7 \cdot \gamma_1(\omega) \cdot x_4 - F_{sat})) \\ \beta_8 (-x_3 + F_{sat}) \\ -\gamma_1(\omega) \cdot x_4 \\ \beta_9 (-x_5 + \beta_{10} x_6) \\ -\gamma_2(\omega) \cdot x_6 \\ \gamma_3(\omega) \cdot x_3 \cdot x_1 - \gamma_4(\omega) \cdot HFP_{meta} / \beta_4 \end{pmatrix} + \begin{pmatrix} \gamma_7(\omega) R_g(t) \\ 0 \\ 0 \\ \gamma_8(\omega) I(t) \\ 0 \\ \gamma_9(\omega) H(t) \\ 0 \end{pmatrix} \quad (6.1)$$

In the paragraph before Equation (17): The unit for  $\gamma_4$  is  $[\sqrt{\%}/\mu g]$ .

$\gamma_7$  (instead of  $\gamma_5$ ) is a coefficient directly related to the concentration of IV glucose infusion and inverse to the body weight. In addition,  $\gamma_8(\omega)^{-1}$  and  $\gamma_9(\omega)^{-1}$  (instead of  $\gamma_6(\omega)^{-1}$  and  $\gamma_7(\omega)^{-1}$ ) are the volumes of peritoneal fluid in which insulin and glucagon are dissolved.

Table 1: The unit for  $\beta_7$  is [mL] (not 1/mL).





Contents lists available at ScienceDirect

Journal of Process Control

journal homepage: [www.elsevier.com/locate/jprocont](http://www.elsevier.com/locate/jprocont)

# Identifiable prediction animal model for the bi-hormonal intraperitoneal artificial pancreas

Karim Davari Benam<sup>a,\*</sup>, Hasti Khoshamadi<sup>a</sup>, Marte Kierulf Åm<sup>b</sup>, Øyvind Stavdahl<sup>a</sup>, Sebastien Gros<sup>a</sup>, Anders Lyngvi Fougner<sup>a</sup>

<sup>a</sup> Department of Engineering Cybernetics, Faculty of Information Technology and Electrical Engineering, Norwegian University of Science and Technology (NTNU), O. S. Bragstads Plass 2D, 7034 Trondheim, Norway

<sup>b</sup> Department of Clinical and Molecular Medicine, Faculty of Medicine and Health Sciences, Norwegian University of Science and Technology (NTNU), Erling Skjalgsons Gate 1, 7491 Trondheim, Norway

## ARTICLE INFO

### Article history:

Received 24 December 2021

Received in revised form 15 November 2022

Accepted 18 November 2022

Available online 8 December 2022

### Keywords:

Bi-hormonal artificial pancreas

Biological system modeling

Biological systems

Diabetes

Parameter identification

## ABSTRACT

To achieve a fully automatic artificial pancreas (AP), i.e., an AP without the need for meal announcements, the intraperitoneal (IP) route is explored. This route has faster dynamics than the typical subcutaneous (SC) route. Model predictive control (MPC) is the most promising control algorithm, but it requires a predictive and identifiable model. This paper presents the design of such a model for MPC-based dual hormone IP APs. This model is trained and tested on recorded data from anesthetized pigs. Animal experiments show that the saturation of the hepatic first-pass effect is essential in how IP insulin and IP glucagon affect glucose levels. These physiological phenomena must be modeled to estimate the system behavior for various conditions. This, in turn, increases the number of parameters and complicates system identification. The availability of rich experimental data from 26 animal trials motivated the design of a technique to exploit this prior information to ensure the identifiability of our model. Through this technique, most parameters were either modeled as body weight functions or common among animals. The correlation between parameter values and body weight is discovered utilizing prior data from various animal experiments, such as blood glucose, plasma insulin, and glucagon levels, in which hormones were administered intraperitoneally or intravenously. This method simplifies the system identification for every new subject while keeping the model's essential details that improve the prediction capability relative to comparable models. The model can be exploited in MPC or any other model-based controller of a bi-hormonal IP AP. It can also be used as a simulator to develop control approaches for single and bi-hormonal IP APs.

© 2022 The Author(s). Published by Elsevier Ltd. This is an open access article under the CC BY license (<http://creativecommons.org/licenses/by/4.0/>).

## 1. Introduction

Type 1 diabetes mellitus (T1DM) is potentially a life-threatening illness in which the pancreas produces little or no insulin [1]. Frequently even glucagon production is impaired [2]. Insulin is the essential hormone to reduce blood glucose levels (BGL) by enabling cellular glucose uptake. The cells either use glucose as an energy source or store it as glycogen, e.g., the liver and skeletal muscle cells. In contrast, glucagon triggers glycogenolysis, a process that involves converting stored glycogen to glucose, releasing it into the bloodstream, and thus raising the BGL.

External insulin therapy is the current solution to control the BGL in T1DM patients. Generally, patients estimate the required

amount of insulin based on their body weight, activity level, and lifestyle. Once the insulin bolus is calculated, they infuse insulin subcutaneously (SC). In an intensive care unit, it can be infused intravenously (IV), but the SC route is the standard in T1DM patients.

Nowadays, the calculations of the required insulin can be made by a device called the artificial pancreas (AP). An AP consists of an insulin pump, BGL sensors, and a control algorithm that calculates the amount of required insulin based on the patient's BGL profile and physical characteristics. The commercially available APs are discussed by Moon et al. [3] and Cobelli et al. [4].

When insulin is delivered via the IV route, as shown in Fig. 1, it is distributed throughout the body by blood circulation. Despite the quickness and reliability of the IV route, blood clots and catheter-related problems make it unsuitable for continuous insulin infusions. The SC route is safer and less invasive than the IV route [4]. Therefore, continuous subcutaneous insulin infusion (CSII) has become a widely used solution since the 1990s, and

\* Corresponding author.

E-mail addresses: [karim.d.benam@ntnu.no](mailto:karim.d.benam@ntnu.no) (K.D. Benam), [hasti.khoshamadi@ntnu.no](mailto:hasti.khoshamadi@ntnu.no) (H. Khoshamadi), [marte.k.am@ntnu.no](mailto:marte.k.am@ntnu.no) (M.K. Åm), [oyvind.stavdahl@ntnu.no](mailto:oyvind.stavdahl@ntnu.no) (Øy. Stavdahl), [sebastien.gros@ntnu.no](mailto:sebastien.gros@ntnu.no) (S. Gros), [anders.fougner@ntnu.no](mailto:anders.fougner@ntnu.no) (A.L. Fougner).

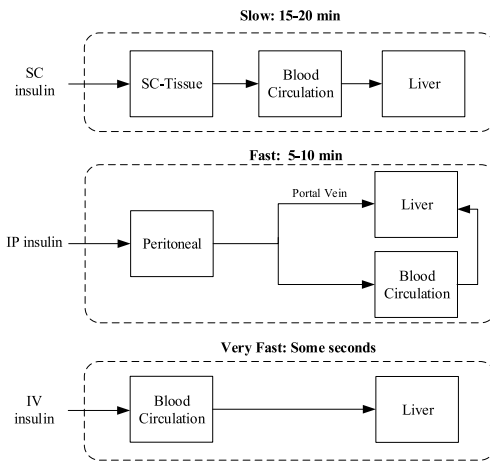


**Fig. 1.** Comparison of the time delays and pharmacokinetics block diagram of the SC, IP, and IV insulin administration. Notice that the HFP is saturated at greater insulin concentrations, and insulin enters the blood circulation system again by bypassing the liver.

advances in the safety and accuracy of the SC pumps and BGL sensors have improved the diabetes management.

Due to the intrinsic delay in the SC route and the slow dynamics of insulin absorption, no matter how advanced the control algorithms are, there is always a trade-off between the performance of the controllers and the risk of hypoglycemia episodes. The slow dynamics and delay can cause oscillations, especially if the control algorithm is aggressive (high gain). It requires precise control tuning to achieve a fully automated AP without meal announcement. Therefore, in commercially available single-hormonal APs, the carbohydrate content of each meal must be estimated and announced to the AP ahead of time [5].

In addition, CSII delivers insulin to the entire body in equal concentrations, whereas the primary target organ of insulin is the liver. Under normal conditions, insulin is secreted from the pancreas and transported directly to the liver via the portal vein (PV). The insulin concentration is consequently much higher in the liver than in the rest of the body. However, the non-physiological nature of CSII leads to a high concentration of insulin in peripheral tissues, which impacts the BGL control quality.

An alternative and feasible approach for delivering drugs to the liver is to deposit the drug into the peritoneal cavity [6–8]. The peritoneal cavity is a space within the abdomen enclosed by the peritoneal lining. It is lubricated by a small volume of peritoneal fluid that facilitates movements of the abdominal organs [9]. Although the peritoneal cavity is small in volume, it has a large surface area and the blood vessels within the lining, together with the blood vessels from the intestines, drain into the liver via the PV. Drug injections via this route are called intraperitoneal (IP) injections.

In addition to mimicking normal pancreatic function with IP injections, this route has significant control benefits, such as faster insulin appearance in the blood due to a higher absorption rate and also faster insulin disappearance rate due to the hepatic first-pass (HFP) effect [10]. The current challenges and solutions of using the IP route are discussed in [5].

Our recent animal studies revealed nonlinear insulin pharmacokinetics and pharmacodynamics behavior of IP route [11]. These results showed that insulin boluses of less than 0.125 U/kg

rapidly affect BGL without causing a significant change in plasma insulin levels (PIL). However, despite a slight extra reduction in BGL, a substantial increase in PIL is found for greater IP insulin boluses. Unlike the IP injections, a dose-dependent relation between insulin dosage and the PIL is observed following SC administration.

These findings are consistent with saturation of the HFP effect, which holds that when insulin concentration in the PV exceeds a certain level, insulin clearance in the liver becomes saturated. As a result, more insulin enters the general blood circulation. Additionally, the insulin effect in the liver is not proportional to the size of the insulin boluses; following a large insulin bolus, the liver's capacity to absorb glucose is saturated. Therefore, the saturation of the HFP effect must be modeled to predict the body's behavior for different insulin bolus sizes.

Taking full advantage of the IP pathways in the AP systems necessitates having a mathematical model. This paper proposes a model to describe IP insulin and glucagon interaction with the BGL. The model aims to be used in APs with model-based control techniques like model predictive control (MPC). Therefore, the model should track the measured data and have a high performance in predicting future BGL. In addition, the parameters must be identifiable, and the system identification procedure must be feasible and noninvasive. It is helpful to have a short identification phase since then; one can rapidly start automated glucose management and reduce the patient involvement in glycemic control. It may be even more critical to have a short identification phase in animal experiments since it is desirable to decrease the duration of these experiments. Therefore, the model is designed with a minimum number of parameters and states necessary for mimicking the real-life behavior of the body's response to IP insulin and glucagon.

In summary, the main aim of this paper is to design a model for blood glucose prediction with IP insulin and IP glucagon with a few parameters to use in model-based control.

The proposed model extends our previous model [12] by including the HFP effect and improvement of the glucagon sensitivity sub-model. The modifications improve the model to predict the response to a wide range of insulin and glucagon boluses. In addition, to overcome the identifiability issues and ease the identification procedure, a novel method based on physiological and practical assumptions is proposed. In this method, called "meta-model identification", one could split the model's parameters into the population and individual parameters. Population parameters are a set of parameters that are functions of body weight or common among individuals/animals, and individual parameters are the parameters that vary from subject to subject. The proposed method enables us to split the invasive sets of excitation and measurements among several animal experiments instead of performing them on each animal. Notably, the population parameters are found using prior information. For every new subject, there is only a need to identify five individual parameters without an invasive excitation.

Using data from several animal experiments, we showed that the proposed model could satisfactorily reproduce the behavior of glucose metabolism in response to a wide range of insulin and glucagon boluses. Furthermore, the new model outperforms other comparable models in prediction performance, which is a crucial feature for the closed-loop performance of MPC-based methods.

The paper is structured as follows. Animal care and surgical procedures are described in Section 2, while pharmacokinetics and pharmacodynamics of insulin and glucagon are modeled in Section 3. We provide identification method and meta-model designation in Section 4. The utilized data sets and evaluation tools are described in Section 5, and the destined model is trained in Section 6. Using the test data, the performance of the proposed model in fitting to the measurements and prediction is compared with other models in Sections 7 and 8, respectively. The conclusions and discussions are provided in Section 9.

## 2. Methods

This section provides an overview of animal experiments and clinical procedures. The procedures are described in more detail in [11,13].

### 2.1. Ethical approval

The Norwegian Food Safety Authority (FOTS number 12948) approved the animal experiments, which were carried out in accordance with “The Norwegian Regulation on Animal Experimentation” and “Directive 2010/63/EU on the protection of animals used for scientific purposes”.

### 2.2. Animals and animal handling

The tests were carried out on 29 non-diabetic farm pigs (*Sus scrofa domestica*) that weighed 30–63 kg. Before the experiments, the animals were given a week to get used to the staff and their new surroundings. The animals were kept together in groups whenever possible. They were fed commercial growth feed twice a day and given unlimited water access.

### 2.3. Anaesthesia

The anesthesia procedure, the drugs used in this procedure, and the environmental factors are described in [11,13] in detail.

### 2.4. Surgical procedure

A venous line for fluid infusion was established in the left internal jugular vein, and the left carotid artery was cannulated for blood sampling and monitoring of physiological parameters. The same cut-down was used to insert both catheters. The catheters from the insulin and glucagon pumps were connected at the end and inserted 10–15 cm into the upper left part of the abdomen through a 2–3 cm long craniocaudal incision in the abdominal wall, 2–3 cm caudally to the umbilicus. The pigs were euthanized with an IV overdose of pentobarbital (minimum 100 mg/kg)(pentobarbital NAF, Apotek, Lørenskog, Norway) at the end of the experiments while fully anesthetized.

### 2.5. Suppression of endogenous insulin and glucagon secretion

Twenty pigs were given IV boluses of 0.4 mg octreotide (Sandostatin 200 g/ml, Novartis Europharm Limited, United Kingdom) every hour and SC injections of 0.3 mg pasireotide (Signifor 0.3 mg/ml, Novartis Europharm Limited, United Kingdom) every three hours to inhibit endogenous insulin and glucagon secretion. The remaining pigs received octreotide as a 5 g/kg/h infusion and no pasireotide injections.

### 2.6. Measurements

PHL was analyzed with Glucagon ELISA (10-1281-01 Mercodia, Uppsala, Sweden), and PIL was analyzed with Porcine Insulin ELISA (10-1200-01, Mercodia, Uppsala, Sweden). The assay ranges for the glucagon and porcine insulin ELISA kits were 2–172 pmol/l and 2.3–173 mU/l, respectively. Blood glucose was analyzed on a Radiometer ABL 725 blood gas analyzer (Radiometer Medical ApS, Brønshøj, Denmark).

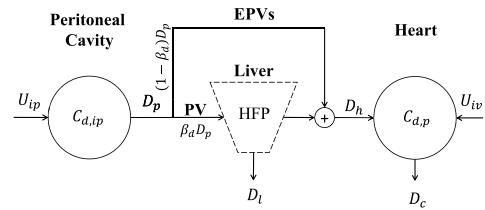


**Fig. 2.** Block diagram of the proposed IP drug pharmacokinetics. The IP and IV drug administration rates are denoted by  $U_{ip}$  and  $U_{iv}$ , respectively.  $C_{d,ip}$  and  $C_{d,p}$  are the drug concentrations in the peritoneal cavity and plasma, respectively. The portal vein (PV) and extra portal veins (EPVs) transport the drug (at a rate of  $D_p$ ) from the peritoneal cavity to the liver and heart. In the liver, the drug undergoes the hepatic first-pass (HFP) effect, and a portion of it (at a rate of  $D_i$ ) is removed from the blood. The remaining drug (at a rate of  $D_h$ ) enters the heart and is cleared from the plasma at a rate equal to  $D_c$ .

## 3. Background and model development

From the pharmacokinetics point of view, drugs deposited in the IP cavity are absorbed by the surrounding capillaries and transported to other organs via blood circulation [14]. The capillaries in the vicinity of the peritoneum can be divided into two groups, (a) capillaries emptying compounds into the PV and (b) capillaries draining into the extra-portal veins (EPVs). The PV carries blood from the stomach, intestines, spleen, and pancreas to the liver and is essential in transferring insulin and glucagon from the pancreas to the liver in the body. The EPVs go directly to the heart. Notably, drugs absorbed into the PV and transported to the liver are subject to the HFP effect, and a significant portion is cleared from the blood before reaching the systemic circulation.

From the pharmacodynamics point of view, the liver can store glucose as glycogen in quantities of up to 6% of its weight, which equates to 100–120 g glycogen for a 70 kg male. Other organs, such as skeletal muscles, kidneys, and lungs, may not substantially influence the BGL, but their cumulative impact is comparable to that of the liver. For example, skeletal muscle glycogen storage can amount to 2% of their weight, allowing for a total of 400 g of glycogen storage in the muscles of the body as a whole [15,16]. Therefore, the liver and other organs' cumulative pharmacodynamics must be modeled separately to describe the effect of insulin.

In the following sections, the mathematical models of the pharmacokinetics and pharmacodynamics of insulin and glucagon are described.

### 3.1. IP insulin and glucagon pharmacokinetics

To simulate the pharmacokinetics of insulin and glucagon in the body, one should model the concentration dynamics of these drugs in peritoneal fluid, the quantity of the drugs entering the liver and the heart, and the concentration of the drug in plasma. The equations are given in the following sections, and the block diagram of the proposed IP pharmacokinetics is presented in Fig. 2.

#### 3.1.1. Concentration of the drugs in peritoneal fluid

The IP cavity fluid is where the drugs are administered, and drug dissemination relies on its dynamics. Similarly to Canal et al. [17] and Zazueta et al. [12], we modeled the concentration of the drugs (i.e., insulin or glucagon) in the peritoneal cavity as a linear system as follows:

$$\dot{C}_{d,ip} = -k_{d_1} \cdot C_{d,ip} + \frac{U_{ip}}{V_{d,ip}} \quad (1)$$



where  $C_{d,ip}$  [mass/ml] is the concentration of drugs in the peritoneal fluid,  $U_{ip}$  [mass/min] is the mass rate of drug injection,  $V_{d,ip}$  [ml] is the volume of the peritoneal fluid, and  $k_{d_1}$  [ $\text{min}^{-1}$ ] is the diffusion rate of the drug from the peritoneal cavity to capillaries. From (1) one can conclude that

$$D_p \triangleq k_{d_1} V_{d,ip} C_{d,ip} \quad (2)$$

is the rate at which the mass of a drug escapes from the peritoneal cavity and gets absorbed into the capillaries that surround the peritoneal cavity.

### 3.1.2. Mass rate of drug entering to liver

A sizeable portion of  $D_p$  eventually drains into the PV, and the rest goes to the heart via EPVs [14]. As shown in Fig. 2, the PV supplies blood from the abdominal organs to the liver, where the main metabolism of glucose takes place. The drug mass rate entering the PV can be defined as  $\beta_d D_p$  where  $0 < \beta_d \leq 1$  is the ratio of drug drained into the PV to the total amount of drug that is absorbed from the peritoneal cavity.

Notably, the HFP effect becomes saturated for a high IP insulin bolus, and the liver cannot remove the drug from the blood in the PV. We used the model suggested in [18] to model the hepatic drug clearance rate and its saturation as follows.

$$D_l = k_{d_2} \frac{\beta_d D_p}{k_{d_3} + \beta_d D_p} \quad (3)$$

where  $D_l$  is the liver clearance rate,  $k_{d_2}$  [mass/min] is the maximum drug clearance rate of the liver, and  $k_{d_3}$  [mass/min] is the half-saturation constant in the liver response function [19].

### 3.1.3. Mass rate of drugs entering to heart

The drug bypassing the HFP effect or absorbed into the EPVs will ultimately reach the heart and spread throughout the body. Therefore, the drug mass rate entering the heart,  $D_h$ , can be found as follows.

$$D_h = D_p - D_l \quad (4)$$

### 3.1.4. Concentration of drugs in plasma

The quantity of drugs available to the different tissues in the body is dissolved in blood plasma. In addition, the concentration of the drug in the blood is a measurable quantity modeled as follows in this paper.

$$\dot{C}_{d,p} = -k_{d4} C_{d,p} + (U_{iv} + D_h) / V_{d,p} \quad (5)$$

where  $C_{d,p}$  is the concentration of drugs in plasma [mass/l],  $U_{iv}$  is IV drug infusion rate [mass/min], and  $k_{d4}$  is the clearance rate of the drug from plasma [ $\text{min}^{-1}$ ], and  $V_{d,p}$  is the volume of the plasma that the drug is solved in [l]. Notably,  $D_c \triangleq V_{d,p} k_{d4} C_{d,p}$  is the drug mass clearance rate from plasma [mass/min].

Please note that peritoneal fluid in people ranges from 50 to 75 ml [20], whereas a 70 kg man's blood volume is 5.81 l [21]. In order to avoid showing low values for  $V_{d,ip}$ , or large values for blood volume, we choose to measure  $V_{d,ip}$  in milliliters and the blood volumes in liters.

### 3.1.5. Summary of the proposed pharmacokinetics model

In summary, a general model for the pharmacokinetics of IP and IV administrations is developed. For insulin and glucagon injections, one needs to replace  $d$  with  $\{i: \text{insulin, and } h: \text{glucagon}\}$  in the notations. The unit [mass] must also change with [U] and [ $\mu\text{g}$ ] for insulin and glucagon, respectively. Notably, mg is the most common unit for glucagon. However, in our animal experiments, due to the size of the pigs, glucagon injection doses were mainly in the range of 0 to 150  $\mu\text{g}$ . Therefore,  $\mu\text{g}$  is chosen as the mass unit for the glucagon in this paper.

The block diagram and the equations are summarized in Figs. 2 and 3. In the next section, the effects of both insulin and glucagon on BGL are modeled using the proposed pharmacokinetics model.

## 3.2. IP insulin and glucagon pharmacodynamics

The purpose of this section is to model the reaction of the organs receiving insulin and glucagon.

### 3.2.1. Effective insulin in liver

In this study, it is assumed that the rate of glucose absorption in the liver is proportional to the quantity of insulin taken up by the liver cells. The liver will then take up glucose based on the insulin sensitivity of the cells and the amount of glucose in the blood. For the sake of simplicity, the amount of insulin taken up by the liver cells is called effective insulin.

To develop a mathematical model for the effective insulin rate in the liver, we assume it is a linear system that responds to the rate at which the liver absorbs insulin from the PV. Since there is a saturation in the insulin uptake from the PV, the effective insulin in the liver will also be saturated for higher amounts of insulin. Therefore, using (1) and the HFP saturation (see Eq. (3)), the concentrations of insulin in the IP cavity and the effective insulin in the liver are modeled as follows:

$$\dot{E}_{i,l} = \frac{1}{\tau_l} \left( -E_{i,l} + k_{i_2} \frac{\beta_i V_{i,ip} k_{i_1} C_{i,ip}}{k_{i_3} + \beta_i V_{i,ip} k_{i_1} C_{i,ip}} \right) \quad (6)$$

$$\dot{C}_{i,ip} = -k_{i_1} C_{i,ip} + \frac{I}{V_{i,ip}} \quad (7)$$

where  $E_{i,l}$  is the effective insulin rate in the liver [U/min],  $C_{i,ip}$  is the concentration of insulin in the peritoneal fluid [U/ml],  $\tau_l$  is the liver response time to insulin [min], and  $I$  is the rate of insulin infusion into the peritoneal cavity [U/min]. In addition,  $k_{i_1}$ ,  $k_{i_2}$  and  $k_{i_3}$  are diffusion rates of the drug from the peritoneal cavity to capillaries [ $\text{min}^{-1}$ ], maximum insulin clearance rate of the liver from blood [U/min], and half-saturation of the insulin HFP effect [U/min], respectively.

### 3.2.2. Effective insulin in the extra hepatic organs

The amount of insulin that reaches the heart is distributed throughout the systemic circulation and to the other organs. For a model developed for control purposes, describing the insulin action in each of these organs is not advisable since it introduces more parameters to the model. Therefore, this paper modeled the cumulative effective insulin in body organs (other than the liver), where effective insulin in body organs is the amount of insulin absorbed by the insulin receptors.

$$\dot{E}_{i,b} = \frac{1}{\tau_b} \left[ -E_{i,b} + \left( V_{i,ip} k_{i_1} - k_{i_2} \frac{\beta_i V_{i,ip} k_{i_1}}{k_{i_3} + \beta_i V_{i,ip} k_{i_1} C_{i,ip}} \right) C_{i,ip} \right] \quad (8)$$

where  $E_{i,b}$  is the effective insulin rate in the body organs other than the liver [U/min] and  $\tau_b$  is the body response time to insulin [min].

### 3.2.3. Effective glucagon

Similar to the insulin sub-model, the effective glucagon in the liver is defined as the number of cells allowed by glucagon to break down glycogen. Notably, the amount of released glucose depends not only on the number of cells receiving glucagon but also on the amount of glycogen stored mainly in the liver or possibly other organs. The cumulative effective glucagon is only considered in the liver to simplify the model and reduce the number of parameters. Additionally, to account for unmodeled glycogenolysis in other organs, we assume that the liver is a linear system that responds proportionally to the amount of glucagon

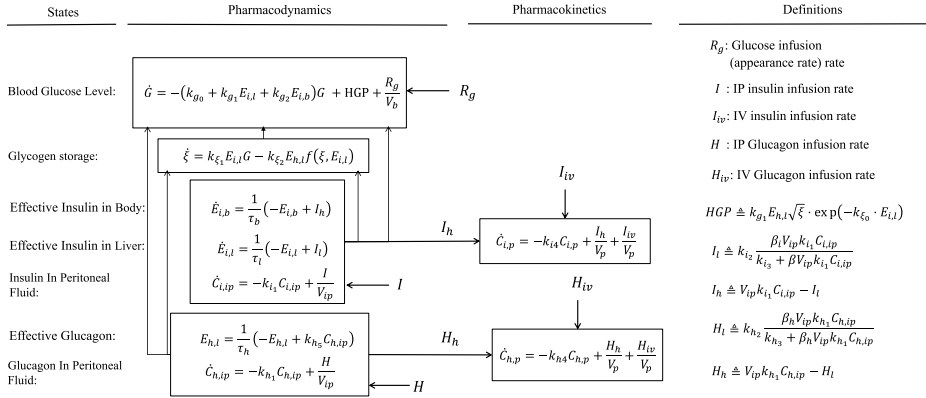


**Fig. 3.** Diagram and equations summary of the proposed model. In this model, inputs are IP insulin ( $I$ ), IP glucagon ( $H$ ), IV insulin ( $I_{iv}$ ), and IV glucagon ( $H_{iv}$ ). Outputs of the model are blood glucose level ( $G$ ), the concentration of insulin in plasma ( $C_{i,p}$ ), and the concentration of glucagon in plasma ( $C_{h,p}$ ). In addition,  $E_{i,j}$  are the effective drug ( $d \in \{i: \text{insulin}, h: \text{glucagon}\}$ ) in the compartments  $j \in \{l: \text{liver}, b: \text{body organs}\}$ . Moreover,  $\xi$  is the glycogen storage level. The rest of the variables are the constant parameters defined in Section 3.

absorbed from the peritoneal cavity without taking the HFP effect into account. The effective glucagon rate is modeled as follows:

$$\dot{E}_{h,l} = \frac{1}{\tau_h} (-E_{h,l} + k_{h5} C_{h,ip}) \quad (9)$$

$$\dot{C}_{h,ip} = -k_{h1} C_{h,ip} + \frac{H}{V_{h,ip}} \quad (10)$$

where  $H$  is the rate of IP glucagon infusion [ $\mu\text{g}/\text{min}$ ],  $C_{h,ip}$  is the concentration of glucagon in the peritoneal fluid [ $\mu\text{g}/\text{ml}$ ],  $E_{h,l}$  is the effective glucagon rate in the liver [ $\mu\text{g}/\text{min}$ ]. Parameters  $k_{h1}$  and  $\tau_h$  are, respectively, the glucagon diffusion rate from the peritoneal cavity to the capillaries [ $\text{min}^{-1}$ ] and the response time of the body to glucagon [ $\text{min}$ ]. Furthermore,  $k_{h5}$  is a constant parameter [ $\text{ml}/\text{min}$ ].

### 3.2.4. Mathematical model for hepatic glucose production rate

Glycogenolysis is the liver's process of producing glucose in response to effective glucagon. The experiments showed that the amount of glucose produced depends on the effective glucagon, insulin, and glycogen stored in the liver.

According to the literature, glycogen is predominantly stored in the cytoplasm of hepatocytes. Zazueta et al. [12] described glycogenolysis sensitivity to glycogen storage level as a linear function. Notably, a high glycogen storage level does not necessarily result in increased glucose production because the glucagon may not diffuse to all liver cells simultaneously, and the liver's glycogenolysis rate can be subjected to saturation. In addition, one can assume that having insulin in the liver decreases glycogenolysis. To account for these assumptions, we define the hepatic glucose production rate as follows.

$$HGP \triangleq k_{g3} \cdot E_{h,l} \cdot \sqrt{\xi} \cdot \exp(-k_{\xi_0} \cdot E_{i,l}) \quad (11)$$

where HGP [ $\text{mmol}/\text{l}/\text{min}$ ] is the hepatic glucose production rate,  $\xi \in [0 - 100]\%$  is liver glycogen storage level modeled as described in (12). The term  $\sqrt{\xi}$  refers to the saturation of the liver in terms of glucose production,  $k_{\xi_0}$  [ $\text{min}/\text{U}$ ] is a constant parameter describing the negative influence of effective insulin rate in the liver on glucose production rate, and  $k_{g3}$  is a coefficient

describing the sensitivity of liver cells to effective glucagon in the liver, glycogen storage level, and effective insulin in the liver [ $\frac{\text{mmol}}{\text{l} \cdot \sqrt{\%} \cdot \mu\text{g}}$ ].

### 3.2.5. Glycogen storage level

We assume that glucose absorbed by the liver is stored as glycogen and thus increases glycogen storage level, whereas hepatic glucose production decreases glycogen storage level. With these assumptions and using (13), one can model the dynamics of the liver glycogen storage level for  $\xi(t_0) \in [0, 100]\%$  as follows.

$$\dot{\xi} = \begin{cases} k_{\xi_1} E_{i,l} G - \frac{k_{\xi_2}}{k_{g3}} HGP & \xi \in [0, 100]\% \\ 0 & \text{otherwise} \end{cases} \quad (12)$$

where  $k_{\xi_1}$  [ $\% \cdot \text{l}/\text{mmol}/\text{U}$ ] and  $k_{\xi_2}$  [ $\sqrt{\%}/\mu\text{g}$ ] are constant values representing the charging and discharging rates of the glycogen storage. One can assume that these parameters are proportional to the weight of the liver. In addition,  $G$  is BGL defined in (13). Notably, the term  $k_{\xi_1} E_{i,l} G$  is proportional to the rate of glucose that liver uptakes.

### 3.3. Blood glucose dynamics

Using the proposed sub-models for insulin and glucagon in the body, it is now possible to model the aggregated effect of insulin and glucagon on the BGL. To achieve this, we employed the following equation.

$$\dot{G} = -(k_{g0} + k_{g1} \cdot E_{i,l} + k_{g2} \cdot E_{i,b}) \cdot G + HGP + R_g(t)/V_b \quad (13)$$

where  $G$  is the blood glucose level [ $\text{mmol}/\text{l}$ ],  $R_g(t)$  is the glucose appearance rate due to meal digestion [ $\text{mmol}/\text{min}$ ], and  $V_b$  [ $\text{l}$ ] is the volume of the blood circulating in the body.  $k_{g0}$  is the insulin-independent glucose uptake rate [ $\text{min}^{-1}$ ] (e.g., brain glucose uptake rate).  $k_{g1}$ , and  $k_{g2}$  are the sensitivity rates of the subjects to effective insulin in liver [ $\text{U}^{-1}$ ], and in the organs other than liver [ $\text{U}^{-1}$ ], respectively.

### 3.4. Summary of model development

An overview of the proposed mathematical model of the pharmacokinetics and pharmacodynamics for both IP insulin and glucagon infusions is shown in Fig. 3. The challenges of the parameter identification for the proposed model are explored in the next section.

## 4. Practical techniques to ensure identifiability and reduce the time needed to identify the parameters

In order to use the model for control purposes, we must ensure that the parameters of the model are identifiable in two ways:

1. **Structural identifiability:** The necessary condition for having structurally identifiable parameters is to have no redundant parameters in the model. Otherwise, there will be a set of parameters that may vary without changing the output. Therefore, the parameters are not uniquely identified [22].
2. **Practical identifiability:** The data used to estimate the parameters provides sufficient information, making it practically possible to identify them. The amount of data required for a reliable estimation of the parameters typically increases with the number of parameters. In addition to the amount of data, we must ensure that the inputs are rich enough to excite the system dynamics [22]. For example, different insulin bolus sizes must be injected to capture the dynamics of the HFP and the insulin pharmacodynamics.

It is worth highlighting that, from a control perspective, the short identification tests and the procedures are desirable because one can start the closed-loop system shortly. However, to excite all the system dynamics in a short time window, one needs extreme inputs, which can be dangerous and invasive.

One solution to increase the identifiability and shorten the identification phase is to embed prior physiological knowledge in the parameter identification process. For example, the model is based on body physiology and drug concentrations in compartments; some parameters strongly correlate to the compartment volume and the body weight. Therefore, we can use past data from different animals to estimate these relationships and embed them in the system identification procedure.

In addition, an easy step in addressing the structural non-identifiability issue is to model additional physical quantities that can be measured. PIL and PHL are two physical quantities that can be measured by taking blood samples and analyzing them in laboratories. However, these measurements are not real-time.

One can use the PIL and PHL measurements to find the parameters correlated to body weight or constant across the subjects in a post-processing manner. For simplicity, one can assume that the observed correlation between body weight and the selected parameters applies generally, and one can extrapolate from these data to all subjects.

Additionally, by combining the PIL and PHL measures with the IV injections, it may be possible to increase identifiability. This is achievable because adding the IV injections to the identification procedure results in a new map from a new input to states while maintaining the original mapping of states to outputs. Consequently, it can increase structural identifiability [22].

Another way to improve identifiability is to use the literature to find the values for the parameters based on the body's physiology. For example,  $V_b$  can be estimated using body weight, and gender [23,24]. These assumptions and information can help improve the model's practical and structural identifiability.

In summary, the following ideas are used in this study to solve the identifiability issues of the proposed model:

1. Perform specific experiments with frequent PIL and PHL measurements to improve the structural identifiability.
2. Perform specific experiments with IV insulin and glucagon boluses to excite dynamics in an efficient way.
3. Find the parameters that are dependent on body weight or are almost constant among subjects.
4. If available, look up the values of the physiology-based parameters in the literature.

In order to find the parameters that have the same values among the subjects or are correlated with body weight, a general model is needed to simulate several subjects together. To put the above concepts into action and analyze the information of different animals, we introduced the "meta-model". It is a generic model that allows us to examine a group of animals (subjects) linked by constant and weight-dependent parameters. Adding other features, such as gender, can also improve the model, but we did not include other features in this study. The meta-model is introduced in the next section.

### 4.1. Meta-model development

This section aims to expand the suggested model (summarized in Fig. 3) to simulate subjects in a population who share parameters related to body weight or that are constant across the population in order to apply the concepts discussed in the previous section. To this end, we categorize the parameters of the proposed model into four groups:

1. **Independent parameter:** A set of parameters that must be identified for each animal (subjects) separately. In this paper, we assumed that the initial values of the states  $\{x_1, \dots, x_7, z_1, z_2\}$  in Eqs. (14b) and (14a) belong to this set, and they are denoted by  $\mathbf{A} \triangleq \{\alpha_1, \alpha_2, \dots, \alpha_9\}$ . Notably, among parameters,  $\alpha_7$  has an essential role in the model since it is the initial glycogen storage level.
2. **Analogous parameters:** A set of parameters which consist of values similar across individuals. However, they must be identified individually, e.g., see the parameters in Eqs. (14a)–(14e) that are noted by  $\mathbf{B} \triangleq \{\beta_1, \beta_2, \dots, \beta_{19}\}$ .
3. **Weight-dependent parameters:** A set of parameters that depends on body weight. This parameter set is defined as  $\mathbf{\Gamma} \triangleq \{\gamma_1, \gamma_2, \dots, \gamma_9\}$  in the Eqs. (16) and (17).
4. **Constant parameters:** A set of parameters that have the same value for all animals in normal situations, e.g., see the parameters denoted by  $\mathbf{\Delta} \triangleq \{\delta_1, \delta_2, \dots, \delta_{15}\}$  in the Eqs. (16), (17), (14d), and (14e).

Using categories for the parameter sets described above, and the proposed model summarized in Fig. 3, a meta-model is introduced in (14a) and (14b) where the detailed comparison with the individual model is given in Table 1. Notably,  $\mathbf{X} \triangleq [G, A_{i,b}, A_{i,l}, C_{i,ip}, A_{h,l}, C_{h,ip}, \xi]^T$  is a vector including the necessary states for model base controllers. The state vector  $\mathbf{Z} \triangleq [C_{i,p}, C_{h,p}]^T$  contains the model of insulin and glucagon pharmacokinetics in the plasma. The model (14b) does not rely on the states of (14a) while it provides necessary information for controllers. Therefore, one may not consider (14a) in the controller (depending on how the complexity of the controller). However, using it in the identification can increase the identifiability of the (14b) because the two models share parameters and (14a) add two new measurable variables.

$$\frac{d}{dt} \begin{pmatrix} z_1 \\ z_2 \end{pmatrix} = \begin{pmatrix} -\beta_{12}z_1 + \beta_{13}(\gamma_5(\omega) \cdot x_4 - F_{sat}) \\ -\beta_{14}z_2 + \beta_{15}(\gamma_6(\omega) \cdot x_6 - F_{sat}) \end{pmatrix} + \frac{1}{\omega} \begin{pmatrix} \beta_{18} \cdot I_{iv}(t) \\ \beta_{19} \cdot H_{iv}(t) \end{pmatrix} \quad (14a)$$

**Table 1**  
Description of the states, inputs and parameters of the proposed meta-model (14b).

States	Units	Description
$x_1$	mmol/L	Blood Glucose Level ( $G$ )
$x_2$	U/min	Effective Insulin in Body ( $E_{i,b}$ )
$x_3$	U/min	Effective Insulin in Liver ( $E_{i,l}$ )
$x_4$	U/mL	Insulin in IP fluid ( $C_{i,ip}$ )
$x_5$	$\mu\text{g}/\text{min}$	Effective Glucagon in Body ( $E_{h,b}$ )
$x_6$	$\mu\text{g}/\text{mL}$	Glucagon in IP Fluid ( $C_{h,ip}$ )
$x_7$	%	Glycogen storage Level ( $\xi$ )
$z_1$	U/L	Insulin in Plasma ( $C_{i,p}$ )
$z_2$	$\mu\text{g}/\text{L}$	Glucagon in Plasma ( $C_{h,p}$ )
Inputs		
$R_g$	mmol/min	IV Glucose Infusion rate
$I(t)$	U/min	IP Insulin rate <sup>(*)</sup>
$I_{iv}(t)$	U/min	IV Insulin rate <sup>(*)</sup>
$H(t)$	$\mu\text{g}/\text{min}$	IP Glucagon rate <sup>(*)</sup>
$H_{iv}(t)$	$\mu\text{g}/\text{min}$	IV Glucagon rate <sup>(*)</sup>
Parameters		
$\omega, \omega_0$	kg	body weight, See Eq. (16)
$\beta_1$	$\text{min}^{-1}$	$k_{g0}$
$\beta_2, \beta_3$	$\text{U}^{-1}$	$k_{g1}, k_{g2}$
$\beta_4$	mmol/L/ $\mu\text{g}$	$k_{g3}$
$\beta_5, \beta_8, \beta_9$	$\text{min}^{-1}$	$\tau_b^{-1}, \tau_l^{-1}, \tau_h^{-1}$
$\beta_6, \beta_{13}$	U/min	$k_{h2}, k_{h3}$
$\beta_7, \beta_{10}$	1/mL, mL/min	$V_{i,ip}^{-1}, k_{h5}$
$\beta_{11}$	Dimensionless	$k_{\xi 0}$
$\beta_{12}, \beta_{14}$	$\text{min}^{-1}$	$k_{i4}, k_{h4}$
$\beta_{13}, \beta_{15}$	$\text{L}^{-1}$	See Eq. (16)
$\beta_{16}, \beta_{17}$	$\mu\text{g}/\text{min}, 1/\text{mL}$	$k_{h2}, V_{h,ip}^{-1}$
$\beta_{18}/\omega, \beta_{19}/\omega$	$\text{L}^{-1}$	$V_{h,p}^{-1}, V_{i,p}^{-1}$
$\delta_1, \delta_4, \delta_7$	— <sup>(**)</sup>	See Eq. (17)
$\delta_{2,3,5,6,8-11}$	— <sup>(**)</sup>	See Eq. (16)
$\delta_{12}, \delta_{14}$	Dimensionless	$\beta_i, \beta_h$
$\delta_{13,15}$	U/mL, $\mu\text{L}/\text{mL}$	$k_{i3}, k_{h3}$
$\alpha_7$	[0 – 100]%	$\xi(0)$

<sup>(\*)</sup> For simplicity, we assumed the insulin and glucagon boluses were given over 5 minute regardless of bolus size.

<sup>(\*\*)</sup> According to the given equations.

$$\frac{d}{dt} \begin{pmatrix} x_1 \\ x_2 \\ x_3 \\ x_4 \\ x_5 \\ x_6 \\ x_7 \end{pmatrix} = \begin{pmatrix} -(\beta_1 + \beta_2 \cdot x_2 + \beta_3 \cdot x_3) \cdot x_1 + HGP_{meta} \\ \beta_5 (-x_2 + (\beta_7 \cdot \gamma_1(\omega) \cdot x_4 - F_{sat})) \\ \beta_8 (-x_3 + F_{sat}) \\ -\gamma_1(\omega) \cdot x_4 \\ \beta_9 (-x_5 + \beta_{10} x_6) \\ -\gamma_2(\omega) \cdot x_6 \\ \gamma_3(\omega) \cdot x_3 \cdot x_1 - \gamma_4(\omega) \cdot x_5 \cdot HFP_{meta}/\beta_4 \end{pmatrix} + \begin{pmatrix} \gamma_7(\omega)R_g(t) \\ 0 \\ 0 \\ \gamma_8(\omega)I(t) \\ 0 \\ \gamma_9(\omega)H(t) \\ 0 \end{pmatrix} \quad (14b)$$

$$HGP_{meta} \triangleq \beta_4 x_5 \sqrt{x_7} \cdot \exp(-\beta_{11} \cdot x_3), \quad (14c)$$

$$F_{sat}(x_4) \triangleq \beta_6 \frac{\delta_{12} \gamma_5(\omega) x_4}{\delta_{13} + \delta_{12} \beta_7 \gamma_1(\omega) x_4}, \quad (14d)$$

$$\bar{F}_{sat}(x_6) \triangleq \beta_{16} \frac{\delta_{14} \gamma_6(\omega) x_6}{\delta_{15} + \delta_{14} \beta_{17} \gamma_2(\omega) x_6} \quad (14e)$$

In summary, the measurable outputs of the introduced meta-model are:

$$\begin{cases} y_1 \triangleq x_1, & \text{blood glucose level (BGL)} \\ y_2 \triangleq z_1, & \text{plasma insulin level (PIL)} \\ y_3 \triangleq z_2, & \text{plasma glucagon level (PHL)} \end{cases} \quad (15)$$

Here  $y_1$  is measured from all animal experiments, while  $y_2$  and  $y_3$  are available from some experiments. Furthermore, (14d) and (14e) are insulin and glucagon HFP effect saturation functions. Notably, we assume that the weight-dependent parameters are as follows:

$$\begin{cases} \gamma_1(\omega) \triangleq \delta_2 \cdot (1 + \delta_3 \cdot f_\omega(\omega)) \\ \gamma_2(\omega) \triangleq \delta_5 \cdot (1 + \delta_6 \cdot f_\omega(\omega)) \\ \gamma_3(\omega) \triangleq \delta_8 \cdot (1 + \delta_9 \cdot f_\omega(\omega)) \\ \gamma_4(\omega) \triangleq \delta_{10} \cdot (1 + \delta_{11} \cdot f_\omega(\omega)) \\ \gamma_5(\omega) \triangleq \beta_7 \cdot \delta_2 \cdot (1 + \delta_3 \cdot f_\omega(\omega)) \\ \gamma_6(\omega) \triangleq \beta_{17} \cdot \delta_5 \cdot (1 + \delta_6 \cdot f_\omega(\omega)) \end{cases} \quad (16)$$

where  $f_\omega(\omega) \triangleq (\omega/\omega_0 - 1)$  is the function describing the effect of body weight on the parameters,  $\omega$  is body weight, and  $\omega_0$  is the maximum body weight among the subjects, e.g., we chose  $\omega_0 = 52$  kg, which is the body weight of the Pig#6 since it was the heaviest pig in our IP experiments.

In Eq. (16),  $\gamma_1$  [ $\text{min}^{-1}$ ] and  $\gamma_2$  [ $\text{min}^{-1}$ ] are the diffusion rates of insulin and glucagon from the peritoneal cavity to the surrounding capillaries (equivalent to  $k_{i1}$  and  $k_{h1}$  introduced in Section 3.1.1), respectively. Since the size of the IP cavity varies with body weight,  $\gamma_1$  and  $\gamma_2$  are considered functions of  $\omega$ . Moreover,  $\gamma_3$  [% l/mmol/U] and  $\gamma_4$  [% l/mmol/ $\mu\text{g}$ ] are the charging and discharging rate of glycogen storage level (equivalent to  $k_{\xi 1}$  and  $k_{\xi 2}$  introduced in Section 3.2.5), respectively. Since the liver size is related to body weight, we assumed that  $\gamma_3$  and  $\gamma_4$  are weight-related parameters.

IV glucose infusion was used in the experiments to simulate meal absorption in the anesthetized pigs. The glucose solution had a concentration of 200 mg/ml. Therefore,  $\gamma_5(\omega)$  is a coefficient directly related to the concentration of IV glucose infusion and inversely to the body weight (blood volume). In addition,  $\gamma_6(\omega)^{-1}$ , and  $\gamma_7(\omega)^{-1}$  are the volumes of peritoneal fluid in which insulin and glucagon are dissolved. These parameters are defined as follows:

$$\begin{cases} \gamma_7(\omega) \triangleq \frac{\delta_1}{\omega}, & \gamma_8(\omega) \triangleq \frac{\delta_4}{\omega} \\ \gamma_9(\omega) \triangleq \frac{\delta_7}{\omega} \end{cases} \quad (17)$$

#### 4.2. Parameter identification

In the animal trials, we assume that the endogenous insulin and glucagon are negligible, and we know there were no IP insulin or glucagon boluses before the experiments. Therefore, the initial values of the states  $x_2, x_3, \dots, x_6$  are zero (i.e., the values of  $\alpha_2, \dots, \alpha_6$  are zero). Moreover,  $\alpha_1, \alpha_8$ , and  $\alpha_9$  are chosen equal to BGL, PIL, and PHL measurements at  $t = 0$ . The initial glycogen storage is a function of different factors, and therefore  $\alpha_7$  needs to be identified individually. In addition, the weight-dependent parameters ( $\Gamma$ ) are designed as body weight functions and constant parameters across the animals. Therefore, we only need to identify  $\Theta \triangleq \{\beta_1, \beta_2, \dots, \beta_{19}, \alpha_7\}$  which are individual parameters and  $\Delta \triangleq \{\delta_1, \delta_2, \dots, \delta_{15}\}$  that are constant parameters across the animals. As previously stated, we expect the individual parameters (except the initial values) of different pigs to be in the same range with a slight variation due to their similar properties.

Objective function (18) is designed for trajectory-fitting and parameter identification. Using the proposed objective function, the modeled BGL, PIL, and PHL tried to fit the measurements in  $N$  animals. Each pig is allowed to have individual parameters, but the objective function contains a penalty on the variation of these

parameters across animals. The designed objective function is as follows.

$$J(\Theta_1, \Theta_2, \dots, \Theta_N, \Delta) = \sum_{i=1}^N \left( E_{G_i}(\Theta_i, \Delta)^T \cdot Q_{G_i} \cdot E_{G_i}(\Theta_i, \Delta) + E_{I_i}(\Theta_i, \Delta)^T \cdot Q_{I_i} \cdot E_{I_i}(\Theta_i, \Delta) + E_{H_i}(\Theta_i, \Delta)^T \cdot Q_{H_i} \cdot E_{H_i}(\Theta_i, \Delta) + (\Theta_i - \bar{\Theta})^T \cdot Q_{\Theta} \cdot (\Theta_i - \bar{\Theta}) \right) \quad (18)$$

where:

- $E_{G_i}(\Theta_i, \Gamma)$ ,  $E_{I_i}(\Theta_i, \Gamma)$  and  $E_{H_i}(\Theta_i, \Gamma)$  are the fitting error vectors of the model in tracking the BGL, PIL and PHL measurements, respectively. They are defined as the following:

$$E_{G_i}(\Theta_i, \Delta) \triangleq \begin{pmatrix} \text{BGL}_i(t_0) - y_1(\Theta_i, \Delta, t_0) \\ \text{BGL}_i(t_1) - y_1(\Theta_i, \Delta, t_1) \\ \vdots \\ \text{BGL}_i(t_{n_i}) - y_1(\Theta_i, \Delta, t_{n_i}) \end{pmatrix}, \quad (19)$$

$$E_{I_i}(\Theta_i, \Delta) \triangleq \begin{pmatrix} \text{PIL}_i(t_0) - y_2(\Theta_i, \Delta, t_0) \\ \text{PIL}_i(t_1) - y_2(\Theta_i, \Delta, t_1) \\ \vdots \\ \text{PIL}_i(t_{n_i}) - y_2(\Theta_i, \Delta, t_{n_i}) \end{pmatrix}, \quad (20)$$

and

$$E_{H_i}(\Theta_i, \Delta) \triangleq \begin{pmatrix} \text{PHL}_i(t_0) - y_3(\Theta_i, \Delta, t_0) \\ \text{PHL}_i(t_1) - y_3(\Theta_i, \Delta, t_1) \\ \vdots \\ \text{PHL}_i(t_{n_i}) - y_3(\Theta_i, \Delta, t_{n_i}) \end{pmatrix}. \quad (21)$$

- $\bar{\Theta}$  is the vector of the average individual parameters identified for the test data:

$$\bar{\Theta} = (\Theta_1 + \Theta_2 + \dots + \Theta_N) / N. \quad (22)$$

- $Q_{G_i}$ ,  $Q_{I_i}$ , and  $Q_{H_i}$  are positive definite matrices that should be chosen according to the variance of the measurement noise and the scale of the measurements. Matrix  $Q_{\Theta}$  is also positive definite and should be chosen according to the expected variability of each parameter. For the animals or the samples that the PIL and PHL are not available, both  $E_{I_i}(\Theta_i, \Gamma)$  and  $E_{H_i}(\Theta_i, \Gamma)$  are zero.

### 4.3. Summary of the proposed identification method

In order to address the practical identifiability issues, we propose a meta-model that can characterize some parameters as either function of body weight or as constant among all animals.

To address the structural non-identifiability, we added PIL and PHL measurements as new outputs and IV drug injections as new inputs to the meta-model. However, measuring the BGL, PIL, and PHL necessitates at least 1–1.5 ml of blood to be extracted at each sampling time, which can interfere with the normal glucose metabolism of the animals. Therefore, due to animal safety, we cannot measure the PIL and PHL in all animals.

Notably, some analogous parameters can have a negligible variation among animals and, therefore, can be considered a constant parameter. In order to find these parameters, the following steps are done in the following sections:

1. Choose training data and test data.
2. Identify the parameters belonging to the sets  $\Delta$  and  $\Theta$  for training data.

3. Analyze the analogous parameters to find more parameters that can be considered fixed among the animals using the sensitivity and inter-subject coefficient of variability.
4. Re-identify the remaining parameters and evaluate the model by assuming the fixed parameters are known.
5. Compare the meta-model with other models for test and training data sets.

## 5. Training data, test data, and evaluation methods

Data collected in 26 animal experiments are used to evaluate the performance of the proposed model and identification method. Experiments are numbered Pig #1–29. Pigs #19–21 received SC insulin injections, which are outside the scope of this paper and were excluded from this analysis. Pigs #1–10 are bi-hormonal IP experiments, Pigs #11–14 are bi-hormonal IP experiments with additional IV boluses, and the rest contain only IP insulin injections. The durations of the experiments are 420–725 min, except Pig #15, which lasted only 250 minutes. BGL was measured every five minutes. In other words, the number of samples for the experiments are 84–145 samples, and 50 samples in Pig #15.

A set of 13 experiments is selected as training data to estimate the parameters of the proposed meta-model and verify its performance, while the remaining 13 experiments are considered test data. Each group of experiments chosen for training has a specific purpose in the identification, to ensure that all dynamics are excited. Table 2 describes experiment IDs, characteristics, and key features of the selected experiments. Group 1 helps to excite the dynamics of insulin, glucagon sub-models, and glycogen storage level. Group 2 helps in the identification of parameters related to body weight and the excitation of insulin and glucagon pharmacokinetics. Group 3 helps to excite the dynamics of the HFP effect since they include a wide range of insulin boluses.

Among the selected experiments, we used BGL measurements of {Pigs #2, 4, 5, 6, 10, 15, 22, 23}, PIL measurements of {Pigs #4, 5, 6, 11, 12, 13, 22, 23}, and PHL measurements of {Pigs #4–7, 11–14} for identifying the parameters of the BGL, PIL and PHL sub-models, respectively.

Notably, to estimate the parameters of (14b), one needs to ensure that the dynamics of all compartments are excited. To this end, we performed four specific experiments, which are Pigs #11–14. In these experiments, we excited the glycogen storage dynamics by injecting insulin and glucagon in different combinations. In addition, IV insulin and glucagon were also infused. The body weight of the pigs used in these experiments was chosen in the range of 30–63 kg to increase the identifiability of the body weight-related parameters.

### 5.1. Parameter coefficient of variability

After the identification using the training data set, the estimated analogous parameters will be analyzed to find the inter-subject parameter variability. This will be used to find the parameters that can be considered as constant across the animals. To this end, the coefficient of variability ( $CV_p$ ) for parameters and sensitivity of the outputs to a parameter ( $S_p^{y_i}$ ) are defined as follows:

$$CV_p = \frac{p - \bar{p}}{\bar{p}} 100\% \quad (23)$$

$$S_p^{y_i} = \left. \frac{\partial y_i}{\partial p} \cdot \frac{p}{y_i} \right|_{p=p^*} \quad \forall i = \{1, 2, 3\} \quad (24)$$

where  $p^*$  is the estimated value of the parameter  $p$ ,  $\bar{p}$  is the average value of that parameter identified for the training experiments, and  $y_i$  for  $i = \{1, 2, 3\}$  is the output defined in (15). Notably, the derivatives in this paper are calculated numerically.

**Table 2**  
Description of the three groups of animal experiments chosen as training data sets, their characteristics, and their key features. I and H refer to insulin and glucagon, respectively.

	Exp. IDs	Weights [kg]	Bolus Types	Injections	Key Features
Group 1	#02	36	IP	I & H	1. Different combinations of I and H boluses to excite the dynamics of Glycogen storage level. 2. Different bolus sizes and body weights.
	#04	37	IP	I & H	
	#05	40	IP	I & H	
	#06	52	IP	I & H	
	#10	43	IP	I & H	
Group 2	#15	50	IP	I	1. Wide range of body weight. 2. IV and IP injections. 3. Wide range of I & H bolus sizes. 4. Regular PIL and PHL measurement.
	#07	48	IP	I & H	
	#11	30	IV & IP	I & H	
	#12	63	IV	I & H	
	#13	40	IV & IP	I & H	
	#14	41	IV & IP	I & H	
Group 3	#22	36	IP	I	1. Wide range of I bolus sizes. 2. Constant Glucose infusion.
	#23	36	IP	I	

### 5.2. Bayesian information criterion

After estimating the parameters and analyzing the inter-subject parameter variability, the rest of the experiments are used to evaluate the performance of the proposed model. The Bayesian information criterion (BIC) is employed to compare the proposed model with the other available models in the literature. The BIC is defined as follows:

$$BIC = n_s \cdot \log(\sigma^2) + p_{\#} \cdot \log(n_s) \quad (25)$$

where  $n_s$  is the number of samples,  $\sigma^2$  is the mean square error (MSE) of the model, and  $p_{\#}$  is the number of the parameters. As the number of samples is equal for all models, The lower MSE of the model with the minimum number of parameters will result in lower BIC values. Therefore, the lower the BIC value, the better the model performance.

## 6. Meta-model parameter identification using the training set

Since the model is developed for control purposes, some simplifying assumptions can be made before identifying the parameters. For example, the precise concentration of insulin or glucagon in the peritoneal fluid is not a critical factor in the control algorithms; rather, the amount (mass) of insulin and glucagon in the peritoneal fluid is required. As a result, there is no need to determine the volume of peritoneal fluid; instead, a value proportional to body weight can be assumed. Therefore, we assumed that  $\delta_4$  and  $\delta_7$  are 1 ml/kg. Furthermore,  $\delta_1$  can be found based on the concentration of the IV glucose solution used in the experiment and the approximation of the blood volume in the body based on the body weight [23]. For example, in our animal trials, we utilized glucose with a 200 mg/ml concentration to simulate the meals. Furthermore, based on our observations and as mentioned in [14], we assumed that 100% of the drugs administered into the peritoneal cavity absorbs to the PV; as a result,  $\delta_{12} = 100\%$  and  $\delta_{14} = 100\%$ . After selecting the data set and having made the assumptions above, we identified the parameters of the meta-model described in the next section.

### 6.1. Performance of the trained meta-model

Table 3 presents the mean error (ME), standard deviation (SD), and mean absolute error (MAE) of the meta-model in estimating the BGL, PIL, and PHL of the selected training data. As an example, the performance of the proposed model for Pigs #4, #5, and #6 in tracking the BGL, PIL, and PHL measurements are plotted in Fig. 4. Notice that the meta-model could fit all BGL, PIL, and PHL measurements of the training data with an average MAE of 0.3 mmol/l, 2.9 mU/l, and 23 pmol/l, respectively.

The PIL and PHL measurements often contain more noise and disturbances compared to BGL due to the measurement method and endogenous secretions.

### 6.2. Identifiability of the model

The models (14b) and (14a) are considered locally structurally identifiable using the assumptions and the available data sets. The identifiability tests are presented in Appendix A.

### 6.3. Inter-subject parameter variability

The inter-subject parameter variability is investigated in this Section in order to find the individual parameters that can be classified as constant across the animals for IP injections. In the proposed meta-model, there are seventeen analogous parameters ( $\beta_1, \dots, \beta_{17}$ ) and one individual parameter ( $\alpha_7$ ) for IP insulin and IP glucagon injections. Using the definitions of coefficient variability and sensitivity of the outputs to parameters given in (23) and (24), the  $|CV_p \cdot S_p^y|$  for the analogous parameters and for  $i = \{1, 2, 3\}$  are shown in Fig. 5. Notably, the violin plots in panel (d) of Fig. 5 shows the %CV of the parameters related to body weight where  $v_b \triangleq \omega/\delta_1$ . Using Fig. 5, the variability of the parameters is discussed in three sections as follows (where they are divided based on categories shown in Fig. 5).

#### 6.3.1. Individual parameters related to blood glucose level

To every new animal experiments, the parameter set  $\{\beta_1, \beta_2, \dots, \beta_{11}, \alpha_7\}$  is required to be identified. As shown in Fig. 5, the values of  $|CV \cdot S_p^y|$  for 7 out of 12 parameters are negligible compared to the others. Therefore, they can be assumed as fixed parameters among the animals. The other five parameters are  $\beta_1, \beta_2, \beta_3, \beta_4$ , and  $\alpha_7$ , which refer to insulin-independent glucose uptake rate, e.g., brain glucose uptake, the sensitivity of the liver to insulin, sensitivity of extra-hepatic organs to insulin, sensitivity of the body to glucagon, and the initial state of glycogen storage level. As a result, instead of identifying all 12 parameters, one needs to identify these five for each new individual. To examine this, we will re-identify only these five parameters while treating the other seven as fixed parameters for all the training and test data. It is worth mentioning that the parameters  $\beta_6$  and  $\beta_7$  are the parameters of the HFP effect on insulin, and they are present both in the BGL sub-model and PIL sub-models (both panels of (a) and (b) of Fig. 5).

#### 6.3.2. Individual parameters of the PIL and PHL sub-models

Among the remaining eight parameters describing the concentration of insulin and glucagon in plasma after IP injections,  $\{\beta_{15}, \beta_{16}, \beta_{17}\}$  are found to be constant across the animals since they have small  $|CV \cdot S_p^y|$  for  $i = \{2, 3\}$  compared to the other parameters. Notably,  $\beta_6$  and  $\beta_7$  are shared parameters between PIL and BGL sub-models, which are already discussed in the previous section and considered as constant parameters.

Recall that the main aim of this paper was to design the BGL model with fewer parameters, and the BGL sub-model does not include  $\{\beta_{12}, \beta_{13}, \dots, \beta_{17}\}$  in its parameters. Therefore, for every

**Table 3**

Mean error (ME), error standard deviation (SD), and mean absolute error (MAE) of the proposed meta-model in tracking the BGL, PIL, and PHL measurements of the training data set. Example graphs for Pigs #4–6 are shown in Fig. 4.

BGL		Exp. ID	Pig #2	Pig #4	Pig #5	Pig #6	Pig #10	Pig #15	Pig #22	Pig #23
Sub-Model	ME ± SD		0.0 ± 0.5	0.0 ± 0.5	0.0 ± 0.5	0.0 ± 0.8	0.0 ± 0.3	0.0 ± 0.4	0.2 ± 0.4	0.0 ± 0.1
	MAE		0.4	0.3	0.4	0.6	0.2	0.2	0.3	0.1
	W [kg]		36	37	40	52	43	50	36	36
PIL		Exp. ID	Pig #4	Pig #5	Pig #6	Pig #11	Pig #12	Pig #13	Pig #22	Pig #23
Sub-Model	ME ± SD		-0.8 ± 2.9	0.0 ± 2.4	0.0 ± 4.5	-1.6 ± 4.6	-1.6 ± 10.4	-0.5 ± 3.5	0.8 ± 4.0	0.2 ± 1.2
	MAE		2.0	1.7	3.2	4.0	6.8	2.5	2.5	0.7
	W [kg]		37	40	52	30	63	40	36	36
PHL		Exp. ID	Pig #4	Pig #5	Pig #6	Pig #7	Pig #11	Pig #12	Pig #13	Pig #14
Sub-Model	ME ± SD		-3 ± 12	-3 ± 9	-4 ± 17	-4 ± 9	-20 ± 31	-21 ± 82	-15 ± 52	-8 ± 14
	MAE		8	7	11	6	27	57	38	26
	W [kg]		37	40	52	48	30	63	40	41

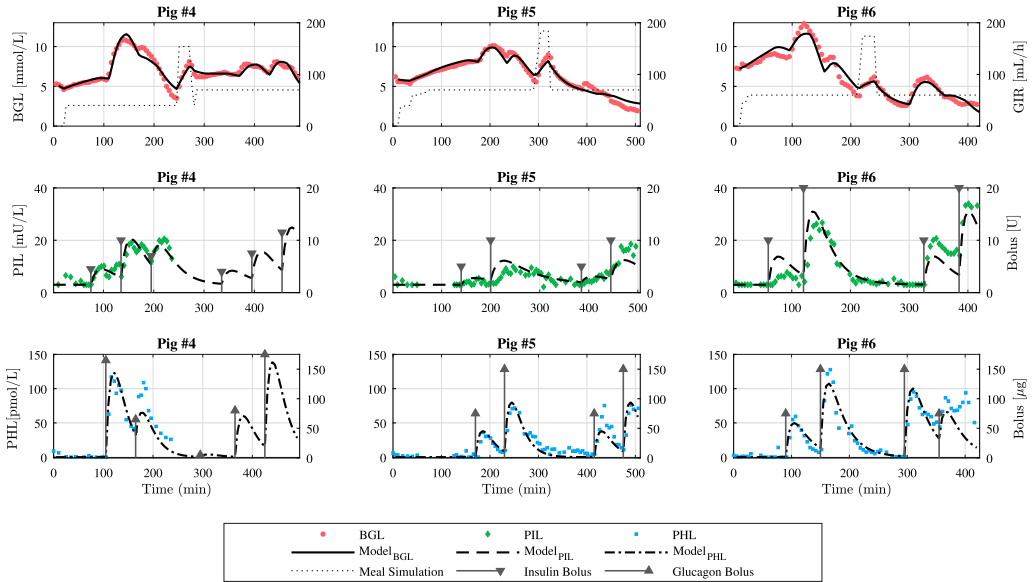


**Fig. 4.** As an example, the figures demonstrate how the proposed meta-model tracked blood glucose levels (BGL), plasma insulin levels (PIL), and plasma phloroglucinol levels (PHL) in three experiments. The three trials shown here are part of the training data utilized to identify the parameters. The performance of the model on the other training data is presented in Table 3. The dashed line in the first row is the Intravenous glucose infusion rate, simulating the meal absorption rate in the intestines.

new pig, one needs to identify only five parameters  $\{\beta_1, \beta_2, \beta_3, \beta_4, \alpha_7\}$ . The other parameters are either constant across animals or are body weight-related parameters that can be identified using the previous experiments. Moreover, if one needs to model the PIL and PHL, then  $\{\beta_{12}, \beta_{13}, \beta_{14}\}$  must be identified.

**6.3.3. Weight-dependent parameters**

Violin plots show the values of the CV% for the weight-dependent parameters in Fig. 5.  $\omega$  is the body weight of the pigs, and  $v_b$  is proportional to blood volume, which directly relates to weight.

$\gamma_1$  and  $\gamma_2$  are insulin and glucagon diffusion rates from the peritoneal cavity to surrounding capillaries. As expected, these parameters are identified to be inversely correlated to weight. The physical explanation may include anatomical features related to size and age, such as thicker peritoneal lining and a lower density of capillaries in the peritoneal lining in heavier animals. Notice that  $\gamma_1 \in [0.54, 1.73]$  and  $\gamma_2 \in [2.00, 3.62]$  which indicates that glucagon diffuses faster than insulin.

$\gamma_3$  and  $\gamma_4$  are glycogen storage charging and discharging rates, respectively. In the training data,  $\gamma_3$  is close to zero, indicating

that the glycogen storage is being charged very slowly. Notably, it is also observed in the experiments that the pigs were responding poorly to glucagon after receiving multiple injections and at the end of experiments. This could be due to a low glucose infusion rate in our 8-hour experiments or the effect of the anesthesia, all of which cause glycogen storage to discharge faster than charging. Since one may experience a faster glycogen refill in humans or awake animal experiments,  $\gamma_3$  was not omitted even if it was close to zero in these experiments.

The value of  $\gamma_4$  has been shown to be inversely related to body weight in the identification, implying that heavier subjects have bigger glycogen storage and can release more glucose than lighter animals.

**7. Performance of the training and testing of the meta-model**

In the previous section, the parameters of the meta-model are identified using the training data set, and it is discovered that for every new experiment, one needs to identify only five individual parameters  $(\beta_1, \dots, \beta_4, \alpha_7)$ . The other individual parameters

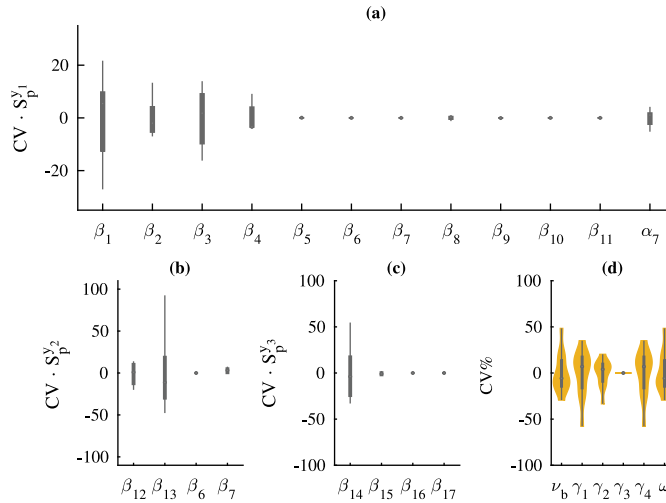


**Fig. 5.** The box-plot (a) shows the  $CV \cdot S_p^{y_1}$  for the individual parameters that are included in the subsystem of the BGL. Panels (b) and (c) show  $CV \cdot S_p^{y_2}$  and  $CV \cdot S_p^{y_3}$  of the parameters that have an influence on the PIL and PHL outputs, respectively. The violin plot (d) shows the  $CV\%$  of the weight-related parameters, and their variation depends on the body weight.

$(\beta_5, \dots, \beta_{11})$  are shown to have negligible variation from subject to subject.

In this section, parameter set  $\{\beta_5, \dots, \beta_{11}\}$  are considered constant among animals and set to the mean value of identified values for the training data in the previous section. Then, the performance of the meta-model is compared with the models in the literature using the training and test data.

There are two important models in the literature; the bi-hormonal low-order model by Zazueta et al. [12] and the single-hormonal linear model by Chakrabarty et al. [25]. Therefore, we split our analysis into bi-hormonal and single-hormonal experiments when comparing the models. In addition, the classical least square method in parameter identification of all three models is used to have a fair comparison. In these identifications, the parameters of the models are identified separately for each experiment using their BGL measurements. In more detail; the following cost function is used for parameter identification of the models:

$$J_{LS}(\Psi_M) = \sum_{i=1}^N P_{LS}(BGL_i - M_i(\Psi_M))^2 \quad (26)$$

Where  $P_{LS}$  is a constant positive number,  $BGL_i$  is the BGL at the sample  $i$ , and  $M_i$  is the model (Meta-model, low-order, or Linear model) output for the corresponding sampling time.  $N$  denotes the number of samples in the experiment. In this cost function, the decision variables are each model's parameter set ( $\Psi_M$ ). Notably, the low-order model has ten parameters (six without the glucagon sub-model), and the linear model has five parameters to identify.

The number of parameters for the meta-model is five. However, frequent blood samples from the jugular vein are taken during the bi-hormonal experiments in bi-hormonal experiments for PIL and PHL measurements. As a result, blood volume is no longer solely dependent on body weight and may be influenced by the number of samples taken. Two meta-models are considered to make up for it: meta-model 1 and meta-model 2, with  $\delta_7$  being treated as a fixed and individual parameter, respectively.

The performance of meta-model 1 and meta-model 2 are compared to the other models in Table 4. Meta-model 1 and

meta-model 2 have similar performance in training and test data. One can conclude that the parameters of the model are identified correctly using the training data set. By looking at the Average values of the errors from different models, one can conclude that all the models have acceptable performance for control purposes, and no significant differences can be found between the models. However, the proposed meta-model 1 and meta-model 2 require fewer parameters to be identified than the other models in the literature.

The BGL, PIL, and PHL measurements from Pigs #01, 09, and 16 versus the meta-model 2 (for Pig#01, and 09) and meta-model 1 (for Pig #15) responses are shown in Fig. 6. Among the test data, Pig #1 and #9 have the inputs with the most excitation inputs, e.g., a wide range of insulin, glucagon, and glucose infusions. Therefore, one can conclude that the proposed meta-model can simulate the behavior of glucose metabolism of various body weights in both complex and simple scenarios.

### 7.1. Summary of training and testing the meta-model

In the previous sections, the parameters of the meta-model are identified using the selected training data. The primary goal of this approach is to identify parameters that are not identifiable when the BGL is the only available data. This is accomplished by utilizing prior data from other animals for whom the PIL and PHL are measured.

The variability of the individual parameters among the different animals is discussed. It is demonstrated that one must identify only  $\{\beta_1, \dots, \beta_4, \alpha_7\}$  for every new experiment. The rest of the parameters are fixed parameters or weight-related parameters obtained from prior information.

Moreover, It is shown that the proposed meta-model can fit the BGL measured from pigs and provide similar performance with fewer parameters compared to the available models in the literature. One can conclude that the identification procedure of the trained meta-model is easier and faster than the other models.

In the following sections, the predicting performance of the meta-model is evaluated and compared with the other models in two different practical scenarios.



**Table 4**

The mean error (ME), standard deviation (SD), mean absolute error (MAE) [mmol/l], and the Bayesian information criterion (BIC) for different models and experiments. In the case of bi-hormonal experiments, two versions of the meta-model were analyzed, meta-model 1, and meta-model 2, when considering  $\nu$  as an individual parameter (to compensate for the volume of the blood taken for BGL, PIL, and PHL analysis). For the single-hormonal experiments, only meta-model 1 is used since there were fewer blood samples taken from them. Notably, the parameters of the BGL sub-model for single-hormonal experiments are not taken into account. Notably, results for Pigs #12–#14 are not presented since they contain IV insulin and glucagon infusions from the beginning of the experiment. However, for Pig #11, the IV infusions were given at the end of the experiment, and the performances of the different models are presented for the IP infusion parts.

Number Of Parameter:	Model:	Meta-Model1				Low-Order Model [14]				Meta-Model2			
	Exp. ID	ME	SD	MAE	BIC	ME	SD	MAE	BIC	ME	SD	MAE	BIC
Insulin & Glucagon Injections (IP)	Pig #01	0.00	± 0.37	0.30	-187	0.02	± 0.28	0.23	-228	0.02	± 0.29	0.24	-242
	Pig #02 <sup>(1)</sup>	0.00	± 0.50	0.40	-110	0.01	± 0.74	0.55	-14	0.00	± 0.50	0.37	-112
	Pig #03	0.04	± 0.55	0.40	-86	0.00	± 0.24	0.19	-219	0.05	± 0.45	0.38	-120
	Pig #04 <sup>(1,2,3)</sup>	0.01	± 0.50	0.30	-123	0.01	± 0.41	0.32	-130	0.05	± 0.47	0.35	-123
	Pig #05 <sup>(1,2,3)</sup>	0.05	± 0.43	0.30	-148	0.07	± 0.48	0.43	-101	0.05	± 0.43	0.31	-179
	Pig #06 <sup>(1,2,3)</sup>	0.04	± 0.71	0.54	-36	0.09	± 0.77	0.59	1	0.05	± 0.71	0.54	-37
	Pig #07 <sup>(1,2,3)</sup>	0.00	± 1.48	0.97	103	0.09	± 0.73	0.51	-18	0.05	± 1.46	0.95	100
	Pig #08	0.07	± 0.80	0.65	-18	0.05	± 0.49	0.37	-92	0.05	± 0.80	0.64	-19
	Pig #09	0.04	± 0.74	0.54	-31	0.04	± 0.54	0.40	-64	0.05	± 0.63	0.49	-59
	Pig #10 <sup>(1)</sup>	0.01	± 0.27	0.23	-191	0.00	± 0.27	0.22	-175	0.05	± 0.28	0.23	-192
	Pig #11 <sup>(2,3)</sup>	0.02	± 0.50	0.41	-77	0.12	± 1.11	0.85	57	0.05	± 0.47	0.39	-87
Average	Training Data	0.02	± 0.63	0.47	-81	-	± -	-	-	0.04	± 0.54	0.44	-110
	Test Data	0.04	± 0.62	0.45	-83	-	± -	-	-	0.04	± 0.62	0.45	-90
	All Data	0.03	± 0.62	0.46	-82	0.05	± 0.55	0.42	-89	0.04	± 0.59	0.44	-97
Number Of Parameter:	Model:	Meta-Model1				Low-Order Model				Linear Model [28]			
	Exp. ID	ME	SD	MAE	BIC	ME	SD	MAE	BIC	ME	SD	MAE	BIC
Only Insulin Injections (IP)	Pig #15 <sup>(1)</sup>	0.06	± 0.41	0.26	-77	0.06	± 0.38	0.23	-71	0.00	± 1.00	0.69	19
	Pig #16	0.04	± 0.23	0.17	-210	0.04	± 0.39	0.30	-118	0.00	± 0.26	0.20	-182
	Pig #17	0.07	± 0.69	0.50	-55	0.02	± 0.38	0.26	-143	0.02	± 0.45	0.26	-111
	Pig #18	0.06	± 0.53	0.43	-94	0.01	± 0.43	0.36	-116	0.01	± 0.48	0.34	-101
	Pig #22 <sup>(1,2)</sup>	0.01	± 0.38	0.33	-155	0.02	± 0.40	0.34	-140	0.00	± 0.38	0.29	-151
	Pig #23 <sup>(1,2)</sup>	0.01	± 0.15	0.49	-336	0.01	± 0.16	0.13	-307	0.00	± 0.37	0.29	-160
	Pig #24	0.05	± 0.33	0.24	-192	0.07	± 0.33	0.22	-181	0.01	± 0.22	0.15	-267
	Pig #25	0.03	± 0.14	0.11	-354	0.00	± 0.10	0.07	-417	0.00	± 0.16	0.12	-329
	Pig #26	0.06	± 0.35	0.32	-182	0.01	± 0.22	0.17	-282	0.00	± 0.35	0.30	-188
	Pig #27	0.04	± 0.30	0.27	-209	0.01	± 0.25	0.21	-229	0.00	± 0.26	0.22	-226
	Pig #28	0.02	± 0.28	0.23	-220	0.01	± 0.12	0.10	-362	0.00	± 0.08	0.05	-456
Pig #29	0.06	± 0.47	0.39	-128	0.05	± 0.46	0.38	-116	0.00	± 0.30	0.25	-204	
Average	Training Data	0.08	± 0.94	0.36	-147	-	± -	-	-	-	± -	-	-
	Test Data	0.05	± 0.37	0.30	-194	-	± -	-	-	-	± -	-	-
	All Data	0.04	± 0.36	0.31	-184	0.03	± 0.30	0.23	-207	0.00	± 0.36	0.26	-196

<sup>(1)</sup> BGL measurement is utilized in training the Meta-model.  
<sup>(2)</sup> PIL measurement is utilized in training the Meta-model.  
<sup>(3)</sup> PHL measurement is utilized in training the Meta-model.

**8. Performance of the meta-model in predicting the BGL**

The combination of MPC with moving horizon estimation (MHE) is one of the most commonly used control approaches in APs [26]. The MHE uses the historical BGL data to estimate state values. Based on the estimated states, the MPC predicts the BGL and finds optimal insulin or glucagon boluses to keep the BGL in the range. As a result, the proposed model should be consistent with past data and effective at predicting.

In this section, we compare the performance of the proposed meta-model (in which  $\{\beta_1, \dots, \beta_4, \alpha_7\}$  must be identified) with the other models in terms of prediction. For that purpose, we proposed the following two scenarios:

**8.1. Scenarios 1: Bi-hormonal model identification and prediction at every sampling time**

This scenario aims to evaluate the proposed meta-model and low-order model fitting the data and predicting each sampling time for bi-hormonal experiments.

The parameters are re-identified for both models after measuring the BGL at every sampling time. Then, based on the identified model and future inputs, a 100 min prediction will be performed. After that, the MSE of the models for both fitting to the measured BGL and the prediction are calculated. For example, at  $i$ th sample, the fitting MSE is the mean squared error of the model in fitting to the BGL samples  $\{1, \dots, i\}$ , and Prediction MSE is the mean squared error of the model in predicting the BGL samples  $\{i + 1, \dots, (i + 100/T_s)\}$ .

In order to have proper initial values for the parameter estimation, one needs to have at least one insulin and one glucagon infusion before starting the identification and predictions. Therefore, this scenario starts after collecting 100 min of the BGL measurements, and the starting model is obtained by the parameter identification over that 100 min time window. Notably, the half-life IP insulin (for the kind of insulin used in our tests) is within the first 100 min of injection, according to our experience. Additionally, glucagon effects fade off after 100 min. Therefore, the 100 min prediction window for IP insulin and glucagon is chosen in this scenario.

To have a fair comparison of the models, an overview of the fitting MSE and prediction MSE are shown in Fig. 7 for the experiments Pig# $\{1, 3, 8, 16, 17, 18, 24, 25, 26, 27, 28, 29\}$ . The selected experiments contain only IP insulin and glucagon with continuous IV glucose infusion that was not used to train the meta-model. Pig#9 was not included since the glucose infusion in this experiment was discontinuous and unrealistic for real-life situations. The supplementary material in Appendix B provides the detailed performance of each model in Scenario 1 on all available experiments with IP injections.

As shown in Fig. 7, the low-order model has a mean model fitting MSE that is 26.6% lower than the meta-model. For both models, the mean fitting MSE is less than 1 [mmol/l]<sup>2</sup>. In prediction, the meta-model has a 39.2% lower mean MSE and a 64.0% lower standard deviation than that of the low-order model. The meta model has a mean prediction MSE of less than 1 [mmol/l]<sup>2</sup>.

In summary, by comparing the performance of the models in scenario 1, one can infer that the low-order model performs better in fitting the measurements. However, the fitting MSE of

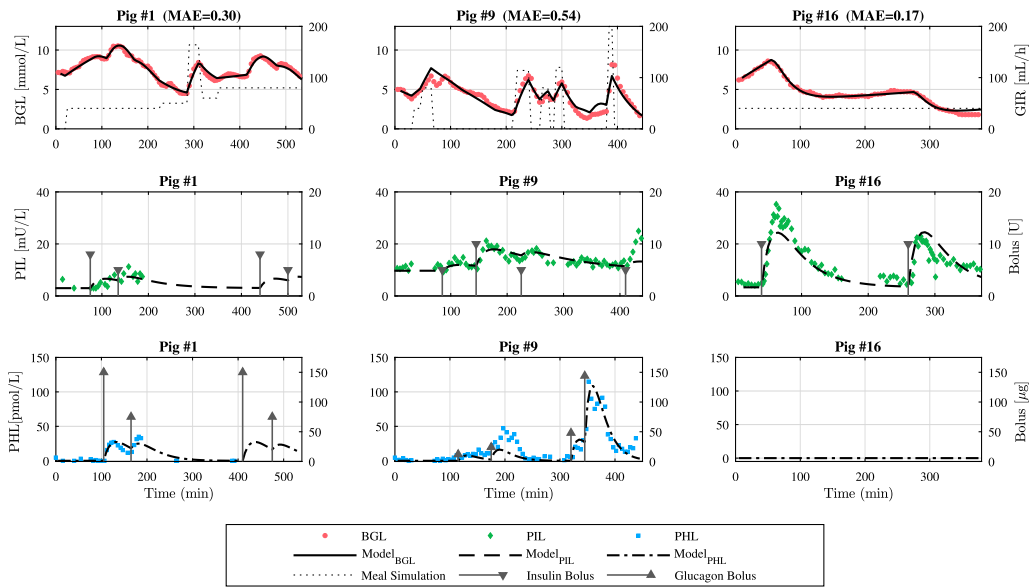


**Fig. 6.** Three examples of meta-model performance on test data are shown in the figure. Notably, meta-model 1 is used for single-hormonal experiment Fig #16 and meta-model 2 is utilized for bi-hormonal experiments in Figs #01, #09. The performance of the presented model in fitting to the BGL measurements for the other experiments is presented in Table 4. However, the MAE (mean absolute error) of the proposed model is for the BGL measurements written in the titles in order to quantify the quality of the fittings. The dashed line in the first row is the IV glucose infusion rate which simulates the meal digestion rate in the intestines.

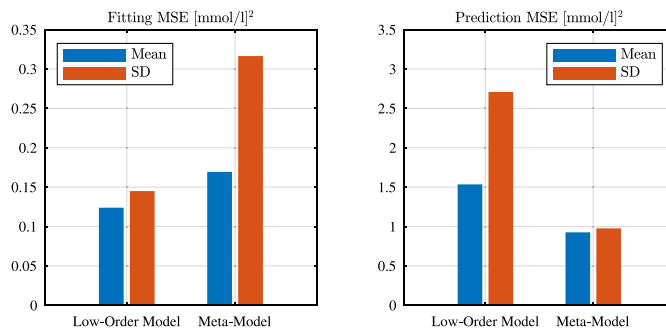


**Fig. 7.** The figure compares the proposed meta-model with the low-order model regarding the fitting MSE and prediction MSE for the selected test experiments in Scenario 1. The panel on the left shows the mean and standard deviation (SD) of fitting MSE at all sampling times of the selected experiments. Similarly, the panel on the right shows the mean and SD of 100 min of prediction MSE at all sampling times for the selected experiments.

both models is in the acceptable range for control purposes. In contrast, the proposed meta-model performs significantly better in prediction, which is more important than fitting when you aim to use the model in control. In summary, the fewer parameters, the acceptable fitting MSE, and the low prediction MSE in the meta-model make it a suitable choice for model-based control.

### 8.1.1. Scenario 2: Prediction of the BGL interaction with different insulin boluses

This scenario investigates the effect of considering the HFP effect on prediction and fitting to the measurements. Among the available animal experiments, Figs #23–28 with weights of 36–41 kg were given a constant basal glucose infusion proportional to their weight and three different insulin boluses, i.e., 2, 5, and 10 Units with various orders. These experiments are performed

to investigate the saturation of the HFP published in [11]. It is shown that the liver of these subjects is saturated after 5U of insulin, and then the insulin enters the central blood circulation. The duration of the experiment chosen for this scenario is about 500 min in which insulin boluses were given approximately at  $t_1 = 75$ ,  $t_2 = 210$ , and  $t_3 = 350$  min.

In this scenario, we first identified the parameters of the different models using the BGL measurements in the time interval  $[0, t_2)$  and evaluated the models' prediction performance in the time interval  $[t_2, 480)$ . Then, we identified the parameters using the BGL measurements interval  $[0, t_3)$  and again evaluated the prediction performance during the time interval  $[t_3, 480)$ . Both identification and prediction MSE of each experiment for the different models are presented in Table 5. Please Note that the Fig #23 was included in the training data while it is also included

**Table 5**  
Mean squared error (MSE) of the different models in identification and prediction for the second scenario. The terms *Iden.* and *Pred.* in this table relate to the identification and prediction MSEs, respectively.

Identification Period	Model	Pig #23		Pig #24		Pig #25		Pig #26		Pig #27		Pig #28		Average	
		Iden.	Pre.	Iden.	Pre.	Iden.	Pre.	Iden.	Pre.	Iden.	Pre.	Iden.	Pre.	Iden.	Pre.
[0, t <sub>2</sub> ]	Linear Model	0.0	0.5	0.1	0.2	0.0	1.8	0.0	26.6	0.1	1.6	0.0	13.7	0.0	7.4
	Low-order Model	0.0	2.6	0.1	10.6	0.0	0.6	0.0	11.8	0.0	1.3	0.0	1.1	0.0	4.7
	Meta-Model	0.0	0.2	0.1	0.8	0.0	0.6	0.0	1.0	0.1	0.2	0.0	0.6	0.0	0.6
[0, t <sub>3</sub> ]	Linear Model	0.1	3.7	0.1	0.4	0.0	0.8	0.1	8.1	0.1	1.7	0.0	0.0	0.1	2.5
	Low-order Model	0.0	3.9	0.1	0.6	0.0	0.0	0.0	0.8	0.1	2.5	0.0	0.2	0.0	1.3
	Meta-Model	0.0	0.1	0.1	1.0	0.0	0.1	0.1	0.5	0.1	0.5	0.0	0.4	0.1	0.4

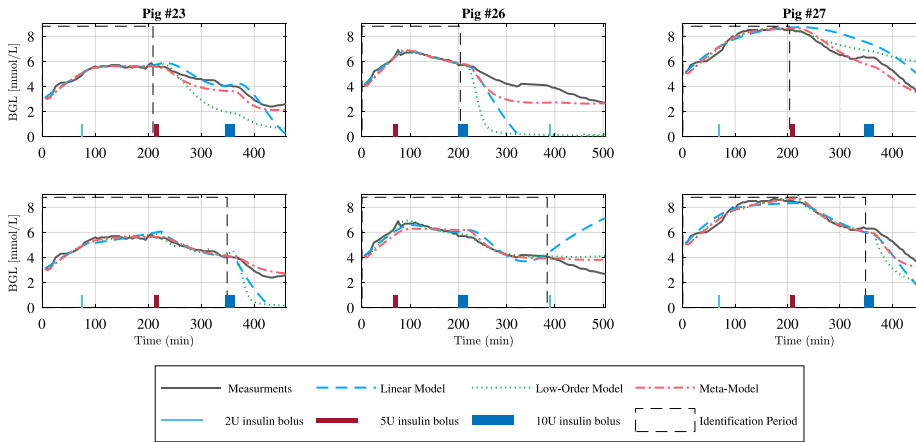


**Fig. 8.** Comparison of different models' prediction performance. The identification period for the upper figures was  $t_2 = 200$  min and  $t_3 = 350$  min for the lower figures. The proposed meta-model has a better prediction for both small and large insulin boluses; this is most notable for the 10U insulin bolus because it is the only model considering the HFP effect. In contrast, the other models fail to respond to smaller and larger insulin boluses.

in this scenario to compare the performance of the meta-model on both training and test data.

The proposed meta-model outperformed the other models' predictions when different insulin boluses were given. As an example, the performance of the models in fitting and predicting the BGL measurement of Pigs #23, #26, and #27 are shown in Fig. 8. Due to the modeled HFP effect and the prior information in the meta-model, it performs better in response to 5 and 10U, while the other models fail to predict the BGL correctly.

By looking at the average error of the models in Fig. 7 and Table 5, one can conclude that the proposed meta-model and the models in the literature for the IP route can track the BGL measurements for anesthetized pigs with acceptable performance. However, the proposed meta-model outperforms the other models in terms of prediction. The average prediction MSE in Table 5 shows that the low-order model performs better than the linear model. Additionally, because of fewer parameters of the meta-model, this model can be set up and used in the controller more quickly than the other models.

**9. Discussions**

In contrast to the SC drug pathway, it is demonstrated in [5] that the insulin absorption from the peritoneal cavity is quick enough to control the BGL without the meal announcement. Furthermore, an important feature of IP injection is the fact that insulin is transported directly to the liver through the PV, where the HFP effect applies before entering the central blood circulation system. It is shown that the HFP effect significantly influences how the body responds to different insulin bolus sizes.

For that reason, a nonlinear model containing the HFP effect is presented.

In order to identify the parameters of the designed model, a large number of tests must be performed to stimulate all the system dynamics. Furthermore, it is necessary to measure both the PIL and PHL to address the identifiability issues for this model. However, invasive tests and measurements are not applicable at a large scale or are dangerous for the animals.

As an alternative to performing all the tests on each subject, the meta-model is designed to allow us to perform the tests on a large group of animals. This approach allows us to conduct less invasive experiments and identify parameters that are weight-dependent or parameters that have a fixed value for all animals.

Using the training data, it is shown that only five parameters must be individually identified for each animal to simulate the BGL dynamics. The remaining parameters are either constant among the animals or can be calculated using body weight.

The model is identified using data and assumptions related to anesthetized pigs weighing between 30 kg and 60 kg. It is shown that the model has an acceptable performance. In addition, it performs accurately in predicting the BGL for various inputs and provides better prediction with fewer parameters, making it ideal for control purposes. In future work, one might design the MPC controller for APs using the model proposed in this paper.

The same procedure used in this paper can also be used for humans. However, some distinctions between the IP structures of humans and pigs must be taken into account. In addition, one can use the proposed meta-model to design less invasive experiments for humans or awake animals.

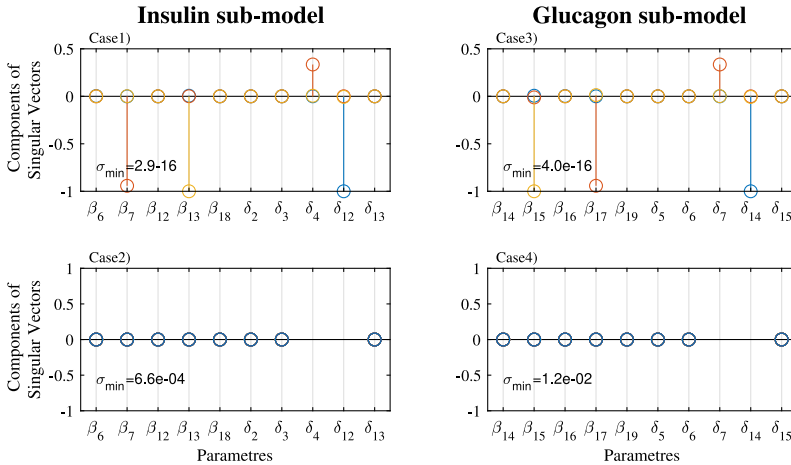


**Fig. A.9.** Components of the columns of  $V^i$  that  $S_r(t, \eta^i)$  has eigenvalues less than  $10^{-6}$  for system (14a). The non-zero (non-vanishing) components are associated with the null space of  $S_r(t, \eta^i)$  as described in Appendix A. Case 1 and case 3 are the identification based on PIL and PHL measurements of all training data. Case 2 and case 4 are with assuming  $\delta_4, \delta_7, \delta_{12}$  and  $\delta_{14}$  equal to one (as explained in Section 6). There are no non-vanishing components in case 2 and case 4. The smallest singular value is printed in the lower-left corner.

Due to limitations with experiments in anesthetized animals, the length of the experiments was shorter than a half-day. Therefore, we assumed that the parameters remained constant throughout the experiments. One might need to consider intra-subject variation in extended experiments or human experiments. In addition, one may need more training data for longer experiments. However, the thirteen training experiments for this paper seem to be enough to identify the parameters of the meta-model.

#### CRedit authorship contribution statement

**Karim Davari Benam:** Conceptualization, Mathematical design, Simulations. **Hasti Khoshamadi:** Data curation, Writing – original draft. **Marte Kierulf Åm:** Data curation, Writing – original draft. **Øyvind Stavadahl:** Supervisor. **Sebastian Gros:** Conceptualization, Mathematical design, Supervisor. **Anders Lyngvi Fougner:** Conceptualization, Mathematical design, Supervisor.

#### Declaration of competing interest

The authors declare that they have no known competing financial interests or personal relationships that could have appeared to influence the work reported in this paper.

#### Data availability

The data that has been used is confidential.

#### Acknowledgments

The animal experiments were performed at the Comparative Medicine Core Facility (CoMed) at the Norwegian University of Science and Technology (NTNU). CoMed is funded by the Faculty of Medicine and Health Sciences at NTNU and the Central Norway Regional Health Authority. This research is also funded by the Research Council of Norway (project no. 248872 and 294828) and the Centre for Digital Life Norway. We would like to thank Oddveig Lyng, Patrick Christian Bösch, and Ilze Dirnena-Fusini for their invaluable contribution to the data collection. We also thank Professor Sven Magnus Carlsen for his help in designing experiments and discussions.

#### Appendix A. Local structural identifiability of the parameters

In this part, we examine the identifiability of the proposed meta-model. To this end, we employ the algorithm described in [27]. In this algorithm, the sensitivity matrix  $S_r(t, \eta)$  defined in (A.1), which is the sensitivity of the output of the model,  $y$ , at each sampling time,  $t = \{t_0, \dots, t_n\}$ , to the parameters,  $\eta = \{\eta_1, \dots, \eta_p\}$ , must be found locally around the identified values for the parameters.

$$S_r(t, \eta) = \begin{pmatrix} \frac{\eta_1}{y(t_0)} \frac{\partial y(t_0)}{\partial \eta_1} & \dots & \frac{\eta_p}{y(t_0)} \frac{\partial y(t_0)}{\partial \eta_p} \\ \vdots & \vdots & \vdots \\ \frac{\eta_1}{y(t_n)} \frac{\partial y(t_n)}{\partial \eta_1} & \dots & \frac{\eta_p}{y(t_n)} \frac{\partial y(t_n)}{\partial \eta_p} \end{pmatrix} \quad (\text{A.1})$$

By considering small random perturbations in parameters sets,  $\eta^i$ , one needs to calculate singular value decomposition (SVD) for  $S_r(t, \eta^i)$  as follows:

$$S_r(t, \eta^i) = U_i \Sigma_i V_i^T \quad (\text{A.2})$$

where  $U_i$  and  $V_i$  are orthogonal matrices, and  $\Sigma_i$  is a matrix containing the  $p$  singular values of  $S_r(t, \eta^i)$  in decreasing order on the diagonal, while all the other elements are zero. It is shown that in [27] that if the smallest singular value of  $\Sigma_i$  is zero or very small, the last column of  $V_i$  shows the parameters that are correlated and non-identifiable. Notable, due to numerical errors, we considered any singular values less than  $10^{-6}$  as zero. Therefore, the columns of  $V_i$  related to any singular values less than  $10^{-6}$  will be considered null space.

This algorithm is used in four stages to evaluate the effectiveness of the proposed meta-model and assumptions in reducing the number of non-identifiable parameters:

##### A.1. Identifiability of the meta-model using single BGL measurements

This section aims at finding which of the parameters of the proposed individual model (14b) are non-identifiable without having the PIL, PHL measurements, and the multiple animal BGL data. To do this, we identified the parameters using the BGL

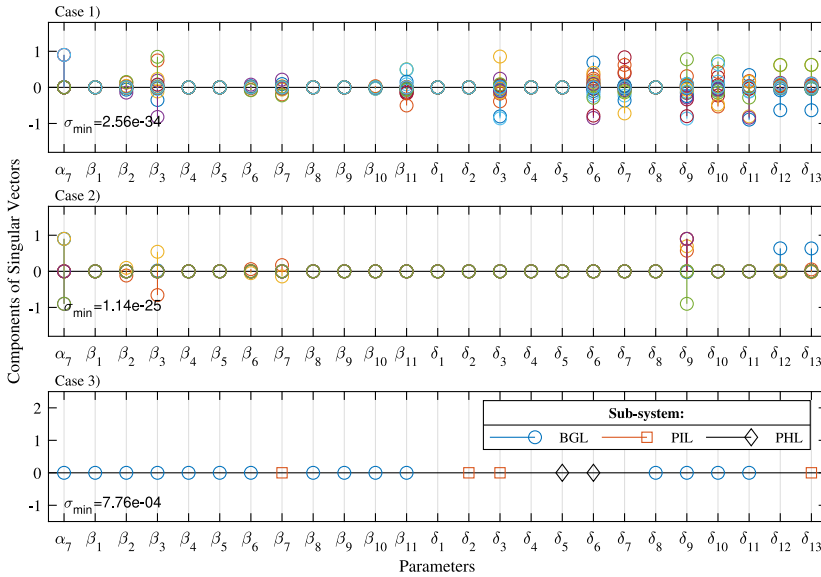


**Fig. A.10.** Components of the columns of  $V^l$  that  $S_r(t, \eta^l)$  has eigenvalues less than  $10^{-6}$  for system (14b). The non-zero (non-vanishing) components are associated with the null space of  $S_r(t, \eta^l)$  as described in Appendix A. Case 1 is the identification based on only BGL measurements of Pig#6, Case 2 is identification based on multiple pig BGL measurements belonging to training data, and case 3 is the identification using the assumption that  $\delta_4, \delta_7, \delta_{12}$  and  $\delta_{14}$  are equal to one (as explained in Section 6) and taking PIL, PHL, and BGL of all training data into account. There are no non-vanishing components in case 3. The smallest singular value is printed in the lower-left corner.

measurements of Pig#6. As shown in the first case of Fig. A.10, thirteen parameters in (14b) are correlated. Notably, the reason for choosing the Pig#6 for this example is that it had received wide ranges of insulin, glucagon, and glucose infusions.

**A.2. Identifiability of the meta-model using BGL measurements from multiple animals**

In this stage, we investigate how many parameters become identifiable by using the BGL measurements of the eight pigs named as training data. As shown in the second case of Fig. A.10, eight parameters in (14b) are correlated in that case.

**A.3. Identifiability of the PIL and PHL sub-models**

By employing all of the PIL and PHL measurements of the training data in identification, four parameters are correlated in both the PIL and PHL sub-models. The correlated parameters are shown in cases 1 and 3 of Fig. A.9. However, as shown in cases 2 and 4 of Fig. A.9, with the assumptions given in Section 6 for preselecting values for  $\delta_4, \delta_7, \delta_{12}$  and  $\delta_{14}$ , no correlated parameters are found. Therefore, the PIL and PHL sub-models are considered structurally identifiable with the parameters found using the selected training data and the assumptions in Section 6.

**A.4. Identifiability of the meta-model using the chosen training data set**

For the meta-model parameters that are identified using the assumption outlined in Section 4 as well as the BGL, PIL, and PHL measurements present in the training data set, the minimum eigenvalue of the sensitivity matrix is greater than  $10^{-2.94}$ . In

other words, all the parameters of the meta-model can be considered structurally identifiable. As it is shown in the third case of Fig. A.10, there are no parameters in (14b) that are correlated in that case.

**Appendix B. Supplementary data**

Supplementary material related to this article can be found online at <https://doi.org/10.1016/j.jprocont.2022.11.008>.

**References**

- [1] A. Katsarou, S. Gudbjörnsdóttir, A. Rawshani, D. Dabelea, E. Bonifacio, B.J. Anderson, L.M. Jacobsen, D.A. Schatz, Å. Lernmark, Type 1 diabetes mellitus, Nat. Rev. Dis. Primers 3 (1) (2017) 1–17.
- [2] P. Herrero, J. Bondia, N. Oliver, P. Georgiou, A coordinated control strategy for insulin and glucagon delivery in type 1 diabetes, Comput. Methods Biomech. Biomed. Eng. 20 (13) (2017) 1474–1482.
- [3] S.J. Moon, I. Jung, C.-Y. Park, Current advances of artificial pancreas systems: A comprehensive review of the clinical evidence, Diabetes Metabolism J. 45 (6) (2021) 813–839.
- [4] C. Cobelli, E. Renard, B. Kovatchev, Artificial pancreas: past, present, future, Diabetes 60 (11) (2011) 2672–2682.
- [5] C. Toffanin, L. Magni, C. Cobelli, Artificial pancreas: In silico study shows no need of meal announcement and improved time in range of glucose with intraperitoneal vs. Subcutaneous insulin delivery, IEEE Trans. Med. Robot. Bionics 3 (2) (2021) 306–314.
- [6] J.A. Nelson, R. Stephen, S.T. Landau, D.E. Wilson, F.H. Tyler, Intraperitoneal insulin administration produces a positive portal-systemic blood insulin gradient in unanesthetized, unrestrained swine, Metabolism 31 (10) (1982) 969–972.
- [7] C. Botz, B. Leibell, W. Zingg, R. Gander, A. Albisser, Comparison of peripheral and portal routes of insulin infusion by a computer-controlled insulin infusion system (artificial endocrine pancreas), Diabetes 25 (8) (1976) 691–700.
- [8] A. Giacca, A. Caumo, G. Galimberti, G. Petrella, M.C. Librenti, M. Scavini, G. Pozza, P. Micossi, Peritoneal and subcutaneous absorption of insulin in type 1 diabetic subjects, J. Clin. Endocrinol. Metab. 77 (3) (1993) 738–742.

- [9] A.M. Albanese, E.F. Albanese, J.H. Miño, E. Gómez, M. Gómez, M. Zandomeni, A.B. Merlo, Peritoneal surface area: measurements of 40 structures covered by peritoneum: correlation between total peritoneal surface area and the surface calculated by formulas, *Surg. Radiol. Anat.* 31 (5) (2009) 369–377.
- [10] M. Schiavon, C. Cobelli, C. Dalla Man, Modeling intraperitoneal insulin absorption in patients with type 1 diabetes, *Metabolites* 11 (9) (2021) 600.
- [11] I. Dirnena-Fusini, M.K. Àm, A.L. Fougner, S.M. Carlsen, S.C. Christiansen, Intraperitoneal insulin administration in pigs: effect on circulating insulin and glucose levels, *BMJ Open Diabetes Res. Care* 9 (1) (2021) e001929.
- [12] C. Lopez-Zazueta, A.L. Fougner, et al., Low-order nonlinear animal model of glucose dynamics for a bihormonal intraperitoneal artificial pancreas, *IEEE Trans. Biomed. Eng.* (2021).
- [13] M.K. Àm, I. Dirnena-Fusini, A.L. Fougner, S.M. Carlsen, S.C. Christiansen, Intraperitoneal and subcutaneous glucagon delivery in anaesthetized pigs: effects on circulating glucagon and glucose levels, *Sci. Rep.* 10 (1) (2020) 1–8.
- [14] V. Claassen, Intraperitoneal drug administration, *Negl. Factors Pharmacol. Neurosci. Res.* 12 (1994) 46–58.
- [15] D.H. Wasserman, Four grams of glucose, *Am. J. Physiol.-Endocrinol. Metab.* 296 (1) (2009) E11–E21.
- [16] J.E. Hall, M.E. Hall, Guyton and Hall Textbook of Medical Physiology E-Book, Elsevier Health Sciences, 2020.
- [17] P. Canal, Y. Plusquellec, E. Chatelut, R. Bugat, J. De Biasi, G. Houin, A pharmacokinetic model for intraperitoneal administration of drugs: application to teniposide in humans, *J. Pharm. Sci.* 78 (5) (1989) 389–392.
- [18] J.M. Collins, R.L. Dedrick, F.G. King, J.L. Speyer, C.E. Myers, Nonlinear pharmacokinetic models for 5-fluorouracil in man: intravenous and intraperitoneal routes, *Clin. Pharmacol. Ther.* 28 (2) (1980) 235–246.
- [19] C. Mulder, A.J. Hendriks, Half-saturation constants in functional responses, *Glob. Ecol. Conserv.* 2 (2014) 161–169.
- [20] V. Rudralingam, C. Footitt, B. Layton, Ascites matters, *Ultrasound* 25 (2) (2017) 69–79.
- [21] K.P. Davy, D.R. Seals, Total blood volume in healthy young and older men, *J. Appl. Physiol.* 76 (5) (1994) 2059–2062.
- [22] A. Raue, C. Kreutz, T. Maiwald, J. Bachmann, M. Schilling, U. Klingmüller, J. Timmer, Structural and practical identifiability analysis of partially observed dynamical models by exploiting the profile likelihood, *Bioinformatics* 25 (15) (2009) 1923–1929.
- [23] S.L. Hansard, H. Sauberlich, C. Comar, Blood volume of swine, *Proc. Soc. Exp. Biol. Med.* 78 (2) (1951) 544–545.
- [24] S. Wolfensohn, M. Lloyd, Handbook of Laboratory Animal Management and Welfare, John Wiley & Sons, 2008.
- [25] A. Chakrabarty, J.M. Gregory, L.M. Moore, P.E. Williams, B. Farmer, A.D. Cherrington, P. Lord, B. Shelton, D. Cohen, H.C. Zisser, et al., A new animal model of insulin-glucose dynamics in the intraperitoneal space enhances closed-loop control performance, *J. Process Control* 76 (2019) 62–73.
- [26] R. Gondhalekar, E. Dassau, F.J. Doyle, Moving-horizon-like state estimation via continuous glucose monitor feedback in MPC of an artificial pancreas for type 1 diabetes, in: 53rd IEEE Conference on Decision and Control, IEEE, 2014, pp. 310–315.
- [27] J.D. Stigter, J. Molenaar, A fast algorithm to assess local structural identifiability, *Automatica* 58 (2015) 118–124.



### 6.3 PAPER 3

**Title: “Blood Glucose Level Prediction Using Subcutaneous Sensors for in Vivo Study: Compensation for Measurement Method Slow Dynamics Using Kalman Filter Approach”**

Published in the Conference Proceedings of IEEE 61st Conference on Decision and Control (CDC) December 6-9, 2022. Cancún, Mexico [3].





# Blood Glucose Level Prediction Using Subcutaneous Sensors for in Vivo Study: Compensation for Measurement Method Slow Dynamics Using Kalman Filter Approach

Martha Halvorsen, Karim Davari Benam\*, Hasti Khoshamadi\*, Anders Lyngvi Fougner

**Abstract**—The continuous glucose monitoring (CGM) system is the most common system used by people with type 1 diabetes to monitor blood glucose levels. However, it measures glucose in interstitial fluid in subcutaneous tissue rather than directly in plasma. Measuring blood glucose level in this method has slow dynamics and introduce a time lag in capturing the blood glucose level. This can reduce the quality of blood glucose regulation and result in hypo- or hyperglycemia. In this paper, a linear Kalman filter is developed to predict blood glucose concentration using CGM data to compensate for that slow dynamics. To this end, an observable input-less model describing the glucose diffusion from plasma to interstitial fluid is utilized. Notably, this model is physiology-based, and its parameters can be obtained from the literature. The designed structure is evaluated on data from two animal experiments conducted on anesthetized pigs. The data sets include CGM measurements every 1.2 seconds and sporadic blood sample analysis during experiments. Results show that the designed approach sufficiently can compensate for the slow dynamics of CGM measurements when compared to blood glucose samples, and the performance is measured using statistical accuracy scores. This compensation can improve the decision-making of control algorithms for glucose regulation during rapid changes in glucose concentration, e.g., during meals and exercise.

## I. INTRODUCTION

Diabetes mellitus is a metabolic disorder or disease that affects approximately 537 million adults worldwide as of 2021 [1]. It is characterized by chronic hyperglycemia in response to ingestion of carbohydrates, fat, and protein, resulting from defects of insulin secretion, insulin action, or both [2]. In a healthy individual, glucose regulation is performed by two hormones, insulin, and glucagon, produced in the pancreas. Insulin secretion makes the glucose concentration in the blood decrease, while glucagon secretion increases the blood glucose (BG) concentration [2]. In type 1 diabetes mellitus (T1DM), the pancreas does not produce insulin due to the destruction of beta cells, which produce insulin in the pancreas [3]. Hence the insulin must be administered by an external source [2]. As a result, people with type 1 diabetes

This research is funded by the Research Council of Norway (project no. 248872), and the Centre for Digital Life Norway. Inreda Diabetic (Goor, the Netherlands) provided transmitters, materials and hormones infusion systems (AP3) for animal experiments at no cost.

M. Halvorsen, K.D. Benam, H. Khoshamadi, and A.L. Fougner are with Department of Engineering Cybernetics, Faculty of Information Technology and Electrical Engineering, Norwegian University of Science and Technology (NTNU), O. S. Bragstads Plass 2D, 7034 Trondheim, Norway. martha.halvorsen@gmail.com, {karim.d.benam, hasti.khoshamadi, anders.fougner}@ntnu.no

\*These authors contributed equally to this work

require daily insulin treatment, regular BG monitoring, and a healthy lifestyle to manage their condition effectively [4].

In 1999 diabetes technology made huge progress when the continuous glucose monitoring (CGM) system was approved by the Food and Drug Administration (FDA) and became commercially available [5]. The CGM sensor is placed in the subcutaneous tissue and measures glucose levels in the interstitial fluid in real-time [2]. The minimally invasive structure of the sensor system allows for continuous glucose measurements, eliminating the need for self-monitoring systems, e.g., finger prick [5]. In addition, continuous glucose measurements provide BG trends and fluctuations.

Despite the sensor's revolutionary qualities, it is not without problems. One of its disadvantages is that the sensor measures ISF glucose level rather than plasma glucose level. Due to plasma-to-ISF glucose dynamics, the CGM measurements are delayed compared to measurements taken directly from the blood during rapid changes in BG [6]. The plasma-to-ISF glucose dynamics refers to glucose diffusion across capillaries and through the interstitial space where the sensor is located [6]. Hence, during both BG rising and falling, the time of the diffusion process will result in the ISF glucose lagging behind the BG. The slow dynamics between these two compartments, together with sensor processing time, causes about, on average, a 4–10 min lag between the BG and the sensor readings [2].

Control algorithms, along with CGM sensors and infusion pumps, are employed in commercially available control devices (artificial pancreas) to regulate BG levels in patients with T1DM. Based on the CGM measurements, the control algorithm will automatically infuse the optimal amount of insulin, and glucagon, in a timely manner. Notably, the absorption and effect of hormones are not instantaneous. Hence, using CGM measurements can lead to a late response to BG level fluctuations which in turn cause severe low or high BG levels. Therefore, predicting the BG levels can help artificial pancreas systems to improve glycemic control.

There are several ways proposed in the literature for predicting or estimating the blood glucose level using CGM measurements. The deconvolution approach is employed to reconstruct the plasma glucose from ISF glucose measurements in [7]. However, it is concluded that perfect linearity and time invariance of the system is required for this method. In addition, various works have addressed the problem through the use of Kalman filtering. In [8], a physiological model is considered for the glucose diffusion from plasma to

ISF glucose dynamic; nevertheless, it is assumed that plasma glucose changes randomly in a step or rate fashion. In [9], the Kalman filter estimates plasma glucose and sensor gain from CGM and fingerstick measurements. In this approach, both plasma glucose level and sensor gain are modeled as ramp disturbances; however, the time lag between plasma and ISF glucose is neglected. A smoothing Kalman filter is used in [10] in an offline manner to interpolate BG measurements when blood samples are taken irregularly utilizing the CGM and fingerstick measurements. The smoothing Kalman filter is based on the central-remote rate model proposed for plasma glucose dynamics. Moreover, the plasma-to-ISF dynamic is also combined in the model. This Kalman smoother was not applied in the current study because it is non-causal.

In this paper, the Kalman filter, together with the input-less model introduced in [10] is utilized to estimate the BG level and compensate for the slow plasma-to-ISF dynamics. The proposed structure is tested on data from animal experiments, and the performance is analyzed using standard statistical methods. To the author's knowledge, the application of the proposed method to the real-life scenarios of anesthetized animal experiments, having the CGM system with a high sampling rate (every 1.2 seconds), frequent measurements of the blood gas analyzer (BGA) to evaluate the performance of the estimator, and together with the use of the intraperitoneal route for insulin and glucagon infusions are novel in the subject.

The paper is structured as follows. The data used in this paper is described in Section II. A brief description of the standard linear Kalman filter is given in Section III, a plasma-to-ISF glucose dynamics model is introduced in Section IV and evaluation tools and metrics for measuring filter performance are given in V. The results are presented in VI, and are discussed in VII, before a conclusion is provided in Section VIII.

## II. DATA

The data used for the simulations in this paper is collected through two animal experiments performed in the animal faculty of the University of Norwegian science and technology. These experiments were conducted on two anesthetized pigs whose endogenous insulin and glucagon secretions were suppressed using Octreotide (Sandostatin) with a rate of 5  $\mu\text{g}/\text{kg}/\text{h}$ . In addition, intravenous glucose infusion (with a concentration of 200mg/ml) was used to simulate different meals in the anesthetized animal experiments. In order to control the BG level, intraperitoneal insulin and glucagon administrations were used.

The CGM sensors used in these experiments were the Medtronic Enlite sensor (Northridge, Canada). These sensors were paired with custom transmitters from Inreda Diabetic (Goor, the Netherlands), providing measurements with a sampling rate of 1.2s. In order to measure the BG level directly, blood samples were taken sporadically, varying between every 5 min-1 hour, and analyzed by ABL800 FLEX analyzer (Copenhagen, Denmark), which is a BGA system.

Data set 1 is the collected data from animal experiment 1 and consists of three meals, where the weight of the pig was 36 kg, while data set 2 the collected data from animal experiment 2 and consists of four meals, where the weight of the pig was also 36 kg. The CGM measurements are plotted together with the BGA measurements for data set 1 and for data set 2 in (1).

## III. KALMAN FILTER

The Kalman filter is a recursive filter that uses a time series of measurements in order to estimate the internal states of a linear dynamical system. Given an output signal  $y_k$ , any time-invariant discrete system can be assumed to be modelled as follows:

$$x_{k+1} = Fx_k + Bu_k + w_k \quad (1)$$

$$y_k = Hx_k + v_k \quad (2)$$

where  $x_k \in \mathbb{R}^n$ ,  $u_k \in \mathbb{R}^p$ , and  $y_k \in \mathbb{R}^m$  is the system state, system input and the system output vectors at time iteration  $k$ , respectively. Moreover,  $F$  is the state transition matrix,  $B$  is the input transition matrix, and  $H$  is the measurement matrix. Assume that the system matrices all have appropriate dimensions. The process and measurement noises are denoted by  $w_k$  and  $v_k$  which satisfy the following conditions:

$$\begin{aligned} w_k &\sim (0, Q) \\ v_k &\sim (0, R) \\ E[w_k w_j^T] &= Q\delta_{k-j} \\ E[v_k v_j^T] &= R\delta_{k-j} \\ E[v_k w_j^T] &= 0. \end{aligned} \quad (3)$$

where  $Q$  and  $R$  are covariance matrices of process and measurement noises respectively. In addition,  $\delta_{k-j}$  is the Kronecker delta function which gives  $\delta_{k-j} = 1$  if  $k = j$ , and  $\delta_{k-j} = 0$  if  $k \neq j$  [11].

The Kalman filter computes an estimate of the internal states,  $\hat{x}$ , as well the estimation error covariance matrix,  $P_k$ , for each time iteration  $k$ .  $P_k$  can be considered as a tool to evaluate of the quality the current estimate  $\hat{x}_k$  quantitatively [12].

The estimation process is performed in two steps, a *prediction step*, and a *correction step*. In the prediction step the filter uses the model from (1) to predict the states one iteration ahead of time. The resulting estimate is known as the *a priori estimate*, and will be denoted as  $\bar{x}_{k+1}$  and  $\bar{P}_{k+1}$ . In the following correction step the *a priori estimate* is used in combination with the measurement  $y_k$  to update and improve the *a posteriori estimate*, which is denoted  $\hat{x}_{k+1}$  and  $\hat{P}_{k+1}$ .

Hence the Kalman filter equations are given by the followings [11]:

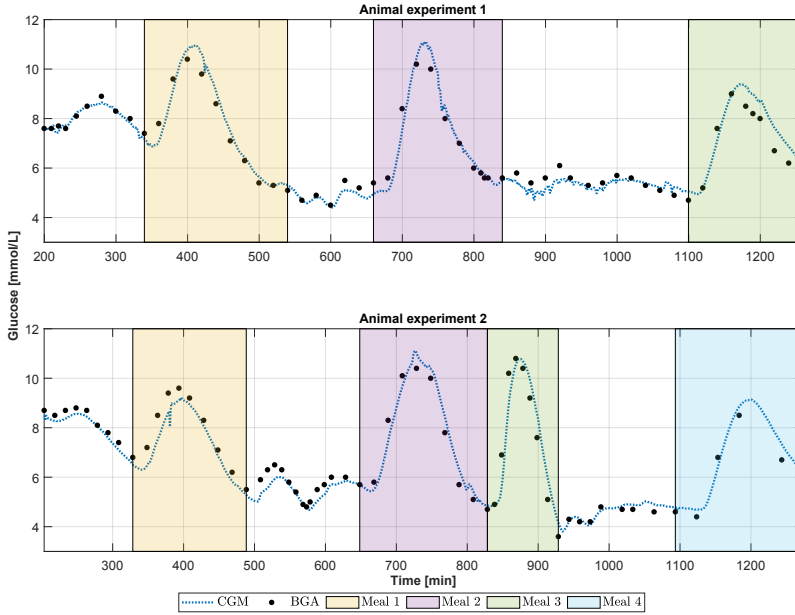


Fig. 1: Continuous glucose monitoring (CGM) and blood gas analyzer (BGA) measurements sectioned by color into specific meal times. The top row describes the data set from animal experiment 1, with three observed meal times, while the bottom row describes the data set from animal experiment 2, with four observed meal times.

Prediction:

$$\begin{aligned}\bar{x}_{k+1} &= F\hat{x}_k + Bu_k \\ \bar{P}_{k+1} &= FPF^T + Q\end{aligned}$$

Correction:

$$\begin{aligned}K_k &= \bar{P}_{k+1}H^T(H\bar{P}_{k+1}H^T + R)^{-1} \\ \hat{x}_{k+1} &= \bar{x}_{k+1} + K_k(y_k - H\bar{x}_{k+1}) \\ P_{k+1} &= (I - K_kH)\bar{P}_{k+1}.\end{aligned}$$

where  $K_k$  is the Kalman gain matrix at time iteration  $k$ . The dynamical system given by (1) and (2) must be fully observable for the Kalman filter to obtain optimal estimates of all internal states. When a system is fully observable, the observability given by (5) is full rank.

$$O = \begin{bmatrix} H \\ HF \\ \vdots \\ HF^{n-1} \end{bmatrix} \quad (5)$$

#### IV. MATHEMATICAL MODEL

Using a Kalman filter requires a mathematical, dynamic model describing the system. Models describing the glucose dynamics are not limited in the literature, and they range

from minimal [13] to quite complex [14]. Models like these describe the glucose dynamics where insulin and meals are inputs of the system. Using such models requires precise information about inputs and parameters, which is not always available or bears the quality needed. In this paper, the introduced model in [10] which combines the ISF glucose dynamics with a plasma glucose dynamical model is used. The combined model makes it possible to have plasma glucose as a state of the system, which is observable with CGM measurement. Notably, insulin and meals are treated as unknown system disturbances in this model.

##### A. Plasma-ISF Glucose Dynamics

The Steil-Rebrin model is a model describing the ISF glucose dynamics, using a two compartmental structure as follows [15], [16] :

$$\frac{dG_{isf}}{dt}(t) = -(k_{02} + k_{12})G_{isf}(t) + k_{21}\frac{V_1}{V_2}G_p(t). \quad (6)$$

where  $k_{02}$  is the glucose uptake rate of subcutaneous tissue from ISF,  $k_{12}$  and  $k_{21}$  are diffusion rates between plasma and ISF compartments,  $V_1$  and  $V_2$  are volumes of the plasma and ISF glucose compartments, respectively [11].  $G_{isf}$  describes the glucose concentration in ISF, and  $G_p$  describes the glucose concentration in plasma. The relationship between the plasma glucose concentration and the ISF glucose concentration can be further simplified:

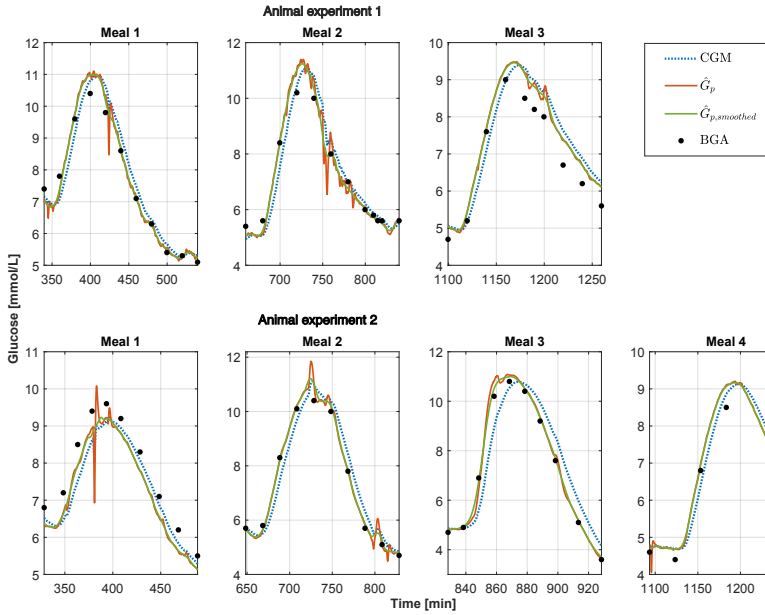


Fig. 2: Kalman filter estimate,  $\hat{G}_p$ , plotted together with the moving average smoothed Kalman filter estimate,  $\hat{G}_{p,smoothed}$ , where Continuous glucose monitoring (CGM) measurements and blood gas analyzer (BGA) measurements are shown for comparison.

$$\frac{dG_{isf}}{dt}(t) = -\frac{1}{T_{isf}}G_{isf}(t) + \frac{g}{T_{isf}}G_p(t), \quad (7)$$

where  $T_{isf}$  is the diffusion time constant, and  $g$  is a steady-state gain. These parameters are defined as follows:

$$T_{isf} \triangleq \frac{1}{k_{02} + k_{12}} \quad (8)$$

$$g \triangleq \left( k_{21} \frac{V_1}{V_2} \right) T_{isf} \quad (9)$$

Notably, in the steady state,  $g = G_{isf}/G_p$ . Physiologically, for a given change in plasma glucose concentration, the same long-term change in the ISF glucose concentration is expected, and thus  $g = 1$  [7], [11].

### B. Central-Remote Rate Model

The plasma glucose model is divided into a central compartment,  $C_c$ , and a remote compartment,  $C_r$ . Insulin or meals going into the system will first affect the central compartment before it diffuses over to the remote compartment by a first-order delay [10], where it finally causes changes in the plasma glucose concentration,  $G_p$ . The state-space equations are as followings:

$$\begin{aligned} \frac{dG_p}{dt}(t) &= C_r(t) \\ \frac{dC_c}{dt}(t) &= -\frac{1}{T_d}C_c(t) \\ \frac{dC_r}{dt}(t) &= \frac{1}{T_d}(C_c(t) - C_r(t)), \end{aligned} \quad (10)$$

where  $T_d$  is a time constant, describing the diffusion rate between the central and remote compartments [10].

### C. Combined Model

The models from (IV-A) and (IV-B) are combined to create a fully observable system in which the plasma glucose concentration is part of the state vector. At the same time, it also provides an insight into plasma glucose dynamics. The state-space form of this combined model is given by:

$$\begin{aligned} \begin{bmatrix} \dot{G}_{p,k} \\ \dot{C}_{c,k} \\ \dot{C}_{r,k} \\ \dot{G}_{isf,k} \end{bmatrix} &= \begin{bmatrix} 0 & 0 & 1 & 0 \\ 0 & -\frac{1}{T_d} & 0 & 0 \\ 0 & \frac{1}{T_d} & -\frac{1}{T_d} & 0 \\ \frac{1}{T_{isf}} & 0 & 0 & -\frac{1}{T_{isf}} \end{bmatrix} \begin{bmatrix} G_{p,k} \\ C_{c,k} \\ C_{r,k} \\ G_{isf,k} \end{bmatrix} + w_k \\ y_k &= [0 \quad 0 \quad 0 \quad 1] \begin{bmatrix} G_{p,k} \\ C_{c,k} \\ C_{r,k} \\ G_{isf,k} \end{bmatrix} + v_k, \end{aligned} \quad (11)$$

TABLE I: Mean absolute error (MAE) and mean absolute percentage error (MAPE) scores for the continuous glucose monitoring (CGM) measurements, the Kalman filter blood glucose estimate,  $\hat{G}_p$  and for the moving average smoothed Kalman filter estimate,  $\hat{G}_{p,smoothed}$ , where blood gas analyzer (BGA) is considered as the reference blood glucose level.

		MAE [mmol/L]			MAPE [%]		
		CGM	$\hat{G}_p$	$\hat{G}_{p,smoothed}$	CGM	$\hat{G}_p$	$\hat{G}_{p,smoothed}$
Data set 1	Meal 1	0.38	0.24	0.21	4.82	2.99	2.61
	Meal 2	0.34	0.31	0.20	4.68	4.17	2.69
	Meal 3	0.55	0.47	0.45	8.02	6.90	6.60
	All	0.32	0.30	0.25	4.68	4.36	3.72
Data set 2	Meal 1	0.46	0.48	0.50	5.78	6.47	6.55
	Meal 2	0.43	0.16	0.17	5.86	2.03	2.22
	Meal 3	0.65	0.21	0.13	9.53	2.71	1.86
	Meal 4	0.44	0.37	0.34	7.30	6.12	5.55
	All	0.40	0.28	0.27	5.84	4.11	3.98

where the dot notation is equivalent to the time-derivative notation, i.e.  $\dot{x} = \frac{dx(t)}{dt}$ . Notably, by assuming  $A$  as the continuous state transition matrix of the combined systems of eq. (10) and eq. (7), the combined system is discretized by setting the discrete state transition matrix equal to  $e^{A\Delta t}$ , where the time step  $\Delta t$  is set to  $\frac{1.2}{60}$  min (in which 1.2 sec is the CGM sampling time).

## V. METRICS

To evaluate the performance of the filter more in detail, the mean absolute error (MAE) and mean absolute percentage error (MAPE) are used, which are defined as below:

$$\text{MAE} = \frac{1}{n} \sum_{i=1}^n |e_i|, \quad (12)$$

$$\text{MAPE} = \frac{1}{n} \sum_{i=1}^n \frac{|e_i|}{y_i} 100\%, \quad (13)$$

with

$$e_i = y_i - \hat{y}_i, \quad (14)$$

where  $y_i$  and  $\hat{y}_i$  are the real value and the estimate of that, respectively, and  $n$  is the total number of samples. The more accurate the method, the smaller the resulting values for MAE and MAPE.

In the calculation of MAE and MAPE, the CGM measurements, the Kalman filter estimate ( $\hat{G}_p$ ), and the smoothed estimates ( $\hat{G}_{p,smoothed}$ ) are compared with the BGA measurement as the reference value. As the BGA samples were taken sporadically while CGM sensor readings and the estimates via Kalman filter are available every 1.2sec, the error is calculated based on BGA samples and their closest corresponding samples in CGM readings or Kalman filter estimates.

## VI. RESULTS

In order to predict the BG level using the CGM measurements, a Kalman filter is utilized. This filter is designed based on the model given in (11). In this model,  $T_d$  is set to 10 min as in [10], and  $T_{isf}$  is set to 7 min, as the middle

point of what has been reported in the literature (4–10 min) [2]. The process noise covariance  $Q$  and the measurement noise covariance  $R$  are given in as followings, respectively.

$$Q = \begin{bmatrix} 0.01 & 0 & 0 & 0 \\ 0 & 0.01 & 0 & 0 \\ 0 & 0 & 0.01 & 0 \\ 0 & 0 & 0 & 0.01 \end{bmatrix}, R = 2 \quad (15)$$

The Kalman filter estimates, as well as CGM measurements and BGA samples for each of the two animal experiments, are shown in fig. 2. This figure describes specifically the meals throughout the experiments, which are recognized by rise and fall in the blood glucose concentration. As is shown in fig. 2, the Kalman filter successfully reconstructed the BG level using the CGM measurements and compensated for what can be interpreted as the time lag due to the glucose diffusion process between plasma and interstitial compartments. The Kalman filter is observed to be oversensitive to small changes in the CGM measurements, hence a moving average smoother is employed to smooth the estimates. Using a moving average function in Matlab with a span of 1000 samples does not make a significant delay in the estimates, but it results in smoothed estimates. The only drawback is the requirement of having enough CGM samples to start the smoother, which is equal to having 20 min of CGM readings.

In table I, the evaluation scores are calculated for every meal registered in each data set, as well as for the whole time window, with the exception of the calibration interval, from about 0–200 min. As demonstrated in this table, there is a clear trend where the Kalman filter outperforms the CGM system due to the prediction, and the moving average filtering improves the performance of the Kalman filter. Meal 1 in data set 2 is an exception to this trend, showing the best score for MAE and MAPE in the CGM measurements. As shown in Meal 1, data set 2, in fig. 2, approximately no time lag exists between CGM and BGA measurements when glucose is decreasing, implying that the poor performance of the Kalman filter in this meal is more related to the sensor itself rather than the Kalman filter. The importance

of smoothing can be observed in meal 2 of data set 1, where the CGM and the Kalman filter performances do not differ to a high degree, while the smoothed Kalman filter estimate has a significantly lower score for both MAE and MAPE, see table I, and follows the slope of the BGA precisely, see fig. 2. Predictions achieved by the Kalman filter and the smoothed Kalman filter bear more resemblance to the BGA measurements compared to the CGM readings, and for most of the meals the estimates can be seen eliminating what can be interpreted as the slower dynamic of CGM. This is especially evident in Meal 1, Meal 2 and on glucose increase in Meal 3, for data set 1, and Meal 2, Meal 3, and on glucose increase in Meal 4, in data set 2, see fig. 2.

## VII. DISCUSSION

For the sake of simplicity, a linear model was used in this study. Future research should examine the impact of model choice on the outcomes and evaluate whether a more sophisticated or even simpler model might enhance the predictions. The parameters of the model are adjusted according to the literature. Hence, given any CGM measurements, the proposed method with the same parameters should be able to predict the BG level without system identification. However, performance degradation might be expected if the CGM sampling rate decreases. In addition, a trial-and-error approach is used to tune the covariance matrices to achieve satisfactory results while a methodical approach to adjust the KF can improve the performance. Moreover, only two data sets have been used in the simulations for evaluation, and in order to achieve more reliable results, the method should be tested on more data sets that are saved for future studies. The proposed method can be used in closed-loop systems and/or state estimators (for example [17]) to decrease the delays in artificial pancreas systems. However, the effectiveness of the suggested method in closed-loop systems may be evaluated by using the control-variability grid analysis (CVGA) method.

## VIII. CONCLUSIONS

The glucose diffusion process from plasma to interstitial fluid causes a time lag between BG levels and CGM measurements as the CGM sensor measures glucose in the subcutaneous tissue. The Kalman filter with an input-less model of the glucose dynamics has been used to estimate the BG level based on the CGM measurement. In addition, the Kalman filter estimates were smoothed in order to reduce the Kalman filter sensitivity to the disturbances of CGM readings. Considering the BGA values as the reference, the performance of the CGM sensor, Kalman filter, and moving average smoothed Kalman filter were assessed. Results showed that estimates obtained from both the Kalman filter and moving average smoothed Kalman filter resembled the BGA measurements to a higher degree, than the CGM measurements.

## IX. ACKNOWLEDGMENTS

The animal experiments were carried out at the Comparative medicine core facility in the Norwegian University

of Science and Technology (NTNU). The study was partly funded by The Norwegian Research Council (with project no. 248872) through the Center for Digital Life Norway. The transmitters and the hormones infusion system are provided by Inreda Diabetic company (Goor, the Netherlands) for this study at no cost. The authors would like to thank Marte Kierulf Åm, Oddveig Lyng, and Patrick Christian Bösch for their contribution to the data collection.

## REFERENCES

- [1] IDF Diabetes Atlas, "Diabetes around the world in 2021," <https://diabetesatlas.org/> (accessed: 22.03.2022), 2021.
- [2] A. Cinar and K. Turksøy, *Advances in Artificial Pancreas Systems, Adaptive and Multivariable Predictive Control*. Gewerbestrasse 11, 6330 Cham, Switzerland: Springer International Publishing AG, 2018.
- [3] Centers for Diseases Control and Preventing, "What is type 1 diabetes?" <https://www.cdc.gov/diabetes/basics/what-is-type-1-diabetes.html> (accessed: 22.03.2022), 2022.
- [4] International Diabetes Federation, "Type 1 diabetes," <https://idf.org/aboutdiabetes/type-1-diabetes.html> (accessed: 22.03.2022), 2020.
- [5] G. Cappon, M. Vettoretti, G. Sparacino, and A. Facchinetti, "Continuous glucose monitoring sensors for diabetes management: A review of technologies and applications," *Diabetes and Metabolism Journal*, vol. 43, no. 4, pp. 383–397, 2019.
- [6] G. Schmelzeisen-Redeker, M. Schoemaker, H. Kirchsteiger, G. Freckmann, L. Heinemann, and L. del Re, "Time delay of cgm sensors: Relevance, causes, and countermeasures," *Journal of Diabetes Science and Technology*, vol. 9, no. 5, pp. 1006–1015, 2015.
- [7] C. C. Andrea Facchinetti, Giovanni Sparacino, "Reconstruction of glucose in plasma from interstitial fluid continuous glucose monitoring data: Role of sensor calibration," *IEEE Transactions on Biomedical Engineering*, vol. 1, no. 3, pp. 671–623, 2007.
- [8] B. Bequette, "Optimal estimation applications to continuous glucose monitoring," in *Proceedings of the 2004 American Control Conference*, vol. 1, 2004, pp. 958–962 vol.1.
- [9] M. Kuure-Kinsey, C. C. Palermo, and B. W. Bequette, "A dual-rate kalman filter for continuous glucose monitoring," in *2006 International Conference of the IEEE Engineering in Medicine and Biology Society*, 2006, pp. 63–66.
- [10] O. M. Staal, S. Salid, A. Fougner, and O. Stavdahl, "Kalman smoothing for objective and automatic preprocessing of glucose data," *IEEE Journal of Biomedical and Health Informatics*, vol. 23, no. 1, pp. 218–226, 2019.
- [11] D. Simon, *Optimal Estimation*. John Wiley & Sons, Inc., Hoboken, 2006.
- [12] F. Auger, M. Hilaret, J. M. Guerrero, E. Monmasson, T. Orłowska-Kowalska, and S. Katsura, "Industrial applications of the kalman filter: A review," *IEEE Transactions on Industrial Electronics*, vol. 60, no. 12, pp. 5458–5471, 2013.
- [13] C. Claudio, M. Chiara, Dalla, T. Gianna, B. Rita, V. Adrian, and R. Rizza, "The oral minimal model method," *Diabetes*, vol. 63, no. 4, p. 1203–1213, 2014.
- [14] C. D. Man, F. Micheletto, D. Lv, M. Breton, B. Kovatchev, and C. Cobelli, "The uva/padova type 1 diabetes simulator: New features," *Journal of Diabetes Science and Technology*, vol. 8, no. 1, pp. 26–34, 2014.
- [15] T. Koutny, "Blood glucose level reconstruction as a function of transcapillary glucose transport," *Computers in Biology and Medicine*, vol. 53, pp. 171–178, 2014.
- [16] K. Rebrin, G. M. Steil, W. P. van Antwerp, and J. J. Mastrototaro, "Subcutaneous glucose predicts plasma glucose independent of insulin: implications for continuous monitoring," *American Journal of Physiology-Endocrinology and Metabolism*, vol. 277, no. 3, pp. E561–E571, 1999.
- [17] K. D. Benam, H. Khoshmadi, L. Lema-Pérez, S. Gros, and A. L. Fougner, "A nonlinear state observer for the bi-hormonal intraperitoneal artificial pancreas," in *2022 44th Annual International Conference of the IEEE Engineering in Medicine & Biology Society (EMBC)*. IEEE, 2022, pp. 171–176.

## 6.4 PAPER 4

**Title: “Estimation and Prediction of Glucose Appearance Rate for Use in a Fully Closed-Loop Dual-Hormone Intraperitoneal Artificial Pancreas”**

Published in IEEE Transactions on Biomedical Engineering on 26 July 2023,  
In press [4].





# Estimation and Prediction of Glucose Appearance Rate for Use in a Fully Closed-Loop Dual-Hormone Intra-peritoneal Artificial Pancreas

Karim Davari Benam, *Student Member, IEEE*, Sebastien Gros, and Anders Lyngvi Fougner, *Member, IEEE*

**Abstract**—Objective: A fully automated artificial pancreas requires a meal estimator and predictions of blood glucose levels (BGL) to handle disturbances during meal times, all without relying on manual meal announcements and user interventions. This study introduces a technique for estimating the glucose appearance rate (GAR) and predicting BGL in people with type 1 diabetes and insulin and glucagon administration. It is demonstrated for intraperitoneal insulin and glucagon delivery but may be adapted to other delivery sites. Method: The estimator is designed based on the moving horizon estimation (MHE) approach, where the underlying cost function incorporates prior statistical information on the GAR in subjects over the course of a day. The proposed prediction scheme is developed to predict GAR using estimated states and an intestinal model, which is then used to predict BGL with the help of an animal glucose metabolic model. Results: The intraperitoneal dual-hormone estimator was evaluated on three anesthetized animals, achieving a 21.8% mean absolute percentage error (MAPE) for GAR estimation and a 10.0% MAPE for BGL prediction when the future GAR is known. For a 120-minute prediction horizon, the proposed predictor achieved an 18.0% MAPE for GAR and a 28.4% MAPE for BGL. Conclusion: The findings demonstrate the effectiveness and reliability of the proposed estimator and its potential for use in a fully automated artificial pancreas and reducing user interventions. Significance: This study represents advancements toward the development of a fully automated artificial pancreas, ultimately enhancing the quality of life for people with type 1 diabetes.

**Index Terms**—Artificial pancreas, Continuous glucose monitoring, Diabetes mellitus type 1, Meal estimation, Moving horizon estimation.

## I. INTRODUCTION

IN people with type 1 diabetes (T1D), the pancreas produces insufficient or no insulin. External insulin delivery is the current approach for these patients to regulate blood glucose levels (BGL). Insulin is a hormone that allows the cells to use glucose as fuel or store it as glycogen. The most common insulin administration method is injecting insulin into the subcutaneous tissue. The amount of insulin required is estimated based on the meal size, activity level, and physical features [1], [2]. The calculation of required insulin can be done by patients or by a control system. A fully automated artificial pancreas (AP) is a system that consists of an infusion

pump, a control algorithm, and continuous glucose monitoring (CGM) system that delivers the required insulin automatically without the need for a meal and exercise announcements [3].

Due to the significant time delay in insulin absorption from subcutaneous (SC) tissue, the carbohydrate content of each meal must be announced to the control algorithms in advance to administer a meal-time insulin bolus at the appropriate time [4]. However, estimating the meal size is challenging [5], and patients occasionally forget to announce it to the AP. Unannounced meals can result in high BGL and increase the risk of insulin overdosing in an attempt to decrease the BGL. In addition, any human interventions in the medical control systems are not desired.

Dual-hormone SC APs, which can deliver insulin and glucagon subcutaneously, effectively decrease the risk of hypoglycemia [6]. However, there is still a high risk of hyperglycemia in the case of an unannounced meal [7] due to the slow pharmacokinetics and pharmacodynamics of the SC route. The intraperitoneal (IP) route is the faster route for insulin and glucagon absorption compared to the SC route [8]. The IP-AP imitates pancreatic function by delivering insulin and glucagon to the peritoneal fluid and ultimately to the liver via the portal vein [9]. The fast insulin absorption in this route is proven efficient in BGL control without meal announcement [8].

Due to the novelty of using the IP route for treating diabetes and the lack of information, fewer studies have been done on the IP route compared to the SC route. However, the IP-AP has garnered interest due to recent developments in medical technology [1], [8], [10]; however, meal estimation is still needed to determine the appropriate insulin dosage even with the faster absorption of insulin from IP route.

Model predictive control (MPC) is a widely used control method in AP systems [11]. It requires a model, predictions, and estimates of GAR, as well as an estimation of immeasurable states to function effectively. Among the models proposed for the dual-hormone intraperitoneal artificial pancreas (DIP-AP) systems, our previously developed meta model [9] is accurate in predictions and offers the advantage of a simple and short identification process. Most meta model parameters were identified and validated through prior information from 26 animal experiments, and only four parameters require identification for each new subject.

The primary focus of this paper is the development of a complete-state moving horizon estimation (MHE) approach. This method utilizes statistical characteristics of GAR obtained

K. D. Benam, S. Gros, and A. L. Fougner are with the department of Engineering Cybernetics, Faculty of Information Technology and Electrical Engineering, Norwegian University of Science and Technology (NTNU), O. S. Bragstads Plass 2D, 7034 Trondheim, Norway. Email: {Karim.D.Benam, Sebastien.Gros, Anders.Fougner}@ntnu.no.

This research is funded by the Research Council of Norway (project no. 248872) and Centre for Digital Life Norway.

through the daily life of the patients to estimate the states and GAR. Moreover, we propose a technique to predict GAR without meal announcements to enable the MPC methods to predict BGL. To evaluate the effectiveness of our proposed estimator and predictor, we conducted animal experiments on three anesthetized pigs for a duration of 24 hours. While our primary objective in this study is to design an estimator for implementation in the MPC methods, it is important to recognize that the estimator can also be utilized in other control techniques, including PID or adaptive control methods. By incorporating the estimated and predicted GAR, these control methods can be better equipped to handle unannounced meals and exercise routines.

Our research group has previously presented a method based on MHE for detecting meals in single-hormonal subcutaneous AP systems in [12], and [13]. This approach showed promising results in simulations and was validated on clinical data. In addition, in a post-processing manner, a Kalman filter was designed to estimate the time and the size of the meal [14]. However, this method was not designed for real-time use. A different approach was investigated for early meal detection based on abdominal sound [15]. Similar studies have been conducted in IP AP systems using a Kalman filter [8] and a nonlinear high gain observer [16] based on the IP model presented in [17]. These methods use complex models with multiple states and require individual identification. This paper presents an estimator designed explicitly for control purposes in dual hormone IP AP systems. One novelty lies in using “meta model” particularly suited for MPC approaches [9], which significantly reduces the number of parameters to be identified, making the identification process more straightforward in closed-loop experiments. Another novelty is that the model includes both insulin and glucagon dynamics (both pharmacodynamics and pharmacokinetics), making the estimator suitable for a dual hormone system, while the other estimators reported in the literature were developed for single hormone systems.

The paper is structured as follows. Animal care and surgical procedures are described in Section II. Section III provides the models for DIP-AP and the intestines used in the estimator. The estimator is designed based on the animal model in Section IV. In Section V, a predictor scheme for closed-loop MPC techniques is suggested using the proposed models and the designed MHE. The demonstrative scenarios are employed in Section VI to examine the accuracy and reliability of the estimates and the predictions. The discussions and conclusions are provided in Sections VII and VIII, respectively.

## II. ANIMAL EXPERIMENTS AND DATA

To evaluate the method proposed in this paper, we employed data from three animal experiments performed by our research group. This section provides a short overview of the experiments and the clinical procedures. The procedures are similar to the experiments described in [9], [18], [19].

### A. Experiments and Animal Handling

These experiments were carried out on three, male non-diabetic farm pigs (*Sus scrofa domestica*). The experiments

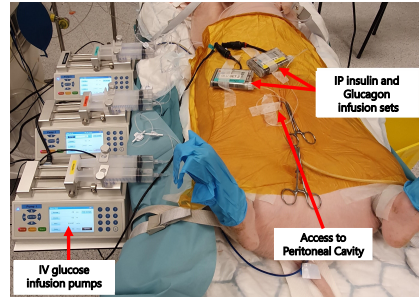


Fig. 1. The experimental setup of the dual-hormone intraperitoneal artificial pancreas for Experiment 1. The experiments were conducted on anesthetized pigs.

were named “Experiment 1”, “Experiment 2”, and “Experiment 3,” in this paper where the pigs weighed 36, 36, and 40 kg, respectively.

Before the experiments, the animals were given a week to adapt to the staff and their new environment. When possible, groups of animals were kept together. Before the experiment, they were provided unlimited access to water and twice-daily feedings of commercial growth feed. The procedure of inserting insulin and glucagon catheter into the peritoneal cavity, anesthesia, and euthanization at the end of the experiments is similar to the presented procedures in [9]. In order to suppress endogenous insulin and glucagon secretion, the pigs received octreotide as a  $5\mu\text{g}/\text{kg}/\text{h}$  intravenous (IV) infusion. The experiments lasted up to 24 hours and the pigs were euthanized with an IV overdose of pentobarbital ( $100\text{ mg}/\text{kg}$ )(pentobarbital NAF, Apotek, Lørenskog, Norway) while fully anesthetized.

These experiments were carried out at the Norwegian University of Technology (NTNU) in accordance with “The Norwegian Regulation on Animal Experimentation” and “Directive 2010/63/EU on the protection of animals used for scientific purposes.” Furthermore, the Norwegian Food Safety Authority (FOTS number 12948) approved the animal experiments.

### B. Data

Each of the experiments lasted nearly 24 hours. In order to simulate a real-life scenario and mimic the intestine functions in anesthetized pigs, an IV glucose serum with a concentration of  $200\text{ mg}/\text{ml}$  is used. The profile of the glucose infusion rate through the day is generated based on a human intestine model (“model 2”) proposed in [20]. The scenarios are further discussed in Section IV-C.

Infusing the glucose intravenously to simulate the intestines in anesthetized pigs provides unique data to evaluate the performance of the estimator in detail. In order to infuse the glucose accurately according to the time, we used three programmable Chemyx Fusion 100 syringe pumps (Chemyx Inc., Stafford, TX, United States). The experimental setup in Experiment 1 is illustrated in Fig. 1. As shown in Fig. 1,

three glucose pumps were used in the experiments in parallel to avoid frequent refills of the syringe during the experiment.

Three Medtronic Enlite sensors (Northridge, CA, USA) with custom-made transmitters from Inreda Diabetic (Goor, the Netherlands) are used to measure the BGL during the experiment. The sensors are attached one day before the experiments. The Data acquisition system can connect to only two transmitters, and one of the sensors was a backup in case the two others failed. Of the two working sensors, the one with the most accurate performance was used in the controller. In order to choose the best sensor, blood samples were taken at varying sampling times between every 5–60 minutes and analyzed by an ABL800 FLEX analyzer (Copenhagen, Denmark). In these experiments, a dual hormone IP AP based on an MPC method was used to regulate the BGL within a normal range. This paper does not address the designed AP system; instead, only the data collected is used to evaluate the effectiveness of the proposed estimator, and the AP system will be reported elsewhere. The controller could give IP insulin or glucagon every 5 minutes using two infusion pumps provided by Inreda Diabetic (Goor, the Netherlands).

### III. BACKGROUND

#### A. Meta Model

The model used in this study is the meta model presented in [9]. Meta model (1) describes the interactions of BGL with IP insulin, IP glucagon, and IV glucose infusions.

$$\frac{d}{dt} \begin{pmatrix} x_1 \\ x_2 \\ x_3 \\ x_4 \\ x_5 \\ x_6 \\ x_7 \end{pmatrix} = \begin{pmatrix} -(\beta_1 + \beta_2 \cdot x_2 + \beta_3 \cdot x_3) \cdot x_1 + HGP \\ \beta_5 (-x_2 + (\beta_7 \cdot \gamma_1 \cdot x_4 - F_{sat})) \\ \beta_8 (-x_3 + F_{sat}) \\ -\gamma_1 \cdot x_4 \\ \beta_9 (-x_5 + \beta_{10} x_6) \\ -\gamma_2 \cdot x_6 \\ \gamma_3 \cdot x_3 \cdot x_1 - \gamma_4 \cdot HGP \end{pmatrix} + \begin{pmatrix} \gamma_7 G(t) \\ 0 \\ 0 \\ \gamma_8 I(t) \\ 0 \\ \gamma_9 H(t) \\ 0 \end{pmatrix} \quad (1)$$

In this model,  $\{x_1, x_2, x_3, x_4\}$  are the states of the insulin sub-model including blood glucose level [mmol/l], effective insulin rate in the organs other than the liver [U/min], effective insulin rate in the liver [U/min], and concentration of insulin in the IP fluid [U/ml], respectively. In This sub-model,  $I(t)$  is the IP insulin infusion rate [U/min], and  $G(t)$  is the IV glucose infusion rate [mmol/min]. Notably, we assume that  $G$  is equivalent to the GAR in awake animals and represents the meal digestion rate in the intestines.

The term  $F_{sat}$  in this sub-model is used to model the saturation of the Hepatic first pass (HFP) effect, which is defined as follows:

$$F_{sat}(x_4) \triangleq \beta_{13} \frac{\beta_{12} \gamma_5 x_4}{\beta_{12} + \beta_{13} \beta_7 \gamma_1 x_4} \quad (2)$$

The states  $\{x_5, x_6, x_7\}$  are the states of the glucagon sub-model that includes effective glucagon rate in the liver [mg/min], glucagon concentration in the IP fluid [mg/ml], and glycogen storage level [%].  $H(t)$  is the IP glucagon infusion rate [mg/min], and  $HGP$  is the hepatic glucose production rate modeled as follows.

$$HGP \triangleq \beta_4 x_5 \sqrt{x_7} \cdot \exp(-\beta_{11} \cdot x_3) \quad (3)$$

In (1), the parameter set  $\{\beta_1, \dots, \beta_4\}$  and the initial value of the glycogen storage level are needed to be identified individually. However, the parameters  $\beta_5, \dots, \beta_{13}$  are shown to be relatively fixed among the different pigs, and they are identified using the prior information of the other subjects. The parameters  $\gamma_1, \dots, \gamma_9$  are body-weight dependant parameters that are known functions (See equations (16) and (17) in [9]).

The equation (1) is discretized using the Euler method. Since 5 minutes is the most typical sample rate for CGM devices, that duration is chosen for the sampling time. The following equation represents the discretized system under the given assumptions.

$$x_{k+1} = F(x_k, G_k, I_k, H_k) + w_k \quad (4a)$$

$$y_k = Cx_k + v_k \quad (4b)$$

where the discretized right hand side of (1) is denoted as  $F(x_k, G_k, I_k, H_k)$ .  $y_k$  is the BGL and  $C \triangleq [1 \ 0 \ 0 \ 0 \ 0 \ 0 \ 0]$ . For the sake of simplicity, the discretized state vector  $[x_1, x_2, x_3, x_4, x_5, x_6, x_7]^T$  is denoted as  $x_k$  where the same notation applied for the inputs and measurements.  $w_k$  is the process noise, and  $v_k$  is the measurement noise.

#### B. Intestine Model

The model for the intestine used in this study to generate scenarios and design the predictor is “model 2” proposed in [20]. This model is given as follows.

$$\begin{cases} \dot{q}_{sto1} = -k_{21} \cdot q_{sto1} + D \\ \dot{q}_{sto2} = -k_{empt} \cdot q_{sto2} + k_{21} \cdot q_{sto1} \\ \dot{q}_{gut} = -k_{abs} \cdot q_{gut} + k_{empt} \cdot q_{sto2} \\ Ra(t) = f \cdot k_{abs} \cdot q_{gut} \end{cases} \quad (5)$$

where  $q_{sto1}$  and  $q_{sto2}$  are the weight of the solid and liquid glucose in the stomach, respectively,  $q_{gut}$  is the mass of the glucose present in the intestines. The size of the meal rate is  $D$ , and  $Ra(t)$  is the glucose that appears in the blood via absorption in the intestines. The coefficient  $k_{empt}$  is the emptying rate of the stomach which is a nonlinear function defined as follows:

$$k_{empt}(q_{sto}) = k_{min} + \frac{k_{max} - k_{min}}{2} \cdot \{ \tanh[\alpha(q_{sto} - b \cdot D)] - \tanh[\beta(q_{sto} - c \cdot D)] + 2 \} \quad (6)$$

where  $q_{sto} = q_{sto1} + q_{sto2}$ . The other parameters of the model are positive constant values that are defined and given more in detail in [20].

Using the similar notation in the previous section and Euler approximation, one can find the discretized version of (5) in the following form:

$$q_{k+1} = F_q(q_k, D_k) + w_{q,k} \quad (7a)$$

$$Ra_k = C_q q_k + v_{q,k} \quad (7b)$$

where  $F_q(\cdot)$  is the discrete form of the right-hand side of the (5),  $q_k \triangleq [q_{sto1}, q_{sto2}, q_{gut}]^T$ , and  $C_q \triangleq [0 \ 0 \ k_{abs}]$ . Moreover,  $w_{q,k}$  and  $v_{q,k}$  are the process measurement noises, respectively.

### C. Comments on the meta model and the CGM devices

In the design of the meta model, it is assumed that glucagon production in the pancreas is also affected in diabetes, and the pancreas is not able to produce glucagon. However, in the case of endogenous glucose production,  $G$  represents the meal digestion rate plus the endogenous glucose production (EGP) rate.

In the experiments, the BGL is measured using CGM devices. This system measures the concentration of glucose in interstitial fluid instead of the blood. The filters used in this CGM system and the process of glucose moving from blood to interstitial fluid cause a time lag in the measurements. In this paper, we ignored the measurement delays. However, the Kalman filter proposed in [21] can be used to compensate for the time lag. However, in this paper, we only used the sensor measurements for the sake of simplicity.

## IV. MOVING HORIZON ESTIMATION

In order to estimate the states of (4a), an approach similar to MHE is employed in this work. MHE is an optimization-based estimation technique for nonlinear systems where the current state of a system is estimated from a finite set of past measurements [22].

Regarding the accuracy of the different estimation techniques in nonlinear systems, MHE commonly outperforms standard state estimation approaches such as the extended Kalman filter (EKF). This is certainly relevant for nonlinear systems, which have been thoroughly considered in MHE. Unlike the EKF, MHE considers a horizon of recent measurements and a nonlinear model to estimate the state trajectories. In addition, using the MHE approach, one can estimate the sequence of the unknown inputs over the estimation horizon.

The capability and ease of accommodating constraints, prior knowledge of the states, or disturbances with non-Gaussian statistics are the other significant advantages of MHE. However, all of these advantages come at a higher computational cost. The basics of a standard MHE scheme are described in the following section.

### A. Design of a Standard MHE with Assuming Glucose Appearance Rate is Known

The fundamental idea behind MHE is that the current state of the system is derived from a finite sequence of prior measurements taken within a time window of length  $N_{ob}$ . This sequence is subject to the disturbances and the model of the system.

The MHE can be expressed as an optimization problem in which the decision variables are the initial values of the states and the sequence of the process disturbances over the time estimation horizon. As an example, for the states (4a) and measurement (4b) with known  $G_k$ ,  $I_k$ , and  $H_k$ , the MHE cost function takes the following form [23].

$$\Phi_1(\hat{x}_{t_0}, w_{t_0-1}, \dots, w_{k-1}) = \Gamma_1(\rho) + \sum_{j=t_0}^k \mathcal{L}_1(w_{j-1}, v_j) \quad (8a)$$

subject to:

$$\rho = \hat{x}_{t_0} - \bar{x}_{t_0} \quad (8b)$$

$$\hat{x}_{k+1} = F(\hat{x}_k, G_k, I_k, H_k) + w_k \quad (8c)$$

$$v_k = y_k - C\hat{x}_k \quad (8d)$$

$$x_k \in \Omega_x, \quad w_k \in \Omega_w \quad (8e)$$

where  $t_0 := K - N_{ob} + 1$ ,  $\Gamma_1(\rho) := \rho^T P^{-1} \rho$  and  $\mathcal{L}_1(w_k, v_k) := w_k^T Q^{-1} w_k + v_k^T R^{-1} v_k$ . Matrices  $R$  and  $Q$  are covariance matrices of process noises and measurement noise, respectively. The term  $\Gamma_1(\rho)$  is the arrival cost that carries prior information on the state of the system before time  $k = t_0$ .  $\bar{x}_{t_0}$  is a priori state estimate and  $P$  represents the covariance of  $\bar{x}_{t_0}$ . Variable  $\hat{x}_k$  is the estimated state vector at time  $k$ . Equation (8e) represents the constraints on the values of the states, process noises, and measurement noise, respectively.

The meals are not announced in the desired fully automated AP systems, and the GAR must be estimated. Similar to [12] and [13], one approach to estimate the GAR and detect the meals is to design and identify a model for the intestines (similar to equation (4) in [12]) to combine it with the meta model.

In the method mentioned above, the parameters of the intestine model need to be identified individually. Moreover, the glucose absorption rate is variable for the different types of meals. For example, the intestines absorb liquids faster than solid meals [20]. In addition, the EGP has different dynamics than the intestine. It is possible to employ a complex model for  $G$  to get around the problems mentioned above. However, it needs parameter identification, adds a higher computational cost, and requires additional information about the initial values and covariance matrices, which are not available.

In the next section, a dual-hormone intraperitoneal moving horizon estimator is designed to estimate the glucose appearance rate independently of the intestine model and based on measurements and prior knowledge about the lifestyle of the subjects.

### B. Dual-hormone Intraperitoneal Moving Horizon Estimator with Unknown Glucose Appearance Rate

The main idea behind the estimator presented in this study is to directly estimate  $G$  over the MHE horizon based on the lifestyle of the patients. For the sake of simplicity, we recall the estimator in this section as Dual-hormone Intraperitoneal Moving Horizon Estimator (DIP-MHE).

We assumed that  $G$  is an input with a probability distribution function (PDF). An intestine and exercise model that generates the  $G$  based on the meals and the activities can be used to find the PDF function from the information gathered about the daily diets and exercise routines of the patients. The idea mentioned above can be formulated as followings:

$$\Phi_2(\hat{x}_{t_0}, \hat{G}_{t_0-1}, \dots, \hat{G}_{k-1}, w_{t_0-1}, \dots, w_{k-1}) = \Gamma_2(\rho) + \sum_{j=t_0}^k \mathcal{L}_2(w_{j-1}, v_j) + \sum_{j=t_0}^k \mathcal{J}(\hat{G}_j) \quad (9a)$$

subject to: (8b), (8d), (8e) and

$$\hat{x}_{k+1} = F(\hat{x}_k, \hat{G}_{g,k}, I_k, H_k) + w_k, \quad (9b)$$

$$\hat{G}_k \geq 0 \quad (9c)$$

in which  $\Gamma_2(\rho) = \rho^T P_2^{-1} \rho$  and  $\mathcal{L}_2(w_k, v_k) = w_k^T Q_2^{-1} w_k + v_k^T R_2^{-1} v_k$ , where  $P_2$ ,  $Q_2$ , and  $R_2$  are positive definite matrices with the same definitions as in Section IV-A. The estimated glucose appearance rate is denoted as  $\hat{G}_k$ .

The term  $\mathcal{J}(\cdot)$  is the prior knowledge embedded in the cost function to impose the feature of the  $G_k$  to the estimator. Therefore,  $\mathcal{J}(\cdot)$  must be designed based on the body weight and the inverse distribution function (IDF) of  $G_k$ . One may use the  $\log(\cdot)$  function or numerical approximation methods to obtain the IDF using the PDF.

We can use the statistics of  $G_k$  to embed the prior knowledge of GAR into the MHE. To achieve this, we must approximate the GAR according to the lifestyle and find its PDF. However, the complete information regarding the lifestyle and  $G$  might not be available, and the information that the approximate PDF provides for the MHE might be incomplete. We know that glucose absorption in the intestines and hepatic glucose production have slow dynamics and are continuous functions. Therefore, one can find the PDF of the  $\Delta G_k := G_k - G_{k-1}$  (rate of GAR) as well and use it as an additional embedded prior knowledge for GAR.

Let us assume  $f_r(G_k)$  and  $f_{dr}(\Delta G_k)$  are PDFs of  $G_k$  and  $\Delta G_k$ , respectively. In this case, one can use the following formulation to embed these PDFs in MHE by designing the  $\mathcal{J}(\cdot)$  as follows:

$$\mathcal{J}(G_j) \triangleq p_r \cdot f_r^{-1}(G_j) + p_{dr} \cdot f_{dr}^{-1}(\Delta G_j) + p_{r_0}(G_j - \bar{G}_j)^2 \quad (10)$$

where  $f_r^{-1}(G_j)$  and  $f_{dr}^{-1}(\Delta G_j)$  are IDFs of  $G_j$  and  $\Delta G_j$ , respectively. As mentioned earlier, the IDFs can be found using the  $\log(\cdot)$  function or numerically from the found PDFs.  $p_r$  and  $p_{dr}$  are positive constant scalars. In (10),  $\bar{G}_j$  is the prior value chosen for the scalar  $G_j$ . Therefore, the term  $p_{r_0}(G_j - \bar{G}_j)^2$  is similar to the arrival cost in the MHE.  $p_r$ ,  $p_{dr}$ , and  $p_{r_0}$  are positive constant scalars.

The defined cost (10) embeds the approximated statistics of  $G_k$  to the estimator. The challenge in this approach is selecting  $f_r(\cdot)$  and  $f_{dr}(\cdot)$ . These PDFs are time-varying, and they can change according to the changes in lifestyle and diet. For instance, the type and size of the meals can be chosen based on the body weight and diet to produce the  $G$  for the entire day, but if the patients change their diet, the type of food they eat, or the number of meals they eat throughout the day, the PDFs must be updated to reflect the new changes. We assumed that the patients followed a relatively consistent routine in their lifestyle regarding the number of meals per day, activity level, and the size of the meals relative to their body weight. Therefore,  $f_r(\cdot)$  and  $f_{dr}(\cdot)$  are considered as time-invariant functions. In the next section, a demonstrative example is provided to find  $f_r(\cdot)$  and  $f_{dr}(\cdot)$  for the animal experiments.

### C. Probability Distribution Functions of Glucose Appearance Rate for a Demonstrative Scenario in Animal Experiment

As mentioned earlier, GAR must be found according to the lifestyle, diet, and physical characteristics of the patients. This section illustrates how to generate  $G$  and then find  $f_r(\cdot)$  and  $f_{dr}(\cdot)$  for the 24-hour anesthetized animal trial.

The IV glucose infusion is used in animal experiments to simulate the GAR. We simulated the EGP, main meals, and exercise events within 24 hours. The GAR is chosen to present significant challenges to the controller used in these experiments. The controller and experiment design are beyond the scope of this paper. The different elements of this scenario are defined as follows.

1) *EGP Simulation*: The basal rate of glucose production in adults is 2–8 mg/min/kg [24]. To prevent hypoglycemia and make sure that the pig received enough glucose during the experiment, we assumed that EGP has a constant rate during the day with a rate of 5 mg/min/kg.

2) *Meal Simulation*: To mimic the behavior of the intestines in the body and generate the GAR for a full-day experiment, we used the intestine (5) with the parameter identified in human trials listed in [20]. The experiments are scheduled to begin at 9:30 a.m. The times and sizes of meals are chosen based on body weight in the following manner:

- 11:00 a.m.: 0.30 gr/kg meal as a small breakfast.
- 01:00 p.m.: 0.70 gr/kg meal as a lunch.
- 06:45 p.m.: 1.00 gr/kg meal as a dinner.
- 09:45 p.m.: 0.60 gr/kg soft drink.
- 11:45 p.m.: 0.00 gr/kg sleeping.
- 03:50 a.m.: 0.70 gr/kg meal as a breakfast.

3) *Exercise/Low Glucose Scenario*: In reality, the impact of physical activity on BGL is multifaceted. Nonetheless, anesthetized animals cannot perform an exercise. Therefore, to simulate the effect of exercise at aerobic (low/medium) intensity, we lowered the glucose infusion from the baseline GAR. It was simulated as a "negative meal" (subtracted from the baseline glucose infusion) with a size of 0.25 mg/kg administered at 04:30 PM.

The designed scenario is illustrated in Fig. 2. Based on the designed scenario, we found the PDFs of  $G$  and  $\Delta G_k$ . The gamma distribution function is chosen to define the probability feature of  $G$  since the glucose appearance rate is always a positive value. For the sake of simplicity, we assumed that  $G$  and  $\Delta G_k$  are independent variables. In addition, it is assumed that  $\Delta G_k$  has a normal distribution. With these assumptions, the estimated  $G$  over the MHE horizon can increase or decrease at the same rate due to the normal distribution of the  $\Delta G_k$  independently of the estimated values for  $G$ .

In order to identify the parameters of the mentioned PDFs, the maximum likelihood method is used. The scenario for the experiments and the found PDFs are illustrated in Fig. 2.

### D. Comments on the Designed DIP-MHE

In order to impose the prior knowledge to MHE, the cost (10) is proposed to embed into the standard MHE cost function. A Gamma PDF is identified for  $G$ . For simplicity, it is assumed that the  $\Delta G_k$  has a normal distribution and is

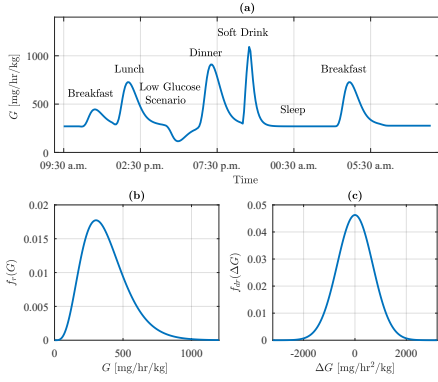


Fig. 2. The glucose appearance rate ( $G$ ) designed for the 24-hour anesthetized animal experiments is shown in panel (a). The glucose was given intravenously. The fitted probability distribution functions of  $G$  (with gamma PDF) and  $\Delta G_k$  (with normal PDF) are shown in panels (b) and (c), respectively.

independent of  $G_k$ . However, this simplification might not be accurate in real life, and the  $\Delta G_k$  has a dependency on  $G_k$ . Additionally, the scenario is intended to last 24 hours due to the restrictions on the duration of the anesthetized animal trials. One should create weekly or monthly routines to achieve more accurate PDFs. Additionally, performing the exercise on anesthetized pigs is unfeasible. Thus, we have lowered the glucose infusion rate to simulate the impact of exercise at a low to medium aerobic intensity. Nonetheless, it is important to perform the actual exercise testing on awake animal subjects or proceed to the human phase for better evaluation of the designed estimator in exercise events.

## V. BLOOD GLUCOSE PREDICTOR SCHEME WITH UNANNOUNCED MEAL

In the MPC methods, the BGL is predicted based on the possible combinations of future insulin and glucagon boluses. However, the future glucose appearance rates over the prediction horizon are needed to perform the predictions, while this information is unavailable when the meals are not unannounced. This section proposed an estimating scheme for short-term prediction of BGL that can be used for control purposes.

The idea is to estimate the states of the model 2 using the estimated GAR and predict it over the prediction horizon of  $N_p$  with assuming no meal over the time window  $\{k, \dots, k + N_p - 1\}$ . Different methods, such as EKF, high-gain observers, and others, can also be used to estimate the states of the digestive model at each sampling time with  $\hat{G}$  (the estimated GAR using the DIP-MHE). However, a standard MHE approach is used in this paper with the following cost function to estimate the

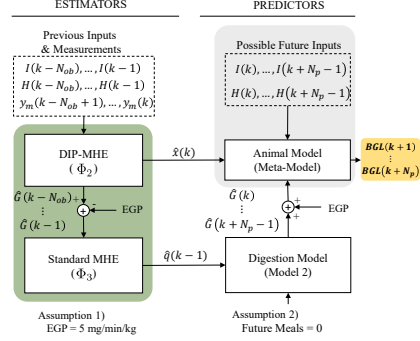


Fig. 3. The proposed BGL predictor scheme with unannounced meals. The estimators are shown in the green box. The problems  $\Phi_2$  and  $\Phi_3$  are solved sequentially to maintain modularity and simplicity of combining other observers instead of  $\Phi_3$ . The gray box can be replaced with an MPC algorithm in the closed-loop system.  $BGL(k+1), \dots, BGL(k+N_p)$  in the yellow box are the predicted blood glucose level.

states of the intestine model (7a) – (7b).

$$\Phi_3(\hat{q}_{t_0}, w_{q,t_0-1}, w_{q,t_0}, \dots, w_{q,k-1}) = \Gamma_3(\rho_q) + \sum_{j=t_0}^k \mathcal{L}_3(w_{q,j-1}, v_{q,j}) \quad (11a)$$

subject to:

$$\rho_q = \hat{q}_{t_0} - \bar{q}_{t_0} \quad (11b)$$

$$\hat{q}_{k+1} = F_q(\hat{q}_k, \hat{G}_k) + w_{q,k} \quad (11c)$$

$$v_{q,k} = (\hat{G}_k - \text{EGP}) - C_q \hat{q}_k \quad (11d)$$

$$q_k \in \Omega_q, \quad w_{q,k} \in \Omega_{w,q}, \quad v_{q,k} \in \Omega_{v,q} \quad (11e)$$

in which  $\Gamma_3(\rho_q) = \rho_q^T P_q^{-1} \rho_q$  and  $\mathcal{L}_3(w_{q,j}, v_{q,j}) = w_{q,j}^T Q_q^{-1} w_{q,j} + v_{q,j}^T R_q^{-1} v_{q,j}$ . Notably, the positive definite matrices  $P_q$ ,  $Q_q$ , and  $R_q$  have the same definition as  $P$ ,  $Q$ , and  $R$  in (8a), respectively. The output of model 2 (7a) – (7b) is the glucose absorbed from the intestines and does not consider the EGP. Therefore, one must deduct the EGP from  $\hat{G}$  as in (11d). For the predictions, we must add the EGP to the predicted glucose absorbed from the intestines to obtain the total predicted GAR.

The proposed block diagram for the predictor is shown in Fig. 3, with having the estimates of the model 2 at time  $k-1$  and assuming no meal consumption in the prediction horizon with the length of  $N_p$ , one can have an estimation of  $G$  for the future time samples of  $\{k, k+1, \dots, k+N_p-1\}$ . Having the  $\hat{x}_k$  together with predicted  $G$  enables us to predict the BGLs for any future insulin and glucagon boluses using the meta model.

### A. Comments on the Designed Predictor

The predictor assumes that no meals will be consumed during the prediction period, which could lead to an underestimation of BGL if a meal will be consumed. However, underes-

timing meals could prevent excessive insulin administration and reduce the risk of postprandial hypoglycemia.

A limitation of the proposed scheme is the increased computational cost associated with solving  $\Phi_2$  and  $\Phi_3$  separately. However, the problems  $\Phi_2$  and  $\Phi_3$  could be combined, but this would lead to undesirable interactions between the parameters of the model 2 and the estimation of the states of the meta model and  $G_k$ . Solving the problems  $\Phi_2$  and  $\Phi_3$  in a sequence is made for ease of tuning the estimators, reducing complexity, and maintaining the modularity of the method.

## VI. DEMONSTRATIVE EXAMPLES

The performance of the DIP-MHE and the proposed predictor scheme is evaluated using the test data from three animal experiments in this section. To this aim, two scenarios are designed; Scenario 1 evaluates the performance of the DIP-MHE in a post-processing manner, and Scenario 2 evaluates the performance of the proposed predictor scheme for closed-loop systems. These scenarios are described in the following sections.

### A. Scenario 1, Performance Evaluation of the DIP-MHE in Post-Processing:

This scenario evaluates the performance of the designed DIP-MHE in estimating the glucose appearance rate, states, robustness of the estimator to model mismatches, and the reliability of the estimates. Three sub-scenarios have been created to simulate real-world situations and test the performance of the proposed method in detail:

1) *Scenario 1.A, Accuracy of Glucose Appearance Rate Estimates:* This scenario aims to evaluate the performance of the DIP-MHE in estimating the GAR. As shown in Fig. 4, the estimated GAR is compared with the rate of the infused IV glucose during the experiments. In this scenario, the parameters of the meta model are identified individually. However, in closed-loop tests and experiments on awake animals, the available data for identification is limited, which could impact the accuracy of the meta model and subsequently and the performance of the estimator. These cases are discussed later in Scenarios 1.C and 2.

2) *Scenario 1.B, Accuracy of the State Estimates:* This scenario focuses on evaluating the ability of the DIP-MHE to estimate the states of the meta model. The estimated states must be compared to their actual values to assess the performance accurately. However, the states  $x_2, x_3, x_4, x_5, x_6, x_7$  are not directly measurable. We assumed that the time lag of the CGM sensors is negligible, the only measurable quantity in these experiments is  $x_1$ , which is obtained using CGM systems.

As previously mentioned, the primary goal of the DIP-MHE is to enable accurate predictions for use in MPC techniques. Therefore, the performance of the DIP-MHE in estimating  $\hat{x}_k$  can be indirectly evaluated by comparing the predicted BGL with the measured BGL in a post-processing manner, assuming that the future glucose infusion is known to the model. As shown in Fig. 3, the predicted BGL is obtained by using the estimated  $\hat{x}_k$ , feature inputs, and the identified meta model.

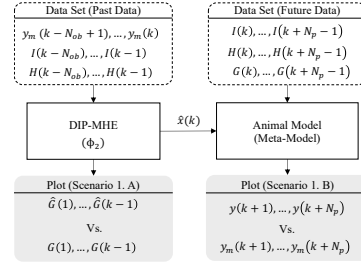


Fig. 4. Scenario 1.A and Scenario 1.B are illustrated. In Scenario 1.A, the performance of DIP-MHE in estimating glucose infusion rate (GAR) is evaluated by comparing it to the actual rate of intravenous glucose infusion during the experiments. In Scenario 1.B, the performance of DIP-MHE in estimating the states is evaluated indirectly by comparing the predicted blood glucose level (BGL) based on an animal model to the measured BGL in a post-processing manner.  $N_{ob}$  and  $N_p$  represent the estimation and prediction horizons, respectively.

The predicted BGL is then compared with the measured BGL. This comparison is considered as an indirect evaluation of the DIP-MHE in estimating  $\hat{x}_k$ . To ensure that the evaluation is accurate, the selected prediction horizon ( $N_p$ ) must be long enough to cover a full meal; in this scenario,  $N_p = 48$  samples, or 4 hours, were chosen.

The initial value selected for the states are  $\hat{x}_0^T = [y_{m0}, 0, 0, 0, 0, 0, 30]$  where  $y_{m0}$  is the first BGL measured at time  $k = 1$ . In addition, the initial glucose appearance rate is set to  $G_j = 5$  mg/min/kg for  $j = [1, N_{ob} - 1]$ , which is equal to the basal body glucose appearance rate [24]. Regarding the initial values chosen ( $\hat{x}_0^T$ ), it is known that there has been no presence of insulin or glucagon in the bloodstream or peritoneal fluid for an extended period of time. However, the selected glycogen storage level is based on previous subjects and there is less confidence in the chosen initial glycogen value for each new subject. Additionally, the accuracy of selecting  $G_j = 5$  mg/min/kg for  $j = [1, N_{ob} - 1]$  is uncertain. To address these uncertainties, a warm-up period was considered for the designed estimator using initial samples of the experiment. During the warm-up period, the arrival cost was set to  $P_3^{-1} = \text{diag}(25, 25, 25, 100, 5, 5, 10^{-3})$ . The warm-up period was set to 180 minutes (36 samples), which is longer than the half-life time of IP insulin, glucagon, and the tail of the glucose absorption due to the meal. After the warm-up period, the arrival cost coefficient will increase to  $P_3^{-1} = 100 \times \text{diag}(50, 50, 50, 100, 50, 50, 0.5)$ .

The matrix  $R_3^{-1}$  is the inverse of covariance of the measurement noise, and generally speaking, it is a scaling penalty on how accurately the model output ( $\hat{y}_k$ ) must be fitted to the measurements ( $y_{m,k}$ ) over the time estimator horizon. In this paper, this matrix is chosen as  $R_3^{-1} = 10^2 \times \mathbb{I}$  where  $\mathbb{I}$  is a  $N_{ob} \times N_{ob}$  identity matrix. Other tuning parameters are  $p_r = 1$ ,  $p_{dr} = 1$ ,  $p_{r0} = 1$ , and  $Q_3 = 0_{7 \times 7}$ . For simplicity, we considered that there is no process noise or endogenous insulin and glucagon production. The parameters are tuned to achieve satisfactory results for the first experiments and then tested on the other experiments.



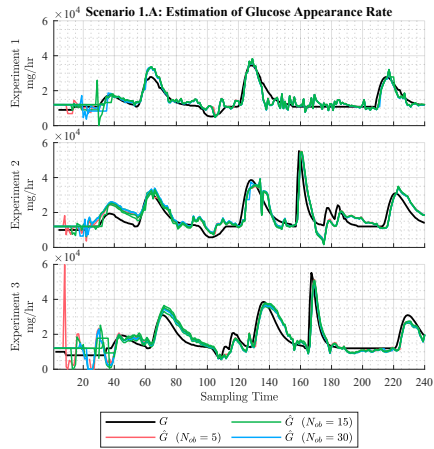


Fig. 5. The figure illustrates the performance of the proposed DIP-MHE in Scenario 1.A, by comparing the glucose appearance rate ( $G$ ) given to the pigs via the IV route to the estimations ( $\hat{G}$ ) made by DIP-MHE for different observation horizons ( $N_{ob}$ ).

It is important to note that the population parameters of model (1) are identified based on short-term anesthetized pig experiments and as it is mentioned in [9], the charging rate of glycogen ( $\gamma_3$ ) is identified near zero. We found a better performance of the estimator when replacing  $\gamma_3$  with  $0.8\beta_3$ . From a philological point of view, it means that the 80% of the up-taken glucose in the liver will be saved as accessible glycogen.

A key parameter in the DIP-MHE design is  $N_{ob}$ , which can impact the estimation accuracy, convergence, and computational complexity. From an accuracy standpoint, longer estimation horizons are preferable as the estimator will have access to more information about the dynamics of the system from measurements. However, using longer horizons can increase computational difficulty.

TABLE I

MEAN ABSOLUTE PERCENTAGE ERROR (MAPE) OF THE PROPOSED DIP-MHE IN ESTIMATING THE GLUCOSE APPEARANCE RATE ( $G$ ) AND THE MAPE OF THE FOUR-HOUR BGL PREDICTION (AVERAGED OVER ALL SAMPLING TIMES) IN SCENARIO 1.A AND SCENARIO 1.B, RESPECTIVELY.

$N_{ob}$	MAPE ( $G$ ) [%]				MAPE (BGL Pre.) [%]			
	Exp 1	Exp 2	Exp 3	Ave.	Exp 1	Exp 2	Exp 3	Ave.
5	16.9	23.9	24.1	<b>21.6</b>	8.3	12.0	9.5	<b>9.9</b>
10	16.6	26.3	23.0	<b>22.0</b>	8.9	12.4	8.3	<b>9.9</b>
15	17.2	26.5	23.1	<b>22.3</b>	9.0	12.2	9.0	<b>10.1</b>
20	17.0	26.0	23.1	<b>22.0</b>	8.9	12.0	9.0	<b>10.0</b>
25	17.8	24.7	24.2	<b>22.2</b>	9.1	11.5	9.7	<b>10.1</b>
30	17.0	23.7	20.6	<b>20.4</b>	9.3	11.3	9.0	<b>9.9</b>
Ave.	17.1	25.2	23.0	<b>21.8</b>	8.9	11.9	9.1	<b>10.0</b>

In order to find the suitable horizon length, performance analysis is done for  $N_{ob} = \{5, 10, \dots, 30\}$ . The sampling time is 5 minutes and, therefore,  $N_{ob} \times dt = \{25, 50, \dots, 150\}$  minutes. We found that the half-life of the IP insulin and

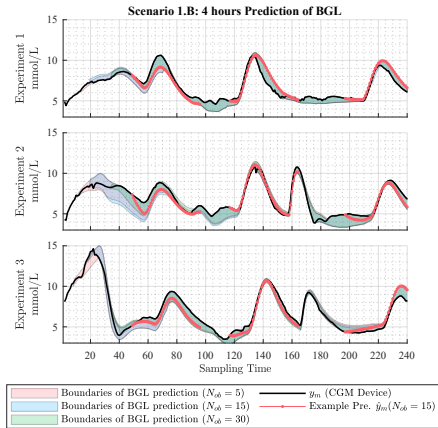


Fig. 6. The figure illustrates the performance of the proposed DIP-MHE in Scenario 1.B by comparing the four-hour BGL predictions (based on estimated GAR and the states) to the measured BGL using the CGM ( $y_m$ ). The predictions are made at every sampling time, and the shaded area shows the boundaries of predicted BGL at each sampling time. As an example, the predicted trajectories are shown for each meal for an observation horizon of  $N_{ob} = 15$ .

glucagon in the pigs is less than 100 minutes [25]. Therefore, the maximum estimation horizon evaluated in this paper is set at 150 minutes.

For the selected set of  $N_{ob}$ , the mean absolute percentage error (MAPE) of estimating glucose appearance rate and the MAPE of the four-hour predictions are shown in Table I. As an example, for  $N_{ob} = \{5, 15, 30\}$  the estimated  $G_k$  and the boundaries of the four-hour predicted BGL are illustrated in Fig. 5 and Fig. 6, respectively. In experiment 1, we did not carry out the simulation of the soft drink as the heart rate was elevated following dinner. Once the heart rate returned to normal, we proceeded with simulating sleep.

A similar performance is achieved for all three experiments with a fixed tuning of DIP-MHE and different values of  $N_{ob}$ . The DIP-MHE has achieved an average MAPE of 21.8% in estimating GAR (Scenario 1.A) and an average MAPE of 10% in predicting the BGL for four hours (Scenario 1.B).

In the third experiment (as shown in Fig. 6), the insulin and glucagon pumps were intentionally misconnected (their reservoirs interchanged) as a simulation of user error. This resulted in elevated glucose levels at the start of the experiment. We believe that this simulated user error also affected the response of the pig to insulin later in the experiment, as the animal did not receive insulin for an extended period of time.

As shown in Fig. 7, when the number of observations,  $N_{ob}$ , is high, the ability to predict BGL is greatest during the transient period. This suggests that the accuracy of state estimation improves as the estimation horizon is extended. However, this improvement comes at the cost of longer computation times. On a regular desktop PC, the average computation time for  $N_{ob} = 5, 10, \dots, 30$  are 2.33, 2.87, 2.90, 3.14, 3.37, and 3.95 seconds, respectively. However, due to

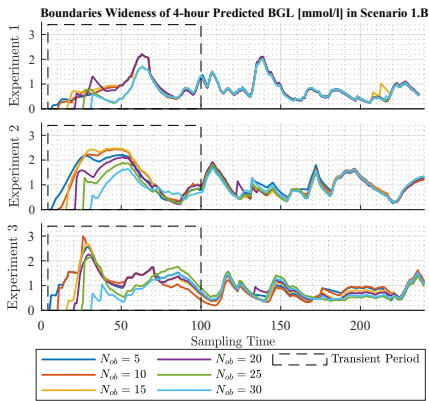


Fig. 7. The widthness of the boundaries of the predicted BGL in Scenario 1.B refers to how much variation there is in the predicted values. It can be an indication of how uncertain or confident the prediction is. It is important to have less wide boundaries when it comes to predicted BGL, which is necessary for managing diabetes.

the large sampling intervals (5 minutes), the calculations are done without optimizing the simulation codes.

### 3) Scenario 1.C, Performance of the DIP-MHE with model mismatches:

In the previous scenarios, a satisfactory performance in estimating the glucose appearance rate and prediction of the BGL is achieved using the proposed DIP-MHE. This is done using the tuned DIP-MHE on the first experiment and the model, identified individually using their full-day BGL measurements. In the short-term closed-loop animal experiments, there are not enough BGL measurements to identify the individual parameters of the meta model ( $\{\beta_1, \beta_2, \beta_3, \beta_4\}$ ). In addition, tuning the parameters of the DIP-MHE is challenging to perform during the experiments.

A practical way to address these challenges is to leverage information from previous experiments, such as utilizing data from a pig with a similar body weight, to tune the parameters of the meta model and DIP-MHE for new experiments. We refer to this data from prior experiments as “training data”. This approach can help overcome the challenges and ensure accurate estimations. However, the insulin and glucagon responses differ from pig to pig. Therefore, the performance of the DIP-MHE in the presence of the model identification error must be studied. To that end, we proposed Scenario 1.C, in which the first experiment serves as training data and the DIP-MHE is then performed on the second and third experiments without re-tuning and model identification.

Fig. 8 and Table II provide details on the performance of the DIP-MHE in Scenario 1.C. The DIP-MHE had the same settings as Scenario 1.A, with  $N_{ob} = 15$ .

The estimator was able to achieve an accurate estimation of the GAR for experiment 2, with a MAPE of 23.3%. Furthermore, it was able to generate a four-hour blood glucose level (BGL) prediction with an average MAPE of 12.9%. For

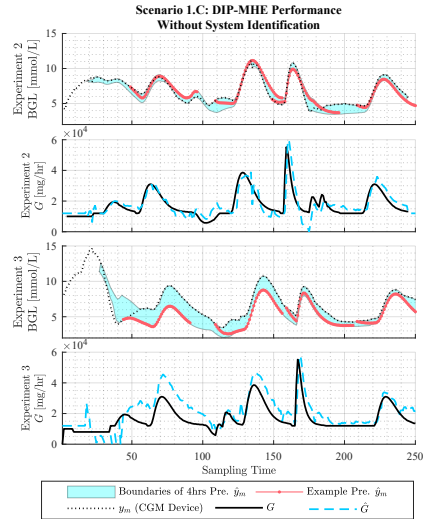


Fig. 8. The figures show the estimated glucose appearance rate and the boundaries of the BGL prediction in Scenario 1.C. Estimations are done with  $N_{ob} = 15$ . The predictions and the estimations are made using the identified meta model [9] for experiment 1.  $y_m$  is the measured BGL using the CGM device,  $G$  is the given IV glucose infusion during the experiments, and  $\hat{G}$  is the estimated GAR.

TABLE II  
MEAN ABSOLUTE PERCENTAGE ERROR (MAPE) OF THE PROPOSED DIP-MHE IN ESTIMATING THE GLUCOSE APPEARANCE RATE ( $G$ ) AND THE MAPE OF THE FOUR-HOUR BGL PREDICTION (AVERAGED OVER ALL SAMPLING TIMES) IN SCENARIO 1.C.

MAPE ( $G$ ) [%]				MAPE (BGL Pre.) [%]			
Exp 2	Exp 3	Exp 3 <sup>(1)</sup> (Part 1)	Exp 3 <sup>(2)</sup> (Part 2)	Exp 2	Exp 3	Exp 3 <sup>(1)</sup> (Part 1)	Exp 3 <sup>(2)</sup> (Part 2)
23.3	41.3	61.3	28.3	12.9	20.2	27.5	17.1

<sup>(1)</sup> Part 1: [0, 500]min. (Effect of the user error simulation).

<sup>(2)</sup> Part 1: [505, 1265]min.

the third experiment, there is a bias and error in estimating the glucose appearance rate in the first 100 samples. As explained earlier, this is due to the simulated user error in the third experiment. The MAPE of GAR estimation and BGL prediction decreased to 28.3% and 17.1%, respectively, for the rest of the experiment.

### B. Comments on the Reliability of the Estimates

The proposed DIP-MHE has been shown to accurately estimate GAR and predict BGL in a post-processing manner. However, when using the estimator in closed-loop systems, it is essential to consider the reliability of the estimator. Various methods have been proposed in the literature for analyzing the stability of the MHE, such as the approaches in [26]. One way to analyze the estimator is by finding the covariance of the estimates, which can be challenging. However, the inverse of the Hessian matrix can be used as an approximation for the

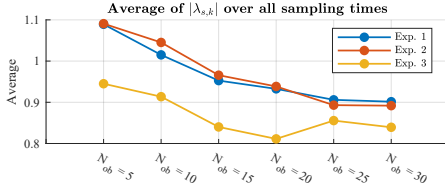


Fig. 9. Average of  $|\lambda_{s,k}|$  over all for different  $N_{ob}$  and experiments.

covariance matrix of estimation error, as shown by Gejadze *et al.* in [27]. The Hessian matrix is defined as:

$$H_{\Phi_s,k} := \nabla^2 \Phi_{2,k} \quad (12)$$

Where  $\Phi_{2,k}$  is the cost function (9a) minimized at the sampling time  $k$ .  $H_{\Phi_s,k}$  is the Hessian matrix found for the estimates at time  $k$ .

The fact mentioned above has been a well-known finding in statistics for decades, and multiple studies offer the same conclusion. Nevertheless, there has also been considerable ambiguity which has been discussed in [27].

As mentioned earlier, the matrix  $H_{\Phi_s,k}$  must be calculated at each sample time after the estimations are complete. The constraints mentioned in (8e) and (9c) are positive constraints, meaning that the states and  $G$  are zero or greater than zero. We assume that the covariances of the active constraints (parameters estimated as zero) are actually zero. For example, the amount of glucagon in the peritoneal cavity ( $x_6$ ) is zero before or after glucagon boluses since there is no glucagon infusion into the cavity except by pumps. Therefore, the rows and columns of  $H_{\Phi_s,k}$  corresponding to the active constraints will be removed. To prevent numerical errors in finding the inverse of  $H_{\Phi_s,k}$ , we calculate  $\lambda_{s,k}$ , which is the smallest eigenvalue of  $H_{\Phi_s,k}$  and defined as follows.

$$\lambda_{s,k} := \min \{ \det(H_{\Phi_s,k}) \} \quad (13)$$

The estimates corresponding to  $\lambda_{s,k} \rightarrow 0$  have large covariance, which indicates less reliable estimates.

Fig. 9 illustrates the average absolute values of  $\lambda_{s,k}$  for all sampling times in all experiments. The trend in this graph shows that longer horizon length results in 10-18% lower values for  $\lambda_{s,k}$ , which means the average reliability of the estimates decreases with large values for  $N_{ob}$ .

The reliability of the estimates for experiments 1 and 2 are similar even though the parameters of their models are different. Experiment 2 had a different glucose infusion profile due to the soft drink consumption. However, DIP-MHE showed less reliable estimates than the third experiment due to the simulated user error at the beginning of the experiment.

The authors believe that the lack of insulin in the blood for a long period of time and a high BGL may affect the dynamics of the metabolic system.  $\lambda_{s,k}$  for the third experiment is shown in Fig. 10. The eigenvalues for the time interval  $k \in [20, 50]$  (the period after simulated user error) are smaller than the rest of the experiment for all  $N_{ob} = \{5, 10, 15, 20, 25, 30\}$ .

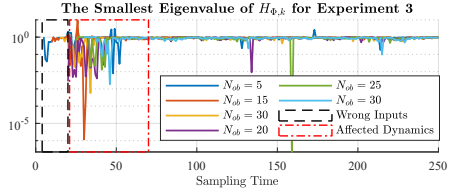


Fig. 10. The smallest eigenvalues of the  $H_{\Phi_s,k}$  of the experiment 3 plotted for different  $N_{ob}$ . The black box shows the period where glucagon boluses were given instead of insulin, and the pig did not receive insulin. The red box indicated the period that the authors believe that the metabolic dynamics have been affected due to the prolonged lack of insulin at the beginning of the experiment.

It is also evident from Fig. 5 and Fig. 6 that the estimates of DIP-MHE are unreliable for this period. The absence of insulin boluses (no exciting inputs) and the prolonged lack of insulin in the bloodstream can contribute to the small  $\lambda_{s,k}$  at  $k \in [20, 50]$  and practical unidentifiability in experiment 3. This is a good indication that the inverse Hessian matrix can serve as an approximation of the covariance matrix and the reliability metric in closed-loop applications.

#### C. Scenario 2, Prediction Performance in Closed-loop Systems:

This scenario uses the tuned DIP-MHE in Scenario 1.C to evaluate the proposed predictor method in Section V. This scenario aims to evaluate the performance of the proposed prediction scheme in MPC methods. The main difference from Scenarios 1.C, is that in Scenario 2 the future GAR is unknown and is instead predicted. At each sampling time, the future insulin and glucagon infusions are assumed to be known, since we want to compare the predicted BGL trajectories with the actual measured BGL in the experiments. In closed-loop systems, the MPC provides the future insulin and glucagon.

In order to tune the cost function (11a), the measurements of Experiment 1 are used as training data. In this tuning, the estimated glucose appearance rate covariance is considered constant and  $R_q = 10^{-2} \times \mathbb{I}$  where  $\mathbb{I}$  is a  $N_{ob} \times N_{ob}$  identity matrix. The other tuning parameters are chosen as  $Q_q^{-1} = \text{diag}(0.01, 0.01, 1)$ ,  $P_q^{-1} = \text{diag}(0.01, 0.01, 0.01)$ , and  $N_{ob} = 15$ .

In a closed-loop experiment, the prediction horizon must be chosen based on the dynamics of the system, available computing power, uncertainties, and disturbances. The main effect (half-life) of IP insulin and IP glucagon is seen within the first 100 minutes (20 samples) after injection; therefore, a prediction horizon of 120 minutes is sufficiently long for the model-based predictive controllers. Additionally, predicting the GAR for a longer horizon can be extremely uncertain because of unannounced meals.

The predicted trajectories of the BGL and the GAR are illustrated in Fig. 11. As shown in Table III, the proposed method could predict the BGL and GAR with an average MAPE of 18.1% and 28.4%, respectively.

As previously stated, the glucose appearance rate is estimated passively from the revolutions in the BGL since the

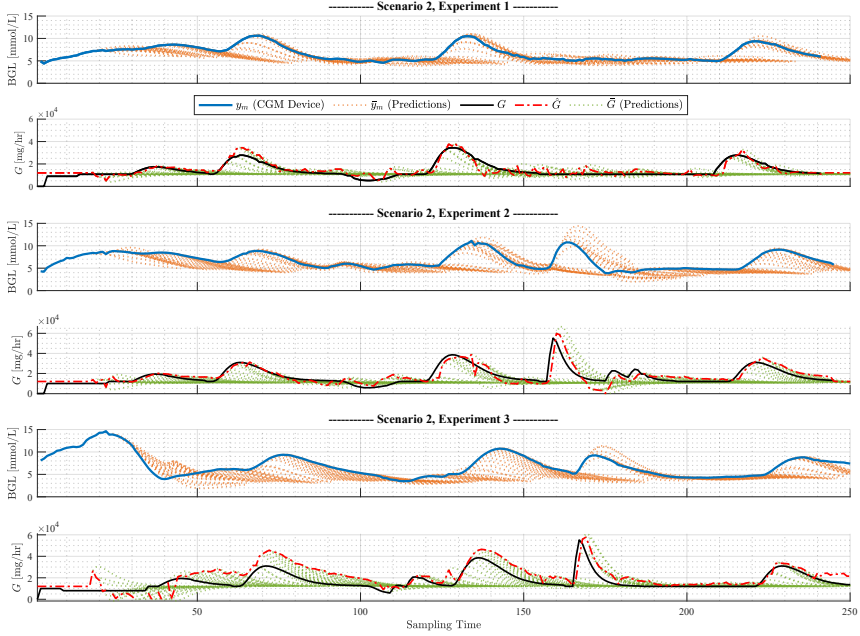


Fig. 11. Performance of the proposed DIP-MHE and the predictor scheme in Scenario 2 for the three animal experiments; In this scenario, the BGL and glucose appearance rate predictions are made using the scheme proposed in Fig. 3. The parameters of the meta model (1), the estimators (9a), and (11a) are identified and tuned using the first experiment.  $y_m$  is the measured BGL via the CGM Device, and  $\hat{y}_m$  is the predicted BGL.  $G$  is the IV glucose infusion rate during the experiments,  $\hat{G}$  is the estimated glucose infusion rate by DIP-MHE, and  $\tilde{G}$  is the predicted glucose infusion rate made for 120 minutes without any meal announcement.

TABLE III  
MEAN ABSOLUTE PERCENTAGE ERROR (MAPE) OF THE PROPOSED METHOD IN PREDICTING THE GLUCOSE APPEARANCE RATE ( $G$  PRE.) AND THE MAPE OF BGL PREDICTION (BGL PRE.) FOR 120 MINUTES IN SCENARIO 2.

$N_{ob}$	MAPE ( $G$ Pre.) [%]			Ave.	MAPE (BGL Pre.) [%]			Ave.
	Exp 1	Exp 2	Exp 3		Exp 1	Exp 2	Exp 3	
15	12.7	19.7	22.0	<b>18.1</b>	23.6	31.4	30.2	<b>28.4</b>

meal amount, meal time, and type of meals are not predictable without the meal announcement. Furthermore, eating is a continuous process; the amount of glucose given to the stomach and intestinal system continuously rises. Therefore, the predicted BGL diverge from the actual future BGL just before the meal absorption starts and during the meal, as seen in Fig. 11. However, as more BGL measurements are obtained, the predictions are updated and become more precise.

The proposed scenario for the second and third experiments is the worst-case scenario. The DIP-MHE and the model have been tuned and identified using data from the first experiment. In real-world situations, such as human trials or longer animal experiments, there would be sufficient data to identify the model and tune the DIP-MHE individually.

In summary, the proposed predictor based on the DIP-MHE performed reasonably well in experiments 2 and 3. The predictions of the GAR over shots during the fast glucose rise (the soft-drink event) in the second experiment. It is important to consider the overshoots of the proposed prediction scheme when designing an MPC controller.

## VII. DISCUSSION

This study focuses on designing an estimator and predictor for the GAR and meta model states, which can be applied in MPC methods. The meta model is based on animal data using intraperitoneal injection of insulin and glucagon. To utilize this method in human trials, the model needs to be adapted to human data. Although designed for dual-hormone systems, the method can also be used in insulin-only APs. However, the use of the intraperitoneal route has some challenges, which are discussed in [8]. Alternatively, the proposed method can also be used in currently available insulin-only APs using subcutaneous injections. To this end, the IP model used in the estimator needs to be substituted with an SC model that provides comparable accuracy. However, this replacement necessitates the recalibration and optimization of the parameters. Specifically, due to the slower dynamics of the SC route, it may be necessary to select a longer estimator horizon

for improved performance. Although the intraperitoneal route is more invasive and costly, it has the advantage of faster insulin absorption, which makes it easier to avoid oscillations and thereby achieve larger safety margins and achieve a lower average glucose level. We utilized data from three comprehensive experiments in anesthetized animals. However, further experiments with longer duration are required before implementing the method in humans.

### VIII. CONCLUSIONS

The proposed DIP-MHE is tested in animal experiments in near-real-life conditions and with model mismatches. It is shown to be a reliable and effective method for estimating the glucose appearance rate and states of the metabolic system. The proposed predictor scheme can be used in closed-loop systems to make accurate predictions of the BGL, allowing for more precise insulin and glucagon bolus calculations without human interventions. Furthermore, the estimator can be utilized to estimate glucose absorption from the intestines to develop and identify an accurate model for the digestive system. The method has been successfully tested in animal trials and has the potential to be adapted for use in human trials.

### IX. ACKNOWLEDGMENTS

The animal experiments were performed at the Comparative Medicine Core Facility (CoMed) at the Norwegian University of Science and Technology (NTNU). The study was supported by the Norwegian Research Council (under project number 248872) and the Centre for Digital Life Norway. In addition, the CGM systems and the infusion pumps are provided by Inreda Diabetic company (Goor, the Netherlands) for the experiments at no cost. The experiments outlined in this paper were conducted by Marte Kierulf Åm, Patrick Christian Bösch, Hasti Khoshmadi, Oddveig Lyng, and Karim Davari Benam. The authors would like to thank this team for their invaluable contribution to performing the experiments and collecting the data. We also like to thank Professor Sven Magnus Carlsen for his help in designing the experiments and discussions. This study was conducted as part of the efforts of the Artificial Pancreas Trondheim research group (APT, apt-norway.com) to develop a fully automated artificial pancreas.

### REFERENCES

- [1] C. Cobelli et al., "Artificial pancreas: past, present, future," *Diabetes*, vol. 60, no. 11, pp. 2672–2682, 2011.
- [2] A. El Fathi et al., "A model-based insulin dose optimization algorithm for people with type 1 diabetes on multiple daily injections therapy," *IEEE Transactions on Biomedical Engineering*, vol. 68, no. 4, pp. 1208–1219, 2020.
- [3] J. Langholz et al., "Fully automated bi-hormonal intraperitoneal artificial pancreas using a two-layer pid control scheme," in *2023 European Control Conference (ECC)*. IEEE, 2023, pp. 1–8.
- [4] A. Haidar, "The artificial pancreas: How closed-loop control is revolutionizing diabetes," *IEEE Control Systems Magazine*, vol. 36, no. 5, pp. 28–47, 2016.
- [5] A. Brazeau et al., "Carbohydrate counting accuracy and blood glucose variability in adults with type 1 diabetes," *Diabetes research and clinical practice*, vol. 99, no. 1, pp. 19–23, 2013.
- [6] T. Peters and A. Haidar, "Dual-hormone artificial pancreas: benefits and limitations compared with single-hormone systems," *Diabetic Medicine*, vol. 35, no. 4, pp. 450–459, 2018.
- [7] E. Fushimi et al., "A dual-hormone multicontroller for artificial pancreas systems," *IEEE Journal of Biomedical and Health Informatics*, vol. 26, no. 9, pp. 4743–4750, 2022.
- [8] C. Toffanin et al., "Artificial pancreas: In silico study shows no need of meal announcement and improved time in range of glucose with intraperitoneal vs. subcutaneous insulin delivery," *IEEE Transactions on Medical Robotics and Bionics*, vol. 3, no. 2, pp. 306–314, 2021.
- [9] K. D. Benam et al., "Identifiable prediction animal model for the bi-hormonal intraperitoneal artificial pancreas," *Journal of Process Control*, vol. 121, pp. 13–29, 2023.
- [10] J. Lo Presti et al., "Intraperitoneal insulin delivery: evidence of a physiological route for artificial pancreas from compartmental modeling," *Journal of diabetes science and technology*, p. 19322968221076559, 2022.
- [11] D. Shi et al., "Adaptive zone model predictive control of artificial pancreas based on glucose-and velocity-dependent control penalties," *IEEE Transactions on Biomedical Engineering*, vol. 66, no. 4, pp. 1045–1054, 2018.
- [12] K. Kölle et al., "Meal detection based on non-individualized moving horizon estimation and classification," in *2017 IEEE Conference on Control Technology and Applications (CCTA)*. IEEE, 2017, pp. 529–535.
- [13] K. Kölle et al., "Pattern recognition reveals characteristic postprandial glucose changes: Non-individualized meal detection in diabetes mellitus type 1," *IEEE journal of biomedical and health informatics*, vol. 24, no. 2, pp. 594–602, 2019.
- [14] O. M. Staal et al., "Meal estimation from continuous glucose monitor data using kalman filtering and hypothesis testing," in *2019 IEEE 58th Conference on Decision and Control (CDC)*. IEEE, 2019, pp. 5654–5661.
- [15] K. Kölle et al., "Feasibility of early meal detection based on abdominal sound," *IEEE Journal of Translational Engineering in Health and Medicine*, vol. 7, pp. 1–12, 2019.
- [16] K. D. Benam et al., "Full order high gain observer design for image-guided robotic flexible needle steering," in *2019 27th Iranian Conference on Electrical Engineering (ICEE)*. IEEE, 2019, pp. 1151–1156.
- [17] C. Lopez-Zazueta et al., "Low-order nonlinear animal model of glucose dynamics for a bi-hormonal intraperitoneal artificial pancreas," *IEEE Transactions on Biomedical Engineering*, 2021.
- [18] I. Dirnena-Fusini et al., "Intraperitoneal insulin administration in pigs: effect on circulating insulin and glucose levels," *BMJ Open Diabetes Research and Care*, vol. 9, no. 1, p. e001929, 2021.
- [19] M. K. Åm et al., "Intraperitoneal and subcutaneous glucagon delivery in anaesthetized pigs: effects on circulating glucagon and glucose levels," *Scientific reports*, vol. 10, no. 1, pp. 1–8, 2020.
- [20] C. Dalla Man et al., "A system model of oral glucose absorption: validation on gold standard data," *IEEE Transactions on Biomedical Engineering*, vol. 53, no. 12, pp. 2472–2478, 2006.
- [21] M. Halvorsen et al., "Blood glucose level prediction using subcutaneous sensors for in vivo study: Compensation for measurement method slow dynamics using kalman filter approach," in *2022 IEEE 61st Conference on Decision and Control (CDC)*, 2022, pp. 6034–6039.
- [22] J. Kang et al., "A simultaneous parameter and state estimator for polymerization process based on molecular weight distribution," in *Computer Aided Chemical Engineering*. Elsevier, 2018, vol. 43, pp. 1117–1122.
- [23] M. J. Tenny and J. B. Rawlings, "Efficient moving horizon estimation and nonlinear model predictive control," in *Proceedings of the 2002 American Control Conference (IEEE Cat. No. CH37301)*, vol. 6. IEEE, 2002, pp. 4475–4480.
- [24] B. Koletzko et al., "Guidelines on paediatric parenteral nutrition: 5. Carbohydrates," *Journal of Pediatric Gastroenterology & Nutrition*, vol. 41, no. Supplement 2, pp. S28–S32, Nov. 2005.
- [25] K. D. Benam et al., "A nonlinear state observer for the bi-hormonal intraperitoneal artificial pancreas," in *2022 44th Annual International Conference of the IEEE Engineering in Medicine & Biology Society (EMBC)*. IEEE, 2022, pp. 171–176.
- [26] C. Rao et al., "Constrained state estimation for nonlinear discrete-time systems: Stability and moving horizon approximations," *IEEE transactions on automatic control*, vol. 48, no. 2, pp. 246–258, 2003.
- [27] I. Y. Gejadze et al., "Hessian-based covariance approximations in variational data assimilation," *Russian Journal of Numerical Analysis and Mathematical Modelling*, vol. 33, no. 1, pp. 25–39, 2018.





## 6.5 PAPER 5

**Title: “Sensor Fusion for Glucose Monitoring Systems”**

Accepted and presented at the 22nd International Federation of Automatic Control Conference (IFAC), Yokohama, Japan, 10 July 2023 [5]





# Sensor Fusion for Glucose Monitoring Systems <sup>\*</sup>

Mohamad Al Ahdab <sup>\*</sup> Karim Davari Benam <sup>\*\*</sup>  
 Hasti Khoshamadi <sup>\*\*</sup> Anders Lyngvi Fougner <sup>\*\*</sup>  
 Sebastien Gros <sup>\*\*</sup>

<sup>\*</sup> *Section of Automation and Control, Department of Electronic Systems, Aalborg University, Aalborg Øst, Denmark, (e-mail: maah@es.aau.dk)*

<sup>\*\*</sup> *Department of Engineering Cybernetics, Faculty of Information Technology and Electrical Engineering, Norwegian University of Science and Technology (NTNU), O. S. Bragstads Plass 2D, 7034 Trondheim, Norway (e-mail: {karim.d.benam, hasti.khoshamadi, anders.fougner, sebastien.gros}@ntnu.no)*

---

**Abstract:** A fully automated artificial pancreas (AP) requires accurate blood glucose (BG) readings. However, many factors can affect the accuracy of commercially available sensors. These factors include sensor artifacts due to the pressure on surrounding tissues, connection loss, and poor calibration. The AP may administer an incorrect insulin bolus due to inaccurate sensor data when the patient is not supervising the system. The situation can be even worse in animal experiments because animals are eager to play with the sensor and apply pressure. In this study, we propose and derive a Multi-Model Kalman Filter with Forgetting Factor (MMKFF) for the problem of fusing information from redundant subcutaneous glucose sensors. The performance of the developed MMKFF was assessed by comparing it against other Kalman Filter (KF) strategies on experimental data obtained in two different animals. The developed MMKFF was shown to provide a reliable fused glucose reading. Additionally, compared to the other KF approaches, the MMKFF was shown to be better able to adjust to changes in the accuracy of the glucose sensors.

*Keywords:* Developments in measurement, signal processing, Diabetes.

---

## 1. INTRODUCTION

Monitoring blood glucose (BG) level in subjects with diabetes is important for managing their treatment. Over the last two decades, continuous glucose monitoring (CGM) systems have become more and more common in patients with diabetes mellitus type 1. Most commercially available CGMs provide measurement samples each 5 minutes allowing for a better description of the subject's glucose variability.

The artificial pancreas (AP) automates BG control by reading levels from a CGM, calculating the insulin bolus dose using a control algorithm, and infusing the insulin with a pump. A reliable system for measuring BG level with minimal supervision is essential to achieve the ultimate goal of reducing supervision. However, real-life situations can cause CGMs to provide inaccurate information or disconnect from APs, posing a risk to BG control in a single-sensor APs.

For simplicity and to reduce the wiring, the common off-the-shelf CGMs have a transmitter to connect wirelessly with the AP. The communication methods are Bluetooth or ANT+, which will lose connection if the CGM and

the receiver/pump are on opposite sides of the body, e.g. during sleep. Furthermore, compression artifacts caused by external pressure on the CGM can rapidly decrease the measured BG level and cause failure of the APs. Many other circumstances make single-sensor APs unreliable, making the supervision of the CGM necessary for patients. These circumstances have been summarised by Facchinetti (2016).

The glucose sensors have a warm-up period, which means that each new sensor attached will not provide accurate data for a while. Warm-up times vary between brands and range from 2 hours to 2 days. In other words, if the CGM fails unexpectedly in single-sensor APs, patients must manually control the BG during the warm-up period of the new sensor. The issue gets aggravated in awake animal experiments since it is challenging to take frequent blood samples to measure the BG. Additionally, since animals are eager to play with the sensors attached to their bodies or exert pressure on them, the circumstances above are more likely to occur in animal experiments. Notably, the warm-up period in the animal experiment is not ideal because it lengthens the experiment and raises the cost of the experiment. In this setting, the animal experiments are used to test controllers.

Redundant sensors are advised in the literature to address the issues above. For example, Jacobs et al. (2014) used

---

<sup>\*</sup> This work was funded by the IFD Grand Solution project ADAPT-T2D, project number 9068-00056B, the Research Council of Norway (project no. 248872), and the Centre for Digital Life Norway.

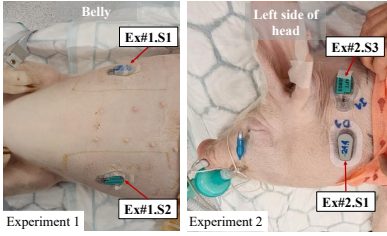


Fig. 1. Placement of glucose sensors. Left: Experiment 1, both sensors Exp1.S1 and Exp1.S2 placed on the pig’s belly. Right: Experiment 2, two sensors on the left side of the neck. Another two sensors were on the pig’s right side, with sensor Exp2.S4 attached at the bottom and Exp2.S2 at the top.

two sensors in their AP where one sensor would replace the active one in the event of a sensor failure. In the present study, instead of using the other sensor(s) only for backup, we developed a method based on a Multi-Model Kalman Filter (MMKF) approach to combine the data from all the glucose sensors attached on the subject to increase the reliability. The proposed method was evaluated using experimental data from anesthetized and awake pigs.

The works in Facchinetti et al. (2013, 2015); Vettoretti et al. (2019) used data batches from multiple CGMs devices together with an accurate reference BG data for the aim of obtaining a detailed parametric model description for the measurement errors in specific CGM devices. Therefore, the methods developed in these works are not suitable for a real time sensor fusion of CGMs for APs.

Kalman Filter (KF) strategies have been used in previously reported studies with CGMs for the purpose of calibrating one CGM device with self monitored blood glucose samples obtained by finger pricking Knobbe and Buckingham (2005); Kuure-Kinsey et al. (2006); Facchinetti et al. (2010). While these solutions primarily focused on sensor calibration, in this paper we aim to fuse information from numerous CGM devices with varying degrees of accuracy considering that one or more sensors can fail and recover over time.

The contributions of this work are as following:

- We show how MMKF can be used for the fusing of CGM devices. In addition, we derive a MMKF with a Forgetting Factor (MMKFF) in Section 4.
- We apply the MMKFF on two sets of experimental data and evaluate its performance in Section 5 comparing it with different types of KFs.

## 2. ANIMAL EXPERIMENTS

The example data sets used in this paper are from two different animal experiments. The tests were carried out in two non-diabetic farm pigs (*Sus scrofa domestica*) of 36 and 40 kg, respectively.

The first experiment (Exp1) was performed in an anesthetized pig for 24 hours. Three Medtronic Enlite glucose sensors (Northridge, Canada) with custom transmitters from Inreda Diabetic (Goor, the Netherlands) were used

(hereafter named Exp1.S1, Exp1.S2, and Exp1.S3) with a 1.2s sampling time. The provided data acquisition system could only receive data from two of the sensors. Therefore, one of the sensors only served as a backup sensor. Blood samples were taken sporadically to calibrate the sensors and compare them. A blood gas analyser (BGA) of ABL800 FLEX (Copenhagen, Denmark) was used to measure the actual BG level throughout the experiment. We compared the performance of the developed MMKFF method with the BGA. Exp1.S1 and Exp1.S2 were attached to each side of the belly as shown in Figure. 1, and Exp1.S3 was attached to the neck as backup. The protocol for this animal experiment was similar to the protocols used in Halvorsen et al. (2022) and Benam et al. (2023).

The second experiment (Exp2) was closer to real-life conditions than Exp1 since it was performed in an awake animal where it could move freely. In this experiment, four sensors were used to decrease the chance of losing data or basing decisions on faulty data. Sensors Exp2.S1 and Exp2.S2 were factory-calibrated Dexcom G6 (San Diego, CA) with 5min sampling time. Sensors Exp2.S3 and Exp2.S4 were Medtronic Guardian sensors 3 (Northridge, Canada) with custom-made transmitters from Inreda Diabetic (Goor, the Netherlands) with 1.2s sampling time. To reduce the connection losses during the experiments, the sensors were mounted on both sides of the neck, as shown in Figure 1. Unlike Exp1, taking frequent blood samples was not possible. However, depending on the sensor connection losses, general behaviours of the sensors compared to others, and position of the pig, the experiment’s operators were giving each sensor a reliability indicator between 0 and 1. Then we calculated a weighted average of the sensors using their assigned reliability indicators. With the weighted average value as a benchmark, we evaluated the performance of the proposed sensor fusion technique. Readings at time  $5k$  [min],  $k \in \mathbb{Z}_{>0}$  from Exp1.S1/ Exp2.S1, Exp1.S2/Exp2.S2, Exp2.S3, and Exp2.S4 will be denoted as  $y_k[1], y_k[2], y_k[3]$ , and  $y_k[4]$ , respectively.

## 3. NOTATIONS

For a random variable  $x$ , we write  $x$  for its realization. We write  $\mathcal{N}(\mu, \Sigma)$  for the normal distribution with mean  $\mu$  and variance  $\Sigma$ . Let two successive time instants  $t_k$  and  $t_{k+j}$  be such that  $t_{k+j} - t_k = jT$ ,  $j \in \mathbb{Z}$  with  $T \in \mathbb{R}$ , then variables  $x(t_k), x(t_{k+j})$  will be denoted as  $x_k, x_{k+j}$ . The symbol  $\mathbb{S}_{>0}^n$  ( $\mathbb{S}_{\geq 0}^n$ ) is used for the set of positive definite (semi-definite) matrices with dimension  $n$ . We write  $[N] = \{1, \dots, N\}$ ,  $N \in \mathbb{Z}_{>0}$ . We write a diagonal matrix with diagonal elements  $v = [v_1, \dots, v_n]^\top$  as  $\text{diag}(v)$ . We use  $\mathbf{I}$  for the identity matrix.

## 4. METHOD

In this section, we will first present the models used for the glucose sensors in 4.1. Afterwards, the MMKFF method will be described in 4.2.

### 4.1 Problem Setup

We consider a setup in which we have  $N \in \mathbb{Z}_{>0}$  CGM sensors. At each sample time  $k$ , a portion of the sensors

$0 \leq n_k \leq N$  will provide readings  $y_k \in \mathbb{R}^{n_k}$ . This setup considers cases when the sensors can fail for some periods of time. For the modeling, we consider in this paper  $N$  linear Gaussian dynamic models  $\mathcal{M}^i$  with  $i \in [N]$  as the following

$$x_{k+1}^i = A^i x_k^i + E^i w_k^i, \quad w_k^i \sim \mathcal{N}(0, Q^i), \quad (1a)$$

$$y_k = C_k^i x_k^i + v_k^i, \quad v_k^i \sim \mathcal{N}(0, R_k^i), \quad (1b)$$

with  $x^i \in \mathbb{R}^{n_x}$ ,  $n_x \in \mathbb{Z}_{>0}$ ,  $A^i \in \mathbb{R}^{n_x \times n_x}$ ,  $E^i \in \mathbb{R}^{n_x \times n_q}$ ,  $n_q \in \mathbb{Z}_{>0}$ ,  $Q^i \in \mathbb{S}_{>0}^{n_q}$ ,  $w_k^i$  is an independent and identically distributed (IID) process,  $C_k^i \in \mathbb{R}^{n_k \times n_x}$ ,  $R_k^i \in \mathbb{S}_{>0}^{n_k}$ , and  $v_k^i \in \mathbb{R}^{n_k}$  is a IID process. Similar to the previous works in Knobbe and Buckingham (2005); Facchinetti et al. (2010) in which integrators of white noise with different orders are chosen to represent a description for the dynamics of BG concentrations, we choose matrices  $A^i = A$ ,  $E^i = E$ ,  $Q^i = Q$  and  $C_k^i = C_k$  for all the models  $i \in [N]$  such that  $A, E, Q$ , and  $C$  represent the discrete output of a triple integrated white noise  $w$  as following

$$A = \begin{bmatrix} 1 & 0 & 0 \\ T & 1 & 0 \\ T^2/2 & T/3 & 1 \end{bmatrix}, E = \begin{bmatrix} T \\ T^2/2 \\ T^3/6 \end{bmatrix}, C_k = \begin{bmatrix} 0 & 0 & 1 \\ \vdots \\ 0 & 0 & 1 \end{bmatrix} \in \mathbb{R}^{n_k \times 3},$$

with  $T$  [min] being the sampling time<sup>1</sup>. The integrated white noise model serves as a prior assumption regarding the stationarity and the power spectrum density of the BG concentration. Additionally, if the model in (1a) is viewed as a discretized version of a continuous time dynamical glucose model, then it captures our knowledge that BG concentration is differentiable with respect to time. This choice is common in time series estimation of physiological processes (see De Nicolao et al. (1997) for e.g.). The higher the order of the integrator, the smoother the continuous time BG concentration is assumed to be. The variance  $Q$  of the driving white noise can be understood as a representation of how confident we are in the assumed model (see Section 5.1 for more details). Note that the model does not reflect the ground truth of the time evolution for BG concentration and different models with different accuracy and inputs (e.g. insulin, physical activity, meals, etc...) can also be considered and used. For the simplicity in this paper, we considered a simple white noise integrator which can work in a general setting in which data regarding more specific inputs is not available. As for the covariance matrix  $R_k^i$  for the measurement noise, it will be chosen differently for each model  $i \in [N]$ . To define  $R_k^i$ , let  $r^i \in \mathbb{R}^N$  such that the  $i_{th}$  element of  $r^i$  is  $\sigma_l^2$  while the rest of the elements in  $r^i$  are  $\sigma_u^2$  with  $\sigma_u > \sigma_l$ . Let  $s_k \in \mathbb{R}^N$  such that the  $i_{th}$  element of  $s_k$  is 1 if the  $i_{th}$  sensor is providing a reading at sample  $k$  and zero otherwise. Then the covariance matrix  $R_k^i$  is chosen as  $R_k^i = \text{diag}(s_k^T r^i)$ . This basically means that for each sensor  $i$ , we have a model  $\mathcal{M}^i$  that assumes a lower variance for the  $i_{th}$  sensor ( $\sigma_l^2$ ) than the variance for the other sensors ( $\sigma_u^2$ ). In other words, each model is more confident with respect to one sensor than the others. Note that it is possible with this structure to have a continuum of models weighting the sensors differently. However, we chose to have a finite number of models for simplicity and tractability. Finally, we define for each model  $\mathcal{M}^i$  a

<sup>1</sup> If the sensors are operating at different sampling rates then  $T$  can be chosen to be the minimum of the different sampling times.

random variable  $m_k^i \in \{0, 1\}$  such that  $p(m^i) = \mathbb{P}(m_k^i = 1) := \mathbb{P}(\mathcal{M}^i \text{ is the best model at step } k)$ . Note that the time dependence for  $m_k^i$  is included to account for the fact that some sensors will become better than others for a period of time. To relate  $m_{k+1}^i$  with  $m_k^i$ , we use the following

$$p(m_{k+1}^i) = p(m_{k+1}^i | m_k^i) p(m_k^i) := (1 - \alpha) p(m_k^i) + \alpha \bar{\beta}^i, \quad (2)$$

with  $0 \leq \alpha \leq 1$  a constant which we call the *forgetting factor*, and  $0 \leq \bar{\beta}^i \leq 1$  with  $\sum_{i=1}^N \bar{\beta}^i = 1$  are predefined probabilities for the models. The dynamic model in (2) is to be understood as a prior model in the absence of measurement updates (similar to (1a)). A measurement correction step will be introduced in section 4.2. To understand more what "forgetting" is meant with (2), assume we start from probabilities  $p(m_k^i) > 0$ ,  $\forall i \in [N]$  representing our knowledge at step  $k$  regarding the models. If we only follow the update in equation (2), then the  $l$ -step prediction is  $p(m_{k+l}^i) = (1 - \alpha)^l p(m_k^i) + (1 - (1 - \alpha)^l) \bar{\beta}^i$ . If  $0 < \alpha \leq 1$ , we can see that  $\lim_{l \rightarrow \infty} p(m_{k+l}^i) = \bar{\beta}^i$ . This means that  $\forall i \in [N]$ , our knowledge regarding the models  $p(m_k^i)$  with equation (2) only is "forgotten" exponentially with a rate  $1 - \alpha$  to converge to a predefined knowledge captured in  $\bar{\beta}^i$ . The predefined probabilities  $\bar{\beta}^i$  can be uniform ( $\bar{\beta}^i = \frac{1}{N}$ ,  $\forall i \in [N]$ ) or prior probabilities regarding the models.

#### 4.2 Multiple Models Kalman Filter with Forgetting Factor

The idea of the MMKF, which was first introduced in Magill (1965), is to run a KF for each model  $\mathcal{M}^i$  in parallel and combine the estimated results to obtain a better new estimate. In this section, we will extend the MMKF with the forgetting factor equation (2) and provide a description for the MMKFF strategy. Note that the MMKFF can be thought of as a specific case for dynamic MMKF where the probabilities of the true models evolve with time and it is different from the one in (Bar-Shalom et al., 2004, chapter 11) since (7) is not a homogeneous Markov chain. For ease of notation, we will use  $\beta_{k_1|k_2}^i := p(m_{k_1}^i | \mathcal{Y}_{k_2})$  with  $k_1, k_2 \in \mathbb{Z}_{\geq 0}$ , and  $\mathcal{Y}_{k_2} = (y_1, \dots, y_{k_2})$  being a tuple of all the available measurement up until sample  $k_2$ . Assume now at iteration  $k$  we have an estimate  $\hat{x}_{k|k} \sim \mathcal{N}(\mu_{k|k}, P_{k|k})$  for the states and probabilities  $\beta_{k|k}^i$ . If there is an available measurement reading  $y_{k+1}$ , then we run a KF for each model  $\mathcal{M}^i$  as following

**Time update:**

$$\mu_{k+1|k} = A \mu_{k|k}, P_{k+1|k} = A P_{k|k} A^\top + E Q E^\top \quad (3a)$$

**Measurement Correction:**

$$\tilde{y}_{k+1|k} = y_{k+1} - C_k \mu_{k+1|k}, S_{k+1|k}^i = C_k P_{k+1|k} C_k^\top + R_k^i \quad (4a)$$

$$\mu_{k+1|k+1}^i = \mu_{k+1|k} + P_{k+1|k} C_k^\top (S_{k+1|k}^i)^{-1} \tilde{y}_{k+1|k} \quad (4b)$$

$$P_{k+1|k+1}^i = \left( \mathbf{I} - P_{k+1|k} C_k^\top (S_{k+1|k}^i)^{-1} C_k \right) P_{k+1|k} \quad (4c)$$

To derive a time update step and a measurement correction step for the probabilities  $\beta_{k+1|k+1}^i$ , we use Baye's rule to write

$$\beta_{k+1|k+1}^i = p(m_{k+1}^i | \mathcal{Y}_{k+1}) = \frac{p(m_{k+1}^i, \mathcal{Y}_{k+1})}{p(\mathcal{Y}_{k+1})}$$

$$\begin{aligned}
&= \frac{p(\mathbf{m}_{k+1}^i, \mathcal{Y}_k, \mathcal{Y}_{k+1})}{p(\mathcal{Y}_{k+1})} = \frac{p(\mathbf{m}_{k+1}^i, \mathcal{Y}_k, \tilde{y}_{k+1|k})}{p(\mathcal{Y}_{k+1})} \\
&= \frac{p(\tilde{y}_{k+1|k} | \mathbf{m}_{k+1}^i, \mathcal{Y}_k) p(\mathbf{m}_{k+1}^i, \mathcal{Y}_k)}{p(\mathcal{Y}_{k+1})} \\
&= \frac{p(\tilde{y}_{k+1|k} | \mathbf{m}_{k+1}^i) p(\mathbf{m}_{k+1}^i | \mathcal{Y}_k) p(\mathcal{Y}_k)}{p(\mathcal{Y}_{k+1})} \\
&= \frac{p(\tilde{y}_{k+1|k} | \mathbf{m}_{k+1}^i) p(\mathbf{m}_{k+1}^i | \mathcal{Y}_k)}{p(\tilde{y})} \\
&= \frac{p(\tilde{y}_{k+1|k} | \mathbf{m}_{k+1}^i)}{\sum_{i=1}^N p(\tilde{y}_{k+1|k} | \mathbf{m}_{k+1}^i) p(\mathbf{m}_{k+1}^i | \mathcal{Y}_k)} p(\mathbf{m}_{k+1}^i | \mathcal{Y}_k)
\end{aligned} \tag{5}$$

with

$$\begin{aligned}
p(\mathbf{m}_{k+1}^i | \mathcal{Y}_k) &= p(\mathbf{m}_{k+1}^i | \mathbf{m}_k^i) p(\mathbf{m}_k^i | \mathcal{Y}_k) \\
&= (1 - \alpha) p(\mathbf{m}_k^i | \mathcal{Y}_k) + \alpha \bar{\beta}^i
\end{aligned} \tag{6}$$

To summarize, (5) and (6) are written as a time update step and a measurement correction step with the notation  $\beta_{k_1|k_2}^i$  as following

**Time update (using (6)):**

$$\beta_{k+1|k}^i = (1 - \alpha) \beta_{k|k}^i + \alpha \bar{\beta}^i \tag{7}$$

**Measurement Correction (using (5)):**

$$\beta_{k+1|k+1}^i = \frac{p(\tilde{y}_{k+1|k+1} | \mathbf{m}_{k+1}^i)}{\sum_{i=1}^N \beta_{k+1|k}^i p(\tilde{y}_{k+1|k+1} | \mathbf{m}_{k+1}^i)} \beta_{k+1|k}^i. \tag{8}$$

with  $p(\tilde{y}_{k+1|k+1} | \mathbf{m}_{k+1}^i)$  being the multi-normal probability density function with zero mean and covariance matrix  $S_{k+1|k+1}^i$ . Finally, let  $\Delta \mu_{k+1}^i := \mu_{k+1|k+1}^i - \mu_{k+1|k}^i$ , then the estimated mean and covariance matrix of the states are computed as following

$$\mu_{k+1|k+1} = \sum_{i=1}^N \beta_{k+1|k+1}^i \mu_{k+1|k+1}^i \tag{9a}$$

$$P_{k+1|k+1} = \sum_{i=1}^N \beta_{k+1|k+1}^i \left( P_{k+1|k+1}^i + \Delta \mu_{k+1}^i (\Delta \mu_{k+1}^i)^\top \right). \tag{9b}$$

Note that the values  $\beta_{k+1|k+1}^i$  in (9a) are acting as weights for the estimates obtained from the different KFs. The values  $\beta_{k+1|k+1}^i$  will be referred to as "trust values for sensor  $i$ " in the next section.

## 5. RESULTS

We compare the MMKFF presented in this paper with the following KFs:

- Linear KF.
- The Distributionally Robust KF (DRKF) from Wang and Ye (2022) with a moment based ambiguity set and an  $\epsilon$ -contamination set for outliers.
- The Adaptive Fading KF (AFKF) based on Xia et al. (1994) but with the fading applied to the covariance matrix  $R(k)$  adapting to sensor changes.
- The MMKF.

### 5.1 Choice of the Kalman Filters' Parameters

All the KFs share the same value of  $Q$ . For a higher value of  $Q$ , the KFs will rely on the measurements more for

their estimates which will make them faster to respond to changes in BG but more prone to noise. On the other hand, a smaller value of  $Q$  will make the KFs rely more on the model predictions but will hinder their ability to respond quickly to changes in BG. The value of  $Q$  in this paper was chosen to be  $Q = 1$ . For the distributionally robust KF, we tuned the parameters denoted in the paper Wang and Ye (2022) as  $\theta_{2,x}, \theta_{2,v}, \epsilon$  to be  $\theta_{2,x} = \theta_{2,v} = 1.02$  and  $\epsilon = 0.005$ . For Exp1, we only compared MMKF and MMKFF due to limited space. For Exp2, the one model KFs share one covariance matrix  $R_k = \text{diag}(s_k^\top r)$  with  $r = [1 \ 1 \ 100 \ 100]^\top$  since our prior knowledge is such that Exp2.S1 and Exp2.S2 perform better than Exp2.S3 and Exp2.S4. For the multi-model KFs, we chose  $\sigma_l^2 = 1$  and  $\sigma_u^2 = 100$  for the both experiments. The forgetting factor was chosen to be  $\alpha = 0.05$ . The KFs for both Exp1 and Exp2 were initialized with  $\mu_{0|0} = [0 \ 0 \ 0.5y_0[1] - 0.5y_0[2]]^\top$  and  $P_{0|0} = \mathbf{I}$  where  $y_0[1]$  and  $y_0[2]$  are the measurements of the first and second sensors of both experiments, respectively. For Exp1, we chose  $\beta_{0|0} = \bar{\beta} = [0.5 \ 0.5]^\top$  based on our prior knowledge (no prior preference over the sensors). As for Exp2,  $\beta_{0|0} = \bar{\beta} = [0.3 \ 0.3 \ 0.2 \ 0.2]^\top$  based on our prior knowledge.

### 5.2 Results from Exp1

In Figure 2, MMKFF and MMKF were tested on data from Exp1.S1 and Exp2.S2 and the result compared to BGA. The MMKF and MMKFF performed similarly, with their fused CGM being close to the accurate BG readings. The fused CGM managed to overcome the drifting in Exp1.S2 and stayed close to the reading from the Blood Gas Analyser (BGA). However, we can see that the trust values  $\beta_{k|k}^1$  and  $\beta_{k|k}^2$  evolved differently with the CGM readings. The trust values from the MMKF converged faster towards Exp1.S1 ( $\beta_{k|k}^1 \approx 1, \beta_{k|k}^2 \approx 0$ ) during the case when Exp1.S2 was being calibrated than the trust values of MMKFF (see Figure 3). In this particular excerpt for Exp1, favoring Exp1.S1 quickly from the beginning as done by MMKF is better since the performance of Exp1.S2 continued to degrade during the period of data collection. However, events like Exp2.S2 improving beyond the calibration point without drifting or Exp1.S1 deteriorating during the trial, for instance, due to connection loss, can still occur. In these events, the MMKFF will perform better than MMKF since it does not immediately converge to trusting one sensor over the others. Additionally, it is able to "forget" past experiences which will enable it to adapt to new changes. This is shown in the findings for Exp2, where the MMKFF outperformed the MMKF in a more realistic case where the quality of the sensors varied over time. It is important to note that even though forgetting can offer better adaptivity to changes in the quality of sensors, it comes with the cost of slower reaction towards abrupt events as seen in Figure 3. The lower the forgetting factor, the faster the reaction of MMKFF to abrupt events and vice versa.

### 5.3 Results from Exp2

Figure 4 shows the results for three different excerpts of Exp2 compared to a fused CGM signal obtained by

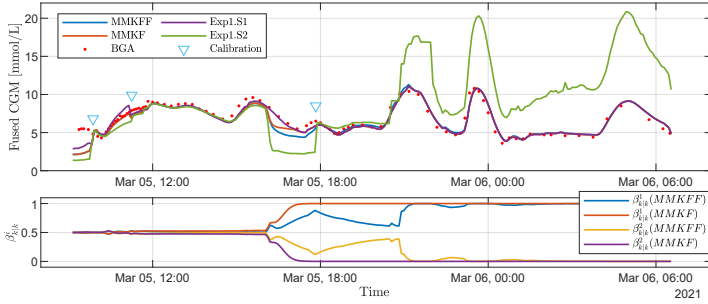


Fig. 2. Results from Exp1. BGA represents the values from the blood gas analyser, and ‘Calibration’ represents points where sensors S1 and S2 were calibrated using the BGA values. The Upper plot shows a comparison between MMKFF and MMKF using the readings from Exp1.S1 and Exp1.S2, while the lower plot shows the trust values  $\beta^i$  in (8) for each of the sensors  $i \in \{1, 2\}$ .

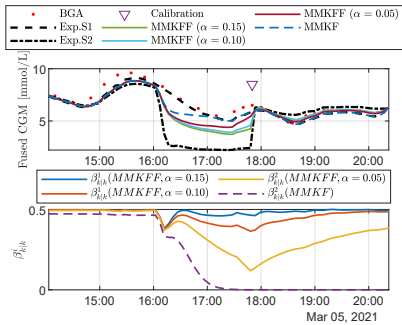


Fig. 3. The upper plot shows the response of MMKFF and MMKF with different forgetting factors, while the lower plot shows the trust values.

manually tuning a weighted average of the four CGMs in an online fashion (labeled Manual in the plots). In the first excerpt (left of the figure), the four sensors were all working as expected and readings were provided each 5 minutes. The MMKFF was the closest to the manually tuned signal. For the second excerpt (middle of the figure), Exp2.S3 was not working properly and stopped providing measurements towards the end. Additionally, Exp2.S2 was performing poorly with missing measurements and reporting readings which were close to 0 [mmol/L] while Exp2.S4 was performing better and close to Exp2.S1. This situation is challenging not only due to the missing and wrong readings of some sensors, but also due to the fact that our prior knowledge prefers Exp2.S1 and Exp2.S2 over Exp2.S3 and Exp2.S4. Despite these challenges, the MMKFF performed the best in the sense of being the closest to the manually tuned reading. Observe how both the MMKF and MMKFF reduced the trust value of Exp2.S4 when it stopped providing readings around 50 [min] of the excerpt. However, the MMKFF increased the trust value of Exp2.S4 when it started providing good readings again, unlike the MMKF. Moreover, the MMKFF started trusting Exp2.S2 more when its readings improved. For the third excerpt (right of the figure), Exp2.S3 was not providing any readings, and Exp2.S4 started providing readings around the time when Exp2.S1 and Exp2.S2 stopped pro-

viding readings. Out of the four KFs, the MMKFF was still the closest to the manually tuned reading on average and had the lowest maximum ARE value. Additionally, notice how it was difficult for the MMKF to increase its trust value of EX2.S4 again when it was providing readings. On the other hand, the MMKFF increased the trust value of EX2.S4 when it started providing readings again. These results show how the MMKFF is able to adapt better to changes in the quality of the sensors.

## 6. CONCLUSION AND FUTURE WORK

For CGM devices, the MMKFF fusing approach was introduced. The technique was evaluated using two separate sets of experimental data, and it was shown to be capable of producing a reliable fused CGM signal. It was demonstrated that MMKFF can respond to variations in the quality of the CGM readings more effectively when compared to other KF approaches. However, it was observed that MMKFF’s ability for adaptation came at the expense of a slower reaction to sudden changes. Future studies could improve this by taking into account an adaptive forgetting factor for MMKFF. Additionally, the past data and inputs can be used with the high gain observer suggested in Benam et al. (2019) and Benam et al. (2022) to estimate the BG levels when the sensor connection is lost. Evaluating the proposed fusing approach on additional data from various experiments can provide a better understanding of the strategy’s performance and its likelihood of being applied in a human environment.

## 7. ACKNOWLEDGMENT

The experimental services were provided by the Comparative medicine Core Facility (CoMed), Norwegian University of Science and Technology (NTNU). CoMed is funded by the Faculty of Medicine at NTNU and Central Norway Regional Health Authority. The transmitters (for Exp1 and Exp2) and the hormone infusion systems in Exp1 were provided by Inreda Diabetic BV (Goor, the Netherlands). We want to thank Marte Kierulf Åm, Oddveig Lyng, and Patrick Christian Bösch for their invaluable contribution to the data collection. We also thank Professor Sven Magnus Carlsen for his help in experimental design and discussions.

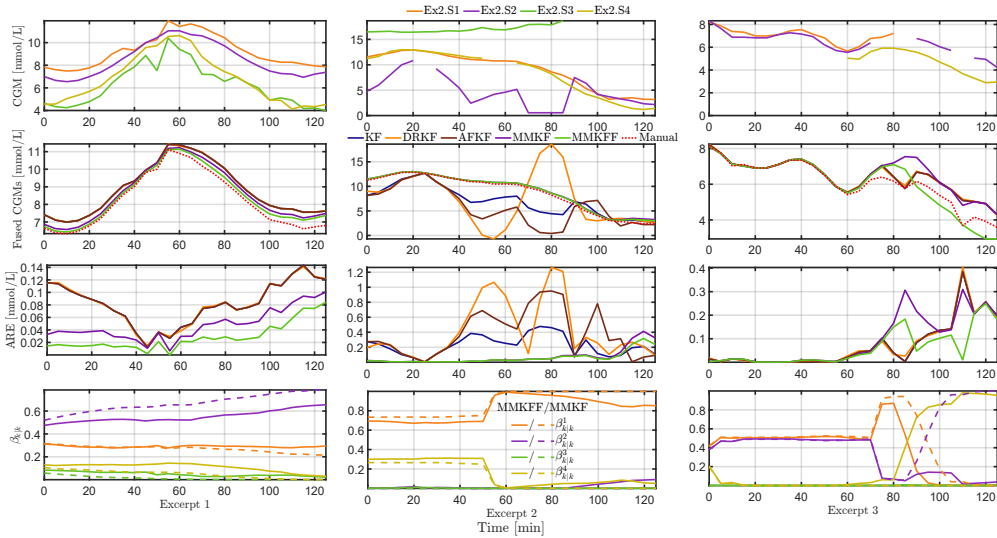


Fig. 4. Results of fusion using four different glucose sensors in the Exp2, for three different excerpts (left, middle, right column). First row: Original glucose sensor values for sensors S1 to S4. Second row: Comparison of fused glucose sensor values for the various sensor fusion methods. Third row: ARE (absolute relative error with respect to manual sensor fusion). Fourth row: Trust values  $\beta_{k|k}^i$  in (8), where solid lines are MMKFF and dashed lines are MMKF.

## REFERENCES

- Bar-Shalom, Y., Li, X.R., and Kirubarajan, T. (2004). *Estimation with applications to tracking and navigation: theory algorithms and software*. John Wiley & Sons.
- Benam, K.D., Khoshamadi, H., Am, M.K., Stavadahl, O., Gros, S., and Fougner, A.L. (2023). Identifiable prediction animal model for the bi-hormonal intraperitoneal artificial pancreas. *Journal of Process Control*, 121, 13–29.
- Benam, K.D., Khoshamadi, H., Lema-Pérez, L., Gros, S., and Fougner, A.L. (2022). A nonlinear state observer for the bi-hormonal intraperitoneal artificial pancreas. In *2022 44th Annual International Conference of the IEEE Engineering in Medicine & Biology Society (EMBC)*, 171–176. IEEE.
- Benam, K.D., Talebi, H., and Khosravi, M.A. (2019). Full order high gain observer design for image-guided robotic flexible needle steering. In *2019 27th Iranian Conference on Electrical Engineering (ICEE)*, 1151–1156. IEEE.
- De Nicolao, G., Sparacino, G., and Cobelli, C. (1997). Nonparametric input estimation in physiological systems: Problems, methods, and case studies. *Automatica*, 33(5), 851–870.
- Facchinetti, A. (2016). Continuous glucose monitoring sensors: past, present and future algorithmic challenges. *Sensors*, 16(12), 2093.
- Facchinetti, A., Del Favero, S., Sparacino, G., et al. (2013). Modeling the glucose sensor error. *IEEE Trans Biomed Eng*, 61(3), 620–629.
- Facchinetti, A., Del Favero, S., Sparacino, G., et al. (2015). Model of glucose sensor error components: identification and assessment for new dexcom g4 generation devices. *Medical & biological engineering & computing*, 53(12), 1259–1269.
- Facchinetti, A., Sparacino, G., and Cobelli, C. (2010). Enhanced accuracy of continuous glucose monitoring by online extended kalman filtering. *Diabetes technology & therapeutics*, 12(5), 353–363.
- Halvorsen, M., Benam, K.D., Khoshamadi, H., and Fougner, A.L. (2022). Blood glucose level prediction using subcutaneous sensors for in vivo study: Compensation for measurement method slow dynamics using kalman filter approach. In *2022 IEEE 61st Conference on Decision and Control (CDC)*, 6034–6039. IEEE.
- Jacobs, P.G., El Youssef, J., Castle, J., et al. (2014). Automated control of an adaptive bihormonal, dual-sensor artificial pancreas and evaluation during inpatient studies. *IEEE Trans Biomed Eng*, 61(10), 2569–2581.
- Knobbe, E.J. and Buckingham, B. (2005). The extended kalman filter for continuous glucose monitoring. *Diabetes technology & therapeutics*, 7(1), 15–27.
- Kuure-Kinsey, M., Palerm, C.C., and Bequette, B.W. (2006). A dual-rate kalman filter for continuous glucose monitoring. In *2006 Int Conf of the IEEE Engineering in Medicine and Biology Society*, 63–66. IEEE.
- Magill, D. (1965). Optimal adaptive estimation of sampled stochastic processes. *IEEE Transactions on Automatic Control*, 10(4), 434–439.
- Vettoretti, M., Battocchio, C., Sparacino, G., et al. (2019). Development of an error model for a factory-calibrated continuous glucose monitoring sensor with 10-day lifetime. *Sensors*, 19(23), 5320.
- Wang, S. and Ye, Z.S. (2022). Distributionally robust state estimation for linear systems subject to uncertainty and outlier. *IEEE Transactions on Signal Processing*, 70, 452–467.
- Xia, Q., Rao, M., Ying, Y., and Shen, X. (1994). Adaptive fading kalman filter with an application. *Automatica*, 30(8), 1333–1338.

## 6.6 PAPER 6

**Title: “Fully Automated Bi-Hormonal Intraperitoneal Artificial Pancreas Using a Two-Layer PID Control Scheme”**

Published in the European Control Conference (ECC) in Bucharest, Romania, June 2023 [6].





# Fully Automated Bi-Hormonal Intraperitoneal Artificial Pancreas Using a Two-Layer PID Control Scheme

Jana Langholz, Karim Davari Benam, Bindu Sharan, Sebastien Gros, Anders Lyngvi Fougner

**Abstract**—Treatment of type 1 diabetes mellitus is significantly improved by using commercially available hybrid closed-loop systems to deliver insulin. These systems, also called artificial pancreas (AP), use the subcutaneous (SC) route to deliver insulin. However, meal announcements are necessary due to the slow insulin absorption from the SC tissue. Thus due to the need for human intervention, it is called “hybrid closed loop” AP. In this work, a bi-hormonal AP with intraperitoneal (IP) infusion is designed to increase the time within the range of 3.9–10.0 mmol/l and alleviate the burden of meal announcements. A two-layer controller is designed to provide safe and effective insulin and glucagon delivery. The primary layer is based on classical PID controllers for insulin and glucagon, and the supervisory layer includes four parts: (A) Zone-based control settings, (B) Extrapolation of sensor data to compensate for sensor delay in SC tissue, (C) Auto-tuning of the PID parameters in the primary layer through simulation in an animal model, and (D) Safety barriers. The controller is designed to prevent hypoglycemia after meals and during physical activity, as well as prevent postprandial hyperglycemia. The designed AP achieved 92.5% of the time within the range of 3.9–10.0 mmol/l on a simulator trained on data from animal experiments. The results indicate that this two-layer control structure with IP infusions makes it feasible to achieve a fully automated artificial pancreas without the need for meal announcements, i.e. without human intervention.

## I. INTRODUCTION

Patients with type 1 diabetes depend on exogenous insulin since their insulin-producing  $\beta$ -cells are destroyed or are not able to produce enough insulin. As a result, the body fails to control the Blood Glucose Level (BGL) [1]. Current diabetes treatment consists of three stages; First, the BGL must be measured, then the amount of the necessary hormone must be determined, and finally, this amount must be injected. The automated system that can perform these procedures is called the artificial pancreas (AP). Commercially available AP systems include a control system to determine the amount of insulin, a pump for injecting the insulin into the subcutaneous (SC) tissue, and a blood glucose sensor for measuring the BGL [2].

Due to the slow insulin absorption from the SC tissue, most control approaches fail to keep the BGL within the

desired range when facing an unannounced meal [3]. Notably, the meal announcements need to be done by the patients well in advance. Otherwise, a delayed meal announcement or underestimated size of the meal can cause hyperglycemia (high BGL). Hyperglycemia is caused by too little (or no) meal insulin or the meal insulin being given too late relative to the meal. If hyperglycemia occurs often, the patient will have a higher risk of microvascular complications and cardiovascular diseases. Improved glycemic control alleviates these risks.

On the other hand, an overestimated meal size can cause hypoglycemia (low BGL). Since hypoglycemia can have serious short- and long-term implications, it is a critical occurrence that must be avoided. As categorized later in Table II by the American Diabetes Association, the first level of hypoglycemia is set at a threshold where neuroendocrine response starts failing. However, the symptoms can be unrecognized, and for that reason, the risk of experiencing hypoglycemic unawareness exists. In the second level, neuroglycopenic symptoms arise, and immediate actions should be taken. If it stays untreated, the patient can experience significant changes in mental and physical functioning, progressing further into consciousness, seizure, coma, or death [1, Chapter 6].

It has been shown in [3] that the intraperitoneal (IP) route has a faster insulin absorption than the SC route, and the AP systems using the IP route do not need the meal announcements. In addition, bi-hormonal AP systems are shown to be effective in avoiding hypoglycemia [4]. Bi-hormonal AP uses a second hormone next to insulin to increase the BGL. This hormone, called glucagon, can stimulate the breakdown of glycogen into glucose in the liver. Thus, glucose is accessible in case of need for energy [5].

Several studies have been done in the literature to design different controller approaches, such as Model predictive control (MPC) and PID controller for single hormonal SC AP [6]–[8]. In addition, a few other research groups are focusing on bi-hormonal SC AP [9]–[11] showing more promising results than single-hormonal APs. However, few controllers have been tested and designed for single hormonal IP AP without meal announcements. This is due to the lack of a simulator for the IP insulin and glucagon infusion. Nonetheless, Toffanin *et al.* in [3] used an MPC approach to control the BGL for single hormonal IP AP, where they used a modified version of the SC simulator. The results showed that IP insulin does not require meal announcement. Huyett *et al.* in [12] used a simulator with intravenous (IV) insulin infusion and assumed that IP and IV insulin infusions have the same

This research is funded by the Research Council of Norway (project no. 248872), and the Centre for Digital Life Norway.

J. Langholz, and B. Sharan are with Institute of Control Systems, Technical University of Hamburg, Eißendorfer Straße 40, 21073 Hamburg, Germany. {jana.langholz, bindu.sharan}@tuhh.de

K. D. Benam, S. Gros, and A. L. Fougner are with Department of Engineering Cybernetics, Faculty of Information Technology and Electrical Engineering, Norwegian University of Science and Technology (NTNU), O. S. Bragstads Plass 2D, 7034 Trondheim, Norway. {karim.d.benam, sebastien.gros, anders.fougner}@ntnu.no

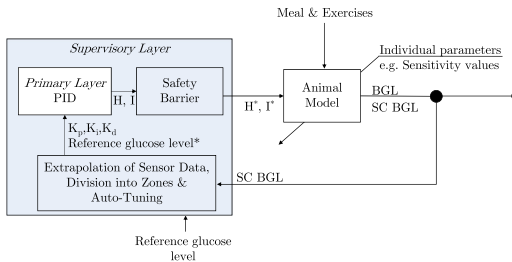


Fig. 1: Block diagram of the proposed two-layer control structure. The primary layer consists of two PID controllers for insulin and glucagon infusions. The supervisory layer manages the safety barriers, extrapolates the sensor data to compensate for the sensor delay, and modifies the set points and PID coefficients in accordance with the BGL values. The inputs to the primary layer are the auto-tuned gains for the controller, the reference BGL of the active zone, the output insulin (I), and glucagon (H). After the safety barrier, the output might be modified, shown by the superscript \*. Meal & Exercises are implemented as glucose infusion rates in the simulator. The simulator outputs are blood glucose level (BGL) and the subcutaneously BGL (SC BGL) measurement.

absorption rates. Then, they designed a PID controller for insulin infusion using the sensors inside the peritoneal cavity. The results showed significant improvements in simulations.

This paper thereby focuses on designing the control algorithm for a bi-hormonal IP AP. To this end, a two-layer control structure is developed and tested on the simulator. As shown in Fig. 1, the primary layer includes two PID controllers for insulin and glucagon, respectively; at every instant only one of them is activated by the supervisory layer depending on the BGL and its derivative. In addition, reference BGL and PID coefficients are specified by the auto-tuning algorithm in the supervisory layer. Moreover, the supervisory layer is responsible for safety barriers, emergency modes, and compensating for sensor delays.

The proposed control structure is tested on a simulator which was trained/identified based on data from 13 animal experiments [13]. The controller was exposed to scenarios aiming for typical real life conditions, e.g., with meals, physical activity, sleep, and model mismatch (tuning the controller for a model that does not match perfectly the simulator it was tested on, e.g., by making a time varying insulin sensitivity). To the best knowledge of the authors, the design and test of a bi-hormonal IP AP on a simulator trained and tested for the IP route is novel.

The paper is structured as follows. First, the simulator used to develop the control structure is described in Section II. Then the different stages of the proposed control structure are presented in Section III. Different metrics are employed to assess the proposed controller, and they are introduced in Section IV. The performance of the controller is assisted

in different scenarios in Section V. Finally, these results are discussed in Section VI, and a conclusion is given in Section VII.

## II. SIMULATOR AND SCENARIOS

The development and evaluation of the proposed control structure take place in a simulator. To the authors' best knowledge, the proposed "meta model" in [13] is the only model available for testing a bi-hormonal IP artificial pancreas. Other models in the literature are developed for IP routes, but they are designed only for control purposes and have simple pharmacokinetics and pharmacodynamics to serve as a simulator [14], [15]. The meta model is generally based on physiology, and its parameters are identified empirically through 13 experiments in anesthetized pigs, making it a suitable option for a simulator.

The control inputs of the meta model are IP insulin and IP glucagon. IV glucose infusion is used as an additional input to mimic the intestines in anesthetized pigs that absorb glucose, but this input is hidden for the controller. It is used to design challenges (such as meals and exercise) for the controller.

There are only five parameters that must be identified for each new subject:

- The insulin-independent glucose uptake rate ( $\alpha_1$ )
- The liver's sensitivity to insulin ( $\alpha_2$ )
- The sensitivity of other organs to insulin ( $\alpha_3$ )
- The liver's sensitivity to glucagon ( $\alpha_4$ )
- The liver's initial glycogen storage level ( $\alpha_5$ )

These parameters are unknown to the controller and the sensitivity parameters ( $\alpha_2, \alpha_3, \alpha_4$ ) can vary over time. In [13], the ranges of these parameters are identified based on the animal experiments as follows:

$$\alpha_2 \in [0.57, 5.84], \quad (1a)$$

$$\alpha_3 \in [4.92, 17.22], \quad (1b)$$

$$\alpha_4 \in [6, 20]. \quad (1c)$$

These ranges are used for challenging the controller with different scenarios in which the sensitivities vary. The other parameters of the meta model are population parameters, which are already identified and known using the information from the previous experiments on different subjects.

The simulator was combined with a subcutaneous sensor model that provides a BGL with a time lag as in actual APs. The inputs and outputs of the simulator are illustrated around "animal model" in Fig. 1. The meta model is thereby the basis of the simulator. Insulin and glucagon are the control inputs, meals and physical activity are unknown to the system and thus can be seen as disturbances, the individual parameters are modifiable internal parameters, and actual BGL and subcutaneous BGL (SC BGL) are the output values. To simulate the SC BGL time lag, we used a first order derivative model with parameters (See equation (7) in [16]). Similar to most commercial AP systems, the sampling time of 5 min is chosen for the simulator.

### A. Sensitivity to Insulin and Glucagon

As mentioned earlier, the sensitivities of the patient to insulin and glucagon are time-varying parameters. They are influenced by various hormones and conditions, which can affect AP performance. Since determining the sensitivity related to hormones is not straightforward, different modeling possibilities are presented in this section to provide realistic challenges to the controller.

To this end, three different modes are introduced in Fig. 2: The first mode represents the constant value identified during the 13 animal experiments [13]. The second mode is a sinusoidal variation representing fluctuations of sensitivities during the a day. Lastly, a sawtooth profile is used to examine the reaction of the controller to discontinuities due to e.g., a replacement of the infusion set, which would typically happen every 2-3 days in a clinical study. In these simulations, the frequency was increased to make it even more challenging for the controller. For modes 2 and 3, a counteracting effect for insulin sensitivity and glucagon sensitivity is implemented using a phase shift. For example, for mode 2, a phase shift of  $90^\circ$  is used. The designed scenario ensures the most significant challenge for the controller because this emulates the fact that when insulin has a high effect on BGL, the glucagon will have the lowest effect, and thus the rescue process is prolonged.

A sinusoidal and sawtooth profile oscillate around a neutral position. Three different neutral positions  $c_{np}$  are defined, given by

$$\text{max: } c_{np,max} = b_u - (b_u + b_l) \cdot \frac{v_r}{2} \quad (2a)$$

$$\text{cen: } c_{np,cen} = b_u - (b_u + b_l) \cdot \frac{1}{2}, \quad (2b)$$

$$\text{min: } c_{np,min} = b_l + (b_u + b_l) \cdot \frac{v_r}{2}, \quad (2c)$$

where  $b$  is defined as boundary value with either index  $u$  as upper or index  $l$  as lower value of the regions from (1a)–(1c). The variable  $v_r \in [0, 100]\%$  ensures that the sensitivity always stays within the regions, no matter which setting is chosen. The amplitude  $a$  is defined as

$$a = (b_u - b_l) \cdot \frac{v_r}{2}. \quad (2d)$$

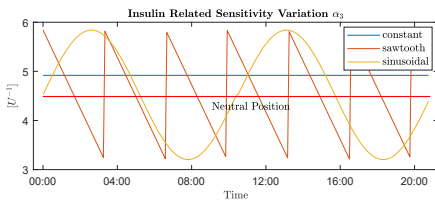


Fig. 2: Visualisation of modes for time-variant hormone sensitivity (using the insulin sensitivity as an example).

### B. Glucose Infusion

As described in [13], the meal and exercises can be simulated by the glucose infusion rate  $R_g$  in anesthetized pigs. In addition, according to [17], the basal rate of glucose production in adults is between  $2\text{--}8 \left[\frac{\text{mg}}{\text{min}\cdot\text{kg}}\right]$ . In this paper, we assumed that the basal glucose infusion rate is  $5 \left[\frac{\text{mg}}{\text{min}\cdot\text{kg}}\right]$ , and it is constant in the simulations.

For modeling different realistic scenarios of glucose infusion, basal glucose production can be taken as a basis. To model the food intake of a normal day, different events such as breakfast, lunch, and dinner, as well as soft drinks, can be taken into account, with different amounts resulting in an increase in the glucose infusion rate. Additionally, physical activities can be modeled by decreasing glucose production below basal glucose in anesthetized pigs. The realistic scenario considered to challenge the controller is shown in Fig. 3. The profile of the glucose infusion rate through the day is generated based on the intestine model ("model 2") proposed in [18].

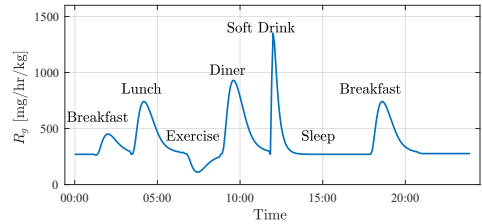


Fig. 3: A demonstrative example of an IV glucose infusion rate in 24 hr to simulate a real-life scenario. Exercise is simulated by reducing the glucose infusion, since it is impossible to perform exercise in anesthetized pigs. The x-axis shows the time (in HH:mm format) since the start of the experiment of the experiment.

## III. TWO-LAYER PID CONTROL SCHEME

With the control of the BGL we want to ensure that the BGL is within the target region most of the time. Additionally, the requirement is set to lower or increase the BGL in a safe way. This is because too much glucagon or insulin injection could lead to a dangerous drop or increase of the BGL and can cause severe side effects. Furthermore, oscillations are unwanted, and the amount of injected glucagon should be as low as possible. Therefore, a supervisory layer is implemented to ensure these requirements are met.

There are four different stages implemented in the supervisory layer. The first stage is sensor data extrapolation, the second is dividing the BGL into different zones, the third is the auto-tuning of the PID coefficients in the defined zones, and the last stage is implementing the safety barriers. The designed control scheme is shown in Fig. 4, and the defined stages are explained in more detail in the following subsection.

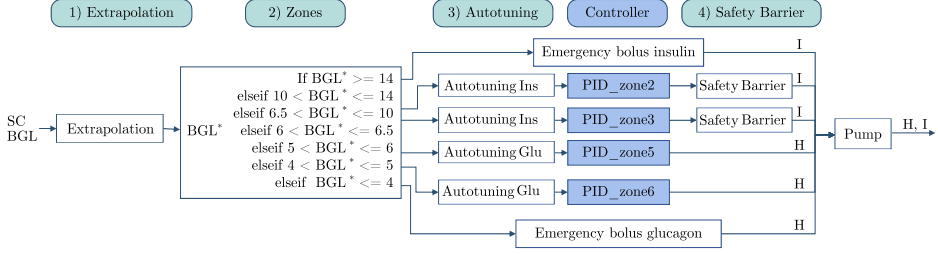


Fig. 4: Detailed block diagram of the two-layer PID controller. The white color denotes the supervisory layer, whereas the blue color represents the primary layer. The four strategies are displayed: (1) Extrapolation. (2) Division into zones. (3) Auto-Tuning. (4) Safety Barrier. As in Fig. 1 shown, the input is the subcutaneous blood glucose level (SC BGL), the extrapolated BGL is presented as  $BGL^*$ , glucagon (H) and insulin (I) are determined during the process and outputted in the end.

#### A. Extrapolation of Sensor Data

SC sensors measurements lag behind the real BGL value due to physiological delays and their slow dynamics [19]. We implement the linear extrapolation method in the supervisory layer to predict the BGL in the next step and compensate for the sensor delay.

#### B. Zones

The first stage of the supervisory layer of the controller splits the BGL into seven zones, as shown in Fig. 5. In zones 1, 2, and 3, insulin is injected, and in zones 5, 6, and 7, glucagon is injected. Zone 4 is called the “quiet” zone, where no controller is activated so that neither insulin nor glucagon can be injected. The first and the last zone are the emergency zones, where in zone 1, an insulin bolus is given, and in zone 7, a glucagon bolus is injected. In total, a PID controller with four sets of coefficients is implemented, two for the injection of each hormone. Zones 2 and 6 consist of a more aggressively tuned PID controller, whereas zone 3 and 5 have a less aggressively tuned PID controller, both for insulin and glucagon respectively. Each zone has a separately chosen setpoint to allow a smooth transition into the next zone. To ensure safety, we opted for a target blood glucose level (BGL) of 6.4 mmol/l. BGLs below this level, falling into zones 4-7, are classified as low BGL. In such cases, no insulin is given to allow the BGL to return to the baseline.

#### C. Auto-Tuning PID controllers

To achieve an optimal performance of the designed PID, we implement a real-time auto-tuning stage to tune the PID controller for different individuals and scenarios. This is done by predicting the BGL for  $N_p$  samples using the individually identified meta-model [13] for each subject and then minimizing the quadratic error of the predicted BGL with the reference BGL value. The reference BGL value is selected according to the active zone as provided in the previous section. The decision variables in the optimization process are the PID coefficients. Notably, this procedure is done online and at every sampling time for zones 2,3,5 and

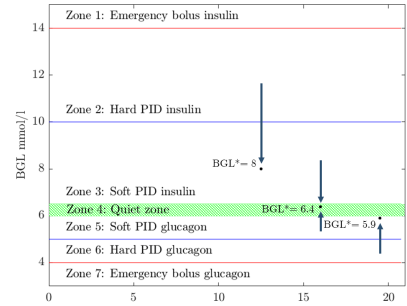


Fig. 5: Division of the BGL into 7 zones with different control types and actions. The borders of each zone as well as the setpoints ( $BGL^*$ ) are illustrated.

6. As explained in the previous section, the reference BGL is defined separately for the different zones. The cost function designed for this end is defined as follows:

$$c = \sum_{i=1}^{N_p} (G_i^* - G_{SC,i})^2, \quad (3)$$

where  $N_p$  is the prediction horizon, and at time  $k$ ,  $c$  is the cost for the prediction interval  $[k, k + N_p]$ ,  $G^*$  is the defined reference BGL for the current zone, and  $G_{SC,i}$  is the  $i$  step ahead prediction of the BGL using the animal model at time  $k + i$ . In order to estimate the future BGL, a glucose infusion rate is needed. Here, for the zones 2 and 3 we assumed that the future glucose infusion rate equals the basal glucose infusion rate (see Section II-B). In contrast, to achieve a pessimistic prediction, a zero glucose infusion rate is assumed for the zones 5 and 6 (where the glucagon must be given).

The optimization problem can have multiple local minima, resulting in sub-optimal solutions. In order to address this

issue, the initial values given to the optimizer must be chosen carefully. In this paper, we choose the initial values using a trial-and-error method performed in multiple simulations for each zone. In addition, the decision variables are constrained in different zones to control the aggressiveness of the PID controller. The selected boundaries and the initial values are shown in Table I. The interior-point method is used to minimize the designed cost function (3).

TABLE I: Initial values and boundaries of the PID controller coefficients for different zones. The values are given in the format  $[K_p, K_i, K_d]$ .

Zone	Initial Value	Lower Boundary	Upper Boundary
2	[0.2, 0, 5]	[0.1, 0, 1]	[0.5, 0, 20]
3	[0.1, 0, 2]	[0.01, 0, 0.02]	[0.2, 0, 10]
5	[-0.5, -0.01, -8]	[-5, -0.01, -10]	[-0.1, 0, -0.1]
6	[-1, -0.01, -5]	[-10, -0.01, -30]	[-1, 0, -5]

#### D. Safety Barriers

The BGL slope is one of the factors we need to consider for patient safety since if insufficient glycogen is stored in the liver, a rapid BGL drop can result in a hypoglycemic event. Thus, if the slope value exceeds a “dangerous value”, the designed controller will be turned off to prevent excessive insulin. Since insulin is only given in zones 2 and 3, this is the only place where this safety barrier is needed. The threshold for the slope must be tuned based on the zone.

Furthermore, due to the pharmacokinetics and pharmacodynamics of the IP insulin, the half-life time of insulin is 60–100 minutes for IP injections [13]. In other words, the maximum effect of insulin and maximum drop in BGL appear 60–100 minutes after injection. Therefore, to prevent a rapid decrease in BGL in the next 60–100 minutes, additional safety parameters are used in zones 2 and 3 to stop the controller from giving more than a specified amount of insulin. The threshold for the amount of insulin must be chosen according to the body weight, sensitivity to insulin, and based on the active zone.

For example, for the pigs with 36 kg of body weight, the “dangerous slope” is defined as less than  $-0.01$  mmol/L/min and 0 mmol/L/min for zones 2 and 3, respectively. In addition, the maximum amount of insulin that can be injected over a rolling time window of 60 min is set to 1.5 U for zone 2 and 2 U for zone 3. These values are chosen using a trial-and-error method in the simulations represented in the paper.

### IV. PERFORMANCE MEASURES

In order to evaluate the performance of the proposed control structure, three metrics are defined as follows:

#### A. Metric 1, Time in Range (TIR)

The Time in Range (TIR) is the first metric used to assess the controller’s performance, indicating the duration for which the BGL remains in the desired range. Table II provides the ideal range, hyperglycemia levels, and hypoglycemia levels specified by the American Diabetes Association. Evaluating the effectiveness of treatments using Time

above Range (TAR, hyperglycemia) and Time below Range (TBR, hypoglycemia) is also recommended [1, Chapter 6].

TABLE II: Glycemic targets for adults according to the American Diabetes Association [1, Chapter 6].

Ranges	BGL range [mmol/L]	Target [%]	Target [Time/Day]
Level 2 hyperglycemia	>13.9	<5	1h 12min
Level 1 hyperglycemia	10.1 - 13.9	<25	6h
Time in range	3.9 - 10.0	>70	16h 48min
Level 1 hypoglycemia	3.0 - 3.8	<4	58min
Level 2 hypoglycemia	<3.0	<1	14min

These glycemic targets can be formulated as

$$T = \frac{\sum_{i=1}^N \mathcal{I}_i}{N_s} \text{ with } \mathcal{I}_i = \begin{cases} 1 & \text{for } G_i \in \text{Range} \\ 0 & \text{else} \end{cases} \quad (4)$$

with  $N_s$  the total number of steps,  $T$  as the resulting target value for each zone, which depends on the current step  $i$ , has to meet a condition based on the BGL value  $G_i$  and the ranges defined in Table II. This produces five different values for the zones. It should be noted that the BGL ranges are defined for humans, while the simulator used in this study is based on pig data.

#### B. Metric 2, Amount of Used Insulin and Glucagon

The second metric measures the control energy. For this, the used amount of insulin and glucagon is calculated to check how much control input was needed to control the BGL. Additionally, these values are used as an indicator, if enough insulin is injected and if the requirement is met that as little glucagon as possible is injected. This yields

$$X_{used} = \sum_{i=1}^N X_i \quad (5)$$

where  $X$  denotes the placeholder for insulin  $I$  and glucagon  $H$ .  $X_{used}$  is the amount of hormone used over the simulation time,  $N$  the total number of control intervals, and  $X_i$  the amount of injected hormone at each sampling interval  $i$ .

#### C. Metric 3, Severity of Hyperglycemia and Hypoglycemia

To compare the severity of hypoglycemia and hyperglycemia with different controllers or setups, we consider the integral of the BGL above or below the defined BGL thresholds. This threshold is chosen to be  $G_{b,he} = 10$  mmol/L for hyperglycemia and  $G_{b,ho} = 3.9$  mmol/L for hypoglycemia. We defined the severity of hyperglycemia [min·mmol/L] as follows.

$$S_{he} = \frac{area}{n_{aB}} = \frac{Q_U(G) - Q_{U,b}}{n_{aB}} \quad (6)$$

where  $G$  is the BGL,  $n_{aB}$  in the number of the samples that  $G > G_{b,he}$ ,  $Q_U(G)$  is integral of the BGL values exceeding  $G_{b,he}$ , and  $Q_{U,b} = G_{b,he} \cdot n_{aB} \cdot \Delta T$ , in which  $\Delta T$  is the sampling time. Similar to  $S_{he}$ , the severity of hypoglycemia is defined as follows.

$$S_{ho} = \frac{Q_L(G_{b,ho}) - Q_{L,b}}{\bar{n}_{bB}} \quad (7)$$

where  $\bar{n}_{bB}$  is the number of the samples that  $G < G_{b,ho}$ ,  $Q_L(G)$  is integral of the BGL values less than  $G_{b,he}$ , and  $Q_{L,b} = G_{b,ho} \cdot \bar{n}_{bB} \cdot \Delta T$ .

## V. RESULTS

This section presents the results of the proposed control approach in different scenarios. For a detailed evaluation, we show the effect of having each of the proposed stages of the supervisory layer (extrapolation, zones, auto-tuning, safety barriers), which are added one by one, yielding the final controller with all implemented stages in the end. As explained in section II, the parameters of the simulator are identified using the animal experiment conducted on anesthetized pigs. Then, the effectiveness of the safety barriers and the zone PID with auto-tuning is assessed on other subjects using the proposed metrics.

In order to challenge the controller, four sets of  $\{\alpha_1, \alpha_2, \dots, \alpha_5\}$  are identified from four animal experiments, and the designed controller is performed on them in the simulator. In addition, three sets of extended simulations with time-varying sensitivity values ( $\alpha_2, \alpha_3, \alpha_4$ ) are done on each of them, resulting in 16 simulations in total. In the extended simulations,  $\alpha_2, \alpha_3, \alpha_4$  are changing in the sinusoidal shape with three neutral positions (max, cen, and min) explained in Section II-A. The effectiveness of the proposed stages in the designed structure is evaluated in the following sections.

### A. Development Stages

As shown in Fig. 4, the input of the controller is represented by the sensor value. In order to compensate the delay, sensor data is extrapolated by predicting a future step. Fig. 6 shows an approximation of the extrapolated BGL value to the actual BGL using the delayed sensor. It can be easily seen that the extrapolated and actual BGL have almost the same sinusoidal peaks.

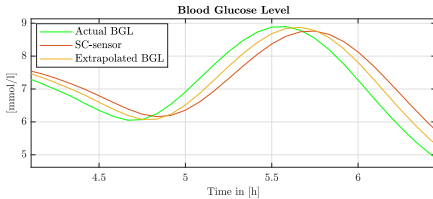


Fig. 6: Extrapolation reduces the time lag of the SC sensors.

A PID controller is chosen as a comparison control structure, which has the same tuning as zone 3 for insulin infusions and the same tuning as zone 5 for glucagon infusions. However, the reference BGL for this single-layer PID is set to 7 mmol/L (middle point of the desired range of 3.9–10 mmol/L) to avoid problems with hypoglycemia. The effect of the control scheme stages can be seen in Fig. 7, 8 and 9. When looking at Fig. 7, the first stage of the two-layer controller injects slightly larger amounts of insulin, and the

transition between injecting the hormones is characterized by small pauses, compared to the single-layer controller.

Auto-tuning significantly increases the use of the control input, which, however, can also considerably decrease the average of the BGL (Fig. 8 and 9). The maximum BGL is noticeably reduced, while the minimum BGL is increased. It is important to note that these are average values of the results of 16 simulations. This reduction in the range of the BGL is also evident from Fig. 7, where the increased aggressiveness of the controller is noticeable from the inputs.

The increase in aggressiveness due to auto-tuning is also noticeable in an increase in hypoglycemic events. Therefore, the safety barrier is implemented for zone 2. This method shows a negligible effect on the total avoidance of hypoglycemic events and reduction of insulin usage. In contrast, when implemented in zones 2 and 3, the amount of insulin can be significantly reduced. This also reduces the need for glucagon injections. However, the activation of safety barrier for both zones leads to a renewed slight increase in the average and maximum BGL. The increased course of BGL is also evident from Fig. 7.

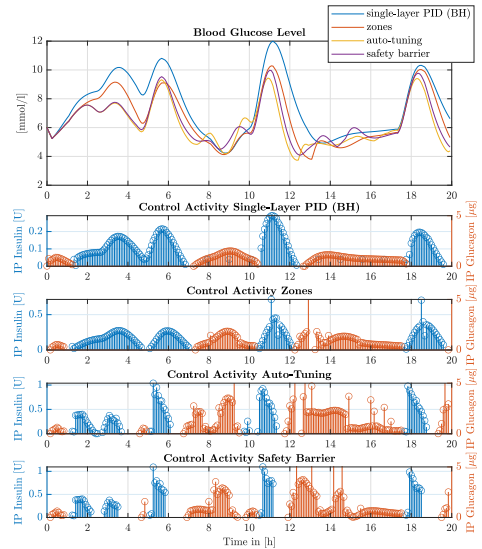


Fig. 7: Comparison of BGL course in 3 stages of proposed 2-layer PID controller (added incrementally) with a single-layer bi-hormonal (BH) PID controller (tuned like zones 3 and 5 of 2-layer). Zones denote 2nd stage, auto-tuning is 3rd, and safety barrier is 4th (activated for zones 2 and 3). Extrapolation is implemented for each stage since it represents the first stage. Subplots show insulin and glucagon control input for each stage.

### B. Final Controller

The proposed PID controller includes auto-tuning, time delay compensation through extrapolation, zone-based switch-

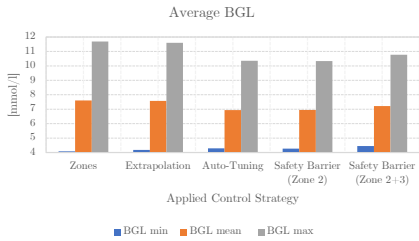


Fig. 8: Comparison of the minimum, average and maximum BGL over the different stages.

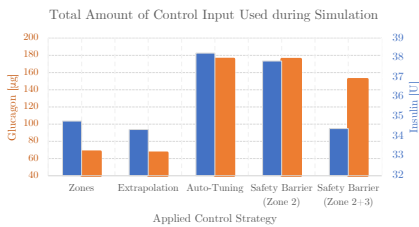


Fig. 9: Course of the control inputs insulin and glucagon over the different development stages of the controller (averaged for the 16 simulations).

ing, and a safety barrier to limit BGL rate. Table III shows the performance of the final PID controller for different sensitivity settings. L2 hypoglycemia and L2 hyperglycemia can be avoided except for the constant sensitivity setting. When considering the TIR, a crucial dependence of the effectiveness of therapy on sensitivity is also apparent. Despite an increase in the amount of insulin, the greatest proportion of hyperglycemia occurs for the minimum sensitivity. With an increase in sensitivity, the TIR and the necessary amount of glucagon increases, while maximum sensitivity achieves the smallest BGL range and mean.

For the constant sensitivity values, one data set has the lowest sensitivity values, leading to hypoglycemic events. Away from this, less insulin but more glucagon is used, which results otherwise in the range of the other sensitivity values.

Fig. 10 shows the comparison of the results when the sawtooth profile and the sinusoidal profile are evaluated. Here, the sawtooth profile shows stronger irregularities, which is due to the fast and abrupt change of the sensitivities. This means that the extremes are stronger, although they are still within a satisfactory range.

## VI. DISCUSSION

The supervisory layer's extrapolation compensates for sensor time delay, resulting in a slight minimum BGL increase and maximum BGL reduction. The zone stage improves glycaemic control, as evident from Fig. 7. However, this improvement comes with the cost of more tuning parameters

TABLE III: Performance metrics (averaged over different data sets): The settings min, cen, and max correspond to the sinusoidal settings, described in Eqs. (2a)–(2c). The constant setting (con) represents the time-invariant sensitivity values. L1 describes regular hyperglycemia or hypoglycemia events, whereas L2 describes severe events.  $N(S_{he})$  and  $N(S_{ho})$  represent the number of hyperglycemic and hypoglycemic events.

	Overall	Min	Cen	Max	Con
L2_hyper [%]	0.00	0.00	0.00	0.00	0.00
L1_hyper [%]	6.57	17.66	5.75	0.91	1.94
TIR [%]	92.51	82.34	94.25	99.09	94.35
L1_hypo [%]	0.93	0.00	0.00	0.00	3.71
L2_hypo [%]	0.00	0.00	0.00	0.00	0.00
I [U]	34.40	42.47	33.86	31.49	29.78
H [μg]	152.25	77.81	100.51	151.50	279.17
$S_{he}$ [min-mmol/L]	0.53	0.87	0.30	0.35	0.48
$N(S_{he})$	1.50	2.50	2.25	0.50	0.75
$S_{ho}$ [min-mmol/L]	0.07	0.00	0.00	0.00	0.28
$N(S_{ho})$	0.19	0.00	0.00	0.00	0.75
min(BGL) [mmol/L]	4.44	4.70	4.66	4.35	4.07
meanBGL [mmol/L]	7.22	8.10	7.34	6.82	6.63
max(BGL) [mmol/L]	10.78	11.89	10.74	10.12	10.36

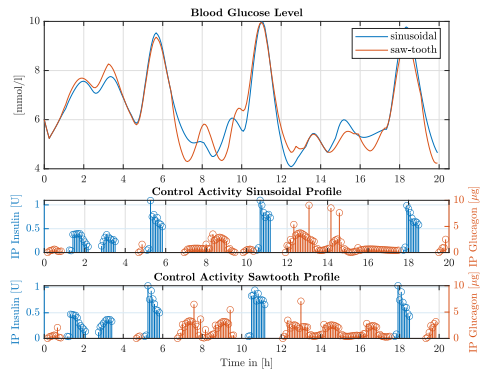


Fig. 10: A final evaluation of the performance of the final controller where the controller is applied to the two different sensitivity profiles, where the insulin sensitivity and the glucagon sensitivity are time-variant as a sinusoidal or a sawtooth function. Apart from the sensitivity profiles everything is identical.

and the complexity of the controller. The tunable parameters must be studied in detail, and sensitivity analysis of the controller to these parameters should be done before implementing the designed method in practice, which is kept for future work. In addition, A high-gain observer can be incorporated with the controller for better functionality and safer control, as discussed in [20], [21]. Auto-tuning adjusts PID parameters automatically for different individuals and scenarios with time-varying settings, resulting in reduced minimum and average BGL for all individuals. However, increased aggressiveness can lead to undershoots close to the lower limit. A penalty could be added to the cost function



to limit hormone use, but this is not included in the current simple cost function. Improvements to the auto-tuning stage are left for future work. The safety barriers in zone 2 and 3 terminate insulin injections early, thus reducing the impact of increased aggressiveness and control activity from auto-tuning. Consequently, there is a significant increase in the minimum BGL, but at the cost of a decrease in mean BGL and some slight hyperglycemic events.

It is important to note that glucagon is an unstable liquid that can cause blockage of the infusion set and the pump. However, in real experiments, we suggest changing the glucagon infusion set every 24 hours similar to [22].

Overall, the proposed control structure meets the requirements specified in Table II. However, the controller's effectiveness is heavily influenced by insulin and glucagon sensitivities. Despite the saw-tooth profile's discontinuities, it produces satisfactory control results. The enhanced performance and safety of the controller are achieved at the cost of increased complexity and tuning parameters compared to the single-layer PID controller.

## VII. CONCLUSION

This paper proposes a two-layer PID controller with four stages to improve glycemic control. The controller compensates for sensor delay, prevents on-off behavior, adjusts PID coefficients automatically, and adds safety barriers to avoid hypoglycemia. Auto-tuning predicts future BGL, making the structure comparable to MPC approaches and computationally efficient for real-time use. The proposed controller is effective on a complex and well-tuned simulator based on an animal model, achieving satisfactory results despite time-varying insulin and glucagon sensitivities. Future studies can evaluate the framework on a human-based simulator to determine if similar outcomes can be achieved without requiring meal announcements.

## VIII. ACKNOWLEDGMENTS

This research is funded by the Research Council of Norway (project no. 248872) and the Centre for Digital Life Norway. We want to thank Professor Sven Magnus Carlsen and Professor Herbert Werner for the discussions.

## REFERENCES

- [1] American Diabetes Association, "Introduction: Standards of medical care in diabetes—2021," *Diabetes Care*, vol. 44, no. Supplement\_1, pp. S1–S2, Dec. 2020.
- [2] Y. Ho, *Patient-Specific Controller for an Implantable Artificial Pancreas*. Springer-Verlag GmbH, 2018. [Online]. Available: [https://www.ebook.de/de/product/34256288/yvonne\\_ho\\_patient\\_specific\\_controller\\_for\\_an\\_implantable\\_artificial\\_pancreas.html](https://www.ebook.de/de/product/34256288/yvonne_ho_patient_specific_controller_for_an_implantable_artificial_pancreas.html)
- [3] C. Toffanin, L. Magni, and C. Cobelli, "Artificial pancreas: In silico study shows no need of meal announcement and improved time in range of glucose with intraperitoneal vs. subcutaneous insulin delivery," *IEEE Trans. Med. Robot. Bionics*, vol. 3, no. 2, pp. 306–314, 2021.
- [4] P. A. Bakhtiani, L. M. Zhao, J. El Youssef, J. R. Castle, and W. K. Ward, "A review of artificial pancreas technologies with an emphasis on bi-hormonal therapy," *Diabetes, Obesity and Metabolism*, vol. 15, no. 12, pp. 1065–1070, 2013.
- [5] K. von der Saal, *Biochemie*. Springer Berlin Heidelberg, 2020. [Online]. Available: [https://www.ebook.de/de/product/38050241/karin\\_von\\_der\\_saal\\_biochemie.html](https://www.ebook.de/de/product/38050241/karin_von_der_saal_biochemie.html)
- [6] R. Gondhalekar, E. Dassau, and F. J. Doyle III, "Periodic zone-mpc with asymmetric costs for outpatient-ready safety of an artificial pancreas to treat type 1 diabetes," *Automatica*, vol. 71, pp. 237–246, 2016.
- [7] R. Gondhalekar, E. Dassau, and F. Doyle III, "Velocity-weighting & velocity-penalty mpc of an artificial pancreas: Improved safety & performance," *Automatica*, vol. 91, pp. 105–117, 2018.
- [8] E. Matamoros-Alcivar, T. Ascencio-Lino, R. Fonseca, G. Villalba-Meneses, A. Tirado-Espin, L. Barona, and D. Almeida-Galarraga, "Implementation of MPC and PID control algorithms to the artificial pancreas for diabetes mellitus type 1," in *2021 IEEE International Conference on Machine Learning and Applied Network Technologies (ICMLANT)*. IEEE, Dec. 2021.
- [9] F. Tang and Y. Wang, "Design of bi-hormonal artificial pancreas system using switching economic model predictive control," in *2017 36th Chinese Control Conference (CCC)*. IEEE, Jul. 2017.
- [10] R. W. Jones, "Glucagon control strategies for the bi-hormonal artificial pancreas," in *IEEE Conf. Ind. Electr. Appl. (ICIEA)*. IEEE, Jun. 2019.
- [11] N. Taleb, A. Quintal, R. Rakheja, V. Messier, L. Legault, E. Racine, and R. Rabasa-Lhoret, "Perceptions and expectations of adults with type 1 diabetes for the use of artificial pancreas systems with and without glucagon addition: Results of an online survey," *Nutrition, Metabolism and Cardiovascular Diseases*, vol. 31, no. 2, pp. 658–665, Feb. 2021.
- [12] L. M. Huyett, E. Dassau, H. C. Zisser, and F. J. Doyle III, "Design and evaluation of a robust pid controller for a fully implantable artificial pancreas," *Industrial & engineering chemistry research*, vol. 54, no. 42, pp. 10311–10321, 2015.
- [13] K. D. Benam, H. Khoshamadi, M. K. Åm, Ø. Stavadahl, S. Gros, and A. L. Fougner, "Identifiable prediction animal model for the bi-hormonal intraperitoneal artificial pancreas," *Journal of Process Control*, vol. 121, pp. 13–29, 2023.
- [14] C. Lopez-Zazueta, A. L. Fougner *et al.*, "Low-order nonlinear animal model of glucose dynamics for a bi-hormonal intraperitoneal artificial pancreas," *IEEE Trans. Biomed. Eng.*, no. 3, pp. 1273–1280, Mar. 2022.
- [15] A. Chakrabarty, J. M. Gregory, L. M. Moore, P. E. Williams, B. Farmer, A. D. Cherrington, P. Lord, B. Shelton, D. Cohen, H. C. Zisser *et al.*, "A new animal model of insulin-glucose dynamics in the intraperitoneal space enhances closed-loop control performance," *Journal of Process Control*, vol. 76, pp. 62–73, 2019.
- [16] M. Halvorsen, K. D. Benam, H. Khoshamadi, and A. L. Fougner, "Blood glucose level prediction using subcutaneous sensors for in vivo study: Compensation for measurement method slow dynamics using kalman filter approach," in *2022 IEEE 61st Conference on Decision and Control (CDC)*. IEEE, 2022, pp. 6034–6039.
- [17] B. Koletzko, O. Guolet, J. Hunt, K. Krohn, R. Shamir, and the Parenteral Nutrition Guidelines Working Group, "Guidelines on paediatric parenteral nutrition: 5. Carbohydrates," *Journal of Pediatric Gastroenterology & Nutrition*, vol. 41, no. Supplement 2, pp. S28–S32, Nov. 2005.
- [18] C. Dalla Man, M. Camilleri, and C. Cobelli, "A system model of oral glucose absorption: validation on gold standard data," *IEEE Trans. Biomed. Eng.*, vol. 53, no. 12, pp. 2472–2478, 2006.
- [19] Ø. Stavadahl, A. L. Fougner, K. Kõlle, S. C. Christiansen, R. Ellingsen, and S. M. Carlsen, "The artificial pancreas: A dynamic challenge," *IFAC-PapersOnLine*, vol. 49, no. 7, pp. 765–772, 2016.
- [20] K. D. Benam, H. Talebi, and M. A. Khosravi, "Full order high gain observer design for image-guided robotic flexible needle steering," in *2019 27th Iranian Conference on Electrical Engineering (ICEE)*. IEEE, 2019, pp. 1151–1156.
- [21] K. D. Benam, H. Khoshamadi, L. Lema-Pérez, S. Gros, and A. L. Fougner, "A nonlinear state observer for the bi-hormonal intraperitoneal artificial pancreas," in *2022 44th Annual International Conference of the IEEE Engineering in Medicine & Biology Society (EMBC)*. IEEE, 2022, pp. 171–176.
- [22] H. Blauw, A. J. Onvlee, M. Klaassen, A. C. van Bon, and J. H. DeVries, "Fully closed loop glucose control with a bi-hormonal artificial pancreas in adults with type 1 diabetes: an outpatient, randomized, crossover trial," *Diabetes Care*, vol. 44, no. 3, pp. 836–838, 2021.

## 6.7 PAPER 7

**Title: “Optimal Experimental Design to Estimate Insulin Response in Type 2 Diabetes”**

Accepted and presented at 7th IEEE Conference on Control Technology and Applications (CCTA) 2023.



# Optimal Experimental Design to Estimate Insulin Response in Type 2 Diabetes

Sarah Ellinor Engell<sup>1,2</sup>, Henrik Bengtsson<sup>1</sup>, Karim Davari Benam<sup>3</sup>,  
Anders Lyngvi Fougner<sup>3</sup>, John Bagterp Jørgensen<sup>2</sup>

**Abstract**—In late-stage type 2 diabetes, automated titration algorithms provide a promising alternative to the current standard-of-care. Many published methods rely on personalized dose-response models to predict a safe and effective insulin dose. In this case study, we address the challenge of how to collect an informative data set to ensure practical identifiability of such models. We apply optimal experimental design to enhance the performance of a published titration algorithm. For a 24-hour experiment, we solve an optimization problem to select the size of three meals and the hourly fast-acting insulin infusion rate. In simulation, we demonstrate how the optimized protocol improves the safety of the algorithm’s dose-predictions. The results indicate that optimal experimental design has the potential to improve model-based algorithms and may be used as a qualitative tool when planning clinical experiments.

## I. INTRODUCTION

Worldwide, one in eleven people lives with diabetes and the prevalence continues to increase. Of all diabetes cases, type 2 diabetes (T2D) accounts for 90%. In T2D, persistent high blood glucose levels occur due to an imbalance between the secretion of the regulatory hormone insulin and the insulin sensitivity in the body. Left untreated, elevated glucose levels can have serious consequences, e.g., vision loss or amputations. Numerous medications exist to enhance insulin secretion or improve the insulin sensitivity. However, as T2D progresses over time, daily basal insulin injections can become necessary to sufficiently lower the glucose levels [1].

Initiating basal insulin treatment is a challenge. The response to insulin is highly individual and overdoses can be both uncomfortable and dangerous. To safely reach the target glucose range, people with T2D *titrate* to find a personalized daily injection dose. Based on daily pre-breakfast finger-prick measurements, the individual adjusts the insulin dose in small steps to reach clinical targets. This process can take several months, and for some even years. Despite a high drug efficacy in clinical trials, up to 60% of the people initiating basal insulin treatment never reach clinical targets. The daily workload is one of many reasons for failed insulin titration [2].

\*This project is funded by Innovation Fund Denmark through the Industrial PhD project 0153-00049B

<sup>1</sup>Novo Nordisk A/S, DK-2880 Bagsværd, Denmark  
sgee@novonordisk.com, hbss@novonordisk.com

<sup>2</sup>Department of Applied Mathematics and Computer Science, Technical University of Denmark, DK-2800 Kgs. Lyngby, Denmark  
saeg@dtu.dk, jbjjo@dtu.dk

<sup>3</sup>Department of Engineering Cybernetics, Norwegian University of Science and Technology (NTNU), Trondheim, Norway  
karim.d.benam@ntnu.no, anders.fougner@ntnu.no

To improve clinical outcomes, the titration burden can be reduced through automation. Published algorithms for automated titration use combinations of data from insulin injection pens, finger-prick measurements, continuous glucose monitors (CGM) and/or insulin pumps to identify a personalized target insulin dose [3]–[7]. Many of these methods rely on identifying a dose-response model for the individual [5]–[7]. The quality of the dose prediction therefore critically depends on successful model identification.

Model-based design of experiments (MBDoe) has been applied in diabetes research to enhance the identification of physiological models and improve control algorithms for artificial pancreas (AP) systems [8]–[13]. Most work in this field dates ten years back, where the aim was to identify when to draw blood samples to obtain the most information about an individual’s physiological response to insulin and meals. Today, improvements in sensor technology have excluded the need for selecting blood sampling times, as CGMs present reliable measurements every five minutes. Still, only a few studies on optimal experimental design have exploited this technological development [12], [13]. To the best of our knowledge, no studies have focused on model-based design of titration experiments in T2D. We believe there is a potential to improve model-based insulin dosing algorithms in T2D using MBDoe.

In this case study, we apply optimal experimental design to improve model identification in a personalized dose-guidance algorithm from [7]. We design a 24-hour experiment with three meals and insulin infusion to estimate parameters in a dose-response model. To evaluate the safety of the new design, we test the protocol in 100 virtual subjects. From the experimental data, we identify parameters in a personalized dose-response model for each subject. With the identified models, we predict a daily insulin dose to reach clinical targets. In simulation, we evaluate the safety and efficacy of the dose prediction and compare the results to [7].

This paper is organized as follows. In Section II, we introduce the model-based dose-guidance algorithm that we aim to improve through optimal experimental design. Section III describes the optimization problem and briefly presents the two models employed for experimental design and simulation. In Section IV, we present the new experimental design and show the performance of the dose-guidance algorithm with the optimal data collection protocol. Section V discusses the design and results in comparison to [7]. In Section VI, we conclude on the main findings from this case study.

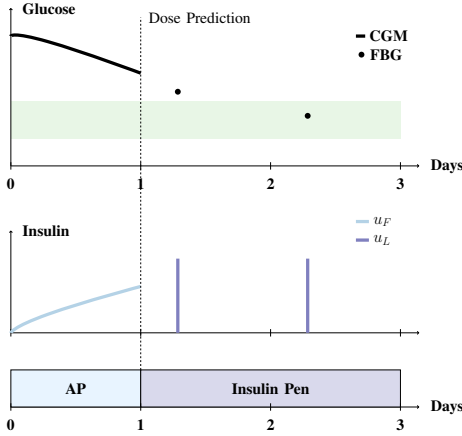


Fig. 1. A visualization of the titration solution from [7]. Data from an artificial pancreas (AP) enables the prediction of an insulin dose for injection-based therapy with long-acting insulin. In the AP period, fast-acting insulin ( $u_F$ ) infusion is based on glucose measurements from a continuous glucose monitor (CGM). We use the AP data to identify parameters in a dose-response model. The model predicts an insulin dose to reach target glucose concentrations. After dose-prediction, a daily dose of long-acting insulin ( $u_L$ ) is injected before breakfast and fasting blood glucose (FBG) measurements are used for daily monitoring.

## II. THE TEST CASE

In previous work, we present a model-based titration algorithm to predict a personalized daily insulin dose [7]. With 24 hours of data from an artificial pancreas (AP), we identify a dose-response model. For parameter estimation, we use a one step prediction error method (PEM) using maximum likelihood estimation (MLE). We apply the continuous-discrete extended Kalman filter (CDEKF) to approximate the likelihood function. We refer to [7] for technical details on the titration algorithm. Figure 1 shows the conceptual setup of the original titration solution. In this paper, we revisit this algorithm and apply optimal experimental design to maximize the information collected with the AP. The former design does not include meals and requires fasting for the 24 hour long AP period. In this work, we solve an optimization problem to find a protocol for both meal and insulin inputs. Figure 2 (adapted from [7]) shows that several dose predictions are unsafe when we use the original data collection protocol. We aim to decrease the amount of unsafe dose estimates, whilst meeting clinical safety requirements during experimental data collection.

## III. METHODS

In this section, we introduce the two models we use for experimental design, prediction, and simulation. We define the optimization problem, the decision variable and the constraints.

### A. Design model

To optimize the experimental design, we employ a physiological T2D model from [14]. We include the adaptations

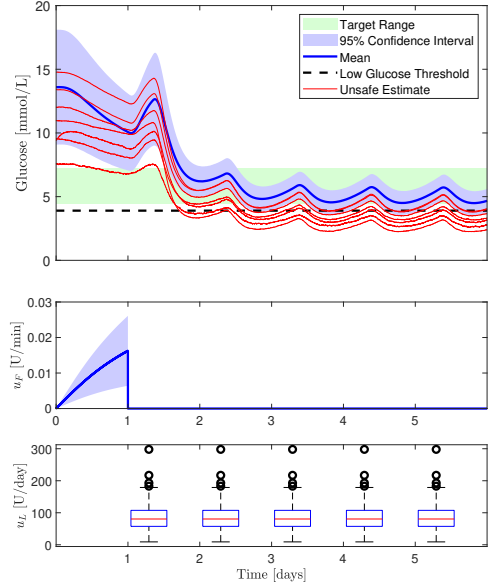


Fig. 2. Simulation results for 100 virtual people using the titration solution in [7]. During the first 24 hours, a closed-loop system gradually increases fast-acting insulin infusion and the plasma glucose drops. After 24 hours, the collected data enables parametrization of a dose-response model. The model predicts a daily insulin dose to reach glucose targets. For the remaining days, the predicted dose is injected prior to breakfast. Seven people have unsafe dose-estimates.

from [15] to ensure structural identifiability. The design model describes the impact of meals and insulin on plasma glucose levels and consists of six differential equations,

$$\dot{D}_1(t) = d(t) \frac{1000 \cdot A_G}{MwG} - \frac{1}{\tau_m} D_1(t) \quad (1a)$$

$$\dot{D}_2(t) = \frac{1}{\tau_m} D_1(t) - \frac{1}{\tau_m} D_2(t) \quad (1b)$$

$$\dot{I}_{sc}(t) = \frac{1}{\tau_I} u(t) - \frac{1}{\tau_I} I_{sc}(t) \quad (1c)$$

$$\dot{I}_p(t) = \frac{1}{\tau_I} I_{sc}(t) - \frac{1}{\tau_I} I_p(t) \quad (1d)$$

$$\begin{aligned} \dot{I}_{eff}(t) &= p_3(I_p(t) + I_{ENDO} \cdot G(t)) - p_3 I_{eff}(t) \\ \dot{G}(t) &= -(GEZI + S_1 I_{eff}(t)) \cdot G(t) \\ &\quad + EGP + R_A(t). \end{aligned} \quad (1e) \quad (1f)$$

$D_1$  [mmol/min] and  $D_2$  [mmol/min] are meal compartments representing absorption of carbohydrate intake,  $d(t)$  [g/min]. The exogenous insulin input,  $u(t)$  [U/min], is absorbed subcutaneously in  $I_{sc}$  [U/min] before reaching plasma,  $I_p$  [U/min].  $I_{eff}$  [U/min] describes the combined insulin effect of exogenous insulin input and the endogenous insulin production,  $I_{ENDO}$  [U·L/mmol·min].  $G$  [mmol/L] is the plasma glucose level.  $R_A(t) = \frac{D_2(t)}{V_G \tau_m}$  [mmol/L/min] is the rate of appearance of glucose from consumed meals. Table I lists parameter descriptions and provides a reference for each parameter value.

The system outputs discrete sensor measurements,

$$y_k = G(t_k) + v_k. \quad (2)$$

affected by independent and identically distributed noise,  $v_k \sim N_{iid}(0, R)$ . Through these measurements, we aim to determine the parameter set  $\theta = [S_I, EGP, I_{ENDO}]$ . To provide dose-guidance, we utilize a personalized version of the model (1) with the individual estimates of  $\theta$ , and for the rest of the model parameters we adopt the published values listed in Table I.

### B. Optimal Experimental Design

The aim of optimal experimental design is to maximize the information collected in an experimental data set [18]. To enhance the estimation of the parameter set,  $\theta$ , we solve an optimization problem to find an experimental design vector,  $\phi$ , that best excites the system,

$$\min_{\phi} \psi(\phi, \theta) \quad (3a)$$

$$s.t. \quad \phi = [u(t), d(t)] \quad (3b)$$

$$x(0) = x_0 \quad (3c)$$

$$\dot{x}(t) = f(t, x(t), u(t), d(t), \theta) \quad (3d)$$

$$\hat{y}_k = h(t_k, x(t_k)) + v_k \quad (3e)$$

$$0 \geq c(t, x(t), u(t), d(t), \theta). \quad (3f)$$

The dynamics of the system we wish to identify are approximated by the model,  $f(\cdot)$ , a discrete measurement function,  $h(\cdot)$ , and measurement noise,  $v_k \sim N_{iid}(0, R)$ . The system states,  $x(t)$ , are a  $N_x$ -dimensional vector and  $x_0$  contains the initial state values. The exogenous insulin,  $u(t)$ , and the meals,  $d(t)$ , are the system inputs.  $\hat{y}$  denotes a vector of discrete measurements estimated by the model. The constraints on the inputs and output are given by (3f).

The cost function of the optimization problem acts on the parameter variance-covariance matrix,  $C_{\theta}$ , which quantifies the parametric uncertainty. Reducing the value of  $C_{\theta}$  is equivalent to improving the parameter estimates. Hence, we wish to determine,

$$\phi = \arg \min \{ \psi[C_{\theta}(\theta, \phi)] \} \approx \arg \min \{ \psi[I(\theta, \phi)^{-1}] \} \quad (4)$$

where  $\psi$  is the design criterion, an assigned measurement function of  $C_{\theta}$ . As an approximation of  $C_{\theta}$ , we apply the inverse of Fisher's information matrix,  $I(\theta, \phi)$ .

Several design criteria exist [18]. To minimize the volume of the hyper box which bounds the variance ellipsoid, we apply A-optimality, i.e. minimizing the trace of the inverse Fisher Information matrix,

$$\psi_A(\phi, \theta) = \text{tr} \left( I(\theta, \phi)^{-1} \right), \quad (5)$$

where Fisher's Information matrix is defined as

$$I(\theta, \phi) = \sum_{k=1}^N S_y(t_k)^T R^{-1} S_y(t_k). \quad (6)$$

$R$  is the covariance matrix of the measurements,  $N$  is the total number of measurements over the length of the experiment, and  $S_y$  is the output sensitivity matrix.  $S_y(t_k)$

is a measure of the change in each of the  $n_y$  outputs for each of the  $n_{\theta}$  estimated parameters at sampling point  $k$ ,

$$S_y(t_k) = \begin{bmatrix} \frac{\partial y_1(t_k)}{\partial \theta_1} & \cdots & \frac{\partial y_1(t_k)}{\partial \theta_{n_{\theta}}} \\ \vdots & \ddots & \vdots \\ \frac{\partial y_{n_y}(t_k)}{\partial \theta_1} & \cdots & \frac{\partial y_{n_y}(t_k)}{\partial \theta_{n_{\theta}}} \end{bmatrix}. \quad (7)$$

We compute  $S_y$  using central differentiation. To avoid numerical issues during the optimization, we normalize the parameters with respect to the (supposed) true values for the subject shown in Table I. We adjust the value for insulin sensitivity,  $S_I$ , to ensure that the design and simulation models reach the same fasting glucose,  $y_0$ , at zero insulin infusion,

$$S_I = \frac{EGP}{I_{ENDO} \cdot y_0} - GEZI. \quad (8)$$

To reduce the risk of numerical errors, we scale the state  $I_{eff}$  by a factor  $c_f = 1000$  and obtain similar orders of magnitude for all states. The equations (1e) and (1f) become,

$$\dot{I}_{eff}(t) = c_f \cdot p_3(I_p(t) + I_{ENDO} \cdot G(t)) - p_3 I_{eff}(t) \quad (9a)$$

$$\dot{G}(t) = -(GEZI + S_I I_{eff}(t)/c_f) \cdot G(t) + EGP + R_A(t). \quad (9b)$$

### C. Decision Variable

We fix the length of the experiment to 24 hours. To ensure that the optimization problem is tractable, we describe the inputs of the design vector,  $\phi$ , in the following way.

$$\phi = [u(t), d(t)] = [u_1, u_2, \dots, u_{24}, d_B, d_L, d_D] \quad (10)$$

We apply a zero-order hold parametrization on  $u(t)$ , and fix the duration and mealtimes for the meal input,  $d(t)$ . For the insulin input, we determine the optimal insulin infusion over 24 one-hour blocks of piece-wise constant input. The three meals are consumed over five minute intervals at 07:00, 12:30 and 18:00. We determine the optimal size of each meal.

### D. Design Constraints

To design a physically feasible and safe experiment, we select a set of input and output constraints. The insulin input must be non-negative and may not exceed an infusion rate of 15 mU/min. All three meals must be within a minimum 20 g and maximum 100 g of carbohydrates. We select a minimal meal size to ensure that the optimal solution contains all three meals.

In current clinical guidelines, the target range for fasting glucose levels is 4.4-7.2 mmol/L [1]. We strive to achieve glucose levels within the range, however a swift drop in glucose concentration can lead to complications, e.g., vision-loss and nerve-damage [19]. To avoid complications, we enforce a maximal drop rate for the glucose concentration. We simulate how much the fasting glucose decreases in an insulin naive cohort after a standardized first dose of 0.1U/kg insulin [1]. Based on the simulation results, we fix the drop rate to  $-0.001$  (mmol/L)/min.

TABLE I  
POPULATION PARAMETERS FOR THE DESIGN MODEL

Parameter	Value	Unit	Description	Reference
$\tau_I$	60	[min]	Time constant for fast-acting insulin absorption	[16]
$\tau_m$	40	[min]	Time constant for meal absorption	[17]
$V_G$	25	[L]	Glucose distribution volume	[16]
$A_G$	0.8	[unitless]	Bioavailability of consumed carbohydrates	[17]
$M_wG$	180.1559	[g/mol]	Molecular weight of glucose	[14]
$p_3$	0.011	[1/min]	Delay in insulin action	[15]
$S_I$	0.44	[L/U·min]	Insulin sensitivity	[15]
$GEZI$	0.0023	[1/min]	Insulin-independent glucose clearance	[15]
$EGP$	0.0672	[mmol/L·min]	Endogenous glucose production	[15]
$I_{ENDO}$	0.0018	[U/mmol]	Endogenous insulin production	[15]

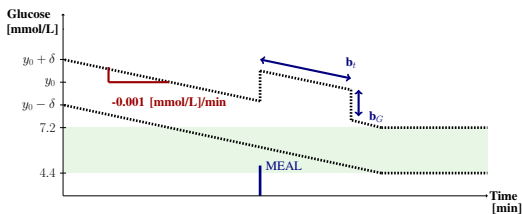


Fig. 3. Output constraints for the optimal experimental design. Over the course of the experiment, the glucose concentration must drop slowly towards the target range. We allow the glucose to fluctuate within the constraints  $y_0 - 0.001 \cdot t_k - \delta \leq y_k \leq y_0 - 0.001 \cdot t_k + \delta$ . Where  $y_0$  is initial fasting glucose,  $t_k$  is the time in minutes,  $y_k$  is the output at time  $t_k$ , and  $\delta$  is half of the width of the target range. Once the target range is reached, it defines the output constraints. After meals, the output constraint is raised by  $b_G = 5.0$  mmol/L for the next  $b_t = 5.5$  hours.

From the initial fasting blood glucose measurement,  $y_0$ , and the 4.4-7.2 mmol/L target glucose range, we select constraints that define how quick the fasting glucose concentration may drop. Following meals, we increase the upper glucose constraint by 5 mmol/L for 5.5 hours to ensure that the optimized insulin input is selected to excite the system, rather than compensating for postprandial peaks. Figure 3 shows the output constraints.

#### E. Simulation model and implementation

We test the optimal protocol in simulation on a model with higher complexity. In [7], Engell et al. employ an augmented version of the integrated glucose-insulin (IGI) model from [20]. We use the same model together with the simulation setup from [7] to generate a virtual cohort of 100 people with T2D.

We implement the simulation, MBDoe and parameter estimation in `Matlab R2020b`, and solve the optimization problem using `sqp`.

## IV. RESULTS

In this work, we investigate how optimal experimental design may improve the performance of an insulin titration algorithm for people with T2D. We solve the optimization problem in (3) to design a 24 hour long experiment to capture data for parameter identification. Figure 4 shows the resulting experimental protocol where all design constraints are met.

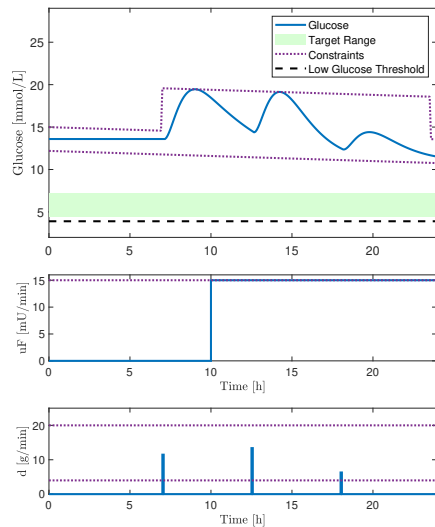


Fig. 4. The optimal experimental design for parameter estimation given the input and output constraints. Meal consumption happens over a five minute interval, hence the three meal sizes are 57g, 67g, and 31g of carbohydrates. The insulin infusion starts three hours after the first meal and remains on the maximal infusion rate, 15mU/min, throughout the rest of the experiment.

The first two meals (57g and 67g of carbohydrate, respectively) drive the glucose concentration to the upper bound and maximize the effect of  $I_{ENDO}$ . The last meal is smaller, 31g of carbohydrate, and lets the insulin input drive the glucose concentration closer to the lower bound emphasizing the influence of  $S_I$ . The insulin infusion resembles a step function. At 10AM, the infusion increases from 0 mU/min to 15 mU/min and remains at maximal infusion until the end of the experiment. The optimal input strategy separates different model dynamics as the insulin input increases three hours after the first meal. Figure 5 presents the output sensitivity of each of the three estimated parameters during the experiment. The sensitivities appear to be somewhat correlated and all three are of similar absolute magnitude.

We test the design protocol in a simulation model which has a higher complexity than the design model. Figure 6 shows how the structural mismatch leads to a different

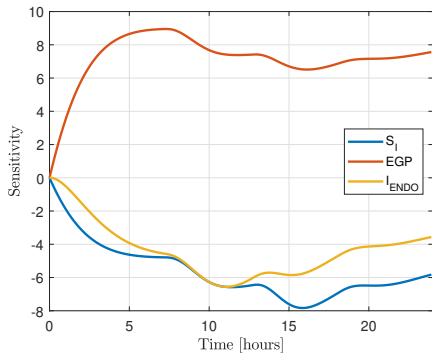


Fig. 5. The output sensitivities for the three estimated parameters over the course of the experiment. The parameters show some correlation.

glucose response. Over the majority of the experiment, the mean glucose curve remains within the output constraints. However, the first two meals cause a slightly higher rise in glucose than the design model prediction in Figure 4. Towards the end of the experiment, the insulin infusion drives the glucose concentration lower than the design model predicts. Still, due to the tight constraints in the optimization problem, the over and undershoot is minimal and the experiment appears to be safe for all the people in the simulated cohort. Compared to the original algorithm performance in Figure 2, the new protocol improves the quality and safety of the dose predictions. In Figure 6, all 100 dose predictions for injection-based treatment drive the glucose concentration into the 4.4-7.2 mmol/L target range.

## V. DISCUSSION

Safety is critical in diabetes treatment. An open-loop implementation of an untested experimental design poses a significant risk and may have limited uptake in clinics. Instead, a qualitative assessment of the new design, rather than a direct implementation, may still improve dose predictions. Figure 6 shows that the system identification improves when insulin infusion starts three hours after the first meal. This split between insulin and meal response could be incorporated when collecting data for parameter estimation. In a real-world implementation, health care professionals may select the maximal insulin infusion rate specifically for the individual or adjust it to match existing treatment guidelines. Closed-loop control could provide an additional safety measure as an artificial pancreas would reduce the insulin infusion in case of too low glucose values.

Compared to the original design, the new protocol has an equivalent amount of insulin input. The mean fast-acting insulin infusion in Figure 2 is 13 U/day. In the new experimental protocol, each individual receives 12.6 U/day. The combined excitation from meals and insulin appears to benefit system identification. However, fixed meal sizes and times can be hard to enforce in a real-world setting. Based on the optimal design, the evening meal needs to have a

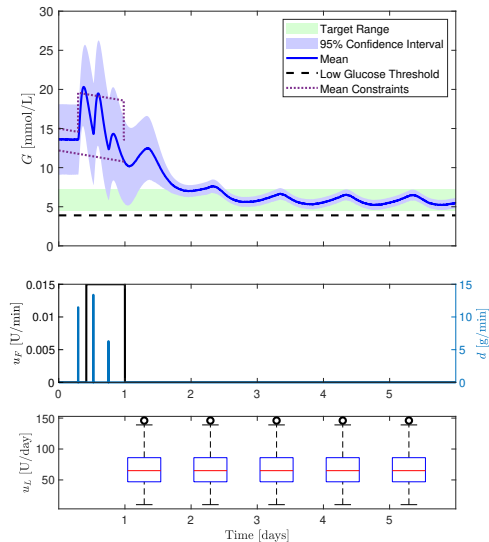


Fig. 6. Test of the experimental design on 100 virtual patients. Over the first 24 hours, we administer the optimized meal,  $d(t)$ , and fast-acting insulin,  $u_F(t)$ , inputs. Meals are consumed over 5 minute intervals. In the experiment, the mean glucose curve mildly exceeds the output constraints after the first and second meal. After 24 hours of data collection, we parameterize a dose-response model for each individual and predict a basal insulin dose,  $u_L(t)$ , to reach the glucose target range. Each subject receives a daily injection with the estimated basal insulin dose at 7AM. To test if the basal insulin dose can control the fasting glucose levels we do not administer meals during the last five days of the simulation. All basal dose estimates are safe and effective.

low carbohydrate content, but the exact number of carbs in each meal may be less important. Still, the timing of and carbohydrate content of meals must be recorded accurately to provide data for system identification. Compared to the original design, meal logging will place a larger work-load on the person with diabetes. Still, one day of logging and counting carbs may pose an appealing alternative to 24 hours of fasting or several months of manual titration.

In manual titration, the slow iterative journey to the clinical target minimizes the risk of nerve- and eye-damage caused by swift drops in glucose concentration. Although the simulation results in this work show that it is possible to find a personalized insulin dose in 24 hours, it can be unsafe to deliver the full dose in an injection of long-acting insulin on the next day. In Figure 2 and 6, the glucose levels drop drastically on the second simulation day when the first long-acting insulin injection is administered. The figures are not meant as implementation proposals to use in clinics. The plots serve to evaluate whether the predicted dose is safe and effective, i.e. that it does not cause low glucose levels and can drive the fasting glucose levels into the 4.4-7.2 mmol/L target range. For a clinical implementation, the person with T2D may step-wise increase the daily dose over a number of weeks, similar to standard-of-care insulin titration. Knowing the target insulin dose, would



allow greater step-wise increases and reduce the length of the titration period. The predicted target dose can help people with T2D and their health care professionals to set goals, balance expectations and evaluate progress of the insulin titration process. Additionally, knowing the target dose size may improve the safety and reduce the fear of overdosing.

In this case study, 24 hours of experimental data is enough to parameterize a dose-response model. In a real-world setting, inter and intraday variations in insulin response may call for longer data collection periods and a different approach to computing the output sensitivities. Due to interday variations, a model identified today may not be representative tomorrow. Hence, data collection over several days, and potentially even weeks, could very well be required to fully understand the dose-response. Additionally, intraday parameter variations can lead to sub-optimal experimental designs, since we base the optimization on output sensitivities we compute from a fixed parameter value.

In this work, we evaluate the output sensitivities locally based on the published population parameters. The local sensitivities provide information about the relevance of  $\theta$  in the proximity of the reference point. Ideally, the reference point should be the true parameter set for the population as a wrong assumption can lead to sub-optimal design protocols. We test our design in a simulation model with structural and parametric differences. Despite model mismatch, the new experimental protocol improves dose predictions hinting that the parameter assumptions are sufficiently representative to design an informative experiment. For future work, testing alternative computation methods for global sensitivities could be a relevant step before clinical implementation of an experimental design in a nonlinear physiological system.

## VI. CONCLUSION

In this case study, we use MBDoE to improve the performance of a model-based insulin titration algorithm. In the framework of a published algorithm, we optimize meal and insulin inputs in a 24-hour data collection period to parameterize a dose-response model. In simulation, we test the safety and efficacy of the model-based dose predictions. The previously published algorithm provides 93% safe and effective insulin doses. By exploiting MBDoE to optimize the titration experiment, the safety and effectiveness is improved and all of the dose predictions are safe in the simulations. We conclude that MBDoE has a potential to improve the performance of model-based dose-guidance solutions. However, it is essential to consider the variations in real-world data before a implementing an *optimal* protocol in clinics.

## REFERENCES

- [1] B. Draznin, V. R. Aroda, G. Bakris, G. Benson, F. M. Brown, R. Freeman, J. Green, E. Huang, D. Isaacs, S. Kahan, J. Leon, S. K. Lyons, A. L. Peters, P. Prahalad, J. E. B. Reusch, D. Young-Hyman, S. Das, and M. Kosiborod, "9. Pharmacologic Approaches to Glycemic Treatment: Standards of Medical Care in Diabetes-2022," in *Diabetes care*, jan 2022, vol. 45, no. Suppl 1, pp. S125–S143.
- [2] K. Khunti, F. Giorgino, L. Berard, D. Mauricio, and S. B. Harris, "The importance of the initial period of basal insulin titration in people with diabetes," *Diabetes, Obesity and Metabolism*, vol. 22, no. 5, pp. 722–733, 2020.
- [3] D. Krishnamoorthy, D. Boiroux, T. B. Aradóttir, S. E. Engell, and J. B. Jørgensen, "A Model-Free Approach to Automatic Dose Guidance in Long Acting Insulin Treatment of Type 2 Diabetes," *IEEE Control Systems Letters*, vol. 5, no. 6, pp. 2030–2035, 2021.
- [4] M. Cescon, S. Deshpande, R. Nimri, F. J. Doyle, and E. Dassau, "Using Iterative Learning for Insulin Dosage Optimization in Multiple-Daily-Injections Therapy for People with Type 1 Diabetes," *IEEE Transactions on Biomedical Engineering*, vol. 68, no. 2, pp. 482–491, 2021.
- [5] T. B. Aradóttir, D. Boiroux, H. Bengtsson, J. Kildegaard, M. L. Jensen, J. B. Jørgensen, and N. K. Poulsen, "Model predictive control for dose guidance in long acting insulin treatment of type 2 diabetes," *IFAC Journal of Systems and Control*, vol. 9, pp. 5–10, 2019.
- [6] T. B. Aradóttir, H. Bengtsson, M. L. Jensen, N. K. Poulsen, D. Boiroux, L. L. Jensen, S. Schmidt, and K. Nørgaard, "Feasibility of a New Approach to Initiate Insulin in Type 2 Diabetes," *Journal of Diabetes Science and Technology*, vol. 15, no. 2, pp. 339–345, 2020.
- [7] S. E. Engell, T. B. Aradóttir, T. K. S. Ritschel, H. Bengtsson, and J. B. Jørgensen, "Estimating a personalized basal insulin dose from short-term closed-loop data in type 2 diabetes," in *2022 IEEE 61st Conference on Decision and Control (CDC)*, 2022, pp. 2580–2585.
- [8] F. Galvanin, M. Barolo, S. Macchietto, and F. Bezzo, "Optimal design of clinical tests for the identification of physiological models of type 1 diabetes mellitus," *Industrial and Engineering Chemistry Research*, vol. 48, no. 4, pp. 1989–2002, 2009.
- [9] F. Galvanin, M. Barolo, F. Bezzo, and S. Macchietto, "A backoff strategy for model-based experiment design under parametric uncertainty," *Aiche Journal*, vol. 56, no. 8, pp. 2088–2102, 2010.
- [10] V. Maheshwari, G. P. Rangaiiah, and L. Samavedham, "A novel multi-objective optimization based experimental design and its application for physiological model of type 1 diabetes," *Ifac Proceedings Volumes (ifac-papersonline)*, vol. 8, no. 1, pp. 638–643, 2012.
- [11] H. E. Silber, J. Nyberg, A. C. Hooker, and M. O. Karlsson, "Optimization of the intravenous glucose tolerance test in t2dm patients using optimal experimental design," *Journal of Pharmacokinetics and Pharmacodynamics*, vol. 36, no. 3, pp. 281–295, 2009.
- [12] F. Galvanin, M. Barolo, and F. Bezzo, "On the use of continuous glucose monitoring systems to design optimal clinical tests for the identification of type 1 diabetes models," *Computer Methods and Programs in Biomedicine*, vol. 109, no. 2, pp. 157–170, 2013.
- [13] A. J. Laguna, P. Rossetti, F. J. Ampudia-Blasco, J. Vehí, and J. Bondia, "Optimal design for individual model identification based on ambulatory continuous glucose monitoring in patients with type 1 diabetes," *Iet Seminar Digest*, vol. 2010, no. 4, p. 0349, 2010.
- [14] T. B. Aradóttir, D. Boiroux, H. Bengtsson, J. Kildegaard, B. V. Orden, and J. B. Jørgensen, "Model for simulating fasting glucose in type 2 diabetes and the effect of adherence to treatment," *IFAC-PapersOnLine*, vol. 50, no. 1, pp. 15 086–15 091, 2017, 20th IFAC World Congress.
- [15] T. B. Aradóttir, D. Boiroux, H. Bengtsson, and N. K. Poulsen, "Modelling of fasting glucose-insulin dynamics from sparse data," *Proceedings of the Annual International Conference of the IEEE Engineering in Medicine and Biology Society*, pp. 2354–2357, 2018.
- [16] S. S. Kanderian, S. Weinzimer, G. Voskanyan, and G. M. Steil, "Identification of intraday metabolic profiles during closed-loop glucose control in individuals with type 1 diabetes," *Journal of Diabetes Science and Technology*, vol. 3, no. 5, pp. 1047–1057, 2009.
- [17] R. Hovorka, V. Canonico, L. J. Chassin, U. Haeter, M. Massi-Benedetti, M. O. Federici, T. R. Pieber, H. C. Schaller, L. Schaupp, T. Vering, and M. E. Wilinska, "Nonlinear model predictive control of glucose concentration in subjects with type 1 diabetes," *Physiological Measurement*, vol. 25, no. 4, p. 905, jul 2004.
- [18] S. Bhonsale, P. Nimmegeers, S. Akkermans, D. Telen, I. Stamati, F. Logist, and J. F. Van Impe, "Optimal experiment design for dynamic processes," *Simulation and Optimization in Process Engineering: the Benefit of Mathematical Methods in Applications of the Chemical Industry*, pp. 243–271, 2022.
- [19] C. H. Gibbons, "Treatment induced neuropathy of diabetes," *Autonomic Neuroscience: Basic and Clinical*, vol. 226, no. September 2019, p. 102668, 2020.
- [20] S. E. Engell, T. B. Aradóttir, H. Bengtsson, M. Ekelund, and J. B. Jørgensen, "Glucose response to fast- and long-acting insulin in people with type 2 diabetes," *IFAC-PapersOnLine*, vol. 54, no. 15, pp. 496–501, 2021.

## 6.8 PAPER 8

**Title: “A Dual Hormone Predictive Controller for a Fully Automated Intraperitoneal Artificial Pancreas in Pigs”**

Submitted to Automatica.

Date of first submission: 17 September 2023, under the title “A Dual Hormone Predictive Controller for a Fully Automated Intraperitoneal Artificial Pancreas in Pigs”. Manuscript no. Automatica 23-1172.

This paper is submitted for publication and is therefore not included.



## 6.9 REFERENCES

- [1] K. D. Benam, H. Khoshamadi, L. Lema-Pérez, S. Gros, and A. L. Fougner, “A nonlinear state observer for the bi-hormonal intraperitoneal artificial pancreas,” in *2022 44th Annual International Conference of the IEEE Engineering in Medicine & Biology Society (EMBC)*. IEEE, 2022, pp. 171–176. Cited on page/s 70.
- [2] K. D. Benam, H. Khoshamadi, M. K. Åm, Ø. Stavadahl, S. Gros, and A. L. Fougner, “Identifiable prediction animal model for the bi-hormonal intraperitoneal artificial pancreas,” *Journal of Process Control*, vol. 121, pp. 13–29, 2023. Cited on page/s 79.
- [3] M. Halvorsen, K. D. Benam, H. Khoshamadi, and A. L. Fougner, “Blood glucose level prediction using subcutaneous sensors for in vivo study: Compensation for measurement method slow dynamics using kalman filter approach,” in *2022 IEEE 61st Conference on Decision and Control (CDC)*. IEEE, 2022, pp. 6034–6039. Cited on page/s 99.
- [4] K. D. Benam, S. Gros, and A. L. Fougner, “Estimation and prediction of glucose appearance rate for use in a fully closed-loop dual-hormone intraperitoneal artificial pancreas,” *IEEE Transactions on Biomedical Engineering*, 2023. Cited on page/s 108.
- [5] M. Al Ahdab, K. D. Benam, H. Khoshamadi, A. L. Fougner, and S. Gros, “Sensor fusion for glucose monitoring systems,” *IFAC-PapersOnLine*, 2023. Cited on page/s 123.
- [6] J. Langholz, K. D. Benam, B. Sharan, S. Gros, and A. L. Fougner, “Fully automated bi-hormonal intraperitoneal artificial pancreas using a two-layer pid control scheme,” in *2023 European Control Conference (ECC)*. IEEE, 2023, pp. 1–8. Cited on page/s 132.